Horizontal and Vertical Transport in a Multilayered Aquifer of the Triassic Sandstone, UK
– Tracer Tests and Modelling –

by
Ralf Lieb

A thesis submitted to
The University of Birmingham
For the degree of
MASTER OF PHILOSOPHY

School of Geography, Earth and Environmental Sciences
The University of Birmingham
JULY 2011

Abstract

The aim of the work was the quantification of horizontal and vertical solute transport of possible contaminants in the close vicinity (<10m) around pumped wells in conurbations. The Birmingham Triassic Sandstone aquifer was chosen to build a borehole array of five wells in the Wildmoor Sandstone. The five wells of the test site at the University of Birmingham approached seven sandstone layers, separated by six mudstone layers, approved with geophysical well logging. Specifically constructed packers were used to process tests quantifying the hydraulic and solute transport characteristics. Hydraulic conductivities between 1.27 m/d and 11.37 m/d were calculated with data of 14 pumping tests. Storage coefficients between 1.76×10^{-5} and 1.32×10^{-5} were determined. Average linear velocities of six sandstones were determined between 0.156 to 3.28m/d. Corresponding hydraulic gradients of 0.033 to 0.288 with up-flow in wells were calculated. Horizontal forced gradient tracer tests, being processed in three aquifers, recovered between 48% to 97% rhodamine WT and fluorescein. Effective porosity values between 0.00225 and 0.346 were calculated. A new setup of vertical forced gradient tracer tests, exploring the connectivity between two sandstone layers separated by a mudstone layer, was processed. Groundwater modelling was carried out to quantify especially dispersivity values for sandstone and mudstone layers.

The tests give a full set of quantified hydraulic data for Triassic Sandstone to estimate contaminate transport within the area of pumped wells. The importance of fractures for the groundwater flow and contaminant transport in Triassic Sandstone, were confirmed by the tests.

ACKNOWLEDGEMENTS

My gratitude and special thanks goes to Richard Greswell who has build a nice pair of packers and with whom I shared weeks on the test site managing the “Scarpheap Challenge” at the University running tests, in good and bad times, and for his kind hospitality. Thanks to his wife Carol, too. I am also thankful to the School of Environmental, Geography and Earth Sciences of the University of Birmingham and the National Environmental Research Council (UK), for supporting me and my research during my stay in Birmingham from June 1998 until September 2001.

Thanks goes to the URGENT team; Abraham Thomas, to whom I sat next to for years in the office and who was always helpful and supportive, Kevin Shepherd bringing order and organisation to our office, Richard Mitchener who provided me with core data of BH4 and taught me about politics. You always helped me on the test site, especially Kevin, when hands were needed to pull, push or carry equipment around. Jane Harris helped in the Laboratory. Thanks go although to Valantim Curião, visiting ERASMUS student, who processed laboratory test on core samples of mudstone of the test site.

I am also thankful to all the Staff of the School and University, supporting the research to be processed, especially staff of workshops who provided me with equipment, material, ... to run the test site. I am glad to have met all the different research and PhD students supporting me, guiding me around and introducing me to the UK.

Of course, I have to thank my wonderful wife Monika, who still supports me in continuing the research, despite we have got three kids and have build a house in the meantime. Furthermore, I like to thank my parents for their help and support, during all these times.

Last but not least, I take the opportunity to thank the fork-lift driver whose name I do not know. Without his help a bundle of packers, transducers and pumps would still stuck in BH1 of the test site.

Table of Contents

List of Figures

List of Tables

List of Equations

Appendices

Appendix III.3.1: Drilling Log of BH1 (Note: The elevations (AOD) given are not correct! See Figure 3.7).

Appendix III.3.2: Double-tube core barrel drilling BH4. A: Core bit removed, B: Taking off the Core Catcher. C & D: Pulling out of the inner tube with the core of the double-tube core barrel

Appendix III.3.3: Core Bits applied to drill Borehole BH 4

Appendix IV 4.1: BH 4 Core Log (Mitchener, 2003)

Appendix IV 4.2: Temperature Logs

Appendix IV 4.3: Conductivity Logs

Appendix IV 4.4: Caliper Logs

Appendix VII.1 a: Mesh Size

Appendix VII.1 a: Computer Model Mesh Size, Rows and Columns

Appendix VII.1 b: Computer Model Layer Setup

Appendix VII.1 c: Computer Model Borehole Coordinates

Appendix VII.2: Computer Model Heads at the Boundaries

Appendix VII.3: Drawdown graphs of the pumping tests fitted against the drawdown graphs of the model results

CHAPTER 1: INTRODUCTION

1.1 Project Setting and Aim

The thesis forms part of the URGENT – Urban Regeneration and the Environment – Programme, a research programme funded by the National Environment Research Council (NERC) with the aim to stimulate the regeneration of the urban environment through understanding and managing the interaction of natural and man-made processes. Over 90% of the population of the UK lives in conurbations covering 10% of its land area. More than 150 years of industrialisation and rapid urbanisation have left a legacy of contamination and dereliction. URGENT focuses on a limited number of urban conurbations and developed generic models and solutions, which should be applicable more widely in the UK and internationally.

An important topic of investigation is the water transport in natural or man-made environment and possible mobilization of contaminates, which was dealt with in this thesis. In this context, UK's Permo-Triassic Sandstone multilayered aquifers, the second most important aquifers in the UK with total abstractions of around 900 Mm^3/a or about 35 % of the groundwater abstraction, were considered for further investigations. The Birmingham Triassic Sandstone aquifer, as a multilayered aquifer, was chosen for this work to explore problems faced by users of single wells when water of usable quality could be sustainably abstracted from the urban aquifer. This issue led to the topic of the thesis: "Horizontal and Vertical Transport in a Multilayered Aquifer of the Triassic Sandstone, UK – Tracer Tests and Modelling". The area of investigation wass the solute migration at borehole scale around an existing pumped well in a distance of less than 10 metre.

Tellam and Barker (2006) confirmed the importance of fracture flow near wells. Tests carried out in Permo-Triassic multilayered aquifers by Green, 1994, Hamilton, 1995, Betts, 1996, Streetly et al., 2002, were processed in horizontal directions within certain aquifer layers. However, to confirm the hypothesis of Tellam and Barker (2006), the **aim of this thesis** was to confirm the interaction between layers within a multilayered aquifer with tracer tests both in horizontal direction and in vertical direction, an experiment not being explored before. The results of the hydraulic quantification should be applicable for similar types of multilayered Permo-Triassic sandstone aquifers worldwide.

1.2 Previous Work

An overview of artificial tracer tests in hydrogeology in Britain was given by Atkinson and Smart (1980), while Davis et al. (1985) discussed groundwater tracer applications in detail. Hiscock (2005) reported on a few tracer tests processed in sand and gravel, limestone chalk aquifer. However, the most appropriate review and guidelines for the use of groundwater tracer tests in British aquifers were presented by Ward et al. (1998). Numerous examples for experimental tracer tests in limestone were given, but only four locations were selected so far where tracer tests were applied in Triassic Sandstone. The first was a forced gradient tracer test in the East Midlands using bacteriophages as a tracer. The second was a dewatering test between a borehole and a tunnel, in Liverpool, using fluorescein as a tracer (Barker et al., 1998). The third location is called Heath House, near Hodnet, in Shropshire (Coleby, 1996), and the fourth location of tracer tests in Triassic Sandstone in the UK is the Haskayne site north of Liverpool, at the Merseysite in NW England (Green, 1994; Hamilton, 1995; Betts, 1996; Streetly et al., 2002). At each of the latter locations, two forced gradient tracer tests were carried out. Semi-quantitative interpretation of the tests at the Haskayne site (Streetly et

al., 2002) found values of dispersivity of 1 - 2 m and of kinematic porosity of 0.14 - 0.2. Joyce et al. (2006) carried out five field tracer tests in the Birmingham Triassic Sandstone Aquifer. From quantitative interpretation of these data, values of 0.7 – 2 m were given for the dispersivity and 0.2 - 0.3 for the effective porosity.

1.3 Approach

The aim of the thesis is the construction of a test site with an array of four boreholes in the vicinity of an existing well; the design of a hydrogeological model of the site; its hydraulic characterization including the horizontal and vertical transport properties; and the development of a hydraulic and transport computer model. To develop such flow and transport models the following steps were processed:

1. Construction of a Test Site in the Triassic Sandstone aquifer of Birmingham

An area in front of the Earth Science Building of the Birmingham University was chosen as test site with an already existing well, BH1, drilled in 1995. The well has a depth of 60 m bgl (below ground level) with an iron casing at the top 13 m bgl and is not grouted. The drilling log of BH1 defines seven sandstone layers separated by six mudstone layers, all connected by BH1 from 13 m bgl to 60 m bgl. Under the expectation of horizontal layered Triassic Sandstone four additional boreholes labeled BH2-BH5 were drilled. To have a better chance of reaching the same layers at the same depth, the additional four wells were drilled in a maximum radius of 7 m around BH1. The distance of 7 m was chosen to be able to account for vertical flow around the pumped wells. Two wells were drilled to approach two different particularly confined sandstone layers. The third well approached the unsaturated aquifer.

2. Development of a Hydrogeological Model of the Test Site

Experimental information of all the wells gained with different logging methods were applied to develop a conceptual model of the Tests Site. A drilling log of BH1 and a core log of BH4 were available after the drilling campaign. For detailed information of all wells geophysical logs were recorded in all wells. The results of the logs were compared for different log types recorded in the same well and compared for the same logging method recorded in different wells.

3. Hydraulic Characterization of the Test Site

Pumping Tests were conducted in all wells to measure hydraulic conductivities, transmissivities and storage coefficients for almost each sandstone layer defined by the conceptual model. A specially designed double-packer system and a plastic tube (lay flat) packer of over 60 m length were used for the test in BH1 to packer off a particular sandstone layer or the whole BH1. The drawdown was recorded with pressure transducers in almost all wells during the tests. Analysis of the drawdown data was processed with pumping test analysis software (Aquifer win32).

4. Characterization of Horizontal and Vertical Transport Properties of the Test Array

Three different types of tracer tests with different set ups were processed on the test site to simulate solute movement and transport within the layered aquifer of the borehole array. Fluorescein and rhodamine WT were applied as tracers. The following three tracer tests were chosen:

- **Point dilution tracer tests** were conducted in BH1 in almost all sandstone layers. The goal of the test was to measure the dilution of the introduced tracer over time in the aquifer and to calculate its natural gradient.

- **Forced gradient tracer tests in horizontal direction** in one sandstone aquifer were conducted in three different aquifer layers where two wells were available for the test set up of an injection and abstraction borehole. The goal was to determine values of effective porosities and longitudinal dispersivities in the Triassic Sandstone.

- **Forced gradient tracer tests in vertical direction** between sandstone aquifers, separated by mudstone layers. The set up of forced gradient tracer tests in vertical direction between two aquifers separated by a mudstone layer was new. All tests were set up in the way that tracer was injected into a confined sandstone aquifer for several hours and that water was abstracted in wells in sandstone layers above and below the injection layer. The goal was to measure the breakthrough of tracer in order to verify whether vertical transport through mudstone layers takes place. Furthermore, the mass of tracer breaking through should be quantified.

5. Development of a Computer Model

At the end of this work all newly gained information of the various tests were used to develop a conceptual flow model of the test site, which is based on the simplified geological layered sandstone and mudstone structure. The data of the hydraulic characterization were used to calibrate the model and the calculated natural hydraulic gradient of the point dilution test was used to define the boundaries of the model. Horizontal and vertical forced gradient tracer tests were quantified by solute transport modeling.

CHAPTER 2: Geology and Hydrogeology

2.1 Aim

The aim of this thesis was to examine the fluid flow and solute transport in horizontal and vertical direction in the Triassic Sandstone. The Birmingham Urban Aquifer was considered to be typical of the Triassic Sandstones in the Midlands, if not for a wider area of Triassic Sandstone in the UK.. The chosen area of the test site lies in the Wildmoor Sandstone of the Triassic Sandstone within the campus of the University of Birmingham. Thus, a review of the sedimentology, geology and hydrogeology of the Triassic Sandstone on a regional and local scale was required, relevant to this project. The focus was laid on matrix flow, fracture flow, aquifer properties and results of previously processed tracer tests in the Triassic Sandstone of the UK.

Groundwater flow and solute transport in the Birmingham aquifer are dependant on the aquifer properties of the Triassic Sandstone. The properties depend on the sedimentation and diagenesis of the aquifer building sandstone, siltstone and/or mudstone. A local, neighbouring test site at the University of Birmingham is presented in more detail with respect to the detailed facies analysis conducted. Tracer tests carried out at this neighbouring test site are presented, as well.

Finally, the regional geology, local geology and hydrogeology of previous information were assigned to the test site built for the purpose of this thesis.

2.2. Regional Geology and Stratigraphy of the Birmingham Area

The Brimingham area is dominated by the geology of the Carboniferous, the Permo-Trias and the Quaternary. The Brimingham aquifer consists of Triassic Sandstone sediments. Figure 2.1 gives an overview of the geology of the Birmingham area after Powell et al. (2000).

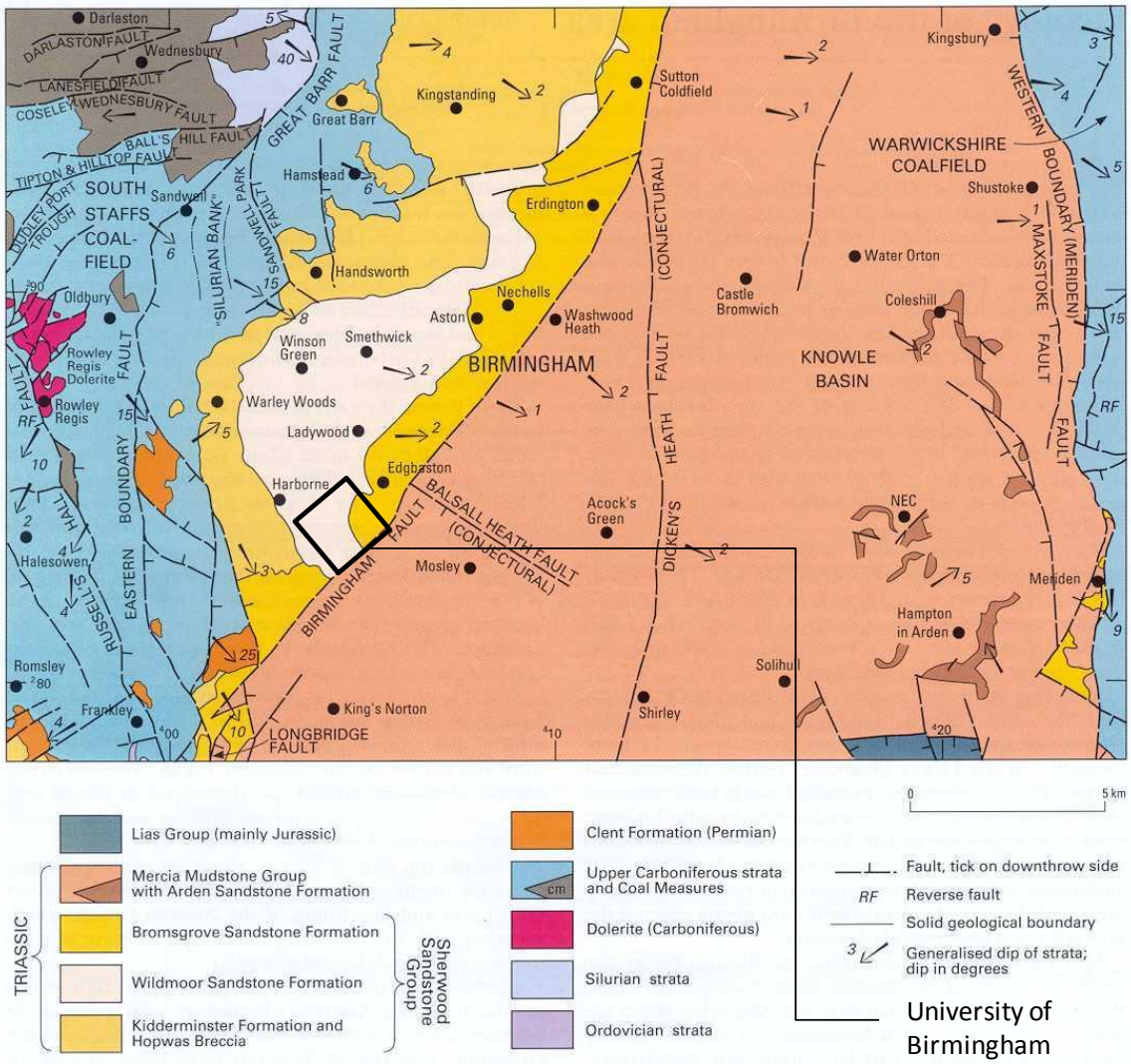

Figure 2.1: Geology of Birmingham with the location of the University main Campus (after Powell et al., 2000)

Triassic rocks are lying unconformly on pretended impermeable Carboniferous Coal Measures, building the basement of a Triassic sediment basin with an approximate northeast-southwest strike. The Birmingham basin is bound in the west by the Black Country of the Carboniferous South Staffordshire Coalfields and in the east by the Carboniferous Warwickshire Coalfields. The filling of the Triassic sediment basin is built by Triassic Sandstones and Triassic Mudstones. The Triassic Sandstones built the Birmingham aquifer, in the north-western part of the basin, lying north-westerly from the Birmingham fault and overlying the Carboniferous strata with a slight angular unconformity, according to Powell et al. (2000). Between the Birmingham fault and the Meridian fault (Western Boundary) is the Knowle Basin consisting of Triassic Mudstones where the sediments were deposited in an extensional setting after Chadwick and Smith (1988). Thus, the boundaries of the Birmingham aquifer are Carboniferous deposits along the western margin, towards the base of the basin and the Birmingham Fault to the east. This is supported by modelling work of the Birmingham aquifer by Knipe et al. (1993).

Warrington et al (1980) defines three groups of Triassic Sandstone:

1. **Sherwood Sandstone Group**: Mainly red sandstones
2. **Mercia Mudstone Group:** Comprising red mudstones and siltstones
3. **Penarth Group:** Mainly marine sediment.

However, the last group was not recorded in the area Birmingham, neither in outcrops nor in boreholes. Extensive quaternary sediments can be found on the sediments of the Birmingham aquifer and on the surface of the Knowle basin. Glacial deposits, fluvio-glacial deposits and locally peat were found also.

The stratigraphy of the Birmingham area shows that the Triassic rocks are subdivided into the older, mainly arenaceous Sherwood Sandstone Group and the younger, mostly argillaceous Mercia Mudstone Group. Table 2.1 shows the general geological succession of the Birmingham area.

Thompson (1970) identified ten lithofacies sequences in the Cheshire Basin, occurring at any stratigraphical level. This reflects the general situation during the sedimentation in the Worcester, Stafford and Needwood Basins close to Birmingham with graben subsidence and the spreading of basin margins. The grain size becomes finer towards the basin centre from proximal coarse alluvial sands and gravels, to distal sandy braided river deposits (Audley-Charles, M.G., 1970, Mader, D., 1992, Wills, L.J, 1976).

Table 2.1: Geological succession of the Birmingham area (Nomenclature after Warrington et al. 1980, in brackets previous stratigrahical nomenclature after Eastwood et al. 1925).

		Thickness
Pleistocene & Recent	Made ground	up to 20 m
	River alluvium	up to 6 m
	Terrace and fluvioglacial sands and gravels Glacial till, sands and gravels, lake clays	up to 40 m
Triassic	Mercia Mudstone Group (Keuper Marl) including Arden Sandstone	up to300 m
	Sherwood Sandstone Group	
	- Bromsgrove Sandstone (Keuper Sandstone)	25 – 120 m
	- Wildmoor Sandstone (Upper Mottled Sandstone)	0 – 90 m
	- Kidderminster Sandstone (Bunter Pebble Beds)	0 – 125 m
Permian	Hopwas Breccia	0 – 30 m
Carboniferous	Coal Measures	600 – 1100 m

Warrington et al. (1980) worked on the correlation of the different formations and divided the Sherwood Sandstone Group into the Bromsgrove, Wildmoor and Kidderminster Sandstone:

1. **Bromsgrove Sandstone** builds the younger division of the Sherwood Sandstone Group. It consists of medium to coarse grained, usually well cemented sandstone with quite variable oxide coatings, giving a red and brown colour with beds of red and blue marl. Narrow outcrops are close to the western site of the Birmingham Fault. To the east of the fault lies the Bromsgrove Sandstone with a maximum thickness of 120 m below the Mercia Mudstone.
2. **Wildmoor Sandstone** Formation is built by well sorted, fine grained sandstone which is little cemented. It builds bedded, soft, uniform, bright red sandstones of up to 90 m thickness with partings and thin bands of marl. Wildmoor Sandstone outcrops are found in much of Western Birmingham.
3. **Kidderminster Sandstone** is formed by up to 125 m of reddish-brown, medium to coarse grained sandstones with abundant pebbles and varying calcite cementation.

The Mercia Mudstone comprises siltstones and mudstones, locally containing dolomitic sandstone horizons close to the base. Evaporite beds are observed throughout the mudstone. The colour is red with some green and grey sandstone bands and the Mercia Mudstone is up to 300 m thick.

Below the Permo-Triassic strata lies the Coal Measures of interbedded fine sandstone and mudstone (with soil and coal horizons) of generally low permeability and storage capacity (Warrington et al., 1980, Audley-Charles, M.G., 1970).

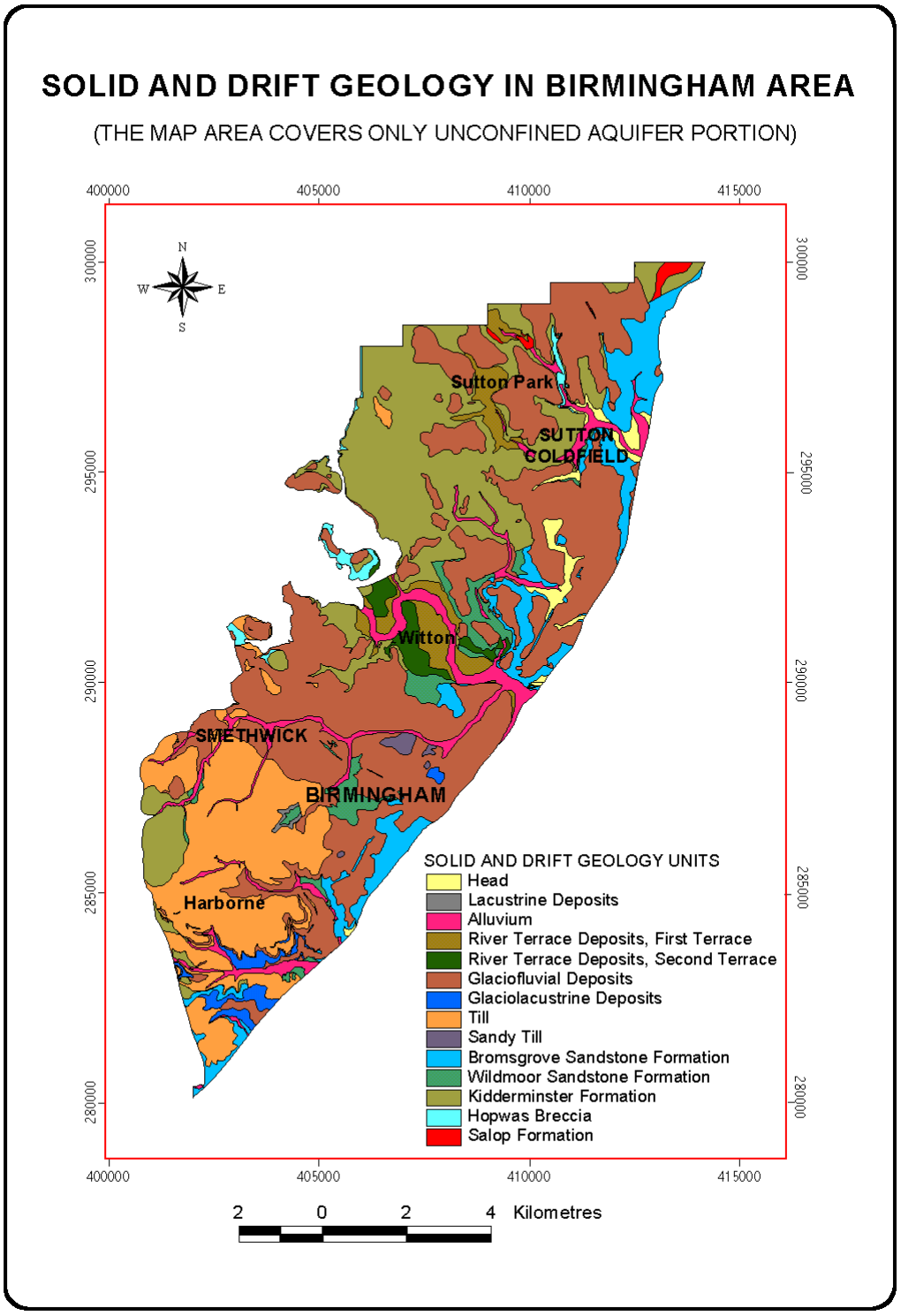

Figure 2.2: The Triassic geology of the unconfined Birmingham aquifer, west of the Birmingham fault (Thomas, 2001)

Drift deposits cover wide areas of the sandstone outcrop around Birmingham with thicknesses of up to 25 m. Specific areas are examined by Pickering (1957), Kelly (1964) and Horton (1974). The glacial deposits consist of a local varying mixture of clay, sand, gravel and boulder. Land (1966) and Horton (1974) examine in detail drift deposits at different localities in the area of Birmingham.

Alluvium overlies glacial deposits and sandstone in places, mainly along the rivers Tame and Rea (see Figure 2.2, after Thomas 2001). Urbanisation and Industrialisation caused a covering with man-made ground in wide areas of Birmingham of up to 20 m. The made ground consists of tarmac hardstandings (e.g. in residential areas) or landfill industrial waste depending on the area. Made ground constituents depend on the local dominant industry and vary in nature. It may consist of ash, clinker, bricks and other demolition materials. Thomas (2001) gives land use classifications and their influence on the recharge for the unconfined aquifer of Birmingham. Figure 2.2 shows the solid and drift geology of the unconfined part of the Birmingham aquifer (after Thomas, 2001).

2.3 Permo-Triassic Sedimentology

To predict the flow and transport conditions within the Permo-Triassic Sandstone, aquifer models should account for the sediment structures at different scales from micro to macro scale. The aquifer architecture of permeable pathways and barriers depends on the lithology and/or facies and increases with their variability (Miall, 1988).

2.3.1 Facies (Depositional Environment)

Tellam and Barker (2006) give a detailed description of the depositional environment during the Permo-Triassic in the UK in respect to solute movement. The Triassic Sandstone is

mainly of fluviatile origin, from a river system comparable with a major braided river system like the Saskatchewan river in Canada of today (Allen et al, 1997). During the sedimentation the climate was semi-arid to arid. Northward flowing braided river systems from the Variscian Mountains in the south (relative to present European geographical orientation) transported finer-grained sediments into tectonic active subsiding basins. Rain events caused flash floods mobilising debris from the mountains. The fluvial and aeolian environment sediment structures comprise plane lamination, cross-lamination, trough and planar tabular cross-stratification, water escape structures, debris flows, paleosols and desiccation cracks (e.g. Thompson, 1970 and Steel and Thompson, 1983, Tellam and Barker, 2006). The bed size varies from few centimetres to more than several metres. Depositional cycles are recorded for less than a metre to more than 100 m which is covered by sequence stratigraphy. Wills (1970) recognised “microcycles” which represent a wet to dry transition at a scale of a few beds. After Wills (1970), microcycles can comprise groups of microcycles up to a thickness of about 100 m. “Magnacycles” comprise a group of microcycles or formations. Microcycles can indicate energy conditions of the sedimentation as shown for an ideal microcycle, according to Thompson (1970) and Wills (1970) (after Tellam and Barker, 2006):

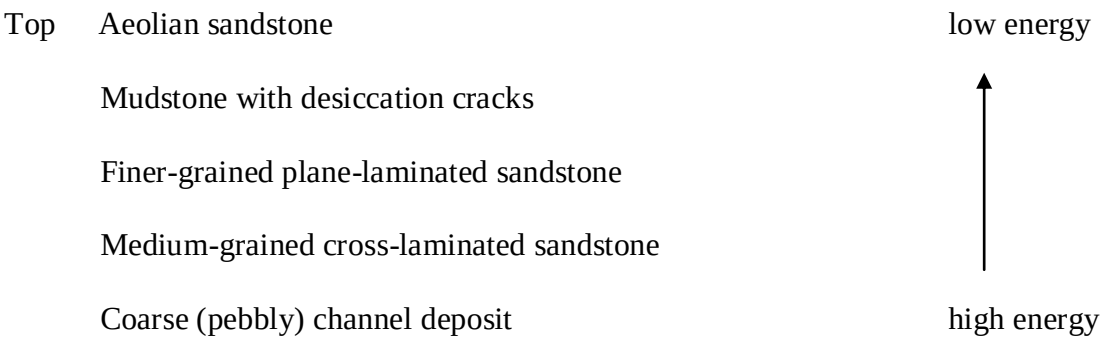

The sedimentation of the cycle base to top or wet to dry stratigraphy is related world-wide to orbital forcing mechanisms (e.g. Mountney and Thompson, 2002). Galloway et al. (1998) describes three simplified principle types of facies and their hydrostratigraphic complexity which can be found at different scales from a few centimetres to several meters and formations of Triassic Sandstone (Figure 2.3):

1. "Layer Cake": Continuous lateral layers with a gradual change in thickness. They have a relatively simple correlation of sheet or lobate geometries of the permeable units.
2. "Jigsaw puzzle": A complex compartmentalised system of cross-bedding cycles. Internal correlation within one cycle is difficult. Correlation and delineation of general zones of higher permeability are relatively easy.
3. "Labyrinth": Numerous partials to completely isolated permeable units. External and internal correlation of the sand-body distribution and interconnectivity are difficult.

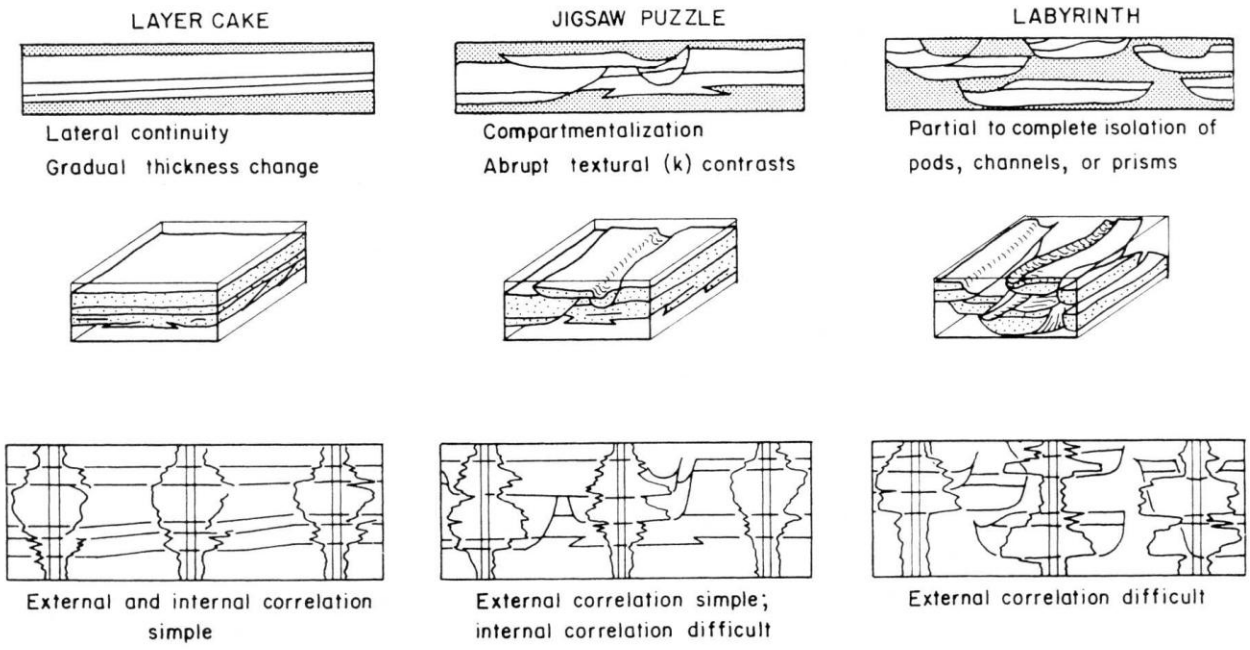

Figure 2.3: Three principle facies types with different hydrostratigraphy applicable for Triassic Sandstone (after Weber and van Geuns, 1990). The scale can vary from a few centimetres to several metres.

2.3.2 Lithology

The Triassic Sandstones are mostly quartz arenites to lithic arkoses (classification after Pettijohn, 1975), mainly composed of quartz with subordinate K-feldspar, albite, mica, carbonate clasts and minor ilmenite, zircon, and apatite (Strong, 1993). The grain size can vary from fine to coarse sands. Fine sands tend to contain some silt and clay matrix. Diagenetic features of the Sherwood Sandstone are similar to those forming today in the red beds of the Sonoran Desert, a basin which reaches only shallow burial depth (Walker et al., 1978, Burley, 1984). Principle diagenetic characteristics are reddening by hematite grain coatings, quartz and K-feldspar overgrowths and cements, calcite, dolomites, with minor albite overgrowth, and kaolinite, illite, smectite and pyrite. Extensive grain dissolution, especially of K-feldspar grains can be traced by oversized pores, residual fragments, hollow overgrowth and ferruginous clay veneers (Strong, 1993). The porosities in the sandstones appear to be dominated by their primary lithology. Fine grained and muddier rocks generally tend to have a lower porosity. Mesogenetic secondary porosity of up to 30 % tends to appear in mature quartz arenites after grain and cement dissolution (Burley, 1984, Strong, 1993). Diagenetic features, especially the presence of pore filling cement in the Sherwood Sandstone, affect the hydraulic properties of the rock. Meteoric water circulating in the sandstone resulted in a carbonate cement removal, mainly in the unconfined aquifer.

Organic carbon contents are less than 0.1% (Steventon-Barnes, 2001; Shepherd et al. 2006).

Mudstones within the sequence are generally less than 1m thick and have a similar mineral composition with clays, quartz, feldspar, mica and hematite.

2.3.3 Burial and Diagenesis of Triassic Sandstone

During the sedimentation of the Permo-Triassic Sandstone sequences the basins often were tectonically active (Audley-Charles, 1970), producing basin fills of no more than a few kilometres thickness (Burley, 1984). The basins were controlled by reactivating basement faults with uplift and inversion at several times since the Jurassic. In general, bedding dips of Permo-Triassic basins are typically less than 10° (Tellam and Barker, 2006). Faults can have a range of morphologies, deformation bands appear often in swarms and slip surfaces exist open or filled with clay or cataclasts (Fisher and Knipe, 1998, Manzocchi et al, 1998, Fowels and Burley, 1994). Jointing occurs to varying degrees and fractures become less frequent with depth (Gutmanis et al., 1998; Jeffcoat, 2002). Dewatering structures are found rarely as large scale dykes. The diagenesis of the sandstones can vary very much locally, but three main phases are differentiated generally by Tellam and Barker (2006, see also Burley, 1984; Metcalfe et al., 1994; Milodowski et al.; 1999):

1. **Early and shallow phase of diagenesis**: Grain dissolution, replacement and precipitation of authigenic minerals (Burley, 1984). For example sandstones of West Cumbria. Burley (1984) suggests that the Midland basins have experienced shallow diagenetic conditions.

2. **Burial or mesogenetic diagenesis**, up to 4 km in the Wessex Basin and the Irish Sea basins. The pororsity has been reduced by compaction during deep burial. Early cementation of high permeable sandstone units. Sutured grain contacts are common.

3. **Post-Inversion or telogenetic diagenesis**, due to ingress of meteoric waters after uplift which the Triassic basins have been exposed to since Jurassic times (Burley 1984). Dissolution of carbonate and sulphate occurred and weathering of some feldspare to clay. An ongoing process which is only in rare cases influencing the hydrogeology significantly (Tellam and Barker, 2006).

The cementation of carbonates and feldspars of the Triassic Sandstone is locally dissoluted (Burley, 1984), especially in the upper 50m to 100m. The unconfined area of the Birmingham aquifer is considered to have a leached zone of around 10 metres at the top, after Knipe et al. (1993).

2.4 Flow Characteristics of Triassic Sandstone

The flow characteristics of an aquifer can be described with aquifer properties: Controls on groundwater flow can be distinguished by properties of matrix flow and fracture flow. Flow characteristics are described for matrix flow of the Triassic Sandstone at different scales.

2.4.1 Laboratory Studies

A variety of studies have examined the porosity and permeability in laboratory studies (Tellam and Barker, 2006). Core sampling of Triassic Sandstones is described by Reeves et al. (1975) and Allan et al. (1997), providing a discussion of core analysis. The latter gives a summary of most of the laboratory studies on Triassic Sandstone. Tellam and Barker (2006) give a general overview.

Porosity data measured in the West Midlands vary from 0.02 to 0.36 for Permo-Triassic sandstones. Average porosities are similar with arithmetic means between 0.24 to 0.28 and a

median of 0.26. (Allen et al., 1997). The porosity mainly depends on the cementation. In cemented areas of the Kidderminster formation the porosity is as low as 4 %. Low porosity values of the Wildmoor Sandstone are measured in silt and clay rich and cemented layers. Low porosity values in the Bromsgrove Formation are corresponding to well cemented, fine grained sands. Maximum porosity values of 34% to 36% correspond to well sorted, medium to coarse grained, and friable sandstones.

Measured values of permeabilities are log normal distributed with geometric means in the range of 0.1m/d to 10m/d. Campell (1982) recorded some variation in formations and between basins. The ratio of horizontal to vertical hydraulic conductivity for the Sherwood Sandstone group in the West Midlands varies between 1.1 to 3.7 (Allen et al., 1997). The ratio can be up to 50 (Tellam and Barker, 2006). No systematic variation in matrix permeability was found by Tellam and Barker (2006) with depth. However, frequent dissolution of carbonates from shallow depth is frequently recorded. Mitchener (2003) suggests a sensitivity of permeability of some sandstones to change in water chemistry.

2.4.2 Pumping Tests

The distribution of transmissivity data from pumping tests performed at 763 sites in Triassic Sandstone (all the sites on the aquifer properties database of the BGS, Allen et al., 1997) nearly forms a log-normal distribution with a geometric mean transmissivity of 189 m^2/d and an interquartile range of 90m^2/d to 436 m^2/d. Comparing transmissivity data of core analysis with those of pumping tests, Lovelock (1977) found that pumping test transmissivity data exceed those of core data. This indicates a non-matrix flow contribution to the aquifer transmissivity, caused by fractures for example. Due to the observed combination of matrix flow and fracture flow towards a borehole, the Permo-Triassic Sandstone is described as a

"dual-permeability" system (Allen et al, 1997). In the West Midlands region pumping test data from 88 tests are available on record (Allen et al., 1997). Transmissivity data range from $2m^2/d$ to $5200m^2/d$ with an interquartile range of $60m^2/d$ to $330m^2/d$ and a geometric mean of $151m^2/d$. A relationship between the length of the pumping tests and the transmissivity values was not observed. Bulk hydraulic conductivity data for the Sherwood Sandstone group of the West Midlands are given in Table 2.2.

Table 2.2: Bulk hydraulic conductivity of the Sherwood Sandstone in the West Midland Region (after Allen et al., 1997)

	Range [m/d]	Interquartile Range [m/d]	Median [m/d]	Geometric Mean [m/d]
Triassic Sandstone in the West Midlands	0.014 - 486	1.02 – 9.90	2.93	3
Bromsgrove Sandstone	0.014 - 486	0.53 – 2.71	1.58	1.58
Wildmoor Sandstone	0.77 – 62.6	3.06 – 19.1	12.1	8.06
Kidderminster Sandstone	0.14 – 69.2	1.14 – 33.3	4.79	4.93

The distribution of storage coefficients of Permo-Triassic Sandstones in Britain varies after Allen et al. (1997) with very low values of about 10^{-8} in confined aquifers and higher values of 10^{-2} to 0.1 in unconfined aquifers. According to Krusemann and de Ridder (1994) the geometric mean of the distribution at 10^{-3} with an interquartile range of $3.6x10^{-4}$ to $3x10^{-3}$ seems to be resonable. Most of the data come from boreholes in unconfined areas rather than in confined areas covered by Mercia Mudstone. Pumping test storage coefficients in the West Midlands are given for 11 test sites by Allen et al. (1997). The values range from $2x10^{-4}$ to 0.15 with a geometric mean at $2.5x10^{-3}$.

The application of borehole packers in wells of Triassic Sandstone in Merseyside has been described by Brassington and Wathall (1985). High hydraulic conductivities of up to 2.52m/d are correlated with fractured sections and low hydraulic conductivities of about 0.24m/d with

marl bands, confirmed by geophysical logging. Outflow packer tests in Bromsgrove Sandstone in Worcestershire described by Ireland (1981) show similar results to those of Brassington and Wathall (1985) for sandstones at Merseyside. Lerner (2000) processed some outflow packer testing in a borehole at Witton, Birmingham. A double packer system built by Owen Baines (University of Bradford) with a packer interval of about 2m was applied. Hydraulic conductivities between 0.56m/d and 9.13m/d were measured.

2.4.3 Fracture Flow

Joints and bedding-plane joints are seen in many outcrops and are often detected in boreholes of Triassic Sandstone (Jeffcoat, 2002). Bedding-plane joints may be partly controlled by lithology, and are considered to be relatively short (less than tens of metres) and having apertures of tens of micrometers up to 10 mm (Allen et al., 1998). Fractures with unfilled apertures of millimetre size are considered to have affects in local flows. Tellam and Barker (2006) discussed fracture flow evidence obtained from borehole studies and found two uncertainties:

- The zone around the borehole may be atypical for the aquifer as it has been developed or clogged during drilling or pumping.
- The detected fractures may not be connected not even via matrix bridges.

They concluded that borehole data appear to be overestimating fracture flow, "... at least in the sandstones with higher matrix permeabilities" (Tellam and Barker, 2006). In summary, fracture flow occurs in sandstone and can be dominating around pumping wells even if intergranular permeability is relatively high.

Antifractures, respectively faults, granulation seems or veins are treated as barriers in porous sandstone reservoirs (Edwards et al., 1993). On-shore sequences indicate many faults with

restricted permeability perpendicular to the slip plane (Allen et al., 1997). Major examples are faults in aquifers of Birmingham and Nottingham (Knipe et al, 1993, see Figure 2.6; Yang et al. 1999, Towsdale and Lerner, 2003). However, faults are acting as barriers or, as recorded by Tellam (2004) and Allen et al. (1997) as high-permeable pathways. The permeability of faults might change along fractures; low permeability at right angles and high permeability parallel to faults. Permeabilities along fractures are not uniform and might even be channelled. Combinations of faults will also have effects on the effective large-scale permeability (Tellam and Barker, 2006).

2.4.4 Vertical Flow in Triassic Sandstone

Salmon (1990), as well as Rushton and Salmon (1993) examined vertical flow through low conductivity zones in the Sherwood Sandstone aquifer at Bromsgrove for an area of about 52km^2 with wells of about 400m depth. A multilayered aquifer system model demonstrated the effect of low permeable bands on the groundwater flow, controlling vertical head gradients in the sandstone. Rushton and Salmon (1993) concluded that the low conductivity zones spread the effect of pumping more evenly across the aquifer and that high groundwater head gradients are required to move water through the low-conductivity zones.

Vertical flow in Triassic Sandstone is recorded with a few percent by Brassington (1992) and Taylor et al. (2003). Segar (1993) recorded head change across most mudstone beds.

2.4.5 Mudstones in the Triassic Sandstone

Mudstones found in Triassic Sandstone are very rarely examined for their hydraulic properties. Tellam et al. (1981) gave a general overview of onshore non-carbonate mudrocks in Britain. Mudrocks are defined as any fine-grained indurated or unindurated sedimentary

rock. In general, laboratory hydraulic conductivities are much lower than in situ measured values, as given by Tellam et al. (1981) in Table 2.3. Generally, the porosity and permeability of Mudstones exponentially decreases with depth and therefore consequently with compaction. Tellam et al. (1981) summarised that mudrocks in Britain can be divided into two groups, a Pre-Mesozoic group, predominated by fissure flow, and a Postpaleozoic group, where interparticle flow may be present and where high rock compressibility may be important.

Table 2.3: Typical range of hydraulic properties for the Mercia Mudstone Group (after Tellam et al., 1981; values were given for rocks up to 20 m below ground level)

	Laboratory Hydraulic Conductivity [m/d]	Field Hydraulic Conductivity [m/d]	Total Porosity [%]	Laboratory Specific Storage[m^{-6}]
Mercia Mudstone Group	10^{-4}-10^{-6}	10^{-1}-10^{-3}	20-40	10^{-4} -10^{-6}

Laboratory measurements of Mudstone permeabilities were processed by Valentim Curião in 2001, as part of an ERASMUS project under the supervision of John Tellam and Richard Greswell (unpublished, see also Tellam and Barker, 2006). The measured values vary between $1.1x10^{-6}$m/d and $8.21x10^{-6}$m/d for the Kelner outcrop (close to Liverpool) and between $1.06x10^{-6}$m/d and $1.40x10^{-5}$m/d for the Alderley Edge outcrop (close to Manchester). The lateral extension and continuity is uncertain and can vary between a kilometre (Thompson, 1970) to no correlation of mudstones within boreholes separated by less than a few tens of metres (Tellam and Barker, 2006). Paleosols may have permeabilities similar to mudstones (Bouch et al. 2006, Newell 2006).

2.5 Solute Transport in Triassic Sandstone

As stated by Tellam and Barker (2006), less work has been completed on solute movement than on flow in Triassic Sandstones. Reacting solute transport mainly describes chemical reactions and is discussed in detail by Tellam and Barker (2006). Here, the focus is put on non-reacting solute transport, as discussed by both authors at the laboratory scale, respectively investigations on core samples, the borehole scale and regional scale.

2.5.1 Borehole Testing – Tracer Tests

The most appropriate review and guidelines for the use of groundwater tracer tests in British aquifers was given by Ward et al. (1998). Four locations are mentioned (see also Chapter 1.2) where tracer tests were applied in Triassic Sandstone. The results of seven breakthrough curves demonstrated the presence of high permeable pathways along joints in the sandstone, allowing very high flow velocities of up to 140m/d over 280m distance (at Liverpool, Barker et al., 1998). The results of two test at Hodnet, in Shropshire (Coleby, 1996) are listed Table 2.4. The distance (radial distance) between the abstraction well and injection well was 20m. About 93% of tracer was recovered.

Table 2.4: Summarized tracer test results after Ward et al. (1998) at Heath House, Shropshire

	Test 1	Test 3
Radial Distance [m]	20	20
Pumping rate [Ml/d]	3.83	3.89
Kinematic Porosity [%]	14	13.5
Tracer injected	40 g amino-G-acid	250 g amino-G-acid
Tracer mass recovered	93% amino-G-acid	32% amino-G-acid
First breakthrough monitored [h]	48	60
Peak breakthrough [h]	100	105

More investigations were made at the Haskayne site north of Liverpool, at the Merseysite in NW England (Green, 1994; Hamilton 1995; Betts 1996; Streetly et al. 2002). Three investigations involving tracer tests using fluorescein, amino-G-acid and bromide tracer were carried out in four boreholes with depths between 85 and 168 m. All were completed within the Omskirk Sandstone Formation, the local upper unit of the Sherwood Sandstone Group. The tracer tests were arranged as forced gradient tracer tests. During Test 1, Green (1994) injected tracer in a piezometer at 7m bgl and pumped in an abstraction well at 5m distance, packered at 10m bgl, increasing the hydraulic gradient for the tests and considering only the top part of the borehole. Water was abstracted with a rate of 0.7l/s at a depth of 7m bgl in the injection well. After steady-state conditions were reached, the dissolved tracer was injected with a short sudden injection or slug into the aquifer. The tracer monitoring was arranged in the abstraction well. The injection well was not monitored. Details are listed in Table 2.5.

The observations of the second tracer test conducted by Hamilton (1995) were not suitable for an interpretation and determination of hydraulic parameters, as it was not possible to fully confirm the reason for no clear breakthrough of tracer, but it is believed that the probable reasons were a combination of the additional initial dilution, and the low flow velocity past the piezometer. The third test was conducted by Betts (1996), set up in a similar way to Green's test, with the pumped well packered at 23.5m bgl (instead of 10m bgl, Green, 1994). Betts (1996) started pumping after injecting the tracer. Details are listed in Table 2.5.

The Tests of Green (1994) and Betts (1996) multimodal breakthrough, making the interpretation of typical transport properties of the sandstone difficult. Streetly et al. (2002) separated the peaks on the basis of their pathways. For quantitative interpretation a radial transport solution of Moench (1989) with a code of Noy (1993) was applied. First peaks,

represented fracture or fast intergranular pathways with dispersivities of less than 10cm. For the last peaks on the breakthrough curves of both tests consistent dispersivities of about 1m to 2m were calculated and a kinematic porosity of 0.14 to 0.2 was determined.

Table 2.5: Observed tracer test results after Green (1994) and Betts (1996)

	Test 1	Test 3
Period	9.08.-13.08.1994	4.08.1996 and 6.08.1996
Pumping rate [l/s]	0.7	0.8
Permeability [m/d]	1 (1.3)	1
Tracer injected at [m bgl]	7	21
Tracer injected	12 g fluorescein	21 g fluorescein
	12 g amino-G-acid	21 g amino-G-acid
	72 g potassium bromide	140 g KBr
Tracer mass recovered	11% fluorescein	9% fluorescein (8% minus background concentration)
	50% amino-G-acid	35% amino-G-acid (17% minus background concentration)
	nil potassium bromide	nil potassium bromide
First breakthrough monitored	All tracer in the first minutes all tracer	
Peak breakthrough	fluorescein after about 19 h	fluorescein after about 9 h
	amino-G-acid after about 16h	amino-G-acid after about 9h

For the tracer tests conducted Tellam and Barker (2006) confirmed that the importance of fracture flow near wells and emphasize that fracture flow can occur over distances of hundreds of meters.

2.6 Hydrogeology of the Birmingham Aquifer

The Permo-Triassic Sandstones are the second most important aquifer in the UK, with about 25 % of total licensed groundwater abstractions in 1977 (figures from Monkhouse and Richards, 1982). Allen et al. (1997) reported variable borehole yields, ranging up to ten thousand cubic metres per day depending on the aquifer properties, which are controlled by a

combination of factors as lithology (mineralogy, grain size, sorting), cementation and fracturing.

Birmingham lies within the West Midlands region of the United Kingdom. Today, Birmingham is the second largest city with about 1.016 million inhabitants (and about 2.285 million including the conurbation, estimated in 2008). Together with the conurbation, including Wolverhampton, Dudley, Sutton Coldfield, and Solihull, Birmingham forms one of the main urban and industrial centres in Britain. The Birmingham aquifer can be defined into an unconfined part to the west of the Birmingham fault, and a confined part to the east of the Birmingham fault, lying confined under the Mercia Mudstone.

The first detailed record of the Birmingham City water supply was recorded by Barclay (1898). Land (1966) addressed the hydrogeological character of the sandstones, groundwater head distributions and the pattern of abstraction. Before abstraction of groundwater, a simple groundwater flow pattern probably existed with recharge dissipated through the aquifer towards the main discharge release of the rivers Tame and Rea (Knipe et al, 1993). It is assumed that with the beginning of significant abstraction in the unconfined aquifer in the 1850s the groundwater level rapidly depressed with the Industrialisation. In 1885, abstraction also started in the confined aquifer. With the development of cities, the aquifer supplies became inadequate and/or polluted (Tellam, 1995). With the increased wealth of the cities Manchester, Liverpool and Birmingham the cities switched to surface water sources in the late 19th and early 20th century, securing the drinking water supply. Abstraction for public supply in Birmingham did not happen before around 1900 when surface water was first imported from Wales. Abstraction for industrial purposes has continuously risen until the period 1938 – 1950. Since the 1950s, a significant reduction in pumping water caused a recovery of the groundwater levels. With decline and transfer of industry, the biggest decrease

in pumping happened during the late 1960s and early 1970s. Today, abstraction is lower than it was at the turn of the 20th century (Figure 2.4). In some areas, groundwater has risen over 22m and is within 5 m of the ground surface in some places. This causes potential problems, as it can be regarded as posing a threat to foundation stability, may modify the characteristics of surface water systems and can mobilise possible contamination in the unsaturated zone. Jackson and Lloyd (1983) and Knipe et al. (1993) gave detailed examinations about the problems of rising groundwater.

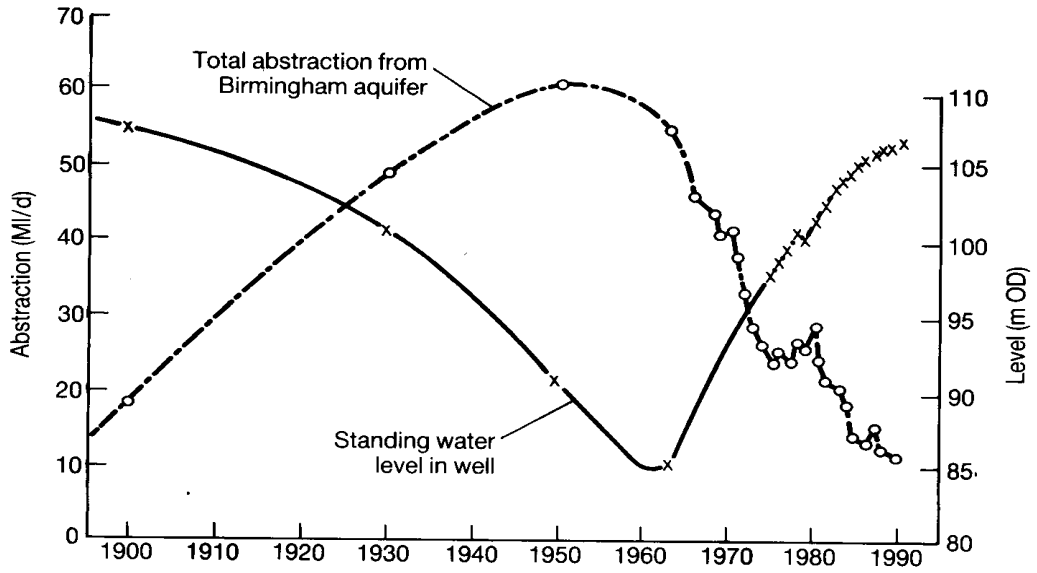

Figure 2.4: Response of the Birmingham aquifer to groundwater abstraction (Knipe et al., 1993)

Results of seven "reliable" pumping tests of the Birmingham aquifer were given by Knipe et al. (1993). The values for the transmissivity vary between 65m²/d and 370m²/d. Three values for the hydraulic conductivity are listed. The lowest is measured at the Queen Elizabeth hospital close to the west gate of the University with 1.2m/d. The second K value is given for

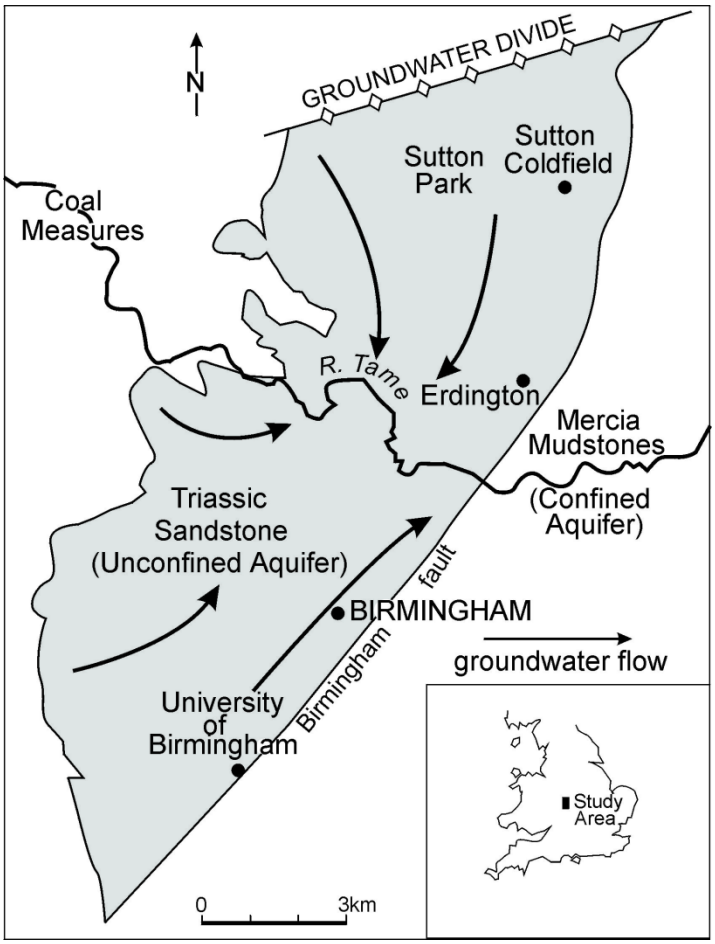

Figure 2.5: Simplified geological and hydrogeological map showing the Birmingham Aquifer (Greswell et al., 2000)

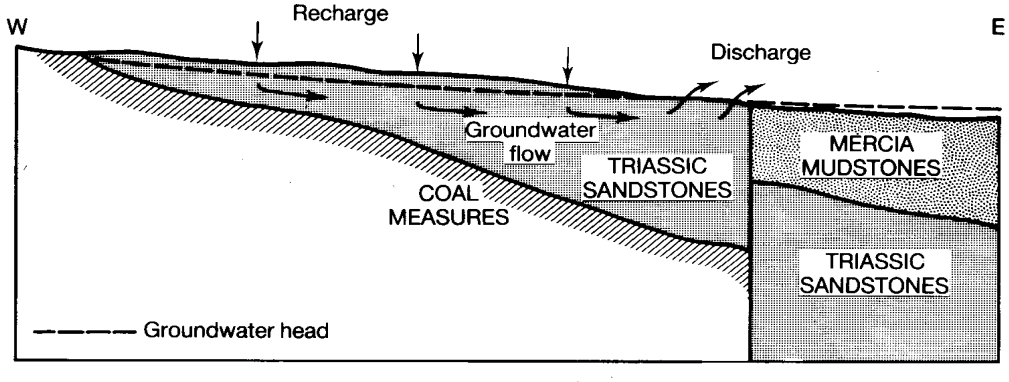

Figure 2.6: Simplified schematic cross-section of the groundwater flows in Birmingham after Knipe et al. (1993)

a well in Aston with 2.95m/d and the third was measured at Witton with a K value of 4.6m/d. The simplified natural groundwater flow in the unconfined Birmingham aquifer is towards the river Tame (Figure 2.5; Greswell et al., 2000). Observations of the groundwater head distribution indicate low permeability of the Birmingham fault perpendicular to the flow direction and limited flow across (Knipe et al., 1993; Allen et al. 1997; Tellam and Barker 2006).

2.7 Local Geology and Hydrogeology

Within a distance of 100m to the south west of the planed test site of this thesis lies the Birmingham Great Hall borehole array (Figure 3.2), comprising three boreholes which were constructed in autumn 2001. All boreholes are about 50 m deep, each with a diameter of about 6 inches, continuously cored (core diameter 4 inches) and cased with solid casing from the ground surface to solid rock at a depth between 12.33m bgl and 15.70m bgl (Joyce et al. 2006). The surface distance between the BH-2 and BH-3 is about 7.55m and the distance of both wells to BH-1 is about 20m. The base of the borehole deviates from the vertical by 1.37m to 2.02m. The overall core recovery was about 80% with poor core recovery at the near surface (to about 10m bgl).

2.7.1 Local Facies

The cores showed typical characteristics of the Wildmoor Sandstone Formation with intra-formational pebbles and extra-formational clasts. Bouch et al. (2006) described the sandstone as typically silty, micaceous, poorly cemented and easily mouldable by hand when disaggregated. Sedimentological core logging indicated that the formation comprises massive sandstone, planar laminated sandstone, ripple cross-laminated silty sandstone, pebbly

sandstone, wind-ripple laminated sandstone, siltstone or claystone and mudstone with dolocrete nodules. Fluvial and subaerial facies are interpreted for these lithologies, to be the result of sedimentation in a moderate to low-sinuosity braided, fluvial environment. The mudstone with dolocrete nodules represents a palaeosol facies. The following facies were recognized by Bouch et al. (2006):

I. Fluvial Facies:

I.a. ***Channel-lag facies*** approximately 5% of recovered cores; coarse grained pebbly sandstone; expected at channel beds with well-developed to pervasive dolomite cement.

I.b. ***Channel-fill facies*** approximately 60%, very fine to coarse-grained, massive, planar-laminated or low-angle cross-bedded sandstones in beds at decimetre to metre scale, up to 5m thick, poorly cemented and porous.

I.c. ***Abandoned channel facies*** approximately 15% fine grained material, lacustrine deposits, ripple cross-laminated sandstones and siltstones. The facies is dominated by mudstones which are typically up to approximately 1m and locally up to 2.5m thick.

II. Subaerial Facies:

II.a ***Aeolian sandsheet facies*** approximately 15% of recovered cores; fine- to medium-grained sandstones, well sorted and round grains; building units of 0.2m-to 2.5m thickness.

II.b. ***Palaeosol (dolocrete) facies*** approximately 5%

Diagenetic events from early and shallow phase diagenesis (or telogenetic diagenesis) with groundwater circulation dissolution were discernible (see Bouch et al., 2006). Hydraulic conductivities were measured for core samples in the range from about 10^{-11}m/s for clay layers to about 10^{-4}m/s for sandy layers.

2.7.2 Local Fractures

Logging of fractures was processed on cores and with the optical televiewer. Bouch et al. (2006) differentiated between artificial horizontal to low angle fractures, as a result of the drilling process, and relatively scare natural fractures. Artificial fractures were mainly recognised at lithological boundaries and were not imaged with televiewer, whereas natural fractures were clearly imaged on the televiewer logs. Natural fractures were described as granulation seams, cemented or filled, and uncemented or unfilled. Natural fractures described by Bouch et al. (2006) were high-angle to vertical (20-90°).

2.7.3 Impact of Heterogeneities on Fluid Flow and Contaminant Transport

The impact of heterogeneities on fluid flow and contaminant transport was described by Bouch et al. (2006) for a larger and finer scale which will be important for modelling of groundwater flow or contaminant transport:

1. **Larger Scale:** The abandoned channel and the palaeosol facies had low permeabilities due to high clay content and/or dolomite-dominated compositions. These features can be up to 1 m thick and have lateral extents of tens of metres, acting as baffles to vertical flow supporting perched water tables as observed in outcrops south to Birmingham (see Wills, 1976).

2. **Finer Scale:** Generally sandstone samples of Bouch et al. (2006) are typically lightly cemented and have high to moderate porosities (primary intergranular macropore volumes of up to 20% modal analysis). Early dolomite and late calcite cements locally degrade severely primary macropore volumes and were significant within

approximately 2-5% of the cored intervals. The cement in coarser grained sandstones of the channel lag facies was prominently developed (0.05 to 0.1m thick). These layers seem to be laterally continuously over distances of bedforms for 10's to 10's of metres. The layers might readily be by-passed by horizontal flow, but may act as a barrier to vertical flow.

2.7.4 Tracer Test Procedures at the Birmingham Great Hall Borehole Array

A number of tracer transport tests were processed by the University of Birmingham through fractures in half metre intervals of fractured regions, applying packers (unpublished,, see Joyce et al 2006). The field tracer test of Joyce et al. (2006) was carried out between July 2004 and August 2005. Tracer appearance was recorded between a few hours to greater than a few weeks. One upwards-directed vertical head gradient of approximately 0.05 was measured. A series of field tracer tests was undertaken to determine the migration and survival of bacteriophage at a field-scale. During all tests, fluorescein was used as conservative tracer together with phages and was added to all tests. In five tests, 2g fluorescein was injected into packered intervals of half a metre. Four tests were carried out on non-fractured rocks and the fifth on fractured rock. A sixth test examinated a full well by injecting 20g fluorescein. The results presented by Joyce et al (2006) showed breakthrough curves, proving that matrix and fracture flow pathways do exist in the Sherwood Sandstone for fluorescein. Dispersivity values of 0.7m to 2m and effective porosity values between 20-30% were calculated with one-dimensional modeling of the tracer tests.

2.8. Conclusions Derived for the Local Geology to be Expected

Constructing the tests site for the purpose of this thesis, Wildmoor Sandstone was to be expected, when drilling was conducted on the Campus of the University of Birmingham, close to the building of the School of Earth Sciences. Lithologically, sandstones of fluvial and subaerial facies and mudstones of paleosol facies should be found. Generally, the sandstones are of fine to medium grain size, weakly cemented and mouldable by hand. Some sandstone horizons are cemented. Together with mudstones of paleosol facies the cemented sandstone horizons result in vertical flow barriers. Regional permeabilities and storage coefficients from a variety of core tests and a number of pumping tests in Triassic sandstones were available for comparison. Locally, permeability values for core samples were measured. The facies analysis of Bouch et al. (2006) concluded that low permeable bands control the vertical flow. For the drilling process after Knipe et al. (1993, see also Taylor et al. 2003) a leached zone of around 10 metres at the top might cause recovery of only lose sand and no core.

A few horizontal tracer tests with conservative tracer were successful in Triassic Sandstone and most of the tracer could be recovered. Pathways for solute transport exist and was regionally differentiated for matrix and fracture flow. Locally, tracer test with phages and fluorescein were carried out in packered intervals. All fluorescein tracer tests measured a breakthrough and most of the tracer was recovered.

CHAPTER 3: Construction of the Test Site

3.1 Aim

For the purpose of this project, it was decided to build a test site around an existing borehole, BH1, drilled by the Environment Agency in February 1994 on the Campus of the University of Birmingham. Figure 3.1 shows the general location of the test site in the unconfined Birmingham aquifer. A map of the University campus and the location of the test site at the School of Earth Science, the Great Hall and the Great Hall borehole array is given in Figure 3.2. Figure 3.3 shows a satellite image of the test site and its location on the lawn next to the School of Earth Science with reference surface elevation (AOD).

BH1 was drilled into the Wildmoor Sandstone formation. Seven sandstone layers (S1 to S7) separated by six clay-rich sandstone or mudstone layers (M1 to M6) are defined according to the drilling log (Appendix III.3.1). Figure 3.4 gives a schematic cross-section of the test site with the existing borehole BH 1. The additional boreholes BH2, BH3, BH4 and BH5 were drilled to approach three different sandstone layers. This would allow to process flow and tracer tests in particular sandstone layers between a packered BH1 and another new borehole. Furthermore, it would be possible to inject a tracer in a packered sandstone layer in BH1 and pump a layer above or below this packered sandstone layer.

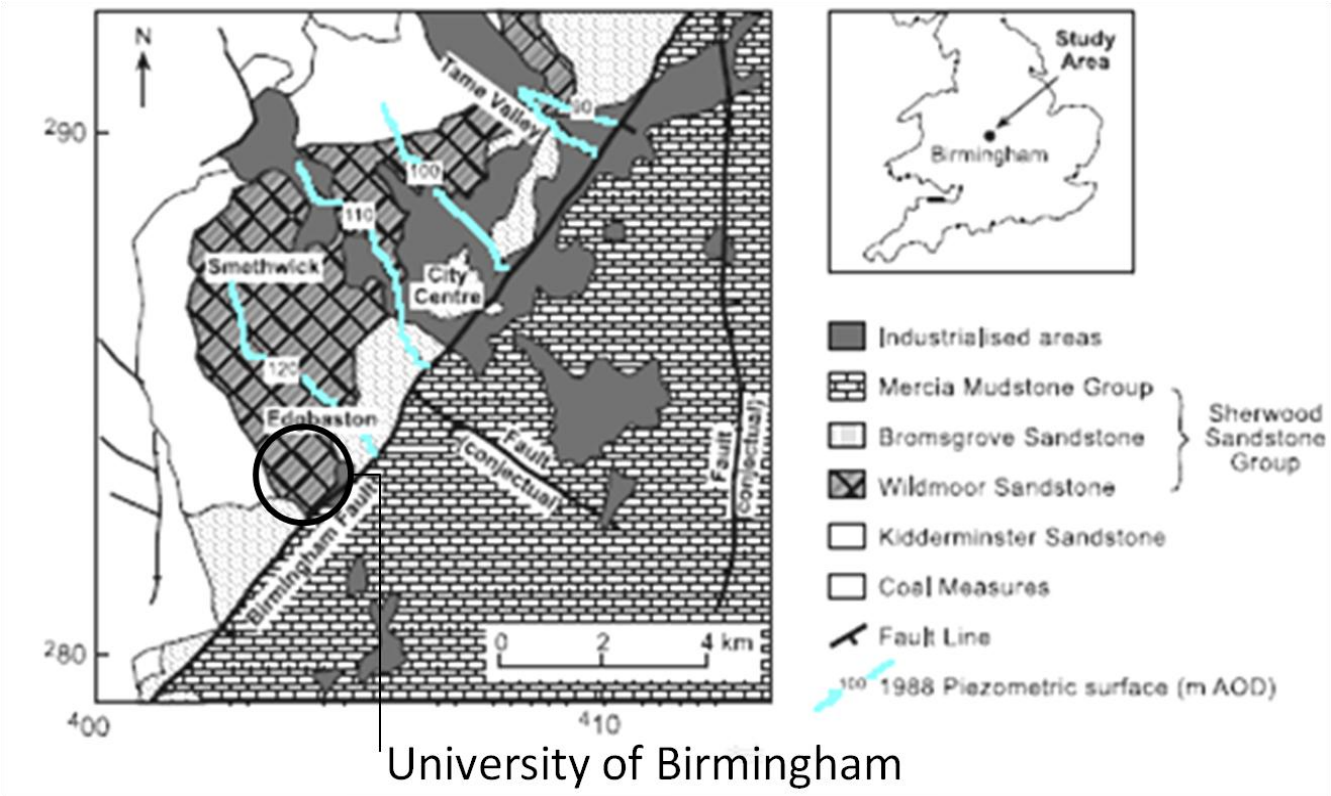

Figure: 3.1: The University of Birmingham and relative location of the test site in the unconfined Birmingham aquifer (after Rivett et al., 2005)

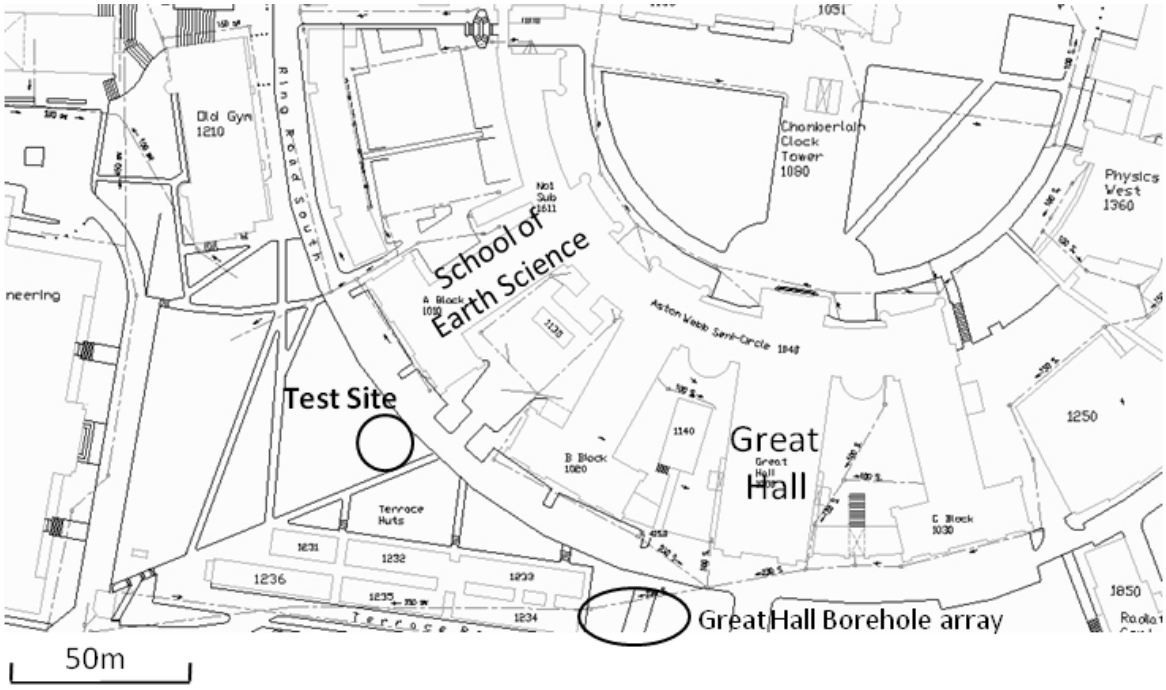

Figure 3.2: Map of the Campus of the University of Birmingham with the location of the School of Earth Science, the test site, the Great Hall and Great Hall borehole array (based on a map of the Estates Services of the University of Birmingham, 2001).

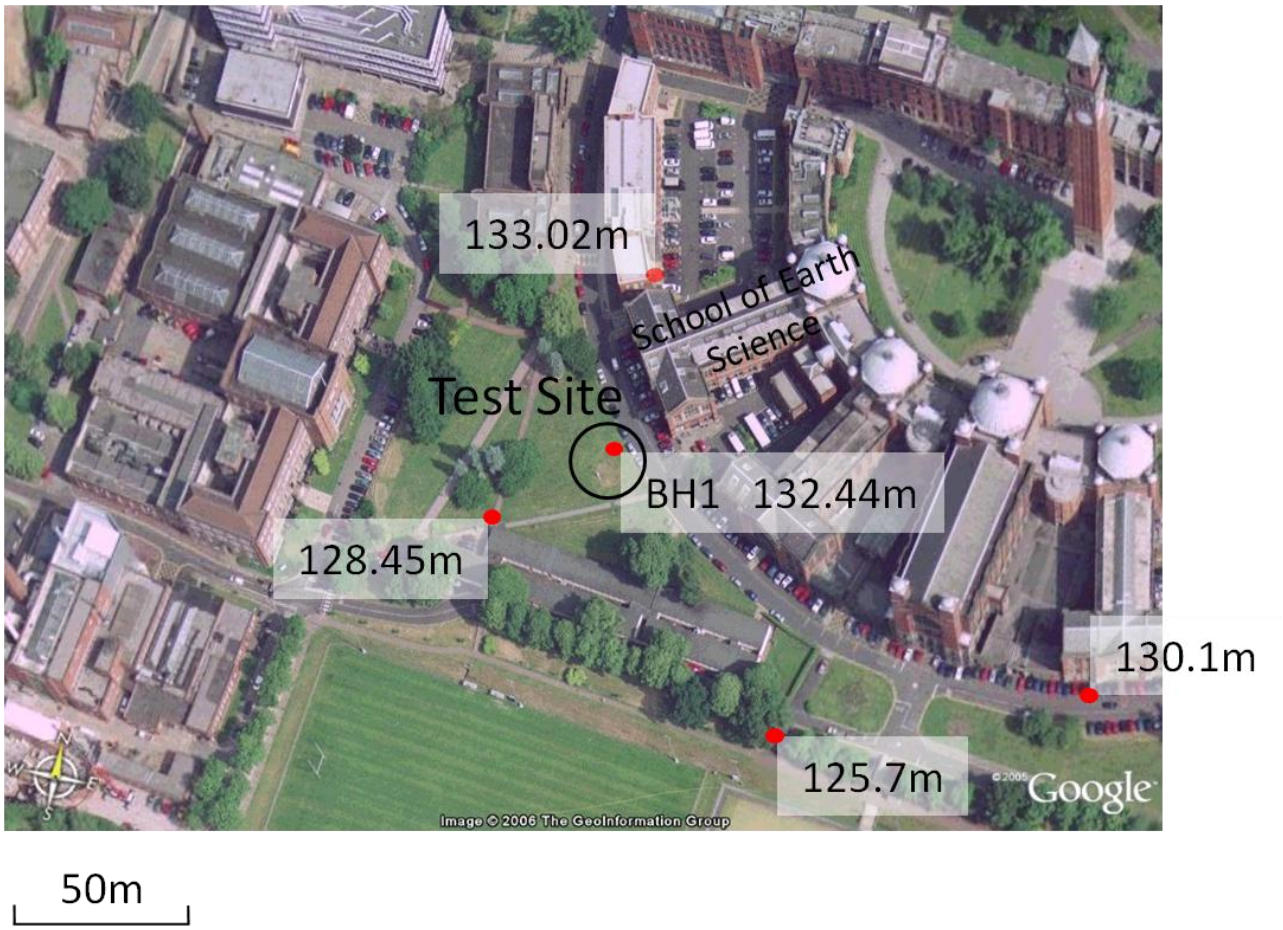

Figure 3.3: Satellite image of a part of the Campus of the University of Birmingham with the location of the School of Earth Science, the test site with BH1 and reference surface elevations AOD (red points). Reference surface elevations are digitalized from a map of the estates services of the University of Birmingham into the satellite image (© Google Maps).

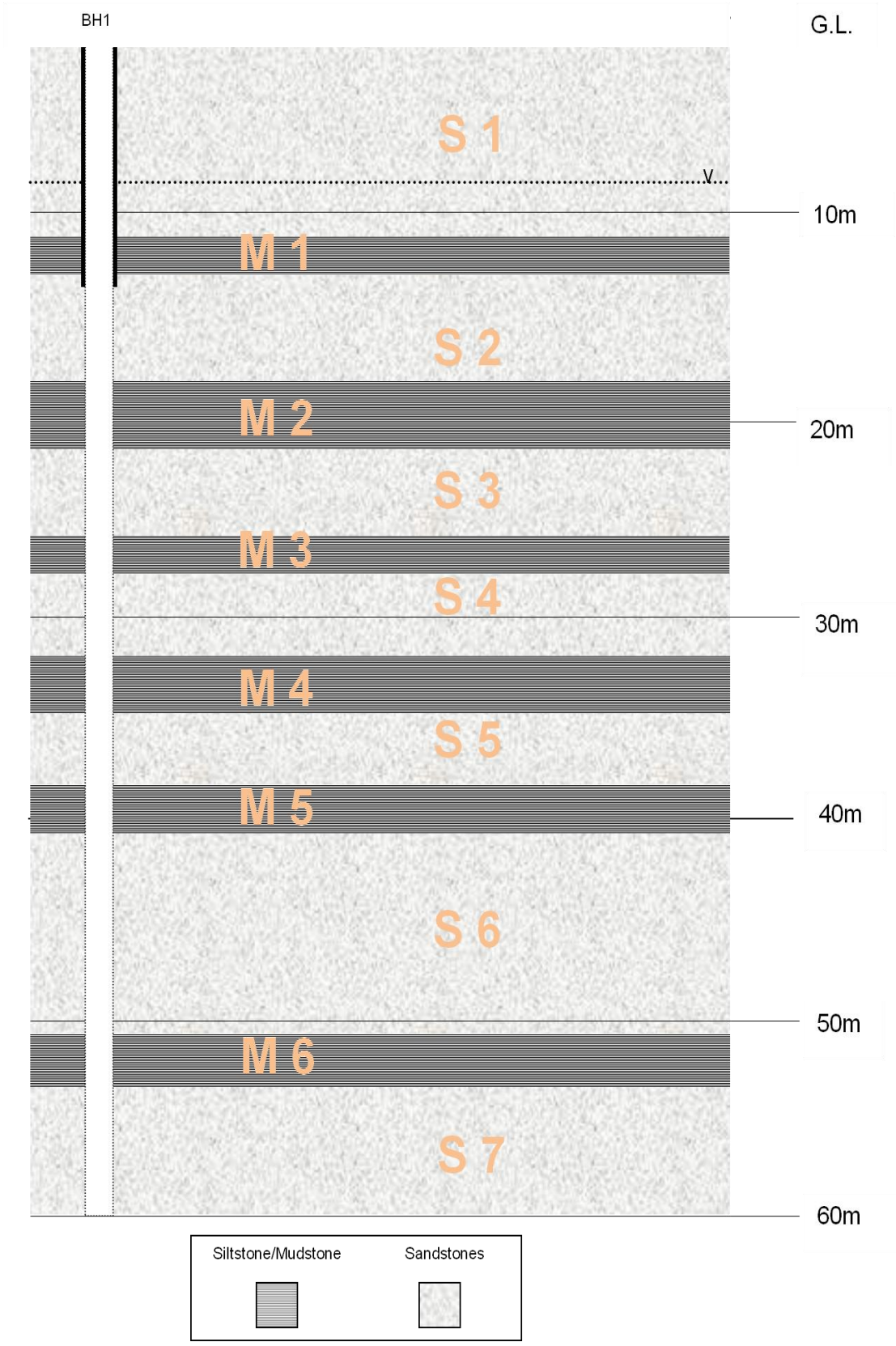

Figure 3.4: Schematic cross-section of BH1.

3.2 Drilling and Well Construction

The wells on the test site were drilled with a rotary drilling rig mounted on a caterpillar. BH4 was drilled with a double-tube core barrel to recover a full core. BH2, BH3 and BH5 were drilled by air drilling with a direct rotary drilling system (Cooper et al., 1977, Driscoll, 1995). The core barrel and drilling bits used are shown in Appendix III.3.2 and III.3.3.

Two grouting methods were applied on the test site. With the first method, the "grout placement method" (Driscoll, 1995), grout was pumped through pipes running in the casing. A float shoe connected to the drilling rig was elevated to a certain interval in the casing which contained prefabricated voids. The interval was sealed above and below the voids with small packers and the grout was injected through the voids into the annular space between borehole wall and casing. This method was applied in BH 4. However, the grout placement method failed. All injected grout flew back into the inner casing and filled the well from 60m bgl to about 19m bgl. The drilling crew tried to rescue BH4 for later tracer tests and almost all grout was air flushed out of the borehole. As grout cement still covered the borehole wall of S7 in BH4, the cleaning of the borehole wall failed, too. Finally the drilling crew tried to pull the casing tube, failing again, and the casing ruptured at a depth of about 10m. To secure the top of the borehole from its collapse, a new casing with a slightly wider diameter was inserted from the top over the remaining eng end of the casing to a depth of about 13m bgl. Because of the grout in the well, BH4 was not applicable for the planned tracer tests. However, BH4 was used, with restrictions, as observation well which approaches S1, M1 and S2 at the top and S7 at the bottom. BH5 was drilled as substitute for BH4.

BH3 and BH5 were grouted with the "tremie pipe outside casing method" (Driscoll, 1995). Grout was placed through a small-diameter pipe, the so called tremie or grout pipe which was connected outside the casing. Grout was pumped into the annular space and the tremie pipe

was withdrawn several times with the rising level of grout in the annular space. BH3 and BH5 were both drilled over the whole depth to be grouted. The casing was inserted into the borehole and the well was grouted. After the grouting of the wells, the uncased parted was drilled. BH2 was drilled in the unsaturated zone in S1 and S2 over its whole depth with supporting iron casing. The plastic casing of the well was inserted into the borehole and the space between the casing and the borehole wall was filled with gravel.

In summary, Table 3.1 lists drilling diameters, installed casing and grouting depth. Figure 3.5 shows a schematic cross-section of all wells drilled on the test site and Figure 3.6. gives a schematic cross-section of the "man-hole" cover and top covers of the boreholes and the distance to the casing of each well. BH4 has no cover and the top elevation is equal to the surface elevation. The elevation difference between the borehole casing and the surface distance of the boreholes is listed in Table 3.2.

Table 3.1: Drilling diameter (Ø), installed casing and grouting depth of BH1, BH2, BH3, BH4, and BH5.

	BH 1	**BH 2**	**BH 3**	**BH 4**	**BH 5**
DRILLING					
Ø 203.2mm	0-60 m bgl	0-16 m bgl	0-32 m bgl	0-52 m bgl	0-52 m bgl
Ø 100mm			32-38.5 m bgl		52-60 m bgl
Ø 152.4mm corebarrel				0-60 m bgl	
CASING					
Ø 127mm plain Polyethylen		0-8 m bgl	0-32 m bgl	8-52 m bgl	0-52 m bgl
Ø 127mm slotted Polyethylen		8-16 m bgl			
Ø 203.2mm plain Polyvinylchlorid				0-12 m bgl	
Ø 203.2mm plain steel	13 m bgl				
GROUTING	not grouted				
with Tremie Pipe			0-32 m bgl		0-52 m bgl
Grout Placement				20-60 m bgl	
filled with gravel		0-16 m bgl		15-20 m bgl	

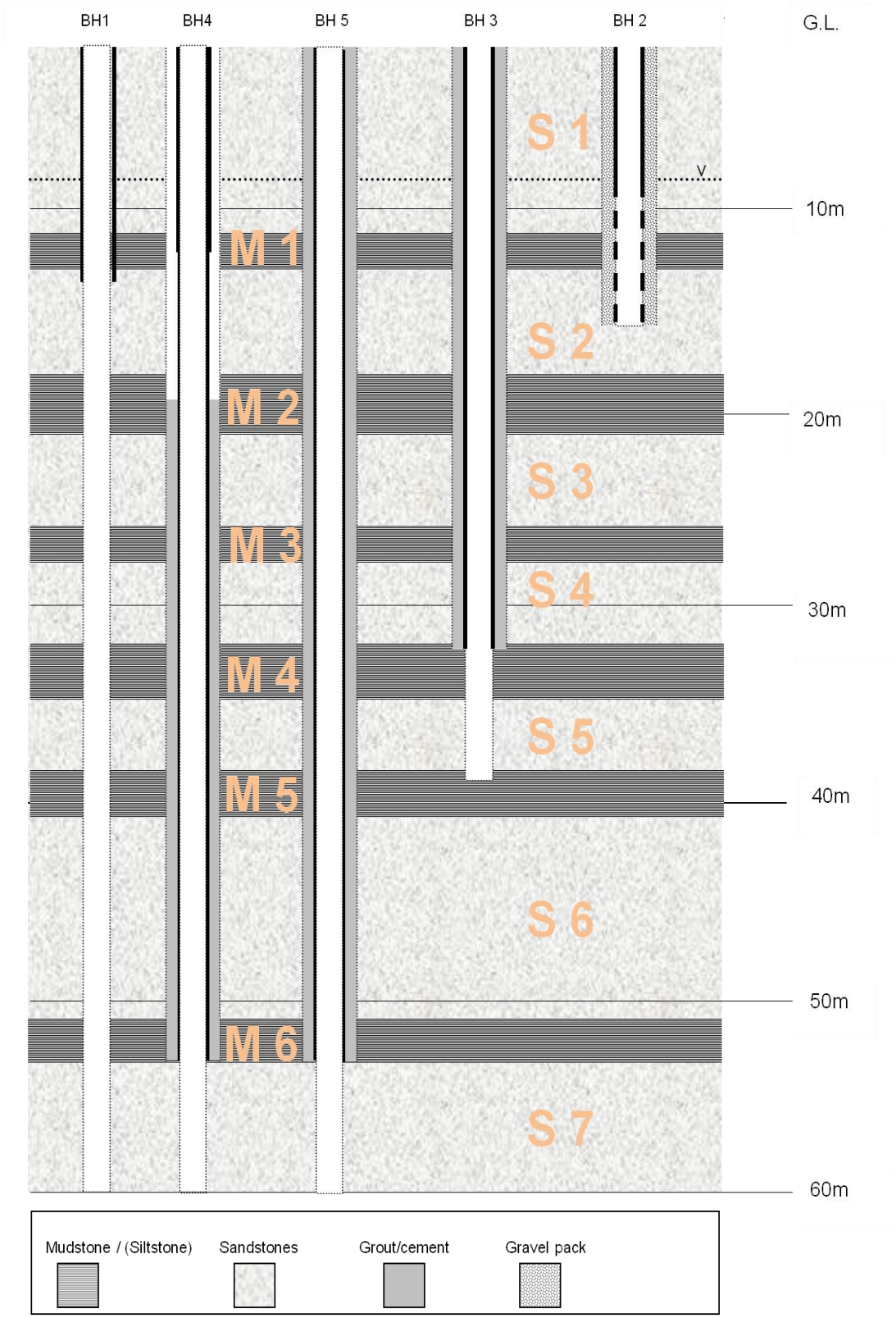

Figure 3.5: Schematic cross-section of all drilled boreholes, casing and grouting, according to the drilling log of BH1.

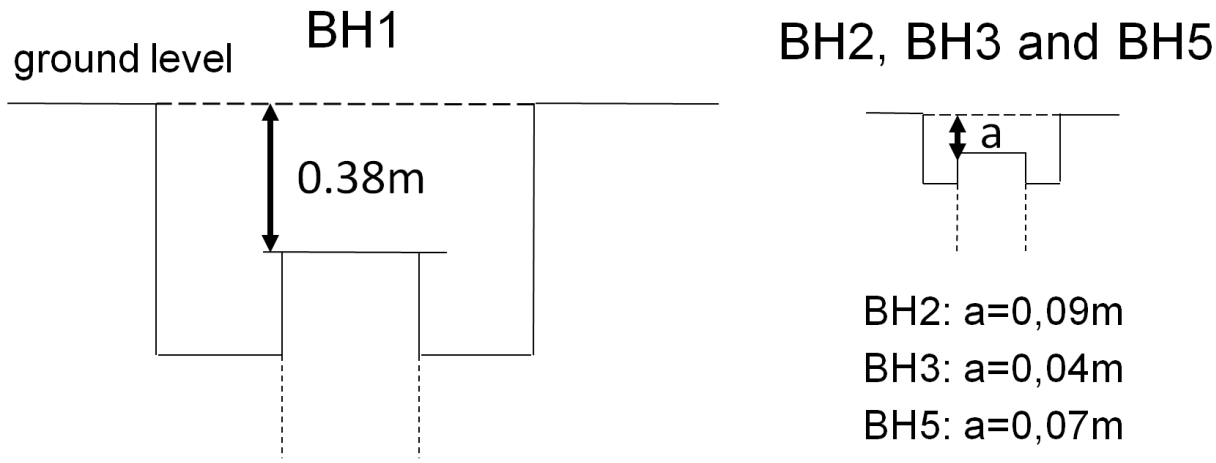

Figure 3.6: Schematic picture of the "man-hole" of BH1 and top covers of BH2, BH3, and BH5.

Table 3.2: Elevations of BH1 to BH5. Elevations differences and surface distances between the boreholes of the test site.

	BH1	**BH2**	**BH3**	**BH4**	**BH5**
Elevation (m AOD)	132,44	132,15	132,22	131,73	131,93
Difference in Elevation between two boreholes in m					
BH1		0,29	0,22	0,71	0,51
BH2	-0,29		-0,07	0,42	0,22
BH3	-0,22	0,07		0,49	0,29
BH4	-0,71	-0,42	-0,49		-0,20
BH5	-0,51	-0,22	-0,29	0,20	
Surface Distance between two boreholes in m					
BH1	0,00	4,20	4,00	7,00	6,85
BH2	4,20		4,90	4,20	6,10
BH3	4,00	4,90		5,20	3,40
BH4	7,00	4,20	5,20		3,00
BH5	6,85	6,10	3,40	3,00	

3.3 Conclusion

The construction of the test site with five boreholes was finished successfully in July 1998. Figure 3.7 gives an overview of the test site with the surface elevations of the borehole covers and topographic lines of interpolated elevations of the surrounding area of the test site (taken from a map of the Estates Services, University of Birmingham, 2001). Four additional wells

in a surface distance of up to 7m around BH1 were drilled. S2, S5, S7 were approached by a pair of two wells, forced gradient tracer tests. The setup of the boreholes was also suitable for vertical forced gradient tracer test by injecting tracer in a sandstone aquifer in BH1 (S3, S4, S6) and abstract water in the sandstone layers above and below the injection layer in S2 and S5 or S5 and S7. The grouting procedure in BH4 failed. However, BH4 could be used as observation well with restrictions.

Figure 3.7: Test site at the University of Birmingham with elevations of the borehole covers of BH1, BH2, BH3, BH4, and BH5, with topographic lines of interpolated elevations of the surrounding area of the test site (taken out of a map of the Estates Services of the University of Birmingham, 2001; satellite image © Google Maps).

CHAPTER 4: Characterization of the Borehole Array

4.1. Aim

The aim of Chapter 4 is to describe the characterization of the borehole array and the location of the sandstone and mudstone layers approached with the boreholes of the test site. For the development, the drilling logs of BH1 and the core log of BH4 were compared. Hydraulic characteristics gained from core data of BH4 are described. The recorded geophysical logs of all wells, BH1 to BH5, were used to compare sandstone layers and mudstone layers throughout the borehole array. Table 4.1 lists the log type, date and persons who recorded the logs in the respective boreholes.

Table 4.1: Logging carried out in the array, boreholes indicating method and date.

	BH1	BH2	BH3	BH4	BH5
Drilling Log	xDrilling Company 1994				
Core Logging				Mitchener 2002)	
Geophysical Logging:					
Natural Gamma Log	x2000			x 1998	x 1998
Gamma Gamma Log	x 2000	x 2000	x 2000	x 2000	x 2000
Neutron Log	x 2000	x 2000	x 2000	x 2000	x 2000
Resistivity Log (E-Log)	x 2000			x 1998	x 1998
Guards Log	x 2000			x 1998	
Calliper Log	x 2000			x 1998, 2000	x 1998, 2000
Temperature Log	x 2000			x 1998	
Conductivity Log	x 2000			x 1998	x 1998
Flow Log	x 1998	x 1998	x 1998	x 1998	x 1998

Performed by Ralf Lieb, John Tellam, Richard Greswell, Richard Mitchener and Kevin Shepard, unless otherwise indicated

The schematic cross-section of the test site shown in Figure 3.3 was drawn with the information of the drilling log of BH1, suggesting a layered setup of sandstone and mudstone layers in the vicinity of BH 1. With the different logs, sections of similar lithology and

stratigraphy could be identified for all boreholes. By constructing diagrams with the logs of all boreholes, a comparison of the logs and the correlation of layers between different wells became easier. The result provided a characterization of the whole test site and a definition of sandstone layers as aquifers and mudstone layers as aquitards for later hydraulic tests, tracer tests and computer modelling. Finally, the vertical differentiation of the test site into seven sandstone and six mudstone layers was confirmed.

4.2 Drilling Log and Core Log

BH1 was drilled in 1994 and logging was achieved, distinguishing chipped fragments of sandstone and mudstone layers which were pumped to the surface during the rotary drilling. The information gained from the drilling log BH1 (Appendix III.3.1) was shown as simplified log in Figure 4.1. The core recovery of the first 12m bgl was poor and almost no complete core was won. This corresponds to information of Knipe et al. (1993), Taylor et al. (2003) that the unconfined area of the Birmingham aquifer is considered to have a leached zone of around 10 metres at the top.

Logging was undertaken using the core recovered from 12m below ground level (bgl) to 60m bgl. The detailed log of BH4 created by Mitchener (2003) describes the colour, grain size, cross layers, etc. (Appendix IV 4.1). Using the initial drilling log of BH1, a correlation between the identified layers S1 to S7 and M1 to M6 of the drilling log and the information of the simplified core log of BH4 was tried, as shown in Figure 4.1.The mudstone layers of the drilling log could not be matched one to one with depths given for clayed sandstone or mudstone layers of the core log. However, by constructing a diagram between the two logs, S1 to S7 and M1 to M6 were identified in both boreholes.

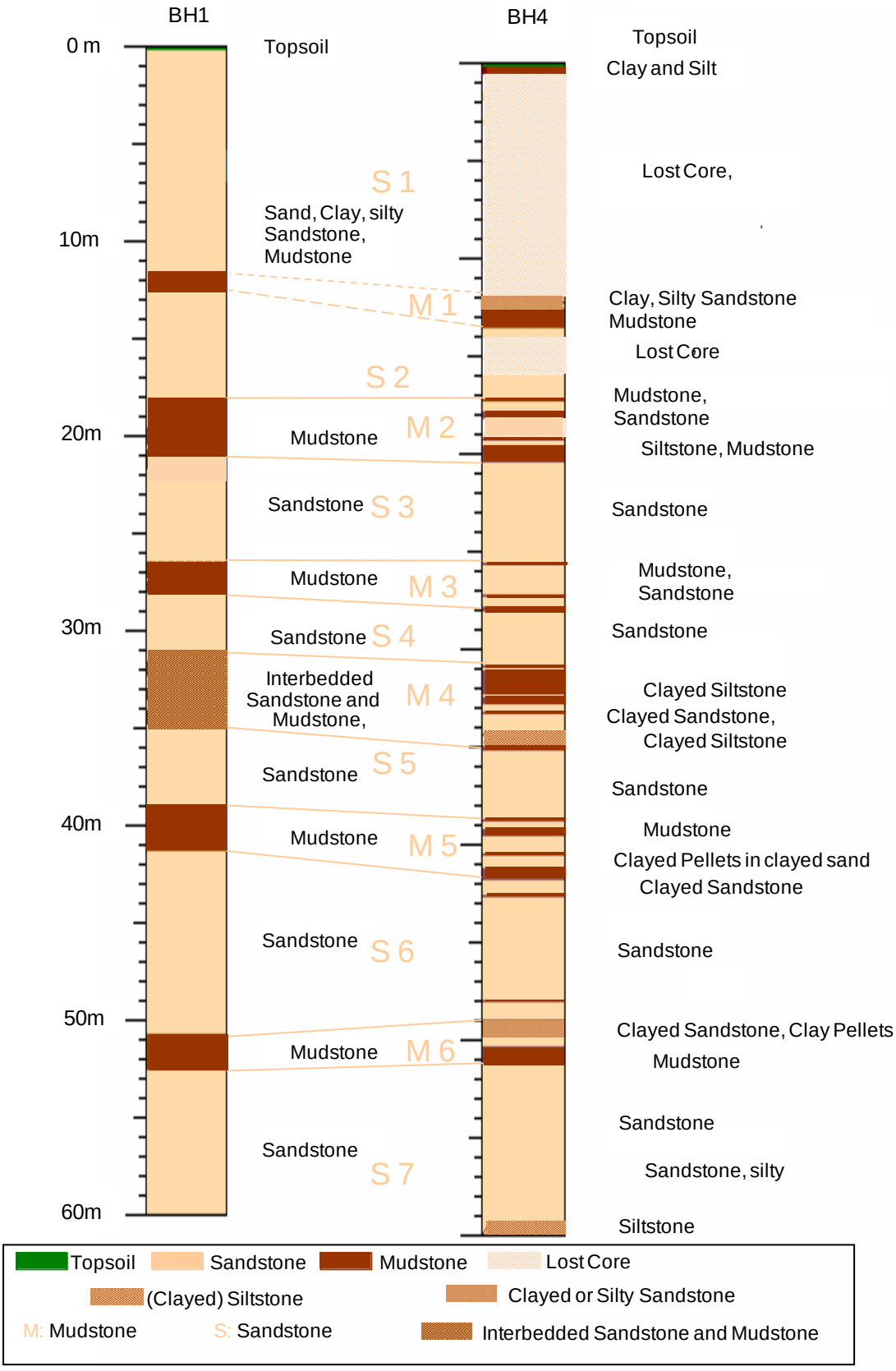

Figure 4.1: Drilling log of BH1 and core log of BH4, comparing sandstone and mudstone horizons.

4.3 Hydraulic Characteristics of Cores Samples of BH 4

Hydraulic conductivity tests on cores of borehole BH4 were carried out by Mitchener (2003) over the whole length of the core on 45 samples of S1 to S7. Curião et al. (2001) examined the permeability of M1, M2, M4, M5 and M6, using 8 core samples from BH4, as well. Curião et al. (2001) and Mitchener (2003) determined the hydraulic conductivity by using a falling head permeameter (Greswell, 1995). Permeability values of sandstones in the horizontal direction varied between 0.564m/d and 5.01m/d. Vertical permeability values of sandstones varied between 1.10m/d and 6.47m/d. Measured permeability values for clay rich sandstone horizons vary between 1.21×10^{-5}m/d and 0.109m/d in the horizontal direction and between 6.76×10^{-2}m/d and 0.101m/d in the vertical direction. The results for the horizontal permeability of mudstone layers vary between 1.08×10^{-6}m/d and 4.86×10^{-5}m/d. Figure 4.2 shows a plot of the measured horizontal and vertical permeabilities of sandstone layers by Mitchener (2003) and the horizontal permeability values of mudstone layers by Curião et al. (2001).

Mitchener (2003) measured the porosity of 44 core samples from borehole BH4 taken from different depths as shown in Figure 4.3. The measured values of porosity of the core samples of BH4 vary between 10.20% and 30.84%. For all measurements, an average value for the porosity of 24.6% was calculated.

In addition to the hydraulic parameter the total organic carbon (TOC) and the carbonate content was defined by Shepherd (2003) on 27 samples taken from the core of BH4. The range of values determined was 0.02% to 0.08%. Mitchener (2003) gives values for the carbonate content of less than 10 % for the unconfined aquifer (S1) and 15-20 % for the confined aquifers (S2 to S7).

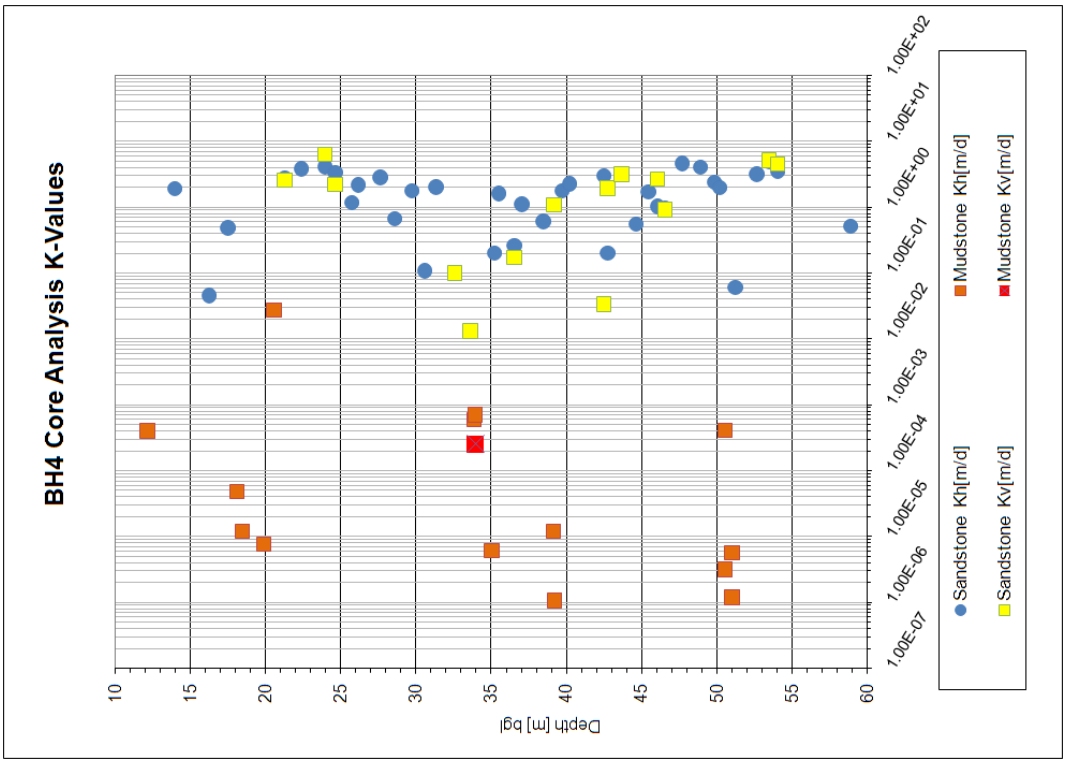

Figure 4.2: Hydraulic conductivity values in horizontal and vertical directions, measured on core samples of borehole BH4 of the test site (data of Curião et al., 2001; Mitchener, 2003).

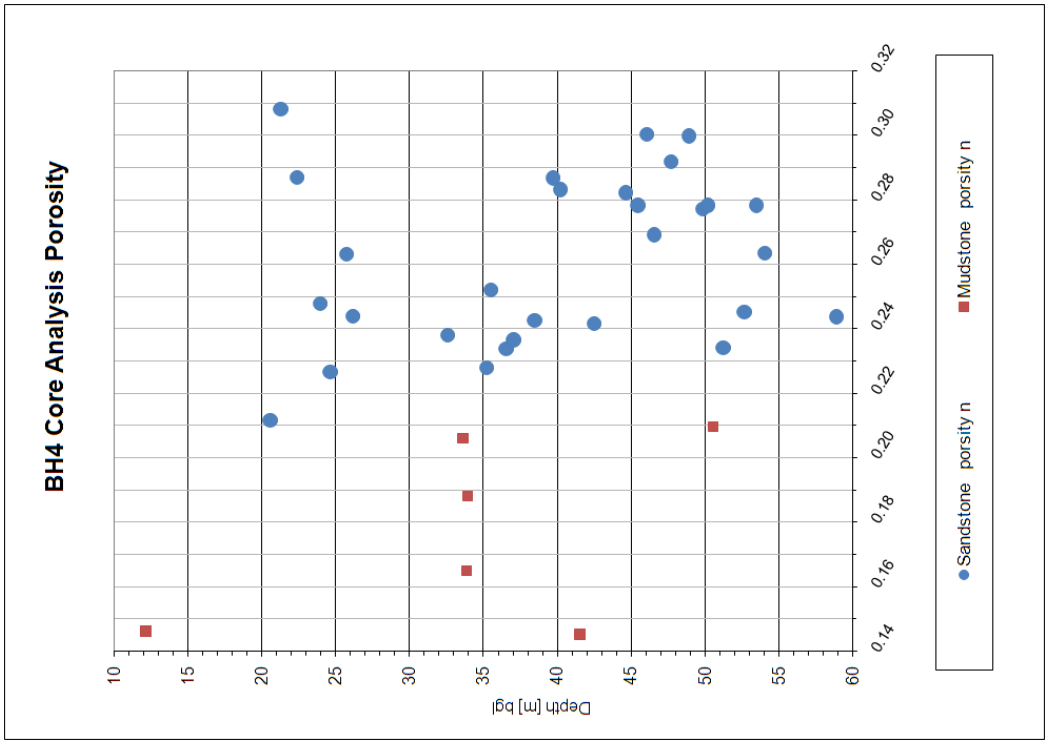

Figure 4.3: Porosity values, measured on core samples of borehole BH4 of the test site (Mitchener, 2003).

4.4 Geophysical Data

Geophysical logging was carried out with a Robertson Geologging Portalog of the early 80's. A data file was recorded for later processing and the log was printed on thermo paper. The log was recorded by positioning the end of the probe at ground level and recording the geophysical data, winching the probe up the borehole. The offset between the top of the probe and the sensor within the probe was considered to allow a correlation of different geophysical logs recorded in one borehole during later data processing. For correlation of the geophysical logs of different boreholes, the top of each log was adjusted to the elevation of BH1 as zero.

The numerical data output of the logger, was recorded in counts per second per centimetre. All recorded data were processed in EXCEL. The recorded data were plotted as values derived from a rolling average over 7cm to 12cm to receive a smoother signal (conversion factors used as recommended and provided by Robertson Geologging manual for the Robertson Geologging Portalog) and to simplify the later visual interpretation. To compare all logs, they were adjusted to the same elevation of BH1, set to 0m bgl, using the surface elevation measurements from Table 3.2. Nuclear, electrical, conductivity, temperature and calliper logs were recorded for all wells. In addition a heat pulse flow meter and a closed circuit television (CCTV) were used in the boreholes. An overview of the recorded geophysical logs is listed in Table 4.1.

4.4.1 Nuclear Logging

Nuclear logging includes all techniques that either detect the presence of unstable isotopes or that create such isotopes in the vicinity of a borehole. This method can be used regardless of the type of fluid in the borehole and is unique because the penetrating capability of the

particles and photons permits the detection of isotopes through the casing and grout. Nuclear logging techniques include natural gamma, gamma-gamma and neutron logs.

4.4.1.1 Natural Gamma Log

Natural gamma logs detect the natural gamma radiation in the vicinity of the borehole with a scintillation counter and give a qualitative interpretation of the startigraphic correlation. Clay minerals and fine particles in shale are enriched with potassium40 and thorium232, a strong gamma emitter. Mature sands and gravels contain mainly silica, which is a stable substance and therefore emits low levels of radiation. Attenuation of the natural gamma radiation intensity can be caused by casing, grouting material and gravel packs between the casing and the rock formation. The gamma radiation was plotted in API units (American Petroleum Institute). The API gamma ray unit was defined as 1/200 of the difference in deflection of a gamma log between an interval of negligible radioactivity in the API standard calibration pit (typically of shale). Conversion from cps (counts per second) to API was made according to the Robertson Geologging Portalog manual. According to Keys (1989), gamma logs should not be interpreted quantitatively by using the amplitude of the gamma response, as Scott et al. (1961) demonstrated that the area under the gamma curve is proportional to the layer thickness multiplied by the quantity of radioisotopes present. For a quantitative interpretation of gamma logs a number possible approaches were described in detail by Killeen (1982). Figure 4.4 shows the natural gamma logs for BH1 for the years 1997 and 2000 and for BH5 for 1998, before and after the setting of the plastic casing. The natural gamma log of BH4 was recorded in 1998, before the plastic casing was set. An interpretation of the logs allowed the conclusion that high gamma emissions trigger mudstones and low gamma emissions indicate sandstone. The mudstone layers were correlated by diagrams. S1 to S7 and M1 to M6 could

be connected with diagrams as horizontal layers. Strong natural gamma emission at about 6.5m bgl to 8m bgl in BH4 and BH5was marked with “M” (for mudstone) in Figure 4.4, which was not detected in BH1, and might be another mudstone layer or a clay rich lens in loose sandstone.

4.4.1.2 Gamma-Gamma-Log

An active source of gamma radiation was lowered into the borehole during Gamma-gamma logging. The gamma radiation source was cesium137. The source and detector were placed about 400mm apart so that the detector could only count the back-scattering gamma radiation. The back-scattered radiation depends on the electron density of the particular formation and is approximately proportional to the bulk density (Keys, 1989). Porosity values were not calculated, as no calibration was made in a representative borehole and because porosity values were gained by Mitchener (2003). For the purpose of defining sandstone layers and mudstone layers, it was sufficient for the interpretation to know that the higher the porosity of water filled the pores, the lower the density of the rock and the back-scattered signal would be. High gamma emissions were measured for clay rich mudstone layers and vice versa. Figure 4.5 shows the gamma-gamma logs for all boreholes recorded after the plastic casing was set. The gamma-gamma radiation was plotted in API units. The mudstone layers were correlated between the different wells with diagrams. S1 to S7 and M1 to M6 were identified in Figure 4.5 as nearly horizontal layers. As detected in the natural gamma log of BH4 and BH5, a high back-scattered radiation was measured in BH5 at about 6m bgl to 8m bgl (marked with “M”).

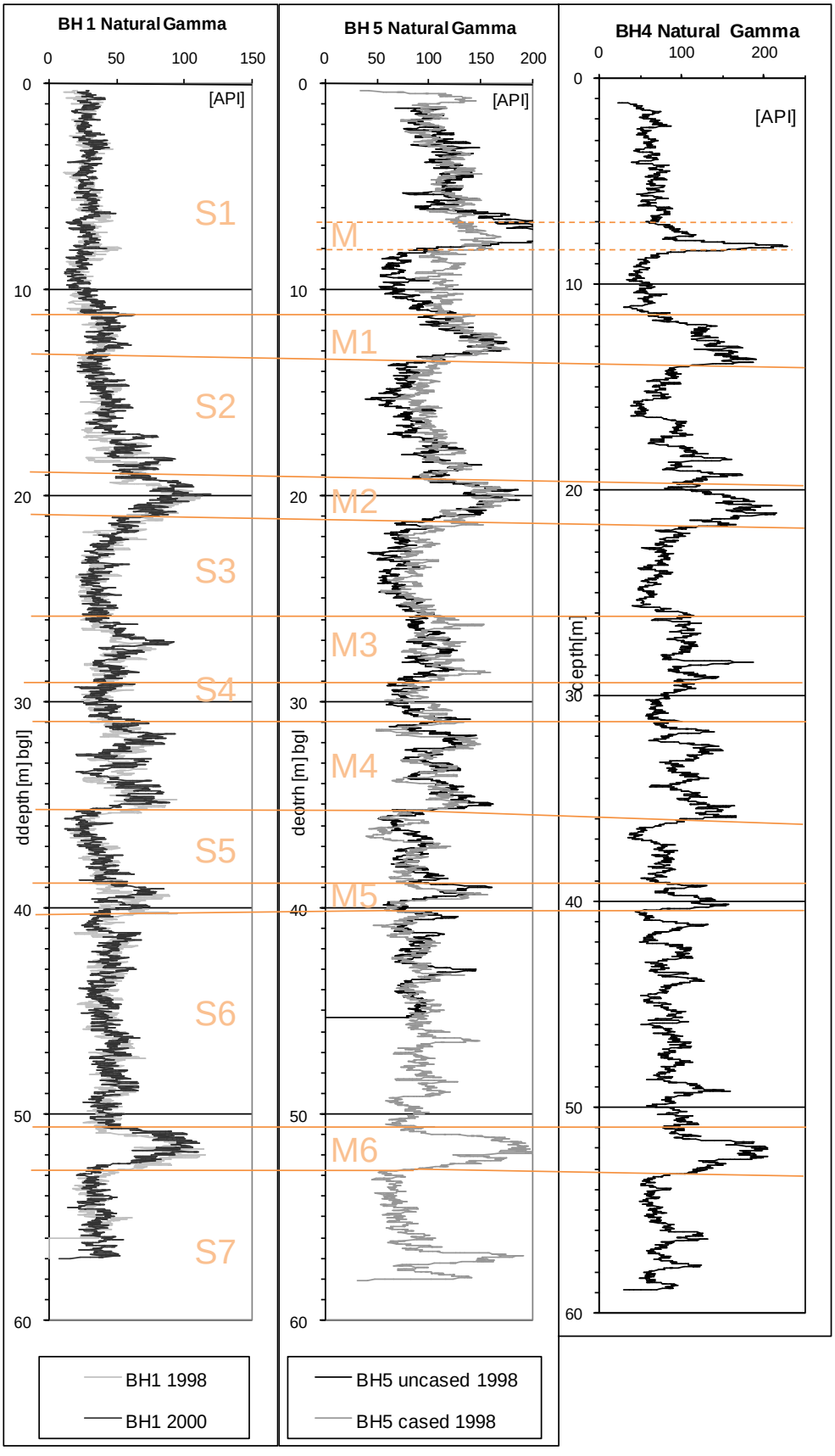

Figure 4.4: Natural-Gamma Logs of BH1, BH2, BH3, BH4, and BH5.

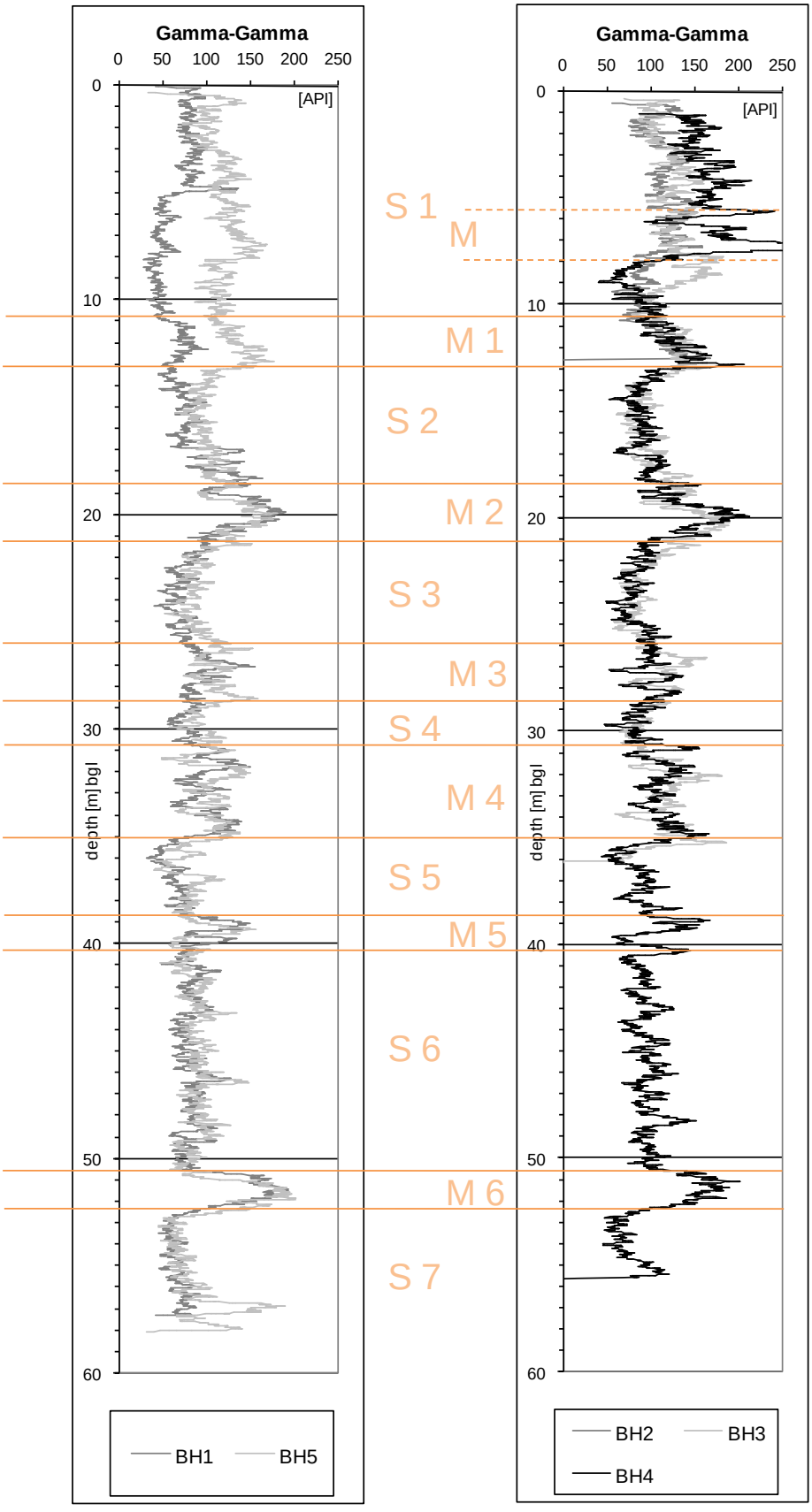

Figure 4.5: Gamma-Gamma Log of BH1, BH2, BH3, BH4, and BH5.

4.4.1.3 Neutron Log

Neutron logs were used to measure the total porosity under saturated conditions. They are used to measure the specific yield in the unsaturated zone or simply to determine lithological and stratigraphical correlations. The latter was required for the test site. The neutrons are emitted from a plutonium/beryllium radiation source when alpha particles of the plutonium strike the beryllium. A detector mounted at a sufficient distance from the source counts the neutrons. The biggest energy loss occurs during the collision with hydrogen ions which are mainly present in the water in the borehole and in the formation. The log reflects variations in the water molecules within the borehole (i.e. depending on the borehole diameter) and in the water of the rock formation, both interstitial water and water bound by clay minerals. Figure 4.6 shows the neutron-neutron logs for all boreholes recorded after casing was installed. The neutron-neutron radiation was plotted in counts per second (CPS). High energy loss indicates formations of high hydrogen content, e.g. sandstone layers or aquifers. Low energy loss indicates formations of low hydrogen content, e.g. aquitards or mudstone layers.M2, M4, M5 and M6 as well as S5 to S7 could be distinguished in the neutron-neutron logs of Figure 4.6 and it was possible to correlate the layers recorded in the logs of different boreholes with diagrams as horizontal. M1and M3 were not clearly detected by the logs. This applies for S1, S2, S3 and S4 as well.

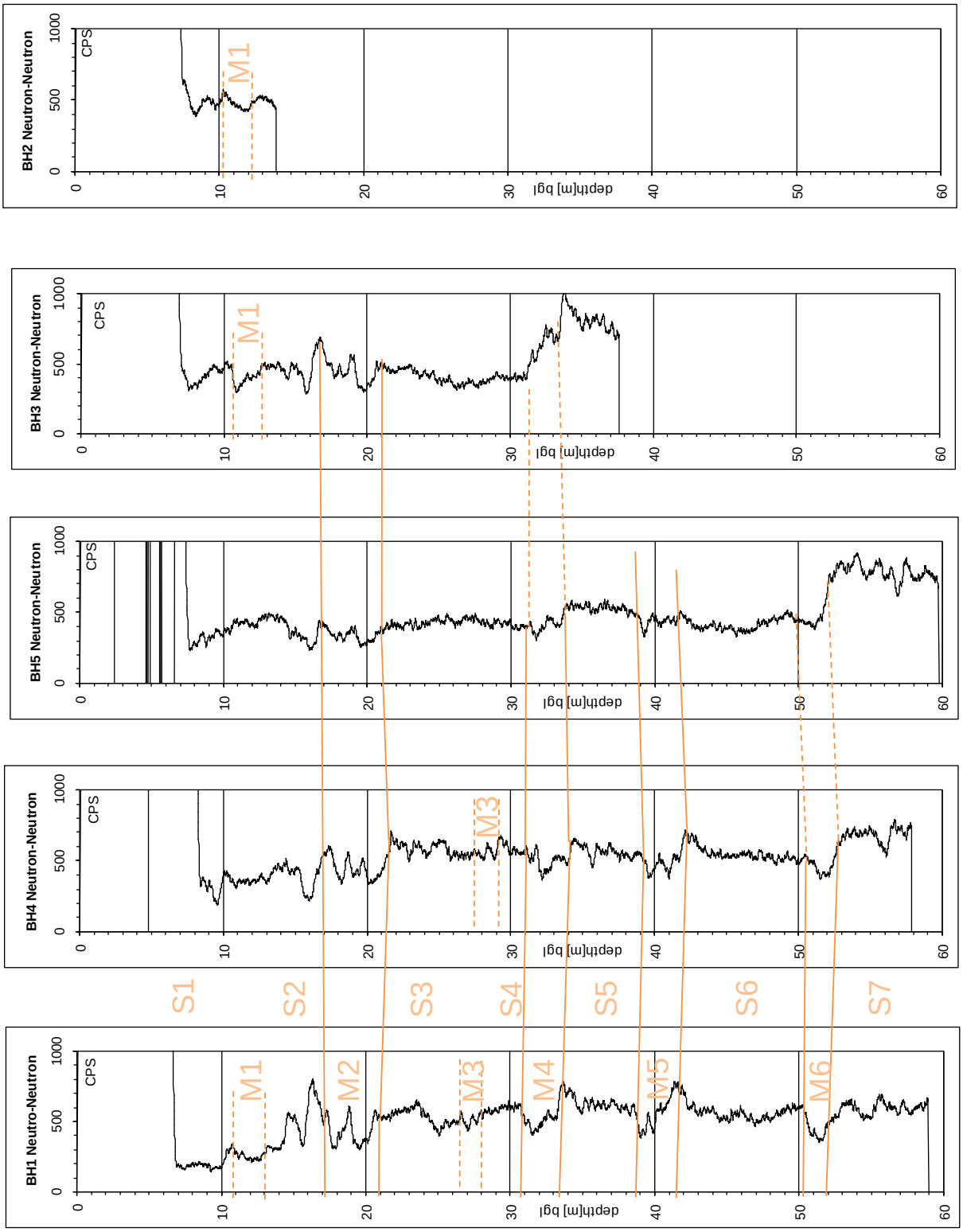

Figure 4.6: Neutron-Neutron logs of BH1, BH4, BH5, BH3, and BH2 recorded at the test site.

4.4.2 Electrical Logging

Electrical logs measure the potential differences of the flow of an electrical current in and adjacent to a well. Three main effects are important for the interpretation of resistivity logs: the borehole diameter, the rock formation and the water quality. The depth of investigation depends on the individual physical configuration of the electrical log. Single Point Resistance (SPR)-logs have an investigation depth as “short normal” log of about 250mm (16 inches) and as “long normal” log of about 400mm (64inches). The University-owned guard log has an investigation depth of 2250mm (Driscoll 1995). In boreholes with a diameter of more than 8 inches (203mm), it was recommended that the sonde is placed close to the borehole wall to avoid a dominating influence of the borehole water (Keys, 1989, 1994). In the electrical log it was tried to position the sonde in the centre of the borehole during logging. General differences in resistivity were recorded for rock formations with different saturation of water. Formations with a higher saturation were controlled by the porosity with high porosities, showing higher resistivities and vice versa. Low resistivities had clay, silt and clay rich sandstones. Low to medium resistivities were shown by silty aquifers with an unusually high content of ion concentration in the groundwater (e.g. caused by pollution), whereas sand and gravel with fresh water had moderate to high resistivity. The highest resistivity values were found in sandstone and limestone saturated with fresh water, as well as in dense igneous and metamorphic rocks (Keys, 1989).

The total dissolved solids (TDS) in the water could be an indicator of the water quality and influence the resistivity. Water dissolves minerals on the grain surface which mainly occurs on clay minerals. This results in low resistivity measurements of the electrical logs in wet clay. In saturated sand formations, water dissolves only very small amounts of minerals which

results in high measurable resistivity values. In general, the resistivity varies inversely with the TDS contained in the water.

Three different electrical logs were used:

4.4.2.1 Spontaneous-Potential Log (SP-Log)

Spontaneous-potential logs or self potential logs record the potential that develops between the different rock formations in a borehole, applied by Schlumberger and Doll (Doll, 1927). An electrode was lowered down the borehole, and connected to a millivolt-meter at the surface which was connected to the second electrode placed at the surface.

4.4.2.2. Single-Point Resistance Log (SPR-Log)

The single-point resistance log is the simplest setup of an active electrical logging method. The configuration of the electrodes is similar to the setup of the spontaneous-potential log. A current induced by a battery is guided down the hole to spread in the rock formation. Parts of the current return to the surface where the current drop is recorded. The depth of investigation is limited, but it has a good vertical resolution, needs only a single conductor cable and is relatively inexpensive in operation. It is not possible to calibrate the log for certain formation resistivities, because of varying distances between the electrodes.

4.4.2.3. Normal-Resistivity Log

The arrangement of two electrodes downhole is called normal log or normal-resistivity log. A current passing between a ground-surface electrode and an electrode on the sonde is measured by its potential difference on a potential electrode on the sonde. Two logs with two distance configurations between one current and two potential electrodes on the sonde are common. A

separation of 16 inches is called short normal and a separation of 64 inches is called long normal. The larger the distance between the electrodes, the greater is the penetration into the formation, but the lower is the resolution of the explored rock formation. As radii of investigation, Driscoll (1995) lists about 400mm for the short normal logs and about 1630mm for the long normal logs. When the normal resistivity log is chosen, the 16 inches configuration is used to detect lithological boundaries, while the 64 inches configuration gives a better estimation on average formation resistivities (Keys, 1989, 1994). Figure 4.7 shows the resistivity logs recorded in BH1 and BH4. The normal resistivity was measured and plotted in Ohm metres (Ohm m).

An interpretation was made by identifying zones of lower resistivity which corresponded to mudstone layers and zones of higher conductivity, corresponding with sandstone layers. The resistivity logging of BH1 (Figure 4.7) started at a depth of about 19m bgl because an iron casing in the top 14m of the well disturbed the "electrical" signal of the log. M2 to M4 were detected by the resistivity logs in BH1 and BH4. The resistivity log of BH4 started recording after the resistivity log entered the ground water (at about 7.36m bgl) and could be analysed from about 10.5m bgl, below the casing set during the drilling process. The measured signal corresponded to the top boundary of M1. However, the lower boundary at 13m bgl was clearly detected by an increase in resistivity. The record of the resistivity log in BH4, at a depth of 31.5 to 32m bgl was disturbed due to interruptions in the electrical circuit. The resistivity log of BH5 started recording in the uncased part of the well from 52m bgl to about 58m bgl. The transition of the mudstone layer to sandstone layer could be assumed to be at or above 52m bgl. In conclusion, it was possible to correlate all mudstone layers and sandstone layers as horizontal layers with some minor variations in thickness between BH1 and BH4.

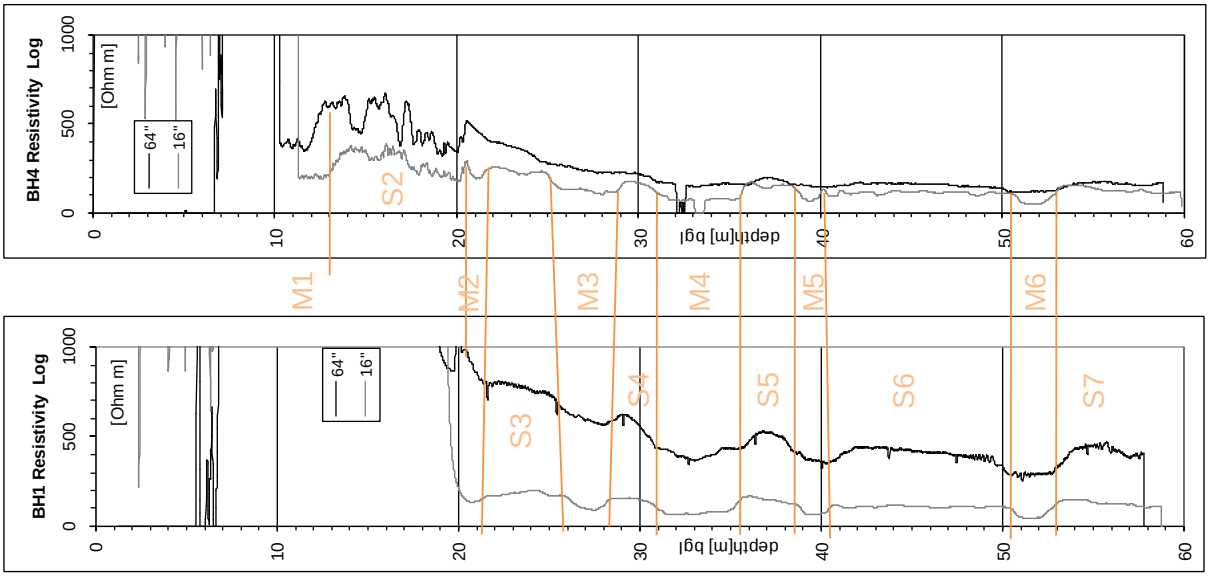

Figure 4.7: Resistivity logs of BH1 and BH4.

4.4.2.4 Guard-Log

Guard-logs are focused resistivity logs, designed to measure the resistivity of thin beds or resistive rocks in wells with conductive fluids. They are also called lateral logs. Guard electrodes are placed above and below the current electrode on the sonde, forcing the current flow in a narrow interval out into the formation surrounding the well. The thickness of the current beam is proportional to the length of the current electrode (usually between 3 inches and 12 inches). The depth of investigation was considered to be about three times the distance between the guard electrodes (Driscoll, 1995) and gives the best results when the distance is twice the electrode spacing (Robertson Research Engineering Ltd, 1982).

Figure 4.8 shows the recorded guard logs for BH1 and BH4. The resistivity of the guard logs was measured and plotted in Ohm metres (Ohm m). The guard logs were interpreted by identifying zones of lower resistivity which correspond to mudstone layers and zones of higher conductivity, corresponding to sandstone layers. S2 to S7 and M1 to M6 could be distinguished in the guard log of BH4. A representative resistivity value noted in BH1 was

recorded from about 18.5m bgl in BH1, as the iron casing disturbed the signal in the top part of the borehole. Due to the iron casing, M1, S1 and S2 were not detected with the guard log in BH1. The identified layers could be correlated between the different wells as horizontal layers.

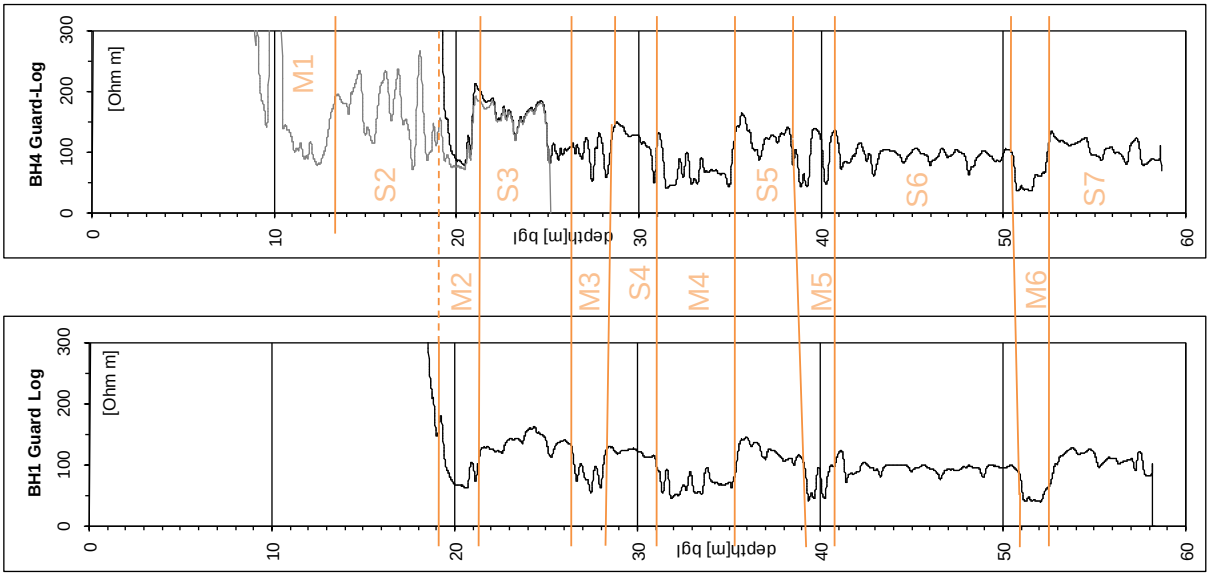

Figure 4.8: Guard logs of BH1 and BH4.

4.4.3 Temperature Log

Temperature logs are obtained by lowering a temperature sensor down the borehole. Local shallow aquifers can disturb the gradient because of their contribution to the total yield. A variety of factors influences the temperature: the depth of the well, background geothermal activity at rifts or volcanoes, the thermal conductivity of rocks, and vertical flow caused by differences in head, water quality or temperature. Temperature logs of all wells were recorded after the setting of the plastic casings. The temperature in BH1 was about 11.5°C at about 7m bgl at the top and 10.8°C at 59m bgl. In BH4, the temperature records 11°C at the top (at about 8m bgl) and 10.3°C at the bottom of the well at 59.5m bgl. Appendix IV 4.2 shows the temperature logs of BH1 and BH4.

4.4.4 Fluid Resistivity Log

Fluid resistivity logs or conductivity logs monitor the electrical conductivity or resistivity of water in the borehole. Changes of the ion concentration are reflected in changes in the fluid resistivity. Conductivity profiles are also affected by pumping, dispersion and convection movement of groundwater. Because the conductivity varies with temperature, a temperature correction is required if temperature changes occur with increasing depth (Keys, 1989). The measured conductivity in BH1 (Appendix IV 4.3) was within the range of 338 microS to 347 microS, remaining constant within this range over the whole depth of the well. The conductivity log of BH4 (Appendix IV 4.3) was recorded one day after the well was drilled, cased from the ground level to a depth of 52m bgl, grouted and air flushed to wash the grout out of the borehole. From the ground level to a depth of 43m bgl, a constant conductivity in the range of 325 microS to 337 microS was measured. Below 43m bgl the conductivity rose slowly to a value of 358 microS at a depth of 53m bgl and decreased to a value of 325 microS at 59.5m bgl. The measured conductivity was caused by an increased ion concentration in the

well of the grouting material. The disturbing influence of the failed grouting procedure and air flush does not represent the natural conductivity of groundwater in BH4.

4.4.5 Calliper Log

Calliper logs measure a vertical profile of the borehole diameter. The measurement was made by three flexible arms connected to the log which were pushed against the borehole wall. Movement of the arms was translated into a variation of a cursor along a resistance which was measured as an electrical output. The vertical profile of the borehole diameter can be used to standardise, calibrate and interpret the response of other logs or to detect casing and its perforation or slotting.

The average diameter of BH1 was 8.4 inches, varying by about 0.5 inches. The average diameter of BH4 in the top ten metres was about 7 inches and 6.2 inches at the bottom of the well (measured before casing and grouting). A diameter of about 4.2 inches was measured from 51.5m bgl to 59.7m bgl in the uncased zone of BH5. Below the casing in BH 1 at 15.50m and at 18m depth, the diameter increased to 10 inches and more than 12 inches. A similar increase in diameter was detected in BH4 with an increased diameter of more than 12 inches at 15.5m bgl. A second increase of the diameter up to more than 12 inches was measured at 10m bgl. The bigger variations in diameter were reasonable because of the looser layers at the top of the well in leached parts of the Triassic Sandstone. The calliper logs of BH1, BH4 and BH5 are shown in Appendix IV 4.4.

4.5 Closed Circuit Television (CCTV)

CCTV was used to record similarities or differences to the drilling log, core log or geophysical logs and to give a possible visual explanation or confirmation of measured values or observed differences. The CCTV available could only give a picture of the borehole wall and was unable to show the direction of the recorded picture (N, S, E or W) or to measure the size, dip direction or angle of certain layers. The CCTV confirmed the depth of mudstone layers M1 to M6 and sandstone layers S1 to S7. Three main observations should be highlighted:

1. The increased diameter recorded by the calliper log at a depth of 15m bgl and 18m bgl in BH1 and at 10m bgl and 15m bgl in BH4 was confirmed. The video recorded a thin clayed sandstone or mudstone layer at these depths.

2. M4 was recorded in BH1 and BH4 as a consistent mudstone layer from about 31m bgl to 33m bgl and from 33m bgl to 35m bgl, alternating fine layers of sandstone and mudstone were recorded.

3. Lowering the CCTV to the bottom of the well, a turbulent inflow into the well of small particles at the bottom of the well could be recorded. Further inflow could not be recorded on video in BH1.

4.6 Comparison of Different Logs of one Borehole

In the following, all recorded logs with different geophysical methods were compared concerning one borehole. The goal was to confirm that S1 to S7 and M1 to M6 could be identified throughout the borehole array at same or similar depths and that a layered model could be characterized for the test site. Diagrams for BH1, BH2, BH3, BH4 and BH5 were constructed in Figures 4.9 to 4.13, connecting sandstone and mudstone layers between the different geophysical logs recorded in each borehole. All mudstone layers were found at similar depths. M4, however, was visibly separated by the CCTV log into an upper mudstone part of 2m and a lower part of alternating fine layers of sandstone and mudstone layers. The neutron-neutron logs of BH1, BH4 and BH5 show a similar differentiation of M4 into an upper part of mudstone with less cps, and a lower part of sandstone with clay and a higher cps, marked by the dotted line. The separation into two parts of M4 was also detected by the natural gamma logs of these wells. The recorded depths of the top and bottom elevations of M1 to M6 in BH1, BH3, BH4 and BH5 are listed in Table 4.2 for each geophysical log. BH2 was not listed as no layer was identified clearly, due to restrictions of the logging setup and the construction with filter gravel. The average depths (arithmetic average) of the top and bottom elevations of each mudstone layer of one borehole were calculated with the depths, empirically read out from each log type of one borehole, and are listed in the last column of Table 4.2 for each well.

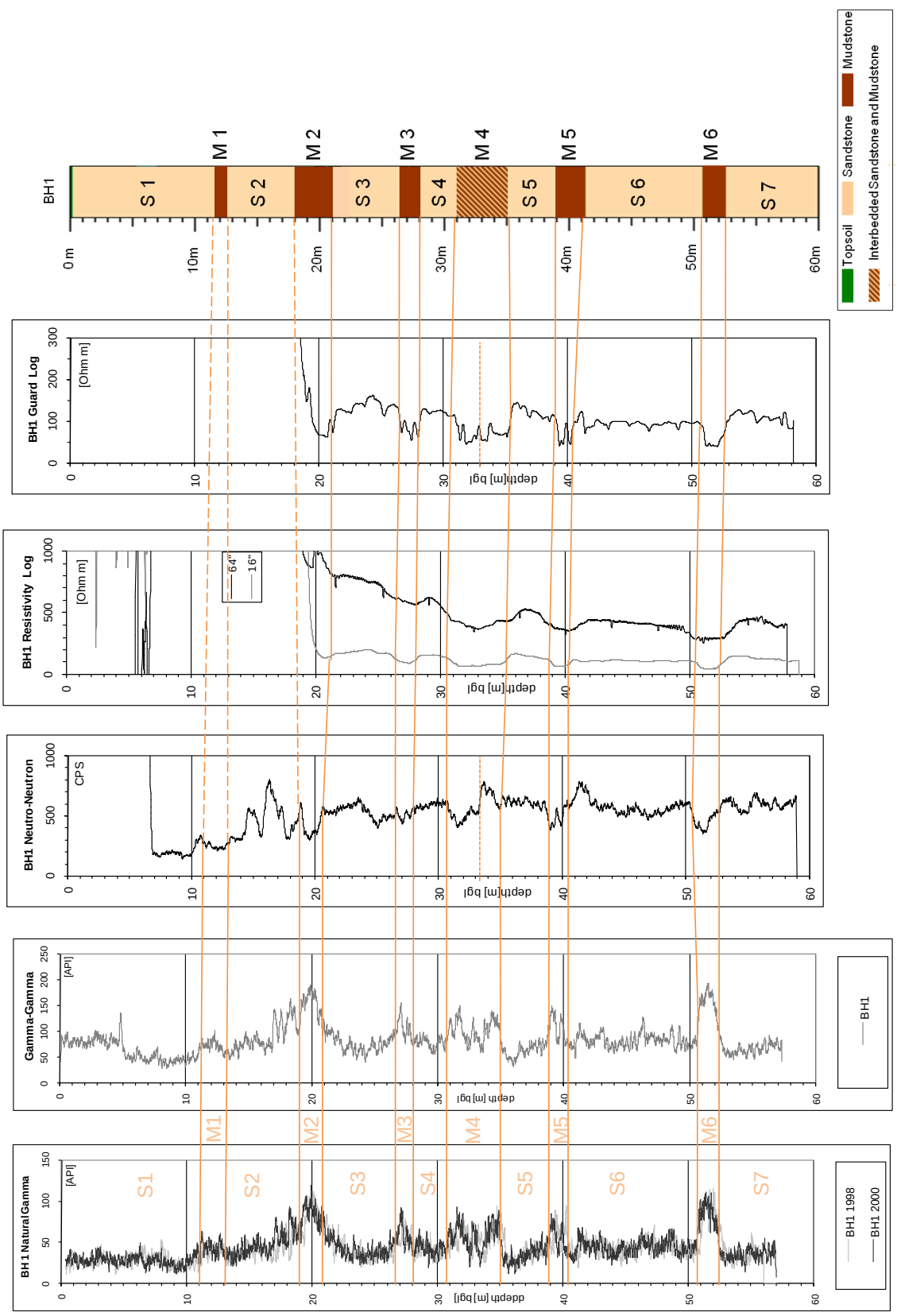

Figure 4.9: Comparison of the drilling log and different geophysical logs of BH1.

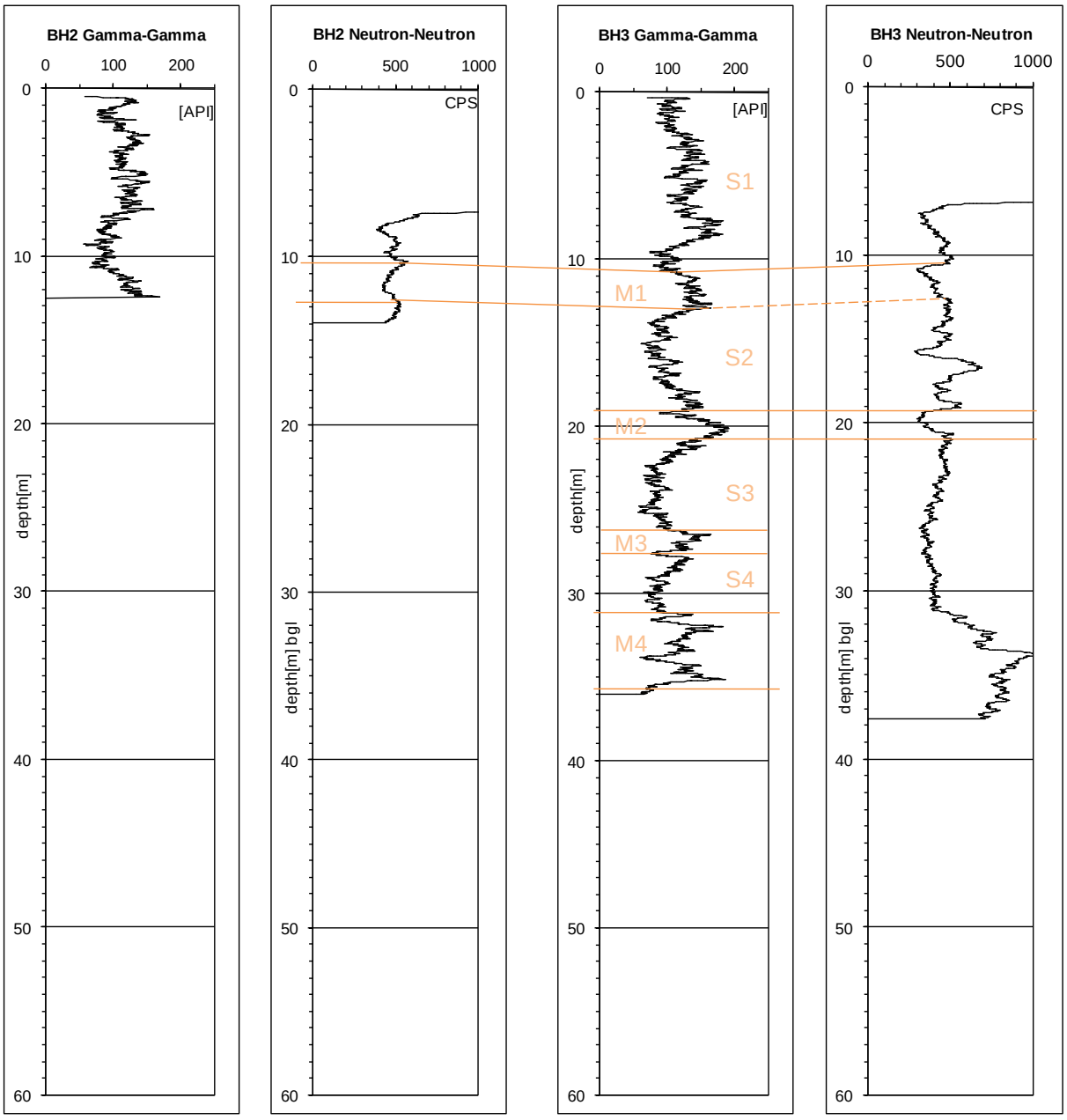

Figure 4.10: Comparison of the gamma-gamma and neutron-neutron logs of BH2 and BH3.

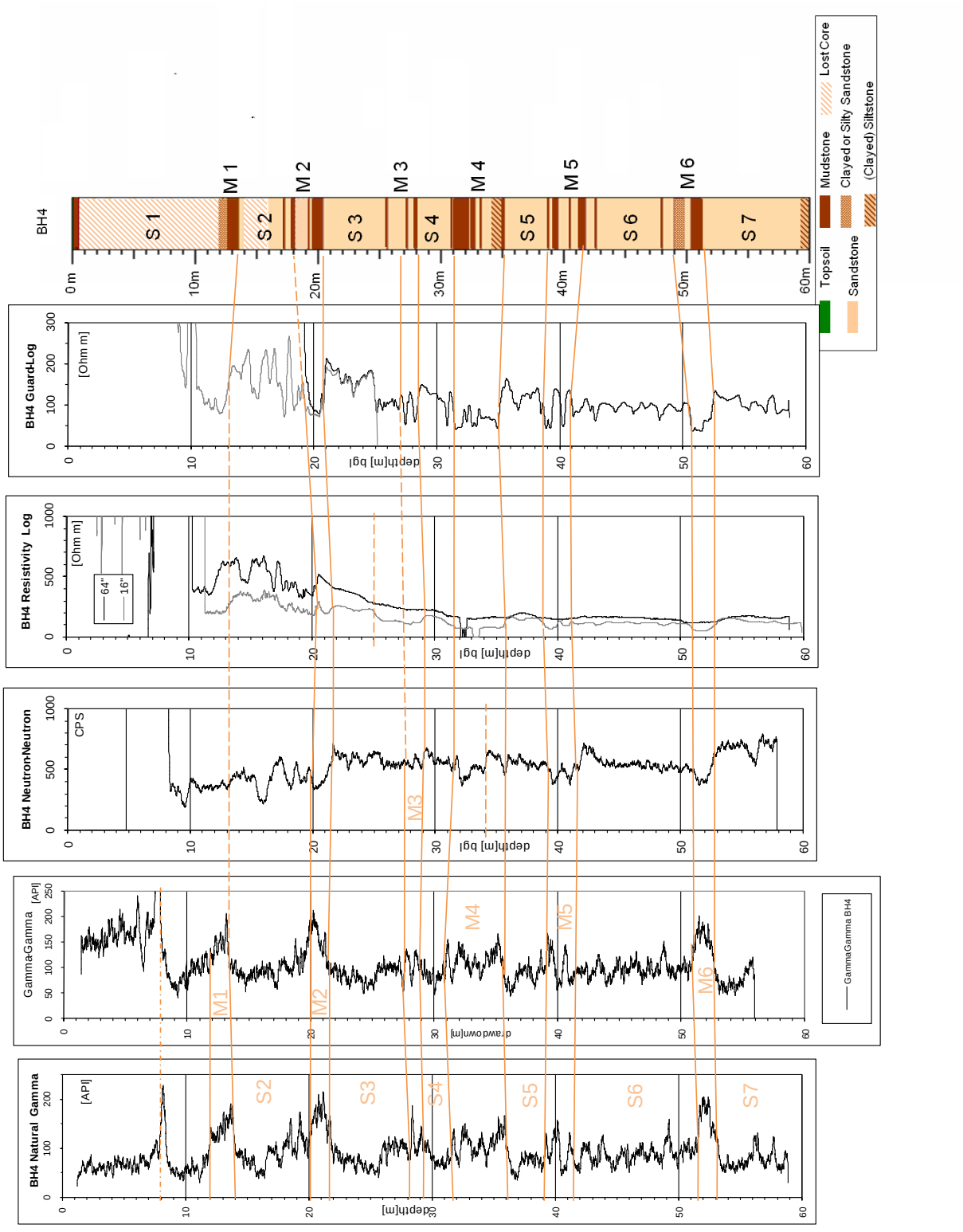

Figure 4.11: Comparison of the drilling log and different geophysical logs of BH4.

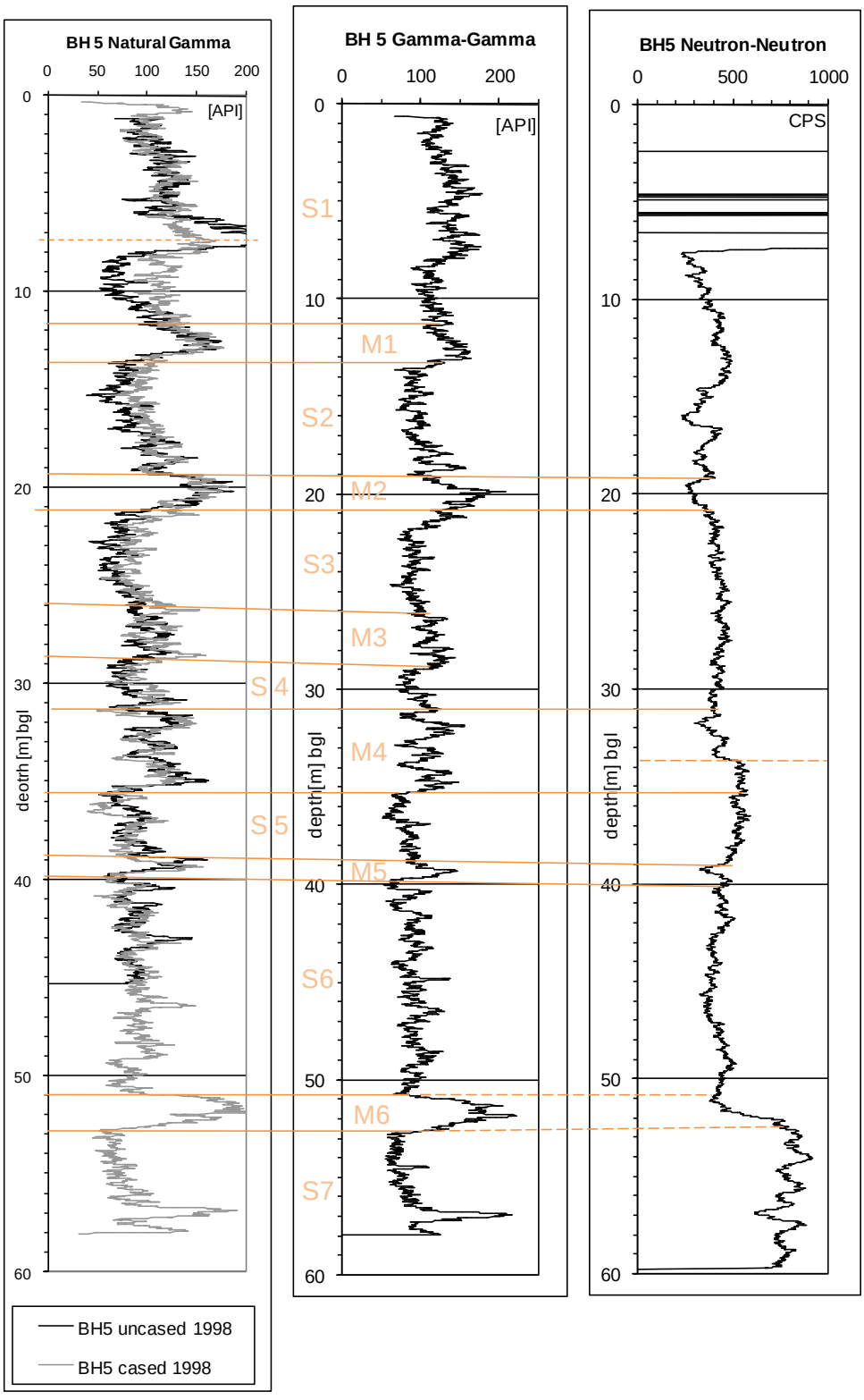

Figure 4.12: Comparison of nuclear logs recorded in BH5. The natural gamma logs were recorded without casing and after installation of the casing. The gamma-gamma and neutron-neutron logs were recorded after the casing and grouting was finished. The bottom end of the casing was installed to 52m bgl which was recorded with the neutron-neutron log with increased values of cps.

Table 4.2: The identified depth of the top and bottom elevation of M1 to M6 in BH1, BH3, BH4, and BH5 were listed for each geophysical method used. The last column lists the average depths (arithmetic average) of the top and bottom elevation of the mudstone layers M1 to M6 identified with the different methods for each borehole.

BH 1	Depth in m bgl	E-Log	Guard-Log	Neutron-Neutron Log	Gamma-Gamma Log	Natural Gamma-Log	Average depth (m bgl) logged for BH 1
M 1	top	n.d.	n.d.	10,50	11,00	11,00	10,83
	bottom	n.d.	n.d.	13,00	13,00	13,50	13,17
M 2	top	19,00	n.d.	19,00	19,00	19,00	19,00
	bottom	21,50	21,25	20,75	21,00	21,00	21,10
M 3	top	26,00	25,50	26,50	26,50	26,00	26,10
	bottom	28,25	28,50	28,00	28,00	28,00	28,15
M 4	top	30,50	31,00	30,75	30,75	30,75	30,75
	bottom	35,50	35,50	33,50	35,00	35,00	34,90
M 5	top	38,75	38,50	38,75	38,75	38,75	38,70
	bottom	40,75	40,50	40,50	40,50	40,50	40,55
M 6	top	50,50	50,50	50,50	50,50	50,50	50,50
	bottom	52,50	53,00	52,50	52,50	52,50	52,60

BH 3	Depth in m bgl	E-Log	Guard-Log	Neutron-Neutron Log	Gamma-Gamma Log	Natural Gamma-Log	Average depth (m bgl) logged for BH 3
M 1	top			10,50	11,00		10,75
	bottom			12,75	13,00		12,88
M 2	top			17,00	18,00		17,50
	bottom			21,00	21,25		21,13
M 3	top				26,00		*26,00*
	bottom				28,00		*28,00*
M 4	top				31,00		*31,00*
	bottom				35,50		*35,50*

BH 4	Depth in m bgl	E-Log	Guard-Log	Neutron-Neutron Log	Gamma-Gamma Log	Natural Gamma-Log	Average depth (m bgl) logged for BH 4
M 1	top	11,00	n.d.	n.d.	11,00	12,00	11,33
	bottom	13,00	n.d.	n.d.	13,00	14,00	13,33
M 2	top	19,00	19,00	17,00	19,00	20,25	18,85
	bottom	21,25	20,00	21,50	21,25	21,75	21,15
M 3	top	26,50	27,00	27,50	27,00	26,00	26,80
	bottom	28,00	28,50	29,50	29,00	29,50	28,90
M 4	top	30,50	31,00	31,50	30,75	31,70	31,09
	bottom	35,00	35,00	34,00	35,50	36,50	35,20
M 5	top	38,50	38,75	39,25	39,00	39,00	38,90
	bottom	41,00	41,75	42,00	41,00	40,50	41,25
M 6	top	50,50	49,00	50,50	50,76	51,50	50,45
	bottom	52,75	51,00	52,75	52,50	53,00	52,40

BH 5	Depth in m bgl	E-Log	Guard-Log	Neutron-Neutron Log	Gamma-Gamma Log	Natural Gamma-Log	Average depth (m bgl) logged for BH 5
M 1	top			n.d.	11,50	11,00	11,25
	bottom			n.d.	13,50	13,50	13,50
M 2	top			17,00	19,00	19,25	18,42
	bottom			21,00	21,00	21,25	21,08
M 3	top			n.d.	26,25	26,00	26,13
	bottom			n.d.	29,00	29,00	29,00
M 4	top			31,50	30,75	31,25	31,17
	bottom			34,00	35,25	35,25	34,83
M 5	top			38,75	39,00	38,75	38,83
	bottom			39,75	40,00	40,00	39,92
M 6	top			*(50,50)*	50,75	51,00	50,88
	bottom			*(52,25)*	52,50	52,75	52,63

4.7 Conclusion - Characterization of the Borehole Array

To process further hydraulic tests and tracer tests, the test site was characterized by distinguishing the main "mudstone" or low permeable layers from high permeable "sandstone" layers, by means of a drilling log, a core log and various geophysical logs. Laboratory tests on core samples of BH4 of the hydraulic permeability with a mean of 1.5m/d and of the porosity with a mean of 25% of the sandstone layers (Mitchener, 2003) were plotted for the different depths. In comparison to the values gained for the sandstone layers the hydraulic conductivity and porosity, values of the mudstone layers gained by Mitchener (2003) and Curião et al. (2001) are plotted. It was shown that the hydraulic conductivities of mudstones were more than 10 times smaller than those of sandstones. The porosity, determined for cores by Mitchener (2003) for values bigger than 21% seem to be typical for sandstone layers and those smaller than 21% seem to be typical for mudstone layers of the test site.

The geophysical logs in BH1 to BH5 confirmed the initial setup of seven sandstone layers (S1 to S7) and six mudstone layers (M1 to M6), as shown in Figure 4.1. To define the depth of mudstone layers for the conceptual model, all average depths calculated for BH1, BH3, BH4 and BH5 (as calculated in Table 4.2) were listed in Table 4.3 and the average depths of mudstone layers according to all geophysical logs were calculated. The last column in Table 4.3 gives the depth of M1 to M6 of the conceptual model, derived from the drilling log, the core log, the average depths of all geophysical logs and the CCTV. Figure 4.13 shows the location of the mudstone layers of the conceptual model in relation to their location recorded in the geophysical logs, the drilling log and the core log. As the location of the mudstone and sandstone layers of the conceptual model was discussed, the location of M1 to M6 was shown with the transparent bars over all log profiles. Figure 4.14 shows a schematic cross section of

the test site with the location of the mudstones, according to their location of the conceptual model, and the construction details (see also Figure 3.2).

A simplified layered model of the test site with parallel layers of seven sandstone layers, separated by six mudstone layers was developed. Thus setup of the borehole array was deemed to be acceptable for the development of a conceptual computer model for applications of a groundwater flow and transport model of the site.

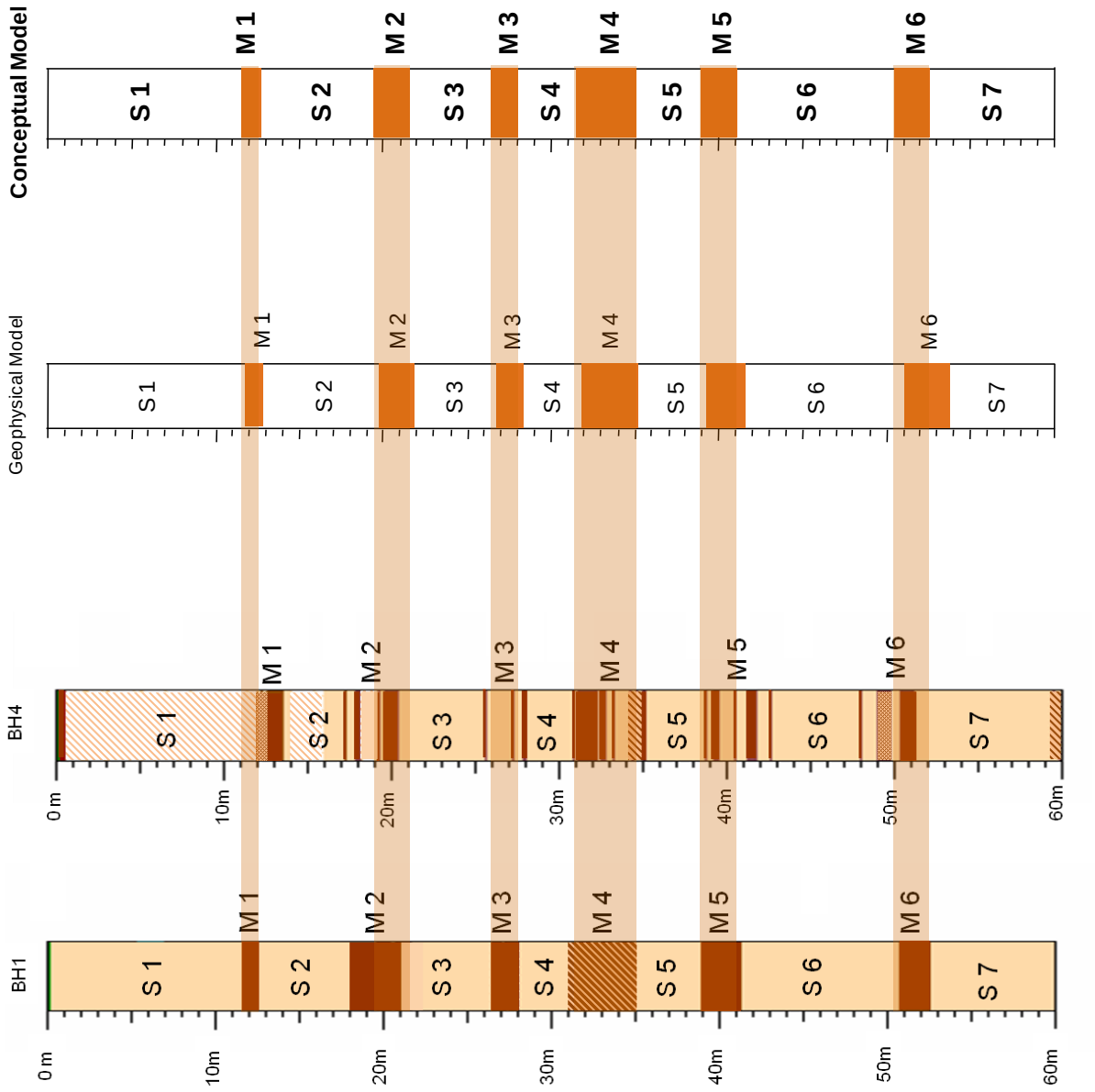

Figure 4.13: Developed simplified log for a conceptual model of the test site, using the recorded drilling log (BH1), core log BH4 and log of all geophysical methods with the calculated average depths of M1 to M6. The mudstone layers were connected between the different generalized logs.

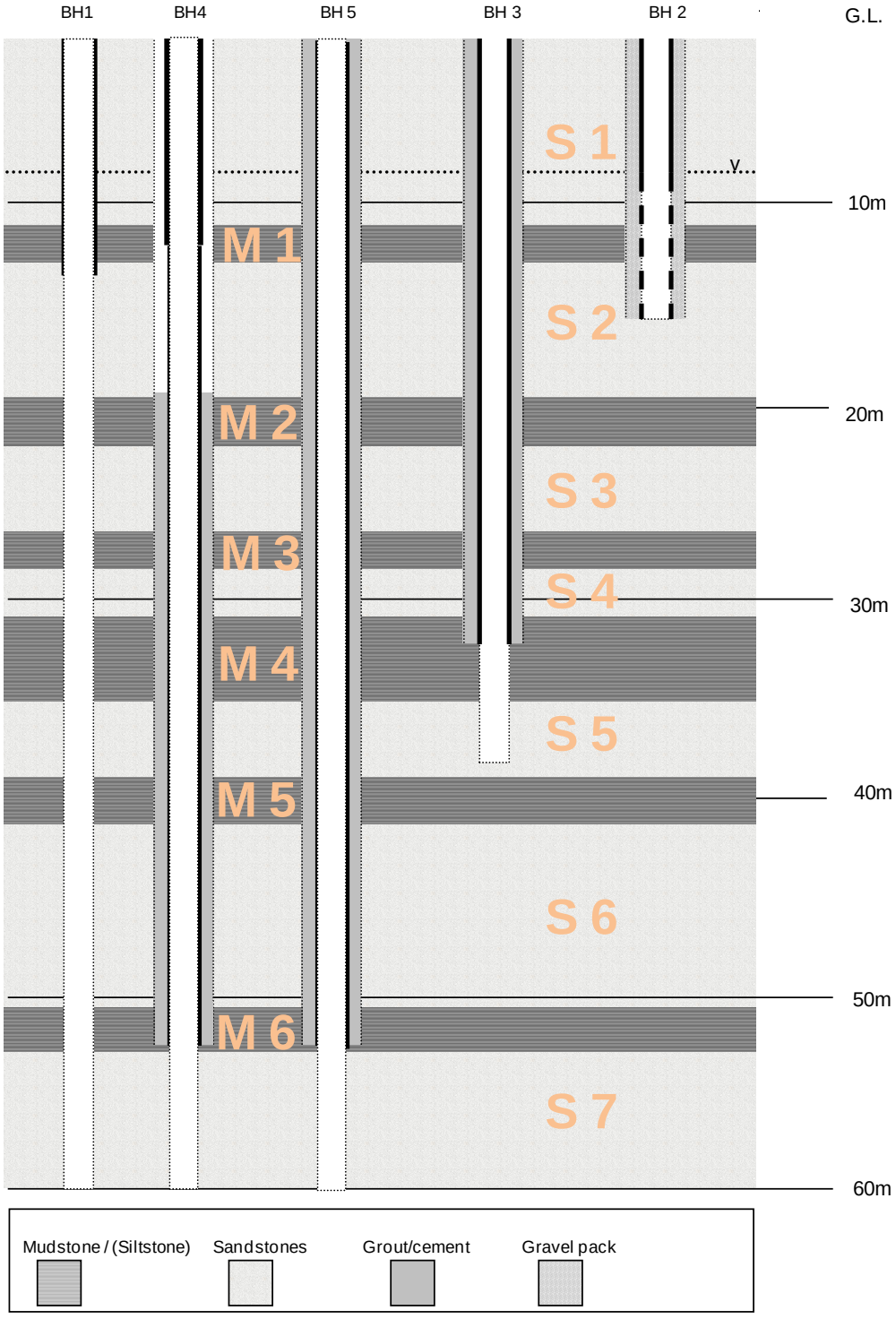

Figure 4.14: Schematic cross-section of the test site, showing the location of the wells according to the depth and layers.

Table 4.3: The calculated arithmetic average of the depths of the mudstone layers taking into consideration all geophysical logs of all wells, by applying the calculated average depths of the top and bottom elevation of the mudstone layers M1 to M6 for BH1, BH3, BH4 and BH5 (Table 4.2). The last column lists the depths of the mudstone layers derived for the conceptual model taking into consideration all geophysical logs, the drilling log, core log and CCTV.

Logs:		**Geophysical**					**Drilling**	**Core**	**All**	**Depth derived for the conceptual model, considering the drilling log, core log and CCTV survey m bgl**
Mudstone Layers		**BH1 Ø depth m bgl**	**BH3 Ø depth m bgl**	**BH4 Ø depth m bgl**	**BH5 Ø depth m bgl**	**BH 1 to BH5 Ø depth m bgl**	**BH1 depth m bgl**	**BH4 depth m bgl**	**Drilling, Core, BH1-BH5 Geophy. Ø depth m bgl**	
M 1	top	10,83	10,75	11,33	11,25	**11,04**	**11,50**	**11,83**	**11,46**	**11,50**
	bottom	13,17	12,88	13,33	13,50	**13,22**	**12,50**	**12,83**	**12,85**	**12,80**
M 2	top	19,00	17,50	18,85	18,42	**18,44**	**19,50**	**19,83**	**19,26**	**19,50**
	bottom	21,10	21,13	21,15	21,08	**21,11**	**21,50**	**21,83**	**21,48**	**21,50**
M 3	top	26,10	26,00	26,80	26,13	**26,26**	**26,50**	**26,83**	**26,53**	**26,50**
	bottom	28,15	28,00	28,90	29,00	**28,51**	**28,00**	**28,33**	**28,28**	**28,00**
M 4	top	30,75	31,00	31,09	31,17	**31,00**	**31,50**	**31,83**	**31,44**	**31,50**
	bottom	34,90	35,50	35,20	34,83	**35,11**	**34,75**	**35,08**	**34,98**	**35,00**
M 5	top	38,70		38,90	38,83	**38,81**	**39,00**	**39,33**	**39,05**	**39,00**
	bottom	40,55		41,25	39,92	**40,57**	**41,25**	**41,58**	**41,13**	**41,00**
M 6	top	50,50		50,45	50,88	**50,61**	**50,75**	**51,08**	**50,81**	**50,50**
	bottom	52,60		52,40	52,63	**52,54**	**52,50**	**52,83**	**52,62**	**52,50**

CHAPTER 5: Hydraulic Conditions of the Test Site

5.1. Aim

The aim of Chapter 5 is to describe the hydraulic characteristics of the test site:

1. Rest water levels were measured from August 1998 until November 2000 when no tests were conducted. Head differences between S1and S2 in BH2, S5 in BH3 and S7 in BH5 were observed (Figure 5.1). BH1 recorded an average head of S1 to S7.
2. Flow logs, conducted in 1998 and 2000 recorded vertical flow in BH1 towards the top between 2.1l/s and 5.8l/s. Packer tests undertaken in 2000 measured pressure changes above and below a single packer installed in BH1 at the levels of M1 to M6. The packer tests recorded a pressure increase below and a pressure decrease above the inflated packer in BH1 for each test interval, apart from M1 (Figure 5.2). The pressure head changes were used later to define the boundary conditions of the groundwater model.
3. A number of pumping tests was undertaken, applying purpose-tailored packers. Curve-fitting analysis were made with AquiferWin32 (Version 1.06, 1997 by Environmental Simulations, Inc. (ESI) developed by J. and D. Rumbaugh), determining values for transmissivities (T), hydraulic conductivities (K) and storage coefficients (S) of S1 to S7. Table 5.1 lists the pumping test details and table 5.2 the applied curve-fitting method and calculated values for T, K and S. All calculated hydraulic values were used as initial input data for the groundwater flow model. The pumping tests could be used for later model calibration.

5.2 Rest Water Level Observation

The water levels in all boreholes were monitored from August 1998 until November 2000. During test periods of pumping tests and tracer tests from May until October 1999 and from May until November 2000, almost no rest water levels for the wells were considered. The hydraulic heads were measured with a dipper or with pressure transducers. As reference point a elevation level of 0 m bgl was defined at the top of the casing of BH1. All other measurements were adjusted to this elevation level for comparison. The rest water levels were plotted in Figure 5.1.

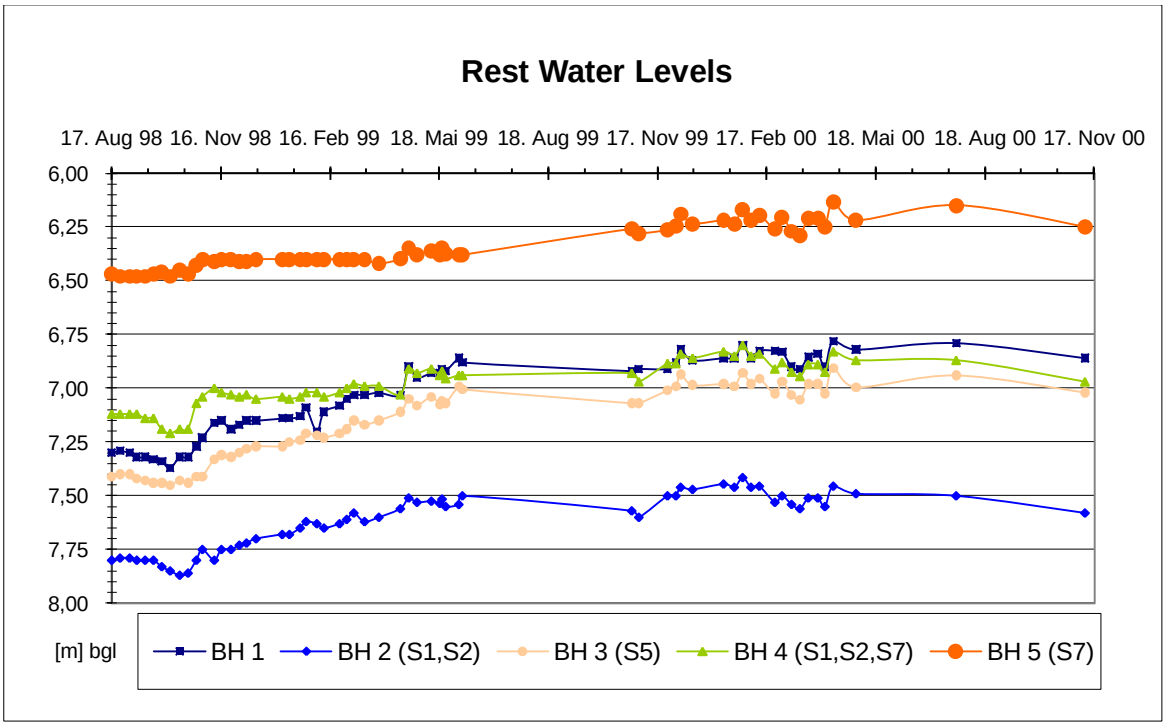

Figure 5.1: Rest groundwater levels monitored in BH1 to BH5.

The highest heads were monitored in S7 (BH5) and the lowest in S1 and S2 (BH2). About the average head of the two layers was monitored in BH4, the borehole which connects S1, S2

and S7. For BH1 which connects all sandstone and mudstone layers a slightly lower head than in BH4 was monitored.

The measurements of the rest water levels implied that the deeper the layer approached on the test site, the higher was the pressure head in the aquifer. As the rest water level in BH1 and BH4 was about the average of BH2 and BH5, a connecting flow in these wells between the layers approached by BH2 and BH5 should occur. However, no information was available of how much each sandstone layer participated in flow into BH1 or from BH1 into a layer.

5.3 Vertical Flow in BH1

Vertical flow measurement in BH1 was performed with the Robertson Geologging heat pulse flow meter, as schematically shown in Figure 5.2 (Keys, 1989). Triggered at the surface, a short pulse of electric current heats the wire heat grid, which was located between two thermistors. The heated water layer moves towards one of the thermistors under the effect of vertical flow in the well. The arrival of the heat pulse was recorded on a chart recorder running on time drive (Figure 5.3). The heat pulse flowmeter used for the measurements could measure vertical velocities in a range of 0.0005m/s to 0.11m/s. or vertical flow between 0.32l/s to 70.22l/s (Roberson Geologging Manual, 1982, Keys, 1989). It was taken into account, that the heat pulse flow meter with a diameter of about 0.06m was moved in the wells with a diameter of 0.1m (BH2 to BH5) or 0.2m (BH1), any movement upwards or downwards in the well could cause turbulence in the fluid column causing large errors at slow vertical flow velocities. Two logs of the heat pulse flowmeter were shown in Figure 5.4. The logs were recorded in an interval of more than two years. Both logs had the same shape and similar values were repeatedly recorded, but the log 2000 recorded slightly lower up-flow velocities.

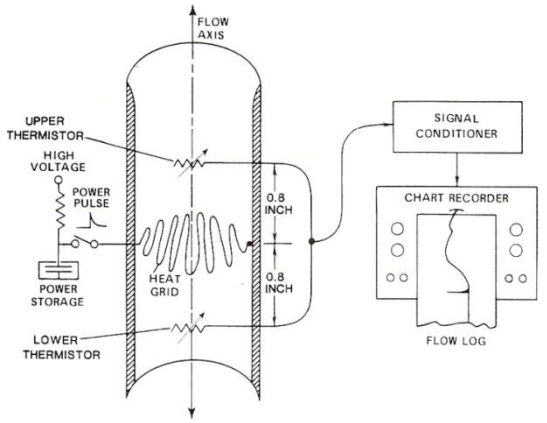

Figure 5.2: Schematic picture of the technical setup of a heat pulse flowmeter (Keys, 1989)

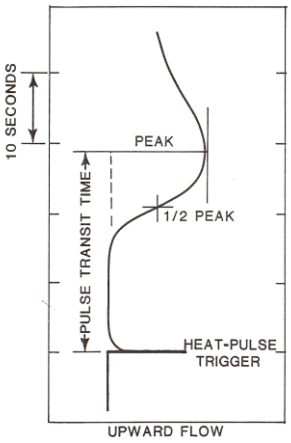

Figure 5.3: Analog record of a heat pulse from a thermal flowmeter (Keys, 1989)

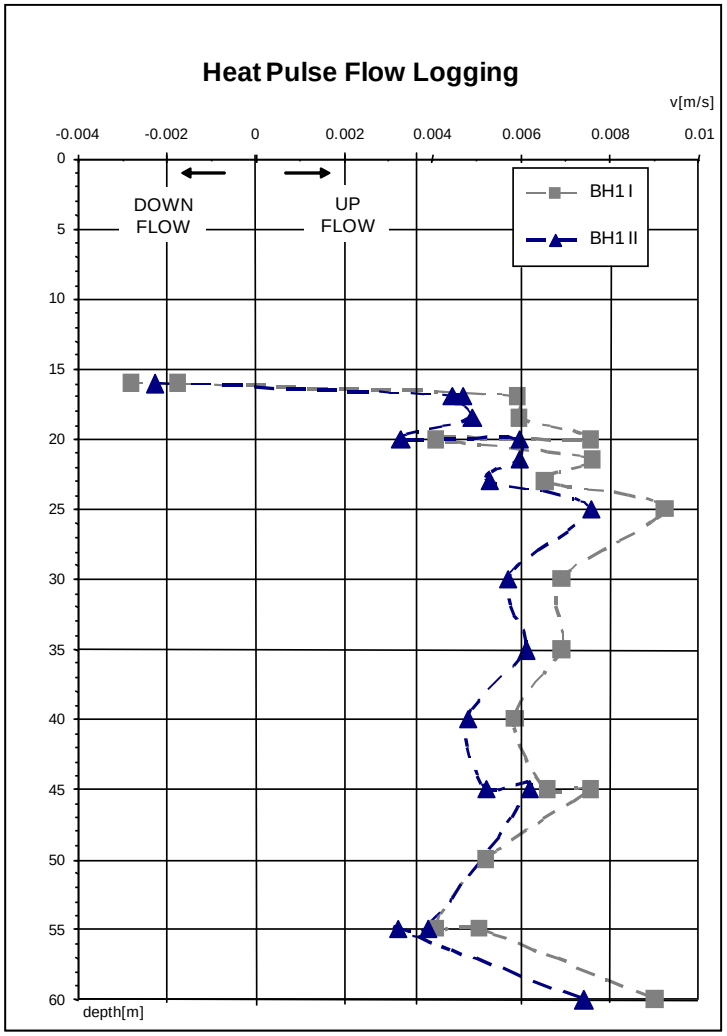

Figure 5.4: Heat pulse flowmeter measurements in BH1 with BH1 I recorded in 1998 and BH1 II recorded in 2000.

The up-flow was measured from the bottom of BH1 up to a depth of 16m bgl with vertical flow velocities varying between 0.0033m/s (about 0.107l/s) and 0.0091m/s (about 0.295l/s). Two flow measurements detected a down-flow in BH1 at 16 m bgl with a velocity of about 0.0028m/s (about 0.091l/s). Variations of the measured up-flow in BH1 at different depths were caused by the different pressure heads of the different aquifer layers approached. The vertical flow measured with the heat pulse flow meter was caused by vertical head differences between the individual sandstone layers S1 to S7.

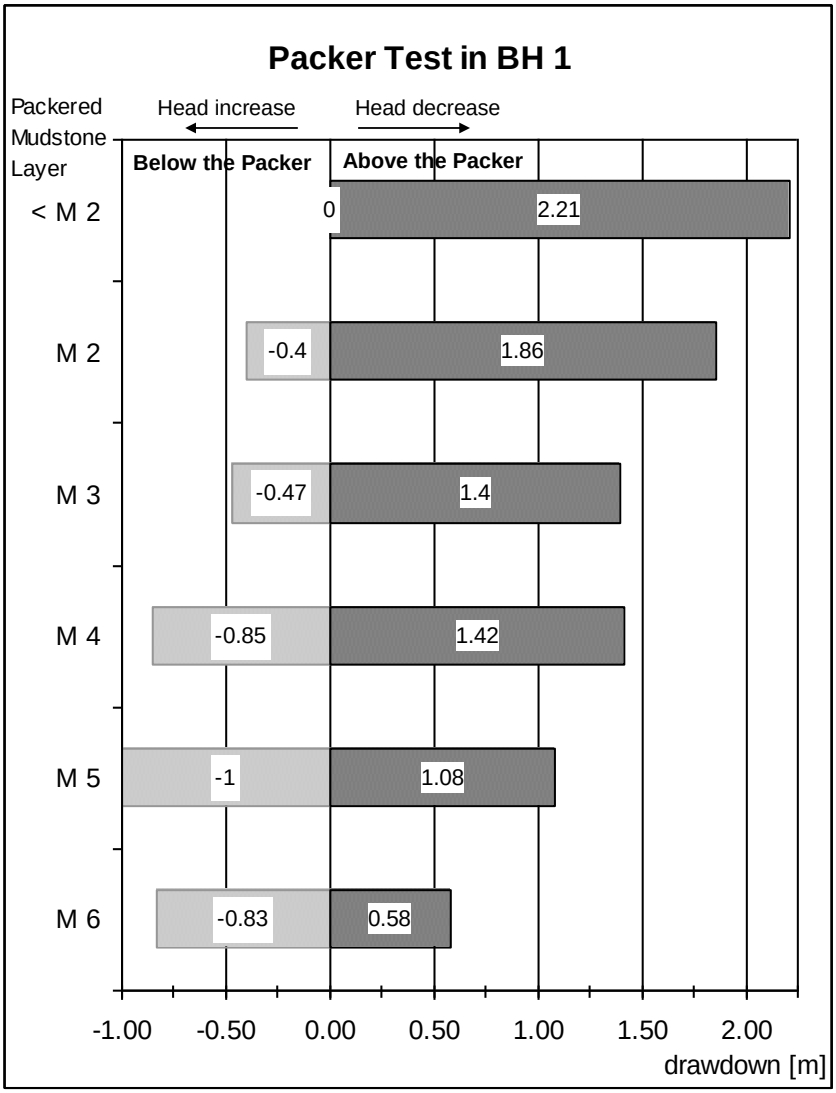

Figure 5.5: Hydraulic head changes due to packered mudstone horizons in BH1. Measurements were taken above and below the packered mudstone layers. Positive values show a head reduction and negative values an increased head.

By introducing a packer into BH1, head changes in BH1 above and below the installed packer were measured with pressure transducers. Figure 5.5 shows the pressure head changes above and below the packer, measured with pressure transducers after the packer was inflated. For each sealed section, a decrease of the head above the inflated packer was observed and vice versa. The head changes and the vertical flow in BH1 were taken into account for the setup of the boundary conditions of the later groundwater model.

5.4 Equipment Applied for the Pumping Tests

In the following, the equipment available for the pumping tests was applied. All equipment was owned by the School of Earth Sciences of the University of Birmingham.

5.4.1 Pumps

Three pumps were used:

1. Godwin F43 FC9 4 inch submersible pump with a 2900 rpm electric motor (415V, 50Hz, rated at 1.5kW) with a maximum discharge capacity of 5l/s.
2. Godwin F43 FC9 4 inch submersible pump with a 2900rpm electric motor (230V, 50Hz, rated at 1.5kW) with a maximum discharge capacity of 1l/s.
3. Submersible Grundfos MP1 with a maximum discharge capacity of 1l/s.

The discharge capacity of the two Godwin pumps was applicable in an on/off modus. Discharge could be adjusted with valves connected to the pump before the tests were started. The discharge capacity of the Grundfos MP1 was electronically adjustable from 0-1l/s with a control box and could be changed during the process of the test.

5.4.2 Transducer

The hydraulic heads in the wells and pressure heads below packers were monitored during pumping tests and tracer tests with Geokon Model 4500 Vibrating Wire Piezometers (GEOKON, Inc., 1989).Two data read out boxes were used during the tests. One was portable with a plug for one transducer, mainly applied for calibration. The other one contained a hard disk and could connect 16 transducers. This read out box was used to record the signal of all connected transducers in an interval of 10 seconds. The power supply was maintained by a regular car battery.

5.4.3 Packer

Different packers were applied for the pumping tests and tracer tests. The following packers were used:

- Bigsock

The term “bigsock” was used for the temporary packer system that sealed the entire borehole wall over the whole depth of borehole BH1. The packer was built from a double skin of polythene “lay-flat” tubing (Figure 5.6). The tube, approximately 65m long, was hung into the borehole BH1 and filled with water, thus inflating the tube in the borehole. The water in the tube pressed the double skin of polythene against the borehole wall, causing the “lay-flat” tubing to seal off BH1. In order to have a higher pressure in the packer than in the surrounding media, a positive head of about 0.2-0.25 bar was tried to be maintained in the packer by filling the water in the bigsock up to 2-2.5m. The hydraulic connection between the aquifer layers through the borehole (S 1 to S 7) was interrupted after the “bigsock” was installed in BH1. The “bigsock” was removed after pumping tests in BH2, BH3 and BH5were finished.

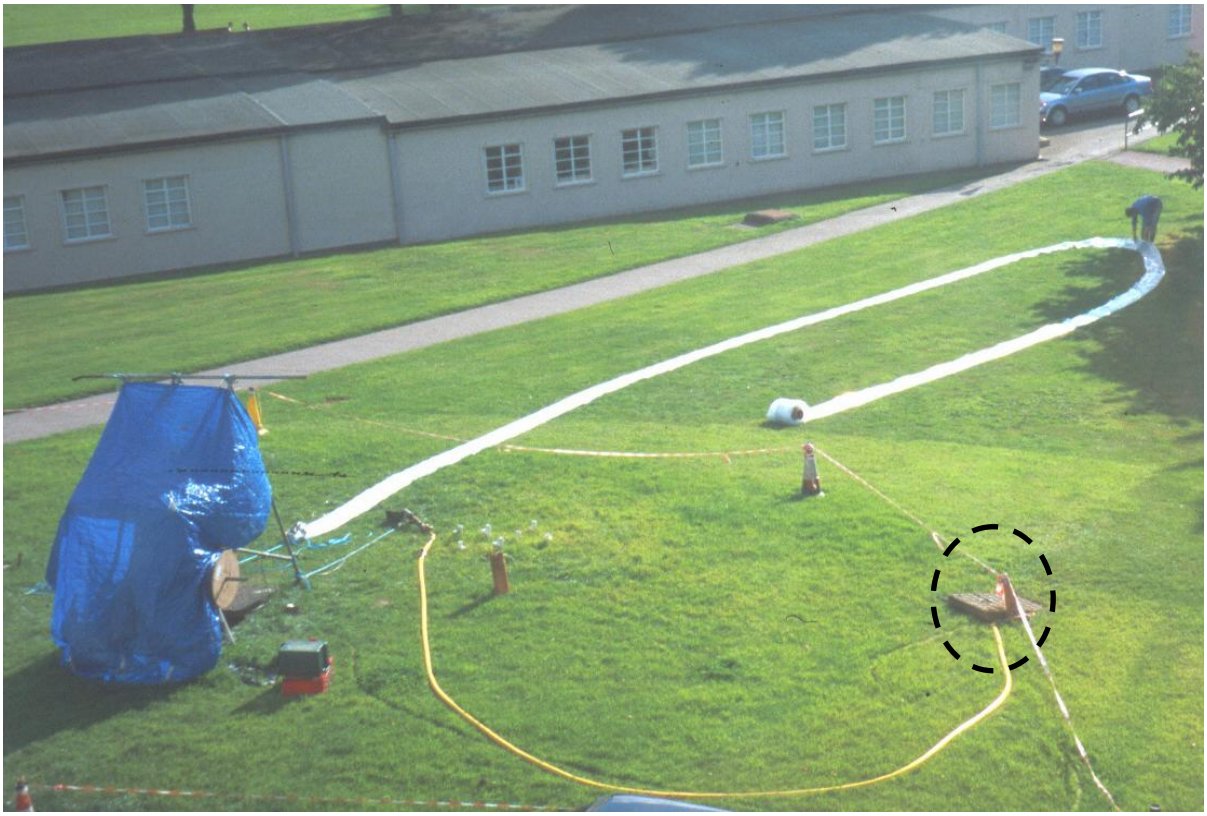

Figure 5.6: Picture of the test site with the “Bigsock” before the installation in BH1. The dotted ring encloses the sewer cover used for discharge.

- Single-Packer

A commercial packer was used in BH4 to interrupt the connecting effect between S1, S2 and S7. The packer was suitable for application in wells with a diameter of 5 inches and could be inflated by pumping water into the inflatable sleeve via a small water tank with a manual hand pump. The inflated state could be controlled by a pressure gauge on the surface. The single packer was always in place during the hydraulic tests and tracer tests in order to interrupt the connection in BH4 between the bottom and top aquifer layer of the test site.

- Double-Packer

A double or dual packer system was designed and constructed by Richard Greswell (in 1999 at the University of Birmingham) to be applied in BH1. This double-packer was convenient

for two persons to handle in a well of 8 inches diameter (Figure 5.7 and Figure 5.8). The design considerations included the practicalities of construction, ease of use and cost (Greswell, 1999). Commonly available ABS pipework and fittings were used. The advantages of this material were the light weight, that it may be solvent welded, and that a large range of components was available that could be adapted for use in packer construction. The inflatable sleeve was a crucial component. It expanded against the borehole wall to form a seal and thus prevented a vertical flow. A 6mm thick natural rubber sleeving was specified and custom-made.

Figure 5.7: A: 1 Bottom packer, 2. Godwin pump (discharge capacity 5 l/s), 3. Geokon Transducer; B: Dual packer system on the surface.

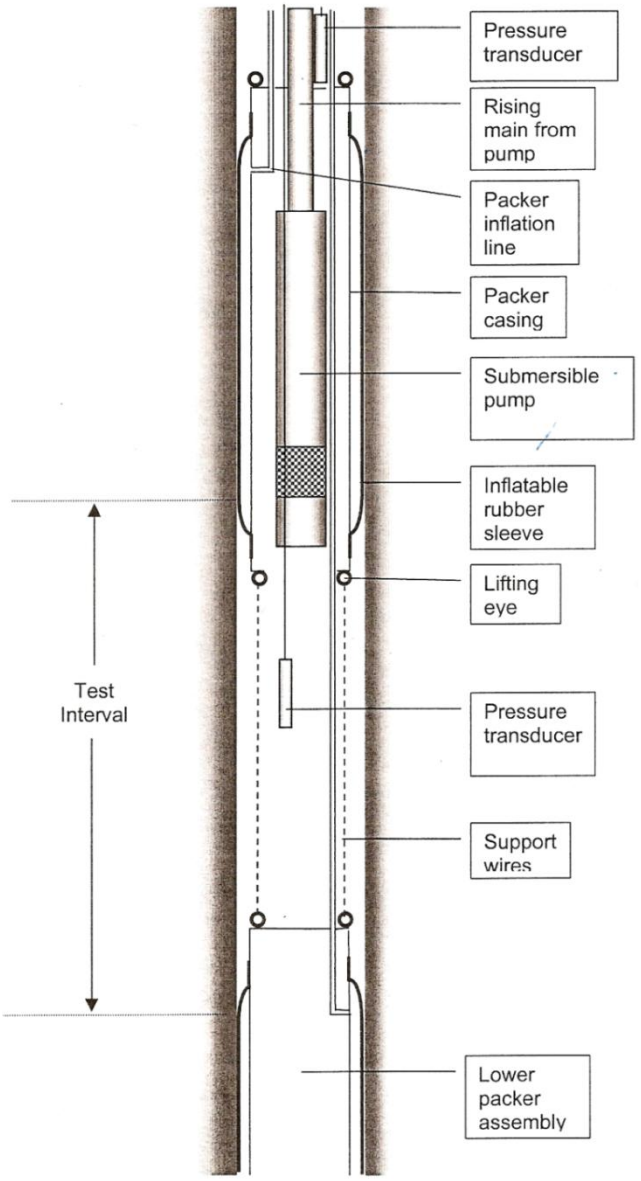

Figure 5.8: Schematic picture of the used dual packer system (Greswell, 1999).

The upper packer housed the submersible pump. The design was such that either of the two available Godwin pumps (1l/sand 5l/s) could be used without modification. Placing the pump within the packer would allow the system to be handled and installed more easily than in separate units. Stainless steel tie rods within the packer bodies were attached to lifting eyes. To these the support cables were tied that suspended the packer/pump module from the

surface. Altering the length of the support cable between the packers allowed the test interval between the packers to be modified. Air lines to inflate the packers, the rising main, the power cable for the pump and transducer cables ran through the plate of the top packer and had to be adequately sealed to prevent water flow. The inflated state was controlled by pressure gauges on the surface. A pressure of about 1 bar to 1.5 bar above the hydrostatic pressure on top of the tested interval was maintained with a compressor or compressed air and a decompression valve. The packer system was connected with a cable and a safety rope to a scaffolding frame above BH1 allowing the lifting of the system with an electric winch or by hand.

5.4.4 Discharge

During all pumping tests, the rising main consisted of one or several lengths of PVC lay-flat hoses with a diameter of 50 mm. Enough space was available during all test for the hose at the well head to bend gently on the surface, ensuring that the diameter of the hose was not reduced and the discharge of the pumped water was not disturbed or interrupted. In addition, 50mm lay-flat hoses were used for the discharge on the surface to a sewer. An analogue flowmeter was installed between the discharge hoses on the surface to measure the discharge rate. Throughout the pumping tests, the water was discharged through a sewer (see Figure 5.6) which discharged into the Bourn Brook River at the south boundary (at the western south gate) of the University Main Campus.

5.5 Pumping Test Setup

The purpose of undertaking pumping tests was to describe the aquifer characteristics and receive data for the transmissivity (T), hydraulic conductivity (K) and storage coefficient (S) of all aquifer layers approached by the test site. During all pumping tests, a packer was

installed in BH4 to interrupt the connection of S7 to S1 and S2, and vice versa. Fourteen pumping tests were carried out on the test site, between May to October 1999 and May to November 2000: Table 5.1 lists the pumping test details such as pumped well, discharge rate, packered section etc..

Table 5.1: Pumping test details of Test 1 to Test 14. Test 13 and 14 were pumped in two different wells with a section in BH1 being packered (see Figure 5.12).

Aquifer layer	Layer Thicknes	Test	Pumped Borehole	Discharge [m³/d]	Pumping time	Water Level Test Start	Packered section BH1		Pump position	Transducer position
							Top	Bottom		
S1 and S2	12.15m	1	BH2	62.99	2h 25min	7.92m bgl	0-60m bglm bgl		14.50m bgl	13.57m bgl
		13	BH2	199.58	178h	7.85m bgl	19.50-21.50m bgl	30.50-32.50m bgl	14m bgl	16.06m bgl
S2	5.5m	4	BH1	61.09	46 hours	8.67m bgl	19.50-21.50m bgl	26.50-28.50m bgl	21m bgl	13.19m bgl
		5	BH1	61.34	141h 45min	8.71m bgl	19.50-21.50m bgl	26.50-28.50m bgl	21m bgl	12.60m bgl
S3	6.5m	6	BH1	66.44	3h 54min	7.87m bgl	19-21m bgl	27.50-29.50m bgl	20.50m bgl	19.73m bgl
S5	5.5m	2	BH3	62.99	4h 25min	7.10m bgl	0-60m bglm bgl		36m bgl	17.84m bgl
		7	BH1	66.44	4h	7.06m bgl	30.50-32.50m bgl	38-40m bgl	32m bgl	32.72m bgl
		11	BH3	95.04	45min	7.10m bgl	not packerd		36m bgl	dipped
		13	BH3	61.34	308h	6.97m bgl	19.50-21.50m bgl	30.50-32.50m bgl	36m bgl	26.47m bgl
		14	BH3	61.34	119h	6.90m bgl	40-42m bgl	50-52m bgl	51.50m bgl	23m bgl
S6	9m	8	BH1	66.44	3h 45min	6.59m bgl	39.50-41.50m bgl	50.50-52.50m bgl	41m bgl	43.48m bgl
S7	8m	3	BH5	62.99	6h	6.91m bgl	0-60m bglm bgl		55m bgl	22.05m bgl
		9	BH1	252.95	20h	6.02m bgl	50-52m bgl		51.50m bgl	54.75m bgl
		12	BH5	246.24	25min	6.91m bgl	not packerd		55m bgl	30.31m bgl
		14	BH5	190.94	93.5 h	6.90m bgl	40-42m bgl	50-52m bgl	51.50m bgl	23.90m bgl
S1 to S7	53.07m	10	BH1	272.16	17h 30min	6.93m bgl	not packerd		35m bgl	13,25m bgl

Pumping Tests 1-3 were undertaken to receive hydraulic information of particular sandstone layers approached by BH2, BH3 and BH5 without having BH1 as connecting well of S1 to S7. To interrupt this connection, the “bigsock” was installed in BH1. The pump was placed in the middle of the slotted casing interval or the uncased interval of BH3 and BH5. Transducer monitored the test in BH2 to BH5. Figure 5.9 shows a schematic cross-section of the test site and setup of Pumping Tests 1-3.

Pumping Tests 4–9 were carried out in BH1 used as pumping well. The aim was to receive data of the aquifer characteristics of each sandstone layer, S1 to S7. Test 7 and Test 9 were undertaken during horizontal forced gradient tracer tests. The double packer system was used

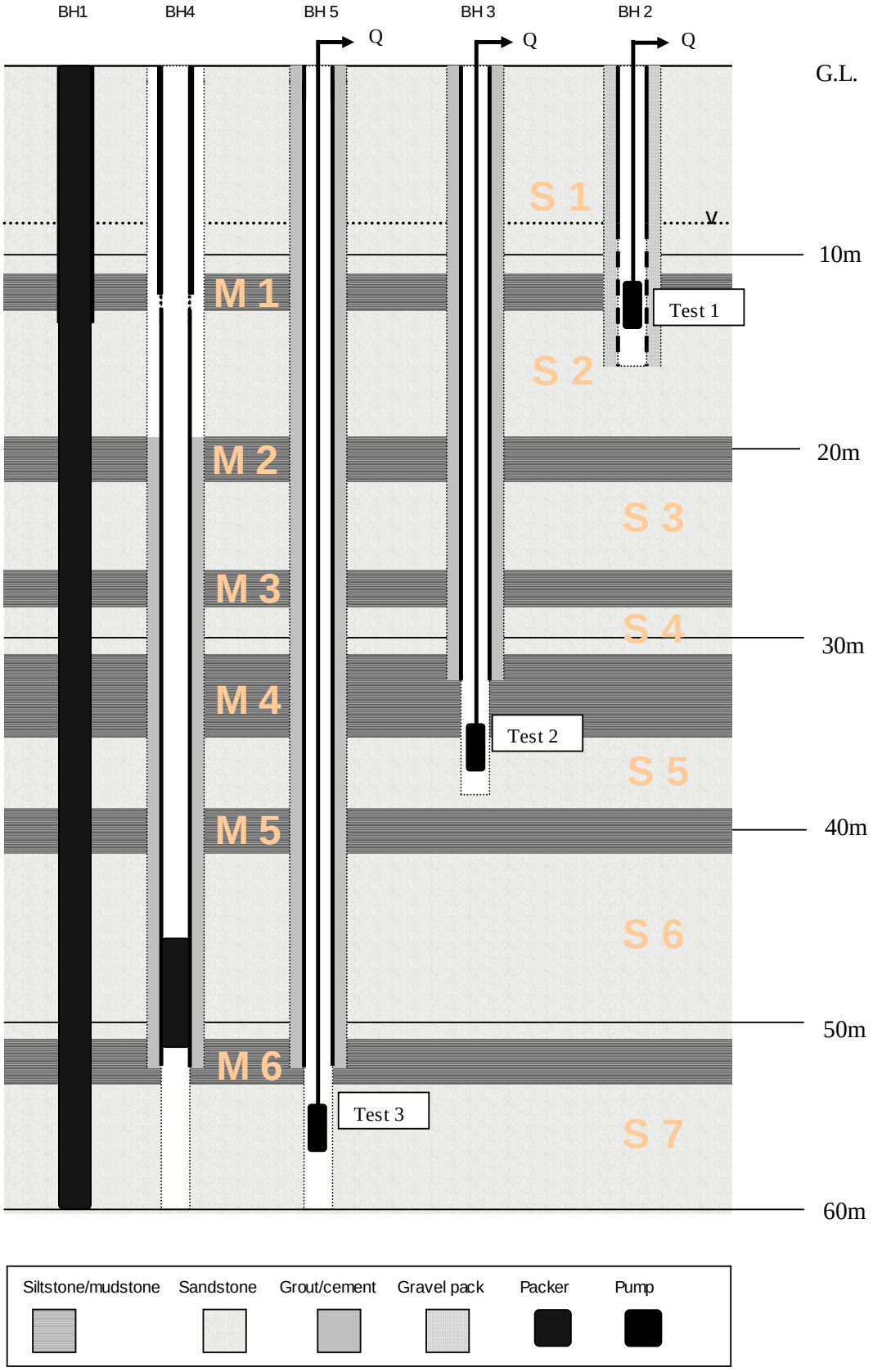

Figure 5.9: Schematic cross-section of the test site and the test setups of pumping tests Test 1 to Test 3.

to seal the mudstone layers at the top and at the bottom of the tested sandstone layer. In Tests 4, 5 and 9 only one packer of the double packer system was applied to seal to the bottom or to the top. Figure 5.10 shows a schematic setup of the tests with the location of the packers and the pumped section of the corresponding tests. The pump was installed in the upper packer of each test, apart from Tests 4 and 5 where the pump was hung into BH1 in the middle of S2. All pumping tests were monitored with transducers in the observation wells and in the pumping well with a transducer placed above, between and below the packered section. The pumping test of S4 failed, as the packers were set inappropriatly in BH1.

Pumping Tests 10, 11 and 12 were carried out without the application of packers. Test 10 pumped all aquifer layers at once in BH1 (Figure 5.11). Transducers monitored the test in all boreholes. Tests 11 and 12 were pumped only a few minutes in BH3 and BH5.

Pumping Tests 13 and 14 were set up so that water was abstracted in two wells (BH2 and BH3 or BH3 and BH5) and injected into a packered interval in BH1. The arrangement of packer and pump was chosen to run vertical tracer tests. The pump was placed in the middle of the slotted casing interval or the uncased interval of BH3 and BH5. Recharge occured through the top packer of the packered layer in BH1. Transducers monitored pressure changes in BH2, BH3, BH5 and BH1, above, between and below the packer. Figure 5.12 shows the setup of the corresponding pumping tests. Pumping two wells, it was tried to pump both wells at a similar pumping rates to avoid the creation of different gradients in the pumped layers. Due to the restrictions of equipment, the Godwin pump with a maximum pumping rate of 5 l/s was installed in BH 2 (Test 13) and BH5 (Test 14). To reduce the pumping rate of 5 l/s, in comparison to the other available pump with a pumping rate of 1 l/s, discharged water was diverted back into the pumping well where the 5 l/s pump was installed. To recharge the pumping well, water was just flushed through a hose at the top of the well.

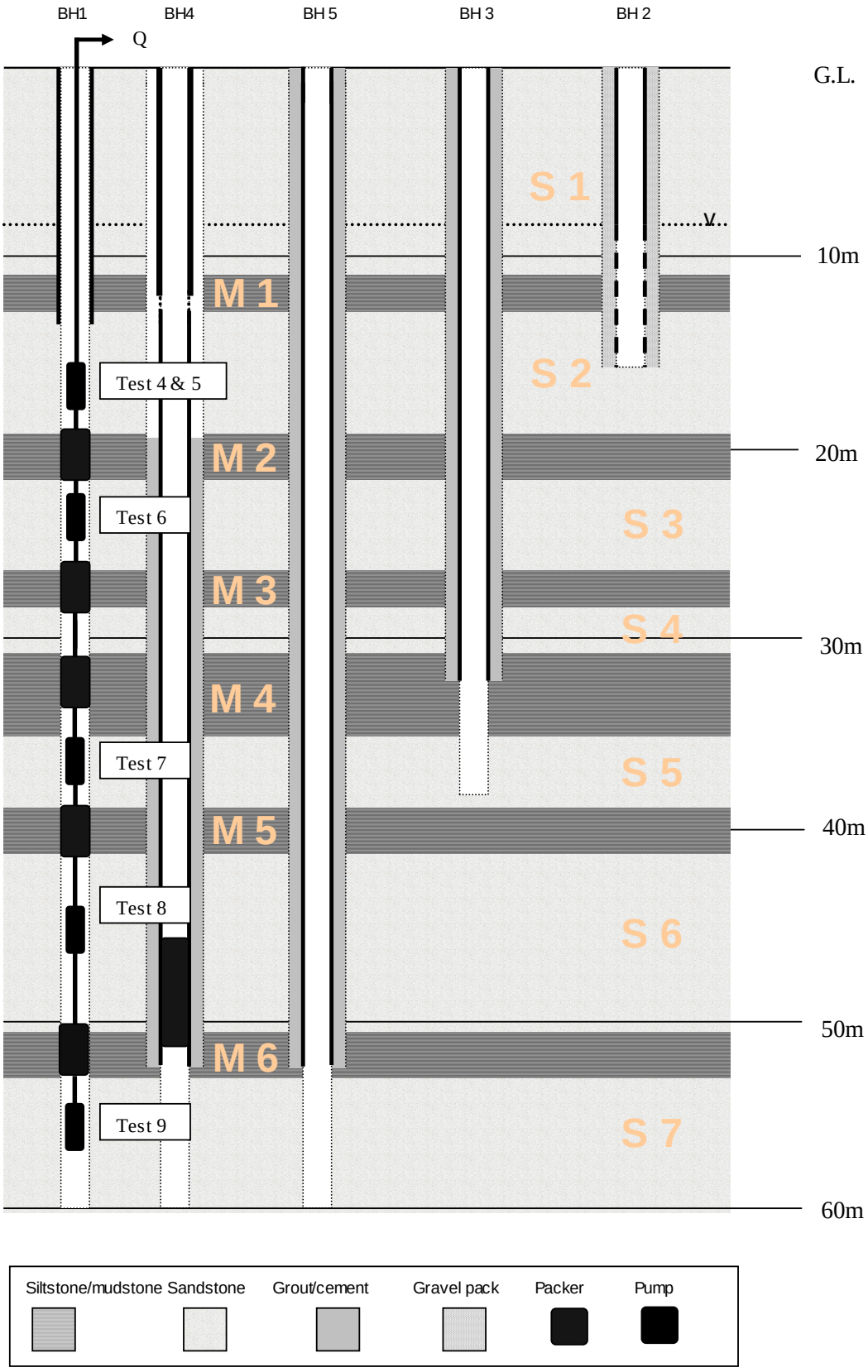

Figure 5.10: Schematic cross-section of the test site and the test setups of pumping tests Test 4 to Test 9. In Test 6 to Test 9, pumps were installed in the upper packer of the test layer.

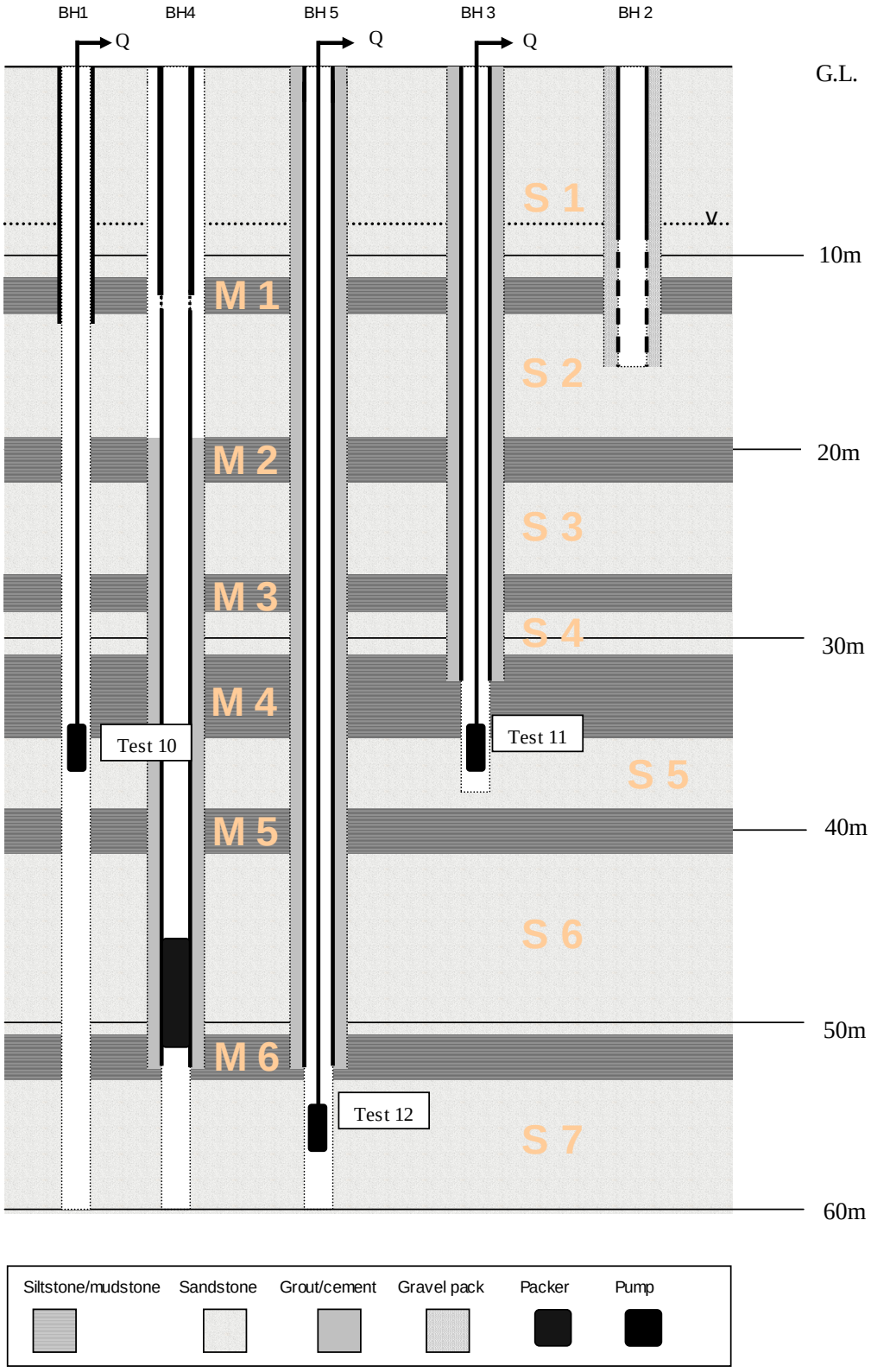

Figure 5.11: Schematic cross-section of the test site and the test setups of pumping tests Test 10, Test 11, and Test 12.

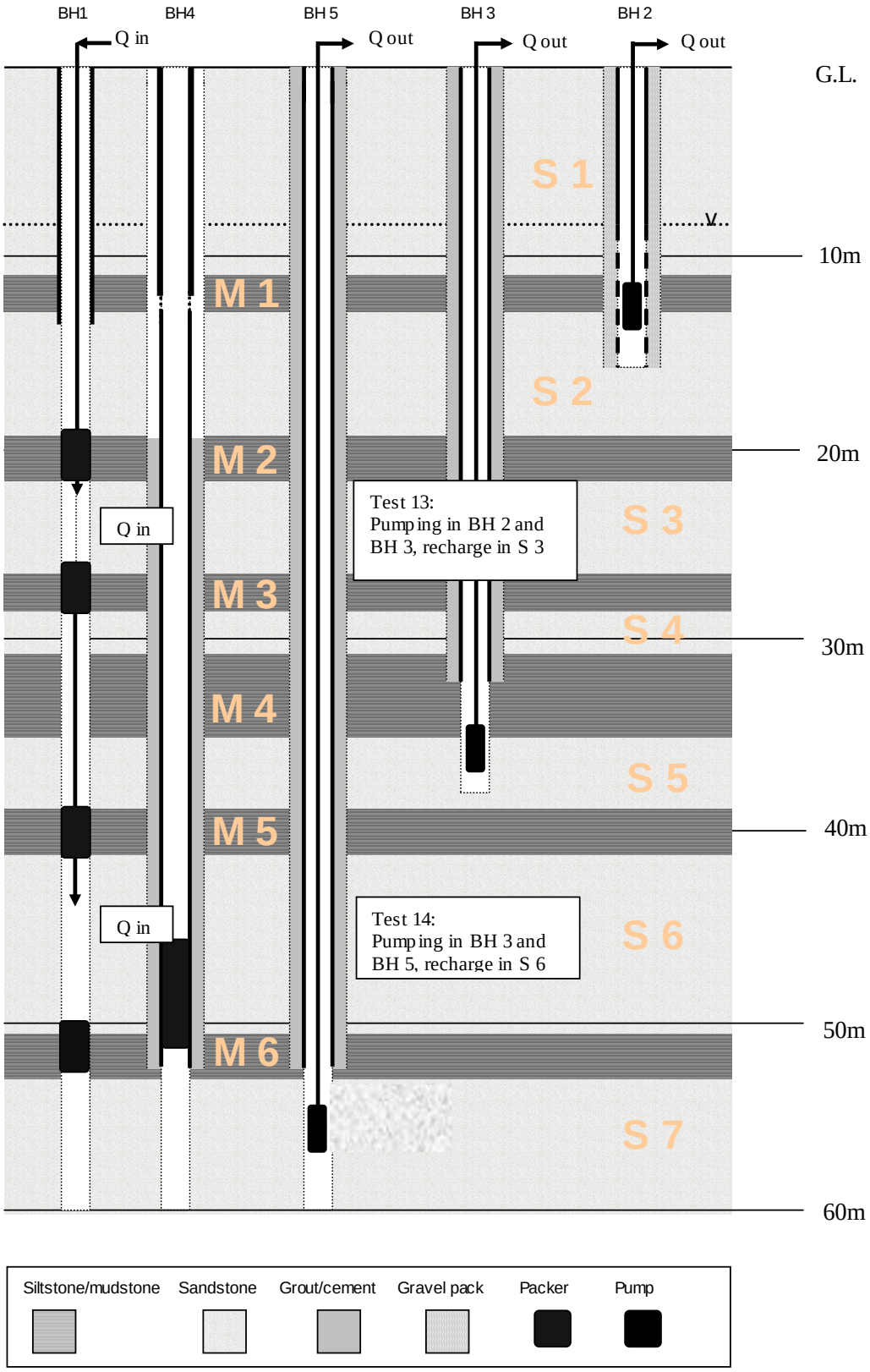

Figure 5.12: Schematic cross-section of the test site and the test setups of pumping tests Test 13, and Test 14.

5.6 Analysis of the Pumping Test

A detailed overview of analysing methods for pumping tests was given by Kruseman and de Ridder (1994). Two aquifer categories are distinguished: unconsolidated and consolidated. However, with respect to the test site, apart from the topmost unconsolidated unconfined aquifer layer only unconsolidated confined aquifer layers were expected. Figure 5.13 shows log-log and semi-log plots of the theoretical time-drawdown relationship which can be used to get a first estimation of the pumping tests conducted. In the following possible methods for the interpretation and effects for the interpretation of the performed pumping tests are described.

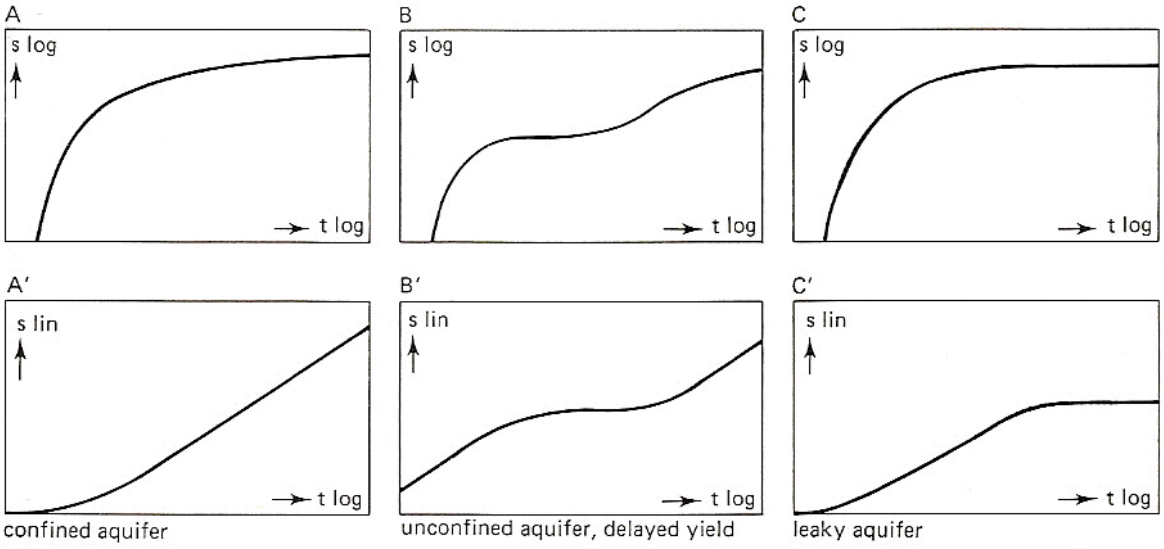

Figure 5.13: Log-log and semi-log plots of the theoretical time-drawdown relationships of unconsolidated aquifers: Parts A and A': Confined aquifer; Parts B and B': Unconfined aquifer; Parts C and C': Leaky aquifer (Kruseman and de Ridder, 1994)

5.6.1 Theis Method (1935)

Theis (1935) was the first to develop a formula for unsteady-state flow to a well taking into consideration the aquifer storativity, radial distance, and time in function. Theis also

introduced the ‘curve-fitting method’ to determine aquifer storativity and transmissivity from time-drawdown response. The assumptions and conditions underlying the Theis equation are:

1) The aquifer is confined.
2) The aquifer has a seemingly infinite areal extent.
3) The aquifer is homogeneous, isotropic, and of uniform thickness over the area influenced by the test.
4) Prior to pumping, the piezometric surface is horizontal over the area influenced by the test.
5) The pumping well discharge rate is constant.
6) The pumping well penetrates the entire thickness of the aquifer, inducing horizontal flow towards the well.

The unsteady-state equation (or Theis equation) can be expressed as:

$$s = \frac{Q}{4\pi KD} W(u), \qquad \text{(Equation 5.14)}$$

s is the drawdown (m) measured in an observation well at a radial distance r (m) from the pumping well .

Q is the constant discharge (m^3/day) of the abstraction well

KD is the transmissivity (m^2/day), where K is the hydraulic conductivity (m/d) and D (m) is the uncased and not grouted length of the pumped well.

where S is the aquifer storativity (dimensionless)

$$S = \frac{4KDtu}{r^2}$$ (Equation 5.15)

and t is the time since the start of pumping (in d=days as applied in this thesis).

The well function or Theis well function of u is an exponential integral:

$$W(u) = \int_u^{\infty} \frac{e^{-y}dy}{y}$$ (Equation 5.16)

W is a function of u [expressed W(u)] (Kruseman & de Ridder, 1994) and indicated as "dimensionless drawdown" and "dimensionless time".

As $\frac{Q}{4\pi KD}$ in equation 5.14 and $\frac{4KD}{S}$ in equation 5.15 are constant, the relation of log s and $\log(r^2/t)$ is similar to the relation between log W(u) and log(u). Plotting s against r^2/t and W(u) against u on the same log-log paper, the resulting curves will be of the same shape. By matching the data curve and the type curve, the coordinates of an arbitrary matching point are the related values of s, r^2/t, u and W(u) to calculate KD and S. Instead of using the "normal type curve", it is more convenient to apply the "reversed type curve" and plot W(u) against 1/u and s versus t/r^2. The assumptions and conditions underlying the Theis equation apply for Theis's curve-fitting method. In addition, the following condition is required: that the flow of the well is in unsteady state, i.e. the drawdown differences with time are not negligible, nor is the hydraulic gradient constant with time.

5.6.2 Jacob's Method

The Jacob method (Cooper and Jacob, 1946) is based on the Theis formula: Jacob's straight-line method can be applied for the following three situations:

1. r = constant
2. t = constant
3. t/r^2 are used in the data plot

However the following assumptions and conditions should be satisfied:

1. The assumptions listed for pumping tests as for Theis (1935)
2. The flow to the well is in unsteady state
3. The values of u are small $(u < 0.01)$, i.e. r is small and t is sufficiently large.

Krusemann and de Ridder (1990) visually inspected the graphs in the range of $u < 0.01$ and $u < 0.1$ and concluded that it is impossible to indicate precisely where field data start to deviate from the straight line relationship. For practical purposes they suggest using values of $u < 0.1$ as a condition for Jacob's method. Due to the conditions Jacobs only considers late time drawdown data.

5.6.3 Leaky Aquifers

Leaky aquifers are more usual in Triassic Sandstone aquifers than perfectly confined or unconfined aquifers. As shown in Figure 5.13, three general principle facies types with different hydrostratigraphy (Weber and van Geuns, 1990) can be expected for the Triassic Sandstone. For the University Test Site, we assume a layered model, as described in Chapter 4. Leaky aquifer can be generally described as aquifer, overlying and/or underlying by a mudstone which is usually leaking to some extent. When the well in the confined aquifer is pumped, the hydraulic head will drop and create a hydraulic gradient not only in the pumped

confined aquifer, but also in the aquitards confining the aquifer. The induced flow is assumed to be horizontal in the aquifer and vertical in the aquitard.

The assumptions and conditions underlying the methods for leaky aquifers as described by Kruseman and de Ridder (1990) are:

1) The aquifer is leaky.
2) The aquifer has a seemingly infinite areal extent.
3) The aquifer and the aquitard are homogeneous, isotropic, and of uniform thickness over the area influenced by the test.
4) Prior to pumping, the piezometric surface is horizontal over the area influenced by the test.
5) The aquifer is pumped at a constant discharge rate.
6) The pumping well penetrates the entire thickness of the aquifer and thus receives water by horizontal flow.
7) The flow in the aquitard is vertical.
8) The drawdown in the unpumped aquifer (or in the aquitard, if there is no unpumped aquifer) is negligible.

And for unsteady-state conditions it is assumed that:

9) The water removed from storage in the aquifer and the water supplied by leakage from the aquitard is discharged instantaneously with decline of head.
10) The diameter of the well is very small, i.e. the storage in the well can be neglected.

5.6.4 Walton's Method

Walton (1962) describes the drawdown in a leaky aquifer under the consideration that the effects of aquitard storage are negligible (Hantush and Jacob 1955). The method can be used

if the assumptions and conditions listed for leaky aquifers are satisfied and if the following assumptions and conditions are fulfilled:

1) The flow in the well is in an unsteady state;
2) The aquitard is incompressible and changes in the aquitard storage are negligible.

The unsteady-state equation (or Theis equation) can be expressed as:

$$s = \frac{Q}{4\pi KD}\int_{u}^{\infty}\frac{1}{y}\exp(-y-\frac{r^2}{4L^2y})dy \qquad \text{(Equation 5.17)}$$

or

$$s = \frac{Q}{4\pi KD}W(u, r/L), \qquad \text{(Equation 5.18)}$$

with

$$u = \frac{r^2 S}{4KDt} \quad . \qquad \text{(Equation 5.19)}$$

Walton (1962, in Kruseman and de Ridder, 1994) developed a modification of the Theis curve-fitting method. Instead of using one type curve, Walton uses a type curve for each value of r/L where the leakage factor L is

$$L = \sqrt{KDc} \qquad \text{(Equation 5.20)}$$

with

$c = D'/K'$ the hydraulic resistance of the aquitard in [d] (Equation 5.21)

and with

D' the saturated thickness of the aquitard in [m]

K' hydraulic conductivity of the aquitard for vertical flow in [m/d].

5.6.5 Unconfined Aquifers

The pumping of an unconfined aquifer underlain by an aquiclude, causes a dewatering of the aquifer and creates a cone of depression in the water table. As the length of the pumping test is increased, the flow towards the well shows clear vertical components. The three major differences between pumped unconfined and confined aquifers are (Kruseman and de Ridder, 1990):

1. A confined aquifer is not dewatered during pumping, but remains fully saturated and the pumping process creates a drawdown in the piezometric surface.
2. The pumped water of a well in a confined aquifer comes from the expansion of the water in the aquifer due to reduction of the water pressure, and from the compaction of the aquifer due to increased effective stresses.
3. The flow in a confined well is and remains horizontal, provided that the well is a fully penetrating one. No vertical flow components occur in such an aquifer.

According to Kruseman and de Ridder (1990), for pumped unconfined aquifers which do not show a delayed watertable response, the time-drawdown curve only follows the late-time segment of the S-shaped curve at this stage. The response to pumping has entered the third phase or the unconfined response (Allen et al., 1997) and approximates to the Theis curve. Because the flow pattern around the well is identical to that of an unconfined aquifer, the Theis method (1935) and the Jacobs method (Cooper and Jacob, 1946) can be used to interpret the pumping tests.

5.6.6 Single-Well Tests

Single-well tests are tests with no observation wells or piezometers available or used. The water-level change during the pumping test is measured only in the pumped well itself. The drawdown in the pumped well is influenced by well losses, skin effect and well-bore storage.

Well losses are separated into linear and non-linear head losses. Linear well losses are caused during the drilling and construction of the well, as head losses due to compaction of the aquifer material during drilling, due to plugging of the aquifer with drilling mud, head losses in the gravel pack and head losses in the screen. Non-linear well losses are friction losses, occurring inside the well and the rising main or suction pipe where the flow is turbulent, and head losses, occurring in the zone adjacent to the well where the flow is usually turbulent (Krusemann and de Ridder, 1990). These well losses cause a greater drawdown in the well than expected on theoretical grounds. The concept of "skin effect" describes the head losses in the vicinity of a well. It is assumed that the head losses are concentrated in a thin, resistant skin against the wall of the borehole. A positive skin effect is measured if the effective radius of the well is larger than the real radius of the borehole. A negative skin effect is measured if the well is poorly developed or its screen is clogged (De Marsily, 1986). A more detailed discussion of effects in well during pumping tests is given by Driscoll (1995).

In the hydraulics of well flow, the well-bore storage can be neglected, as the well is considered to be a line source or line sink with an infinitesimal radius. However, in reality wells have finite radius and thus a certain storage volume. Well-bore storage effects exist if the early-time drawdown (drawdown versus pumping time) plot is a unit-slope straight line in a log-log plot. Papadopulos and Cooper (1967) observed that the influence of well-bore storage on the drawdown decreases with time. Well-bore storage becomes negligible at

$$t > \frac{25 r_c^2}{KD}$$ (Equation 5.22)

where r_c the radius of the unscreened part of the well

The bigger T gets, the smaller t becomes and the earlier well-bore storage becomes negligible.

Table 5.2 gives example calculations for t if the well-bore storage becomes negligible.

Table 5.2: Example calculations applying equation 5.20 to calculate t if the well-bore storage becomes negligible (Papadopulos and Cooper, 1967). r of BH 1 to BH 5 is applied. For T a lower value of 20 m²/d and a higher value of 140 m²/d were taken into consideration.

	BH1	BH2- BH5	BH1	BH2- BH5
r [m]	0.1016	0.0625	0.1016	0.0625
KD [m²/d]	20	20	140	140
t > [d]	0.013	0.0049	0.0018	0.0007

5.6.7 Analyse of Pumping Tests with Curve-Fitting Methods

In the following, the drawdown data of the pumping tests were analysed with curve-fitting methods applying the student version of AquiferWin32 (Version 1.06, 1997 by Environmental Simulations, Inc. (ESI) developed by J. and D. Rumbaugh). Curve-fitting was possible with the non-linear least-squares technique when it was considered to be reasonable, using an application offered by Aquifer Win 32. Otherwise, manual curve-fitting was processed in Aquifer Win32. Each test is discussed with reference to the relevant aquifer or sandstone layer in which the test was conducted. Table 5.2 lists the results of the curve-fitting analysis and the calculated values for T, K and S.

5.6.7.1 Sandstones Layer S1 and S2

S1, S2 and M1 were approached by BH2 where Test 1 and Test 13 were carried out. As there was no appropriate analytical solution derived for a multilayered aquifer system with an

unconfined top layer and a confined bottom layer separated by an aquitard, an attempt was made to analyse Test 1 and Test 13 with the Theis method (1935). For the interpretation, the following assumptions were made: First of all, S1, M1 and S2 were one aquifer and the layers were pumped in BH2 together. Secondly, S2 was fully penetrated by BH2, and thirdly, S1, M1 and S2 were acting as a confined aquifer with a horizontal flow towards the well.

Figure 5.14 shows the curve fitting result of Test 1 after Theis (1935). Even though the optimized curve-fitting method in AquiferWin32 was applied, the Theis curve and the drawdown curve of Test 1 do not match very well. The observation wells BH4 and BH5 in Test 1 showed no response to the abstraction.

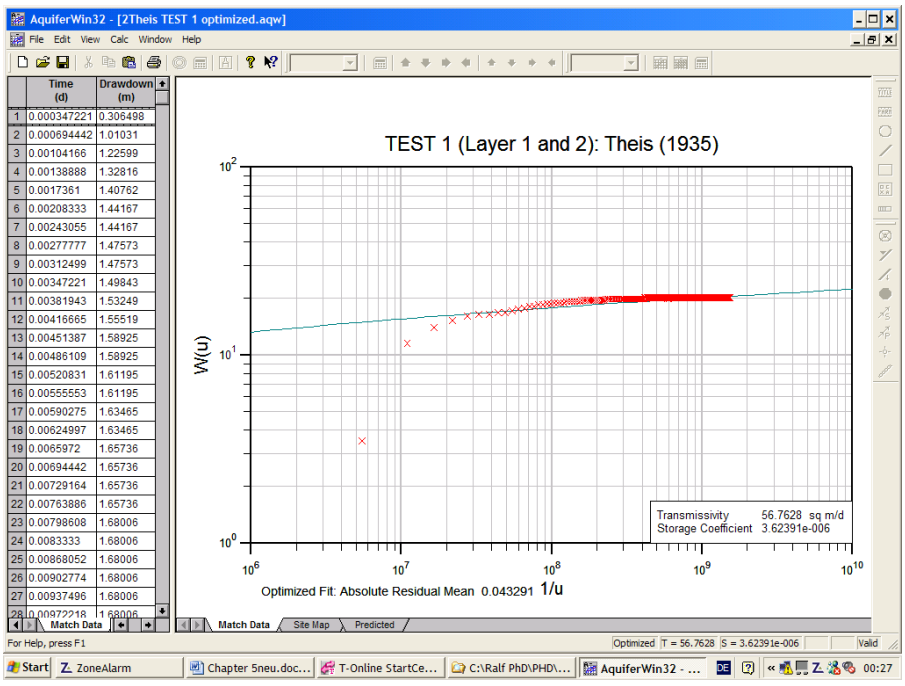

Figure 5.14: Interpretation of Test 1(in S1 and S2), using the Theis method (1935). The residual mean of the optimised fit was 0.043 m (ESI, 1997).

After 6 minutes, the drawdown increased again and a delayed yield was recorded. Water in layers S1 and S2 seemed not to have been discharged instantaneously at the same rate over both layers for the first minutes. However, after 6 minutes the drawdown increased again and towards the end of the test the drawdown curve flattened, getting a shape similar to those of

the drawdown of leaky aquifer. The interpretation of Test 13 was made under the same assumptions and conditions as for Test 1. However, due to the test setup in which BH2 was pumped and water was injected into the well again (see Chapter 5.5) the early-time drawdown oscillated continously towards the end of the tests. Figure 5.15 shows the curve fitting of Test 13 with Theis (1935).

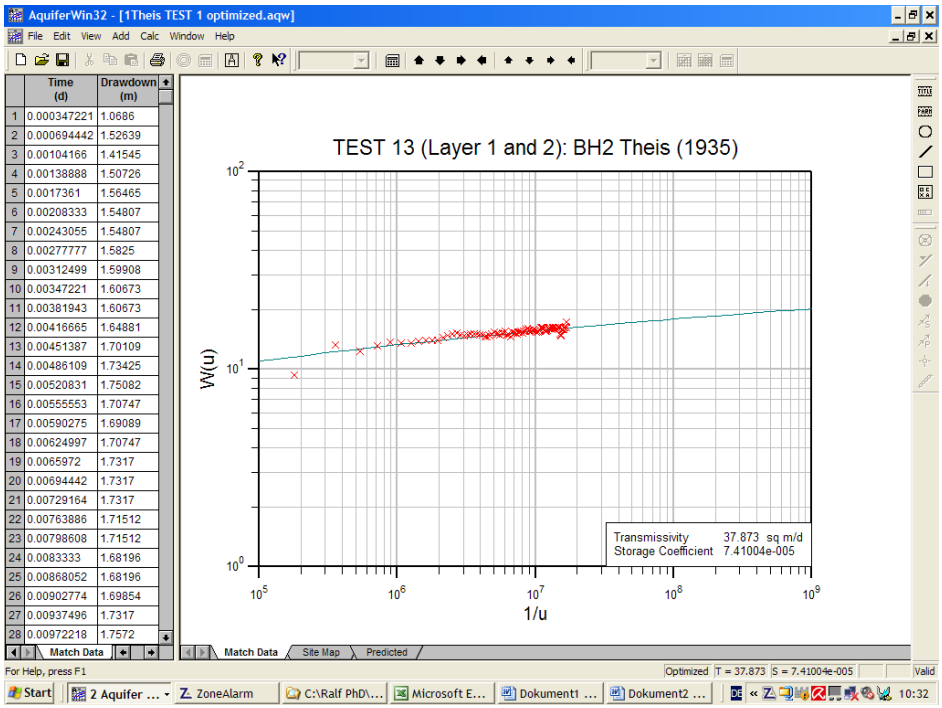

Figure 5.15: Interpretation of Test 13 using the Theis method (1935). The residual mean of the optimised fit was 0.032 m (ESI, 1997).

Comparing the interpretations of Test 1 and Test 13, the curve fitting of the Theis method (1935) with the drawdown data of Test 13 seems to fit in a better way than the data of Test 1. The storativity S of Test 13 is realistic, compared to the results of Test 1, and within a realistic range given by Kruseman and de Ridder (1994). However, the calculated T and S values of Test 13 have to be regarded carefully, due to the test setup. Test 1 does not fit well with Theis (1935) as late time drawdown data show “severe” effects of leakage (Kruseman and de

Ridder, 1994). Unfortunately, they do not fit with Walton (Hantush and Jacob, 1955), either, considering leakage.

5.6.7.2 Sandstone Layer S2

Test 4 and Test 5 were conducted in sandstone layer S2. BH1 was used as abstraction well. The pumped section of BH1, the section below the packer in BH1, and observation well BH4 were monitored with transducers, but showed only response within 5 to 10 cm. BH2 was not monitored as it was used for tracer injection and the transducer signal was disturbed by other electrical equipment on site. This caused also disturbance of the first three drawdown measurements (90 seconds) during the test which could not be consider for later analysis.

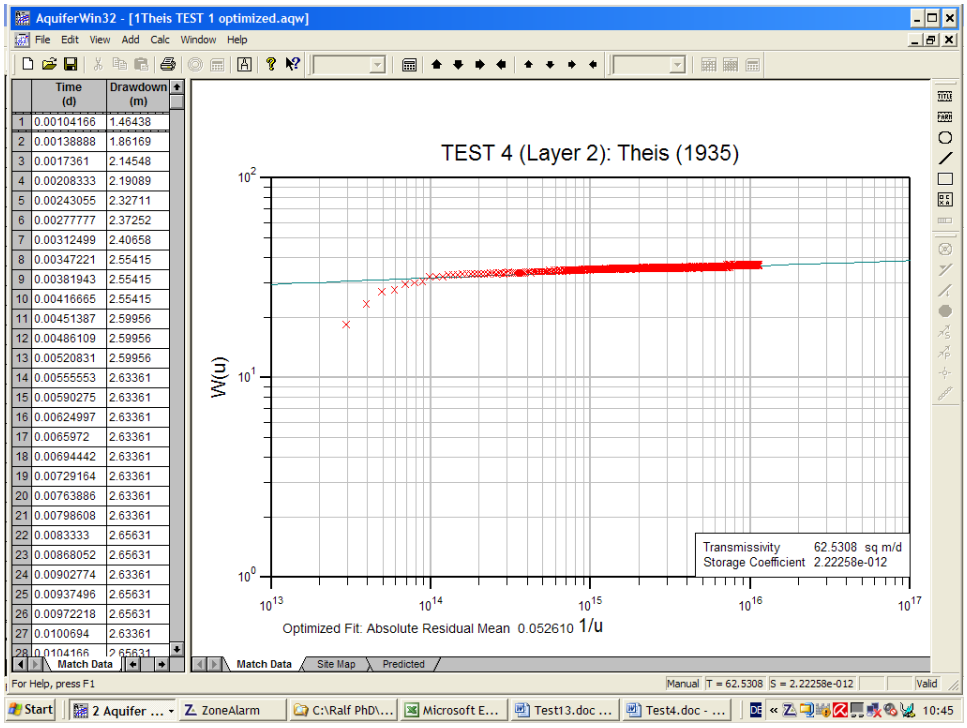

Figure 5.16: Interpretation of Test 4 using the Theis method (1935). The residual mean of the optimised fit was 0.053 m (ESI, 1997).

As leaky conditions were expected, it was tried to use fitting methods for leaky aquifers after Hantush (1960) and Walton (Hantush and Jacob, 1955). However, no fit could be generated. Therefore, Theis (1935) curve-fitting method was used to analyse Test 4 and 5. Only the analysis for Test 4 gave a fit for the late-time drawdown data (Figure 5.16), delivering a reasonable transmissivity value. The calculated value for the storage coefficient is very small but realistic compared to values given by Kruseman and de Ridder (1994).

5.6.7.3 Sandstone Layer S3

The interpretation of Test 6 with the Theis curve fitting methods for confined aquifers (Theis, 1935) is shown in Figure 5.17. The observation wells show nearly no drawdown. Applied curve fitting methods for leaky aquifers after Hantush (1960) and Walton (Hantush and Jacob, 1955) do not fit with the drawdown data of the test.

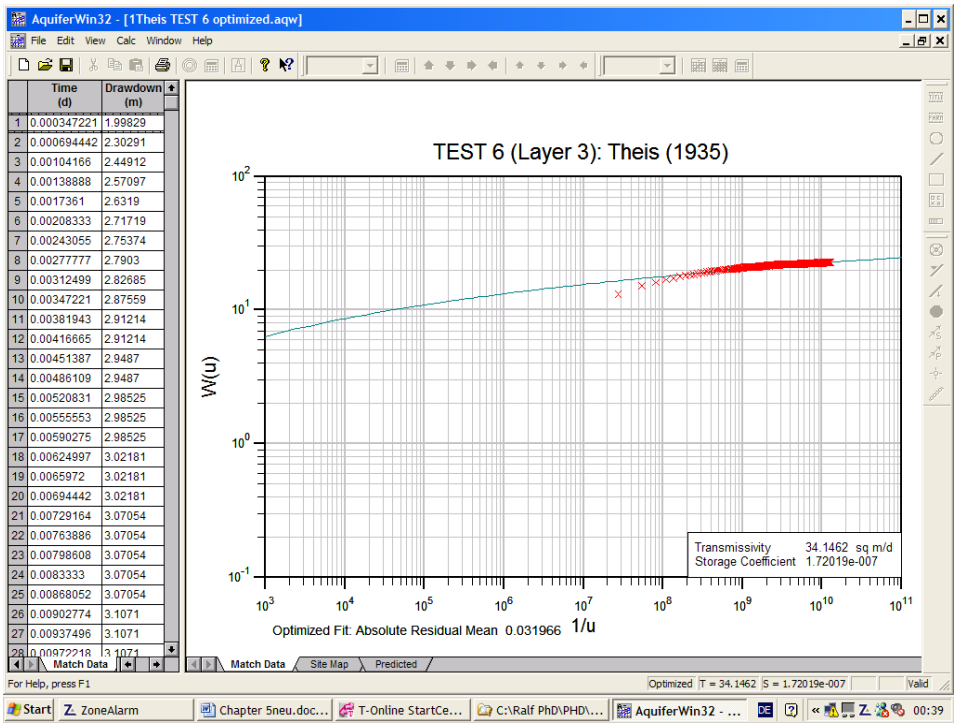

Figure 5.17: Interpretation of Test 6 using the Theis method (1935). The residual mean of the optimised fit was 0.032 m (ESI, 1997).

As described for Test 4, only the late-time drawdown data gave a reasonable optimized fit, delivering a transmissivity value.

5.6.7.4 Sandstone Layer S5

Sandstone layer S5 was approached on the test site by BH1 and BH3. Three pumping tests were carried out in S5:

- Test 2 was processed in BH3.
- Test 7 was undertaken in BH1 (S5 packered) with BH3 used as observation well.
- Test 10 was undertaken in BH1 (not packered) with BH3 as observation well.

Test 2 showed no fit using Waltons or Theis-Method (1935). Figure 5.17 shows the curve-fitting of the drawdown data of the pumped well BH1 of Test 7 with Theis (1935). The initial drawdown after the first measurement is 6.21 m. For the first 7 minutes, the drawdown increased slowly and plotted nearly as a straight line. After 7 minutes, the drawdown increased again. With the first drawdown record well-bore storage was measured followed by "leakage effects" of the pumped section, possibly because of negative skin effects caused by a poorly developed layer S5 in BH1. As a section of BH3 was possibly clogged, the drawdown increased again. Clogging of S5 in BH1 was slightly removed during the test and the drawdown increased only slightly towards the end of the test. The late time drawdown neither fit with the method of Papadopulos and Cooper (1967), considering well-bore storage, nor with Walton (1962, Hantush and Jacob 1955). The best fit was with Theis (1935), as shown in Figure 5.18, giving reasonable values for T and S.

Figure 5.19 shows the curve-fitting for the observation well BH3 of Test 7 with Walton (1962; Hantush and Jacob 1955), giving reasonable values but smaller values for T and S, compared to Figure 5.18.

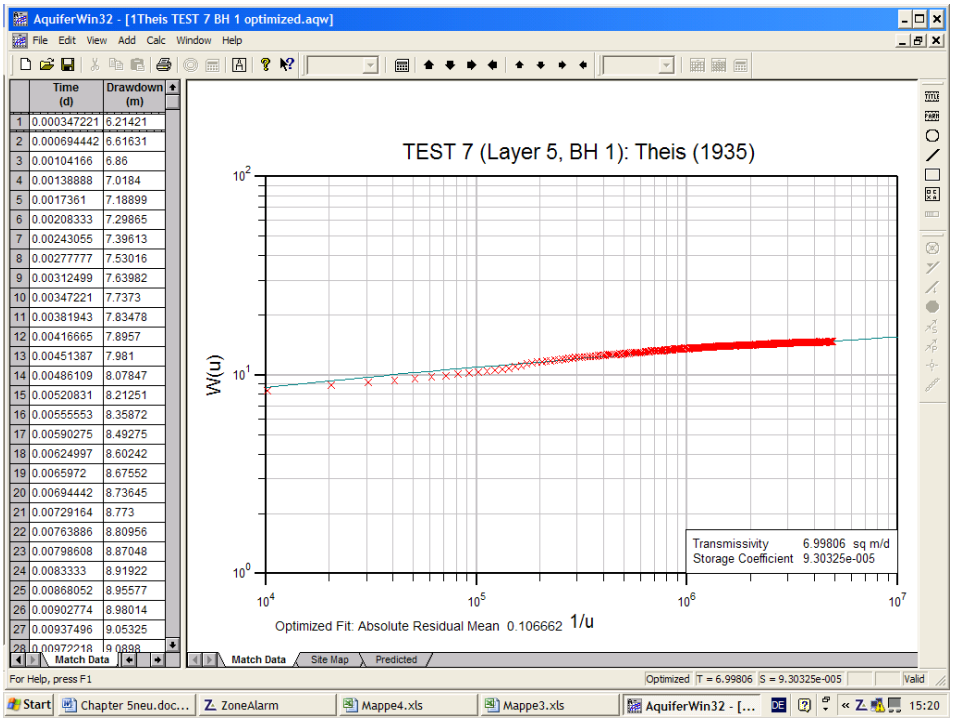

Figure 5.18: Interpretation of Test 7 using the Theis method (1935) for drawdown data of BH1. The residual mean of the optimised fit was 0.106 m (ESI, 1997).

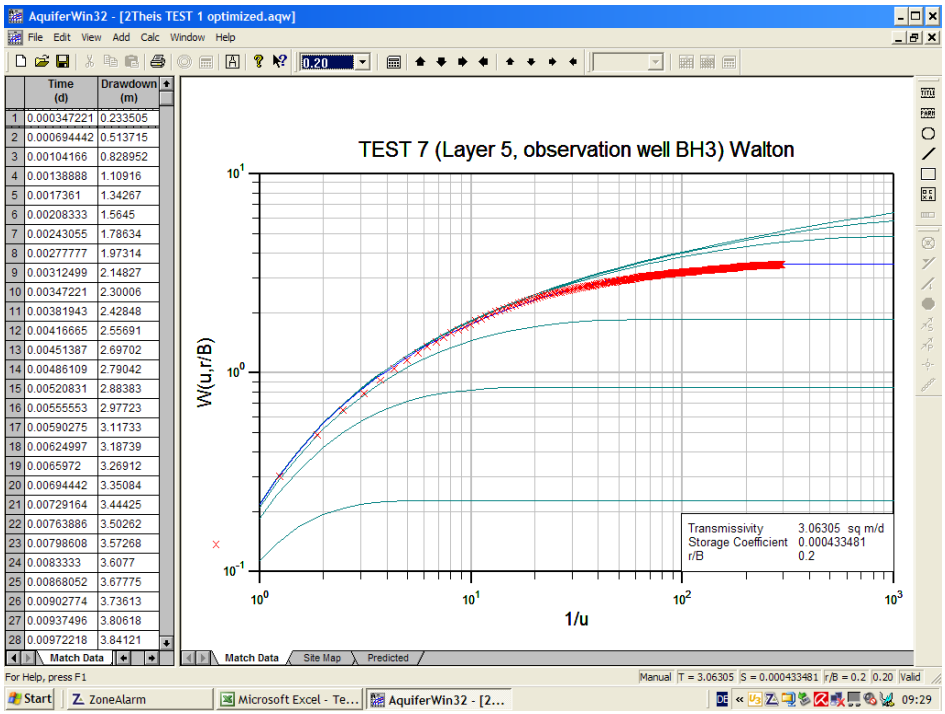

Figure 5.19: Interpretation of Test 7 observation well BH3, using the method of Walton (1962; Hantush and Jacob 1955). The residual mean of the optimised fit was 0.046 m (ESI, 1997).

The analysis of Test 10 with the drawdown data collected from observation well BH3, applying Theis method (1935) is shown in Figure 5.20. The first drawdown record was made after 5.5 minutes, as the connection to the transducer was interrupted when the test was started. However, the drawdown data show the best fit with the Theis (1935) compared to the the curve-fitting results of the observation well BH3 of Test 5.

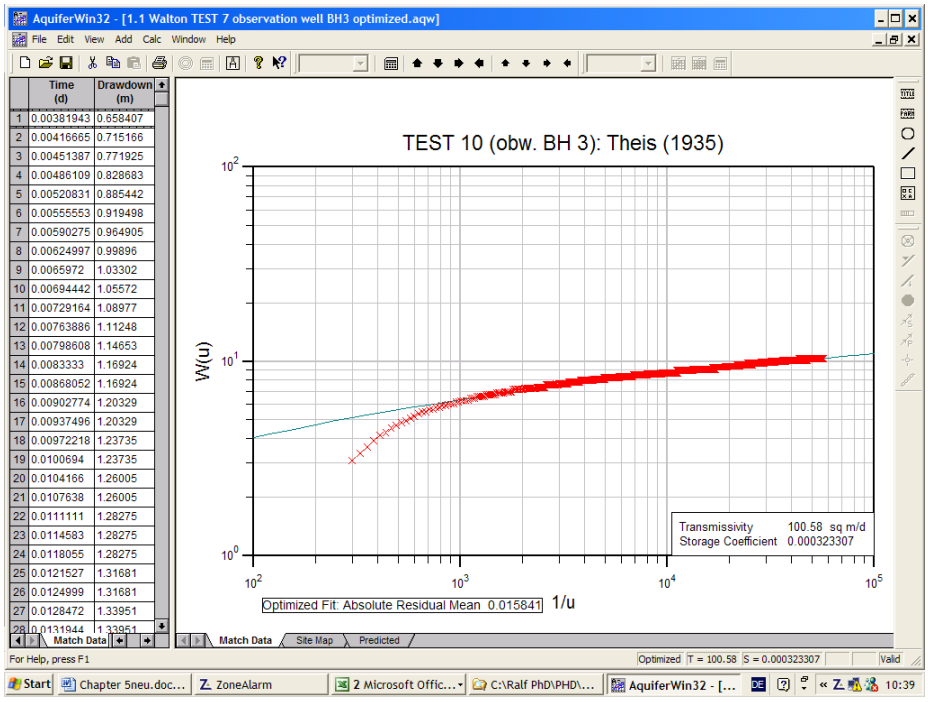

Figure 5.20: Interpretation of observation well BH3, Layer 5, Test 10 using the method of Theis (1935). The residual mean of the optimised fit was 0.016 m (ESI, 1997).

5.6.7.5 Sandstone Layer S6

Test 8 was conducted in BH1, exploring aquifer layer S6. The late-time drawdown data flatten and leaky conditions, but the fit with Walton was not successful. The test was analysed with Theis method (1935) and the applied curve fitting is shown in Figure 5.21.

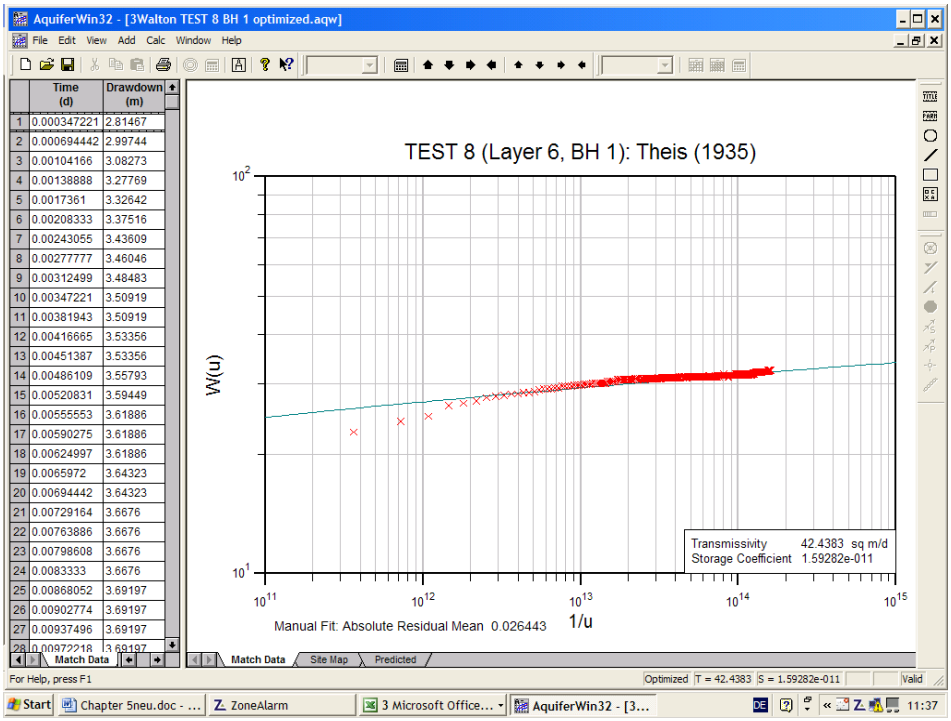

Figure 5.21: Interpretation of Test 8 using Theis method (1935). The residual mean of the optimised fit was 0.026 m (ESI, 1997).

5.6.7.6 Sandstone Layer S7

Sandstone layer S7 was approached by BH1 and BH5. Test 9 and Test 14 were carried out in BH1 as pumping well. Test 3 was processed in BH5.For the interpretation of sandstone layer S7, it should be considered that the aquifer was partially penetrated by BH1 and BH5. Only the top boundary of S7 was identified. The results of Test 3 could not be matched with available curve-fitting methods. Test 9 matched not well with Theis (1935) or Walton. The best curve-fit could be gained with the results of Test 14, using the Theis (1935) and Waltons (1962) curve-fitting method. However, both methods delivered unrealistic values calculated for S (see Figure 5.22 and 5.23 for Test 14). The drawdown values oscillated during the whole tests, as the pumping rate of the installed pump with a maximum pumping rate of 5 l/s was reduced with a valve to a pumping rate of 2.2 l/s. The oscillation was caused by the pump, as it pumped against the valve with inconsistent rates trying to maintain its maximum pumping rate (the pump had to be repaired after Test 14).

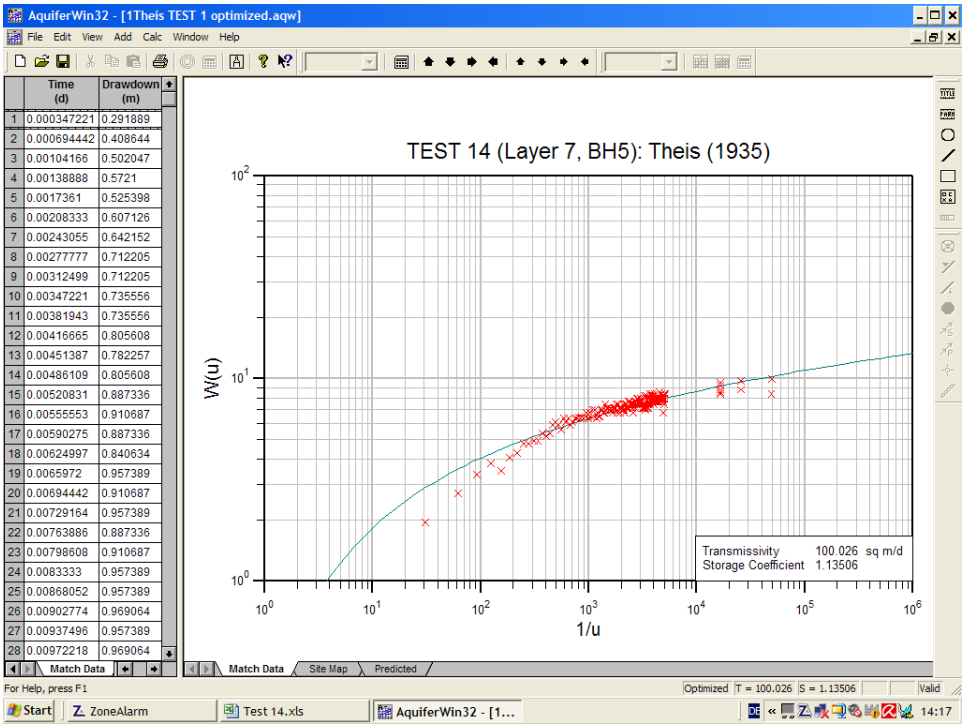

Figure 5.22: Interpretation of Test 14 using the Theis method (1935). The residual mean of the optimised fit was 0.027 m (ESI, 1997).

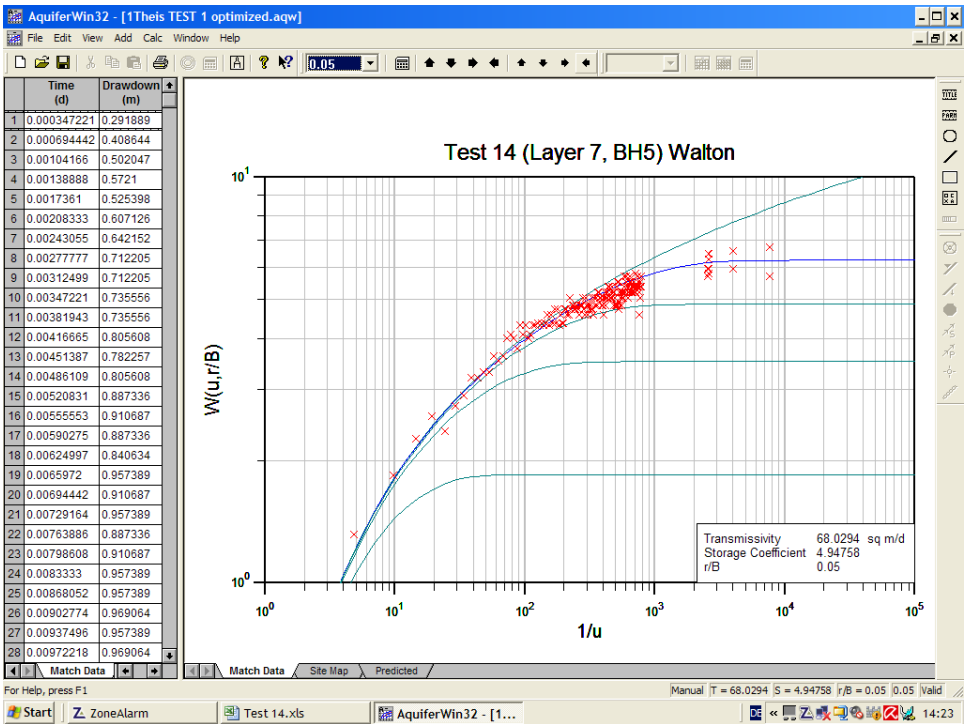

Figure 5.23: Interpretation of Test 14, using the method of Walton (1962; Hantush and Jacob 1955). The residual mean of the optimised fit was 0.026m (ESI, 1997).

5.6.7.7 All Sandstone Layers (S1 - S7)

In Test 10, water was abstracted from borehole BH1 with no application of packers other than in BH4. S1 to S7 were pumped together, BH2, BH3 and BH5 were used as observation wells. The drawdown data of the pumping well BH 1 were analysed using the Theis method (1935) and Jacob's method (Cooper and Jacob, 1946). The latter was applied since the calculated value for S with Theis (1935) was small (Figure 5.24 and 5.25).

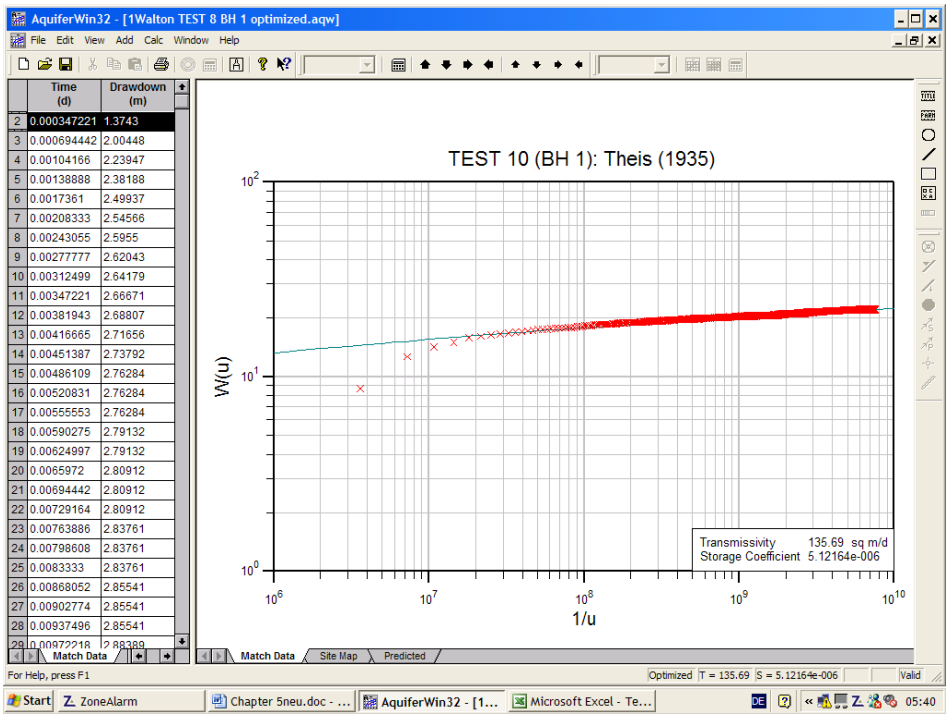

Figure 5.24: Interpretation of Test 10 using Theis (1935). The residual mean of the optimised fit was 0.014 m (ESI, 1997).

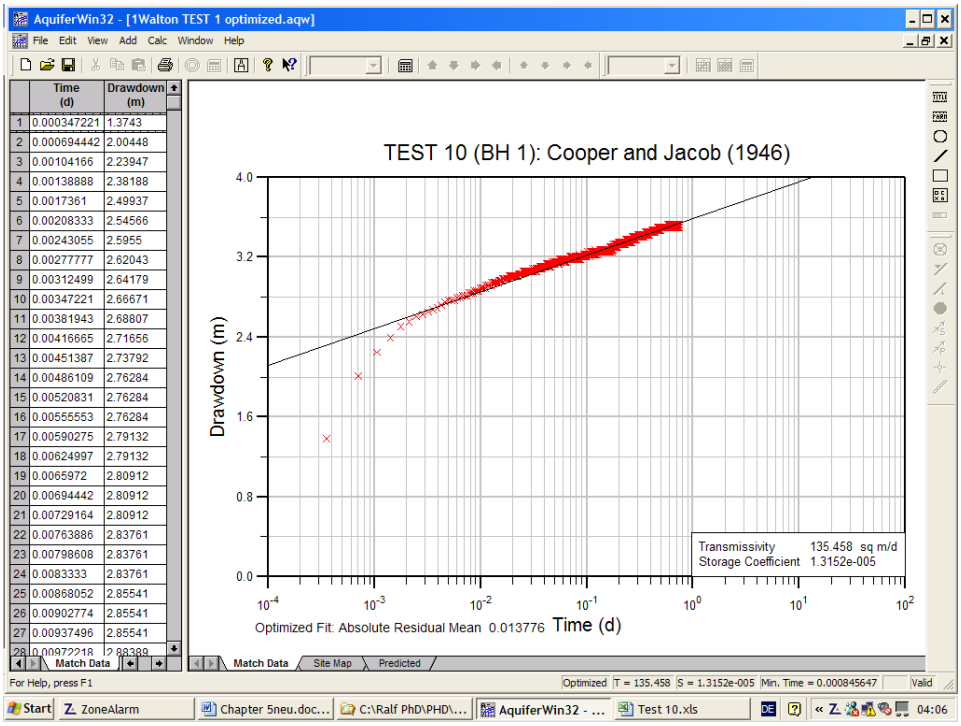

Figure 5.25: Interpretation of Test 10 using Copper and Jacob (1946) straight line method. The residual mean of the optimised fit was 0.014 m (ESI, 1997).

5.7 Conclusion of the Pumping Tests

Pumping tests were undertaken and curve-fitting methods of Theis (1935), Walton (1962; Hantush and Jacob, 1955) and Jacob ("Jacob's method", Cooper and Jacob, 1946) were applied successfully. Aquifer characteristics could be determined for the aquifer layers S1 to S7. The calculated values for T and S of the curve-fitting methods are listed in Table 5.2. The values of T were in the range of transmissivities given by Allen et al. (1997) for Triassic Sandstone. S values were not always within the range of $5x10^{-3}$ to $5x10^{-5}$ as proposed by Kruseman and de Ridder (1996), because of difficulties in matching the drawdown data with the different methods. The bolt marked values of T and S in Table 5.1 were used as first input for the groundwater flow-model. The drawdown data of the tests were used for calibration of the hydraulic flow model.

Table 5.2: Applied curve-fitting method and calculated T, K and S values of S1 to S7 gained from the pumping test data of Test 1 to Test 14. The column Borehole lists the pumped wells of the pumping tests when no observation wells were marked ("ob. well"). Bold marked tests were chosen as the curve-fitting gave the best fit. Cursive marked tests were not shown as the curve-fitting figures do not match very well.

Aquifer layer	Test	Borehole	Max. Drawdown	Curve-Fitting Method	T[m²/d]	K[m/d]	S
S1 and S2	*1*	*BH2*	*2.35m*	*Theis*	*56.76*	*4.68*	$3.62x10^{-6}$
	10	*ob. well BH2*	*0.79m*	*Theis*	*135.95*	*2.43*	$7.83x10^{-2}$
	13	**BH2**	1.98m	Theis	37.87	4.59	$\mathbf{7.41x10^{-5}}$
S2	**4**	**BH1**	2.81m	**Theis**	**62.53**	**11.37**	$2.22x10^{-12}$
	5	*BH1*	*2.76m*	*Theis*	*49.18*	*8.94*	$1.16x10^{-8}$
S3	**6**	**BH1**	3.46m	**Theis**	**34.15**	**6.21**	$1.72x10^{-7}$
S5	*2*	*BH3*	*13.50m*	*Walton*	*0.79*	*0,14*	*0.25*
	7	**BH1**	11.00m	**Theis**	**6.99**	**1.27**	$\mathbf{9.30x10^{-5}}$
				Walton	*5.05*	*0,92*	$1.76x10^{-3}$
		ob. well BH3	5.94m	**Theis**	**9.99**	**1.81**	$\mathbf{9,30x10^{-5}}$
				Walton	*3.06*	*0.56*	$4.3x10^{-4}$
	10	ob. well BH3	2.19m	**Theis**	**100.58**	**1.90**	$\mathbf{3.23x10^{-4}}$
	14	*BH3*	*8.64m*	*Theis*	*11.08*	*1.94*	$1.1x10^{-4}$
S6	**8**	**BH1**	3.46m	**Theis**	**42.44**	**4.72**	$1.59x10^{-11}$
S7	*3*	*BH5*	*1.19m*	*Walton*	*27.42*	*3.43*	$\boldsymbol{3.92x10^{-3}}$
	9	*BH1*	*6.75m*	*Walton*	*37.17*	*4,65*	$\boldsymbol{1.83x10^{-3}}$
				Theis	*91.32*	*11.42*	$5.68x10^{-10}$
		ob. well BH5	*4.51m*	*Walton*	*81.49*	*10,19*	$3.59x10^{-9}$
				Theis	*120.35*	*15.04*	$9.49x10^{-12}$
	14	BH5	1.49m	***Walton***	***68.09***	***8.51***	*4.95.*
				Theis	*100.03*	*12.50*	*1.13*
	10	ob. well BH5	2.19m	Theis	128.61	**2.43**	$5.98x10^{-8}$
S1 - S7	**10**	BH1	3.52m	Theis	135.69	2.56	$5.12x10^{-6}$
				Cooper and Jacob	**135.46**	**2.55**	$\mathbf{1.32x10^{-5}}$

5.8 Conclusion

Chapter 5 describes the hydraulic conditions of the test site. Rest water level observations detect vertical flow in BH1 and BH4. Heat pulse flowmeter measurements quantified the up-flow in BH1 and packer tests in BH1 measured the relative head changes between the different aquifer layers by inflating a packer on the level of each mudstone layer, M1 to M6. The relative head changes could be used for later adjustment of the boundaries of the groundwater model.

Pumping tests were carried out in all sandstone layers, S1 to S7. The purpose-tailored double-packer system (Greswell, 1999) was successfully used to run the tests which were performed up to a period of about 13 days (Test 13 in BH 3). Curve-fitting methods were successfully applied to the drawdown data of the processed tests and values of the transmissivity T, the hydraulic conductivity K and the storage coefficients S for the aquifer layers S 1 to S7 were calculated (Table 5.2). T and K values of the pumping tests lay within the range of parameters given by Allen et al. (1997) and Tellam and Barker (2006) for the Triassic Sandstone in the U.K. In a few tests calculated S values were very small and below the range for storage coefficients generally defined by Kruseman and de Ridder (1994). However, the values of T and K, and – with restriction – the values of S were applicable as first input data for the hydrogeological computer model of the test site. The drawdown data of the pumping tests could be applied to calibrate the groundwater flow model.

CHAPTER 6: Characterization of Horizontal and Vertical Transport Properties with Tracer Tests

6.1 Objective

The aim of this chapter was to process tracer tests to gain values of natural linear groundwater velocities, effective porosities and dispersivities of the Triassic Sandstone, UK. Three different types of tracer tests were chosen to be appropriate to achieve data to quantify these values:

1. **Point Dilution Tracer Tests** were carried out to calculate natural linear groundwater velocities and the natural hydraulic gradient of the sandstone layers S1 to S6.
2. **Horizontal Forced Gradient Tracer Tests** were chosen to define values of the effective porosity and dispersivity of sandstone layers.
3. **Vertical Forced Gradient Tracer Tests** were carried out to quantify values of the effective porosity and dispersivity of mudstone layers.

All tests were successful, as tracer breakthrough could be detected. Breakthrough curves for almost all tests were recorded. During the horizontal and vertical forced gradient tracer tests, the tracer concentration in the injection well was monitored for all tests, showing strong correlations between concentrations in the injection well and the pumped well for certain tests.

6.2 General Tracer Application and Detection

The use of different tracers throughout the history in hydrology and hydrogeology was described by Käss (1998). First, dye tracer tests were carried out at the end of the 19th century, using discovered fluorescein together with slate oil and NaCl (Germany; Knopp 1875, 1878). A variety of tracer experiments were also carried out in France and Italy during the 19th and 20th century to find sources of typhus epidemics (Flury and Wai 2003, Käss, 1998). The amount of tracer injected was chosen mainly to find a connection between two points and to receive a visible confirmation at the point of observation by coloured water. Later, image analysis techniques were used to receive detailed spatial resolution of tracer concentrations, e.g. two-dimensional imaging of fluorescent dyes in soil profiles (Aeby et al., 2001; Vanderborght et al., 2002). Collecting dye tracers with active charcoal or cotton strips was first recorded in the late 1950's (Flury and Wai, 2003). This method allows detection of lower concentrations of dyes and measurement of the tracer concentration over a specific period of time. Fluorescence spectroscopy and fiber optic sensors offer the possibility of detecting low concentrations of dye tracer and measuring the tracer concentrations in situ.

Fluorescent dyes make ideal groundwater tracers as they have very low detection limits, may be measured over a concentration range of several orders of magnitude and can be simply analysed using online equipment. Reviews on the use and characteristics of groundwater dye tracers were given by a variety of authors (Drew, 1968; Smart and Laidlaw, 1977; Davis et al, 1985; Mull et al., 1988; Viriot and André, 1989; Flury and Wai, 2003; Käss, 2004). Flury and Wai (2003) listed recommended dye tracers on the basis of solubility, sorption, mobility, and stability for different chemical environments: fluorescein (Na-flourescein, uranine) (Trillat, 1899), sulforhodamine G (Moser and Sagl, 1967), rhodamine WT, liassamine yellow FF, and amino-G-acid (Smart and Laidlaw, 1977) as well as rhodamine WT and rhodamine B (Wilson

et al., 1986). The toxicology and ecotoxicology of tracers has been explored by Smart (1984), the German Federal Environmental Agency (Umweltbundesamt, 1997) and Behrens et al. (2001).

6.3 Theory of Flow and Solute Transport

The theory of flow and solute transport which could be expected on the test site was given by Scheidegger (1961), Bear (1961a/b, 1972), Bear and Buchlin (1991), Batu (2006) and Maloszewski (2007). A detailed discussion contaminant transport can be found in Fetter (1994 and 1999).

6.4 Introduction to Tracer Tests

Tracer tests were useful tools to measure and understand hydrogeological properties. Ward et al. (1998) define properties which can be determined by six different tracer tests methods, as shown in Table 6.1: 1. laboratory tests, 2. single borehole dilution tests, 3. natural gradient tests (without a borehole), 4. natural gradient tests (multi-well), 5. drift (or injection) and pump-back tests, and 6. forced gradient tests (multi-well).

- **Single borehole dilution tests, "method 2",** were conducted by Hiscock (1982, see also Hiscock 2005, p191) in Chalk aquifer. Ward et al. (1998) did not record any existing dilution test in the Triassic Sandstone of the U.K. Single borehole dilution tests are part of this thesis and are further discussed under 6.5.

- **Forced gradient (multi-well) tracer tests "method 6"** were carried out in a sand and gravel aquifer by Bateman et al. (2001, see Hiscock 2005, p192) to establish a connection between a road soakaway and a well in Wales. Ward et al. (1998) listed four tracer tests processed in Triassic Sandstone of the U.K. (discussed in 2.5.1).

Table 6.1: Hydrogeological properties which can be measured using tracer tests (after Ward et al., 1998).

Property to be determined	**Suitable test methods**
Measurement of flow paths:	
Connection between two or more points	3, 4, 6
Direction of flow	3, 4
Measurement of velocity:	
Average linear water velocity	3, 4, 5, 6
Specific discharge/darcy velocity	2
Contaminant migration velocity	3, 4, 6
Measurement of aquifer properties:	
Hydraulic Conductivity	2
Effective porosity	5
Heterogeneity	4
Fracture Characterization	4
Matrix Diffusion	1, 4, 6
Measurement of solute/contaminant transport properties:	
Dispersion	3, 4, 5, 6
Sorption	1, 4
Dilution	3, 4, 6
Measurement of recharge/groundwater catchments	3, 4
Measurement of groundwater age	3, 4

Apart from the tracer tests listed above, Hiscock (2005) and Atkinson et al. (1980) gave an overview of tracer tests applied in the UK, which were mainly processed in limestone or Chalk aquifers. Further important test sites where tracer test were carried out are:

- Borden: Extensive field experiments were conducted at the Canadian Air Force Base Borden, Ontario, Canada, to investigate the transport of organic tracers under natural gradient conditions (e.g. Mackay et al., 1986; Freyberg, 1986; Curtis et al., 1986; Roberts et al., 1986; Sudicky, 1986).

- Cap Cod test site running natural gradient tests (multi-well "4", after Ward et al., 1998) were conducted by LeBlanc et al. (1991), Garabedian et al. (1991), and by Hess et al. (1992).

- Drigg: Radial injection experiments were performed in a shallow, confined sandy aquifer at the Drigg British Nuclear Fuels site in Cumbria, England (e.g. Williams et al, 1985).

- Moffett: Experiments at a site located within the Moffett Naval Air Station, California. Induced- or forced-gradient tracer tests were conducted using bromide and chlorinated organic chemicals as tracers (Roberts et al. 1990, Semprini et al., 1990).

Fracture flow was explored at different sites with tracer tests. At Tono (Japan; Iwatsuki et al., 2002), Äspo (Sweden; Pedersen et al. 1997) and for the Triassic Sandstone in Sellafield (Cumbria, UK; Milodowski et al., 1999; Bath et al., 2000) and for Triassic Sandstone in Derbyshire-Leicestershire (UK; Bouch et al., 2004) fracture flow and the relationship of groundwater chemistry, calcite chemistry and calcite morphology were taken into account.

6.5 Tracers Applied

The dyes fluorescein and rhodamine WT (RWT) were selected for the tracer tests discussed in the thesis. Table 6.2 gives details for both tracers. They can be used

Table 6.2: Details of the dye tracers fluorescein and rhodamine WT (RWT) used as tracers on the University test site (Käss, 1998 and 2004).

	Fluorescein (Uranine/Na-Fluorescein)	Rhodamine WT (RWT)
Color Index Number	45350	
Color Index Name	Acid Yellow 73	Acid Red 388
Molecular formula	$C_{20}H_{12}Na_2O_5$	$C_{29}H_{29}O_5N_2Na_2Cl$
Molecular weight	376.276	566.5
Solubility in Water	600 g/l (20°C)	180 g/l
Maximum Excitation	491 nm	555 nm
Maximum Emission	512 nm	580 nm
Minimum Detection	10^{-12} g/l (0.001 ppb)	1.3×10^{-11} g/l (0.013 ppb)
Visibility	10^{-8} g/l (10 ppb)	$\approx 10^{-8}$ g/l (10 ppb)
Sorption	low (pH < 5.5 high)	high

simultaneously, having their fluorescence maximum at different wavelengths. This allowed additional flexibility in the timing of experiments as more than one dye could be measured in the system at any time without detriment.

RWT is not present in nature, whereas fluorescein can be present in nature. However, fluorescein is used to dye different products, e.g. shampoos. It was also used for entertainment, for example to dye the Chicago River green on an annual basis on St. Patricks Day. In 1962, about 45 kg and in 2005, about 16 kg of fluorescein were introduced into the Chicago River to colour the river green (http://de.wikipedia.org/wiki/Fluorescein (2007)). Such sources of fluorescein can significantly influence the background concentration. Fluorescein shows lower fluorescence in water with pH of less than 5 (Olsen and Tenbus. 2004; Sabatini and Austin, 1991 and Mull et al., 1988). However, for pH values above 5 and aquifers with low clay and organic content, fluorescein showed low sorption and was considered as a conservative tracer (Käss, 1998). According to Mitchener (2003) and Shepherd (2002) the pH value of groundwater in the Triassic Sandstone was above 5. Laboratory batch and column experiments using Triassic Sandstone in conjunction with dyes had shown that fluorescein behaved conservatively (Bashar, 1997). The fluorescence intensity of RWT was not affected by changes in pH for values above 6 in the water (Smart and Laidlaw, 1977). A number of studies showed that RWT sorbs during field-scale groundwater tracer tests (Ptak and Schmidt, 1996), laboratory column and batch experiments (Sutton and Kabala, 2001). Bashar (1997) reported that RWT was sorbed by the Triassic Sandstone in laboratory batch and column experiments. Hofstraat et al. (1991) and Shiau (1993) isolated two RWT isomers and showed that they had different sorption properties. Sutton et al. (2001) recommended the application of RWT as a conservative tracer for the first isomer as this exhibits only a small affect of sorption. The second isomer was not recommended as a tracer

because it sorbs to a relatively large extent. For simplicity, Derouane and Dassargues (1998) considered RWT as a conservative tracer with a negligible sorption. This was supported by experiments of Käss (1998) who recorded a small sorption for RWT. From tracer experiments with chloride and RWT as tracers, Pang et al. (1998) concluded that RWT behaves as a conservative tracer, as well.

Most dyes will be absorbed on fine particulate material including organic fragments and clays as discussed by Davis et al. (1985) and reported by Smart and Laidlaw (1977). Table 6.3 shows the absorbed dye depending on the amount of clay or, in this case, Kaolinite in water.

Table 6.3: Adsorption of dyes on Kaolinite, results of experiments (Smart and Laidlaw, 1977; Davis et al. 1985).

Absored Tracer Amount in [%]	Kaolinite Concentration in g/l			
	5	10	15	20
Fluorescein	6	12	17	18
Rhodamine WT	11	19	25	31

The results shown in Table 6.3 support the idea of conducting the tracer experiments using a mixture of both fluorescein and RWT so that possible insight might be gained into geochemical differences between the sandstone units and their clay content revealed by the relative retardation of RWT.

6.6 Estimating Tracer Mass Requirements

For single borehole dilution tests Ward et al. (1998) recommended a quantity of tracer which raises the concentration in the injection borehole 100 to 1000 times the background concentration; For radial convergent flow or combined pumping and tracer test a tracer

injection which results in a peak of 10 to 100 times the background concentration at the sampling point was proposed.

For point to point tracer tests it must be taken into account that too little tracer injected would not raise the tracer concentration enough and breakthrough could not be measured if it was below the detection limit. On the other hand, too much tracer injected causes coloured water, influencing the water supply and might cause health problems, depending on the tracer used. Equation 6.1, based on the one-dimensional Fickian dispersion term, was used to estimate the minimum mass of tracer required in natural gradient tests:

$$M = c_m A\sqrt{4\pi r\alpha} \qquad \text{(Equation 6.1)}$$

with

α estimate of dispersivity, e.g. 1/10 of the distance between injection and sampling point;

A the cross-sectional area of injection pulse;

r distance between injection and sampling points;

c_m maximum peak concentration expected;

M mass of tracer.

The calculation of the required mass of tracer (M) might underestimate the effects of radial flow for radial converging tests. To determine an upper limit for M_2 required for a radial test, the following equation should be applied:

$$M_2 = M \times \left(\frac{n_e 2\pi R}{d} \right) \qquad \text{(Equation 6.2)}$$

with

α estimate of dispersivity;

A the cross-sectional area of injection pulse;

r distance between injection and sampling points;

R distance between injection well and sampling point;

d diameter of the injection well.

Another method to define the mass of tracer was described by Lenda and Zuber (1970) (see also Malozewski, 2007). Ward et al. (1998) listed a Monte Carlo approach for estimating tracer quantities if few of the relevant physical parameters controlling the movement of the tracer could be ascribed without confidence.

6.7 Setup of Tracer Injection

The tracer was injected over the whole thickness of the aquifer in all tracer tests. In BH2 tracer was injected over the whole depth of the slotted casing. In all tests, the tracer was injected at the top of the tested interval and pumped continuously at the bottom of the test interval in a recirculating loop, back to the surface and injection point, and down to the top of the test interval again. Continuously mixing the water in the test interval was performed to deliver the same tracer concentration over the full thickness of the tested aquifer layer. Brouyère et al. (2005) described and modelled tracer injection and well-aquifer interaction. Brouyère (2003) and Brouyère et al. (2005) concluded that the chosen tracer injection in the well aquifer system acts similar to a double porosity system. The injection of tracer could influence the tracer test results due to the capture of tracer in the well bore and gradual release into the aquifer leading to enhanced concentration attenuation and recorded tailing of tracer concentration in the breakthrough curve of the observation well.

6.8 Tracer Detection

The tracer concentrations in the injection wells were usually measured with a fluorescence spectroscope on water samples taken over time, or with fluorometers using optical sensors. The tracer concentrations within the system at the discharge well were determined with a fluorometer, using optic sensors. Such detected tracer in the injection and observation wells was calibrated against water samples analysed with the fluorescence spectroscope and vice versa. Three fluorometers were used to analyse the tracer concentration:

1. Perkin Elmer 204-A fluorescence spectrophotometer: a laboratory based fluorometer with a sensing head where the concentration of the tracer was measured. As the detection sensitivity for fluorescein and RWT was $>10^{-11}$ g/ml, the samples had to be diluted before the concentration measurement. The significant photo-decay of fluorescein and amino-G-acid has been explored by Streetly et al. (2002). Two separate 250 ml samples of 10 mg/l for each tracer were prepared. One was exposed to the sunlight and the other was wrapped into aluminium foil and stored in a dark cupboard. The sample exposed to sun light showed significantly lower tracer concentrations in the measurements, compared to the concentration measured in the sample stored in the dark. To avoid photodegradation, samples and tracer solutions were stored in the dark, and exposure to sunlight was kept to a minimum. For the detection of the tracers, the samples needed to be diluted before measurement. Any sediment in the samples appeared to have negligible affects on the fluorescence measured with the Perkin Elmer 204-A fluorescence spectrophotometer, as unshaken and shaken samples gave indistinguishable results (Streetly et al., 2002)
2. A GGUN-FL 20 (Geomagnetism Group University of Neuchâtel) (Schnegg and Doerflieger, 1992) or “Schnegg fluorometer”, comprising a sensing head where the

concentration of the tracer was measured and a data-logger that records the data reading every 10 seconds or every 4 minutes. The head was originally designed for down-hole use but was adapted to work as an in-line device with a take-off pipe from the rising main of the pump. The fluorometer was linked to a PC to allow observation of the current reading and to store the data. The Schnegg fluorometer could detect different tracers and the sediment concentration simultaneously. Three groups of two tracers could be detected:

Group I (excitation with blue light): Uranin (fluorescein) and pyranin

Group II (excitation with green light): Amido rhodamine G (acid red 50), amido rhodamine G (acid red 52), rhodamine B, rhodamine WT

Group III (excitation with UV light): Naphtionate, Tinopal CBS-X.

Two tracers could be selected among the three groups, one from each group. The sensitivity for fluorescein was 10^{-9} g/ml. The detection threshold for fluorescein was 10^{-11} g/ml.

3. A constructed fluorometer by Richard Greswell in 2000, "Schneggli", comprising a sensing head where the concentration of the tracer was measured and a data-logger that was applied to record the data reading every 60, 120 and 300 seconds. The head was connected to an in-line device with a take-off pipe from the rising main of the pump. The fluorometer was linked to a PC to allow observation of the current reading and to store the data. The Schneggli fluorometer did not measure as accurately as the other two fluorometers. However, it was able to detect a concentration range of up to a maximum of five orders of magnitude. The "Schneggli" fluorometer was applied during the vertical tracer tests to detect the tracer concentration of fluorescein in one of two abstraction wells and to detect the fluorescein concentration in the packered

injection section of the vertical tracer tests. The sensitivity of the Schneggli was 10^{-5} g/ml (fluorescein) and the detection threshold at 10^{-6} to 10^{-7} g/ml (fluorescein).

All spectrophotometers were zeroed using pre-tracer test groundwater samples, as the natural groundwater fluoresces, albeit at low intensities.

6.9 Point Dilution Tests

6.9.1 Introduction to Point Dilution Tests

The borehole dilution or point-dilution method was developed in the USSR in the late 1940's (Freeze and Cherry, 1979). A point dilution test can be performed in a single well over a short period of time. Velocities of the groundwater can be estimated using the rate of dilution of a tracer added to the tested well. The theory of point dilution tests was well described by Halevy et al. (1967), Drost et al. (1968), Freeze and Cherry (1979), and Gasper (1987). Moser and Neumaier. (1957), Neumaier (1960), Moser and Sagl. (1967), Halevy et al. (1967) and Drost et al. (1968), for example, applied radioactive tracers in different point dilution tests in porous media of column experiments in the laboratory and in wells at different depths. Lloyd et al. (1979) used point dilution methods and applied fluorescein to determine permeabilities of land-fill materials. Kearl et al. (1988) considered the point dilution method as one method to measure groundwater velocities in unconfined aquifers. Lamontagne et al. (2002) described the successful application of point dilution techniques in soft sediments of riparian zones in Australia (Wollombi Brook, NSW) using saline tracers. Pitrak et al. (2007) applied borehole dilution techniques in a Tertiary sandstone aquifer near Leipzig (Germany) to measure the horizontal groundwater flow with the food colour Brilliant Blue FCF (Euro code E-133).

6.9.2 Point Dilution Theory

The method aims to relate the observed dilution of a tracer introduced into a well to the rate of undisturbed groundwater flow in the aquifer. The theory of the point dilution method requires that the following assumptions were met (Freeze and Cherry, 1979):

1) The borehole dimensions were well known, particularly the cross-section through which groundwater flow could occur.
2) The tracer concentration is homogeneous at any particular time in the flow section.
3) Measurements of tracer concentration were performed under steady groundwater flow conditions.
4) The vertical hydrodynamic potential had no gradient (Dupuit's Assumption).

Goal of the point dilution test was to know the average linear velocity v of the sandstone aquifer or the rock adjacent to the well which was calculated as follows (Freeze and Cherry, 1979):

$$v = \frac{v^*}{n_e \alpha} \qquad \text{(Equation 6. 3)}$$

n_e is the effective porosity of the rock formation around the well;

α is an adjustment factor that depends on the geometry of the well screen and on the radius of the sand or gravel pack around the well screen;

v^* apparent velocity (Freeze and Cherry, 1979) in the tested well which could be calculated by measuring the concentration versus time:

$$v^* = \frac{-V}{At} \ln\left(\frac{C}{C_0}\right) \qquad \text{(Equation 6.4)}$$

V volume of the borehole open section with radius r and height h;

A cross-section of the tested well section perpendicular to the direction of the groundwater flow.

The factor α is a correction factor or well-shape factor and takes into consideration the flow field of the well distortion. This factor depends on the geometry and hydraulic conditions of the well screen and the sand or gravel pack around the well screen. In the introduction to Point Dilution Tests, the authors mentioned, listed well-shape factors for a variety of rocks and well setups. Drost et al. (1968), for example, gave values for α of 0.5 to 4 in sand and gravel aquifers, and of 2.35 and 3.21 for wells with well screens and gravel packs with a diameter of 4 inches. Gasper and Oncescu (1972) assumed that α = 1, which seems to be reasonable for boreholes with a diameter of up to 100 mm (Lloyd et al., 1979). Applying α = 1 for wells with larger diameters might lead to inaccuracy considering the effect of hydraulic distortion by the construction of boreholes. Under the assumption that the flow was laminar, the following formula (Drost et al., 1968) was used to calculate α of SPD 6:

$$\alpha = \frac{8}{\left(1+\frac{K_3}{K_2}\right)\left(\left[1+\left(\frac{r_1}{r_2}\right)^2\right]+\frac{K_2}{K_1}\left[1-\left(\frac{r_1}{r_2}\right)^2\right]\right)+\left(1-\frac{K_3}{K_2}\right)\left[\left(\frac{r_1}{r_3}\right)^2+\left(\frac{r_2}{r_3}\right)^2\right]+\frac{K_2}{K_1}\left[\left(\frac{r_1}{r_3}\right)^2-\left(\frac{r_2}{r_3}\right)^2\right]}$$

(Equation 6.5)

where

r_1 inside radius of the well screen;

r_2 outside radius of the well screen;

r_3 radius of boring (well, well screen and gravel pack);

K_1 well-screen permeability;

K_2 permeability of the gravel pack and

K_3 permeability of the aquifer.

For wells with a single filter zone (e.g. only with a well screen and no gravel pack), α could be estimated from Ogilvi's formula (Ogilvi, 1958; cited in Halevy et al., 1967, and Drost et al., 1968), used to calculate α of SPD 1 to SPD 5:

$$\alpha = \frac{4}{\left[1+\left(\frac{r_1}{r_2}\right)^2\right]+\frac{K_2}{K_1}\left[1-\left(\frac{r_1}{r_2}\right)^2\right]} \qquad \text{(Equation 6.6)}$$

The equations listed above are valid for groundwater velocities in the range of 0.01 to 15 m/d (Gasper 1987). Under laminar flow conditions in the adjacent rock (Domenico and Schwartz, 1998), Darcy's law could be written as follows

$$v = Ki \qquad \text{(Equation 6.7)}$$

v as average linear velocity according to Freeze and Cherry (1979).

Rearranging equation 6.5, the hydraulic or groundwater gradient i could be calculated as follows:

$$i = \frac{v}{K} \qquad \text{(Equation 6.8)}$$

6.9.3 Setup of the Point Dilution Tests

Figure 6.1 shows the schematic setup of the six point dilution tests processed on the test site during the summer and early autumn 2000. The water in the tested interval was constantly recirculated at flow rates of 0.167 l/s to 0.217 l/s. This test setup maintained approximately a constant concentration of tracer in the water column over the whole packered test interval. For each point dilution test, Table 6.4 lists, the length of the tracer test, tracer amount and volume injected, recirculating pumping rate of the water in the test interval and discharge rate of the test interval after the test was finished. Test SPD 6 in BH 2 considered S1, M1 and S2 intersected by the well. The Grundfos MP 1 pump was installed at the bottom of BH2. Tests

SPD 1 to 5 were carried out in BH1 in the packered layers S3, S4, S5, and S6. The pump was installed at the bottom of each test interval in BH1. Diluted in previously pumped groundwater of the test interval, the tracer was injected through a small valve into the recirculating main at the surface. The tracer concentration was measured during all tests with the GUNN-FL 20 fluorometer. After each dilution test, the water was discharged until the RWT concentration in the packered section reached a concentration of $C < 5x10^{-5}$g/l (Figure 6.2). In Figure 6.3, the processed dilution tests SPD 1 to 6 were drawn as a semi-log plot of the RWT concentration over time. The recirculating cycle was switched on prior to the injection of the tracer so that an undisturbed natural steady state groundwater flow field developed before the start of each test.

Table 6.4: Point dilution tests: Length of the tests, tracer amount, and volume injected, recirculating pumping rate of the water in the test interval and discharge rate applied to withdraw the tracer from the test interval after the dilution test was finished.

Test	Tested Aquifer Layer BH 1	RWT injected	Injected Fluid	Injection Time	Recycling Pumping Rate	Discharge Rate	Length of the Dilution Test
	S 6	0.21 g	50l	47 min	0.217 l/s		45h 50min
SPD1	discharge					0.217 l/s	1h 28.5min
	S 3	0.21 g	10l	35min	0.2127 l/s		43h 35min
SPD2	discharge					0.2127 l/s	1h 15min
	S 6	0.21 g	10l	52min	0.1669 l/s		45h 18min
SPD3	discharge					0.1669 l/s	6h 30min
	S 5	0.21 g	10l	40min	0.1669 l/s		11h 22min
SPD4	discharge					0.1669 l/s	2h 25min
	S 4	0.21 g	10l	48min	0.1669 l/s		22h
SPD5	discharge					0.1669 l/s	1h 24min
SPD6	S1 & S 2 in BH2	0.21g	10l	40min	0.1669 l/s		15h 45min

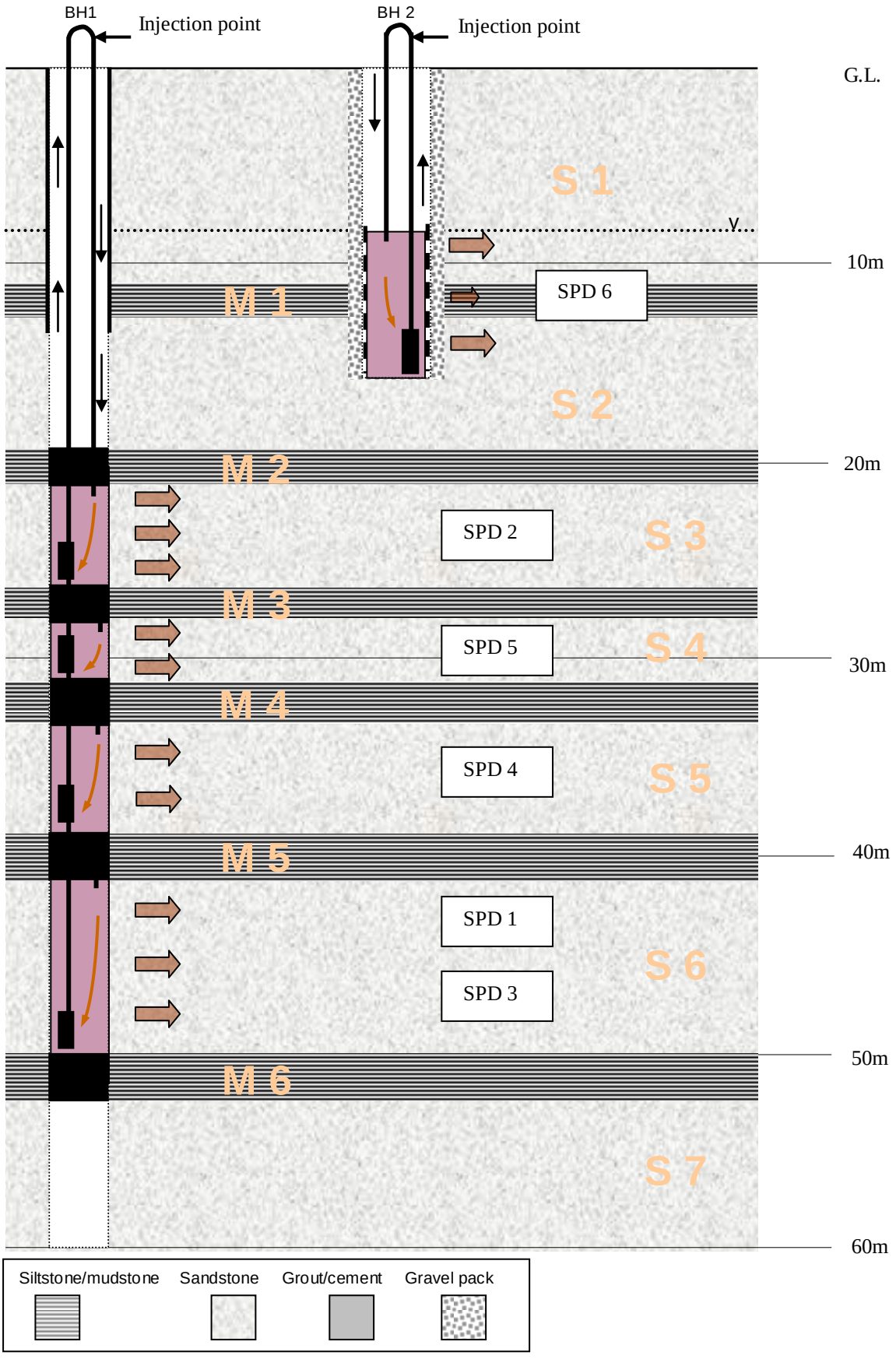

Figure 6.1: Schematic cross-section of the Single-Point Dilution Test Setups.

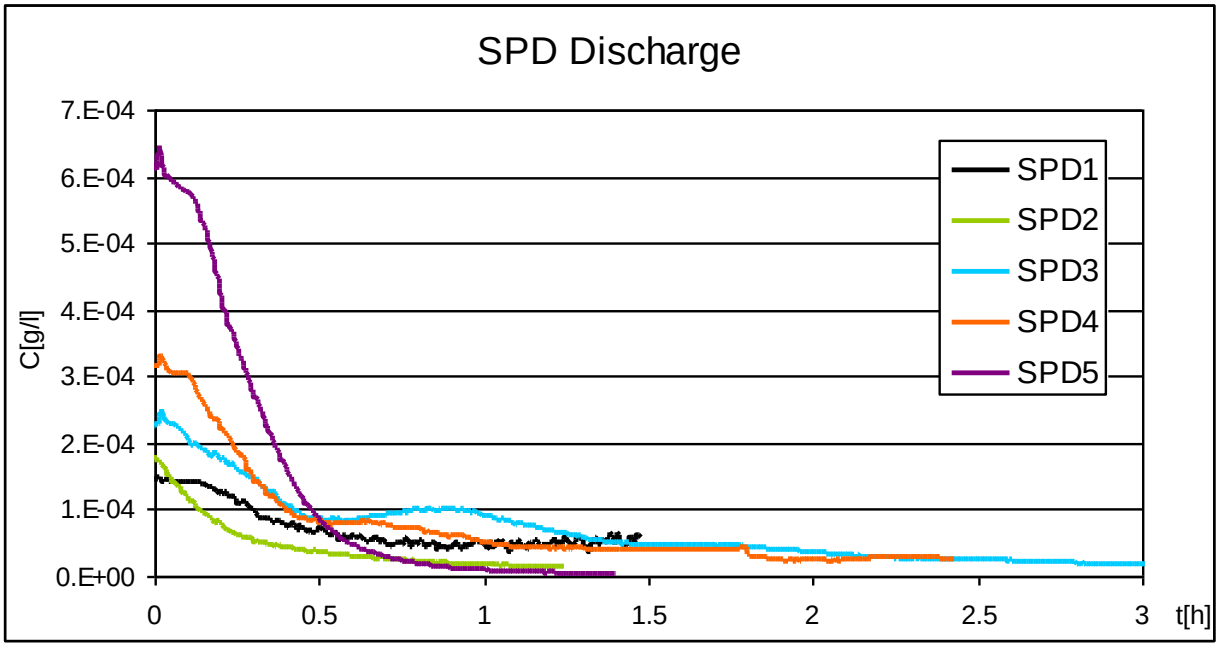

Figure 6.2: RWT concentration over time in BH1 after the termination of the single-point dilution tests (SPD). Each test interval was pumped for at least one hour to abstract as much as possible tracer injected.

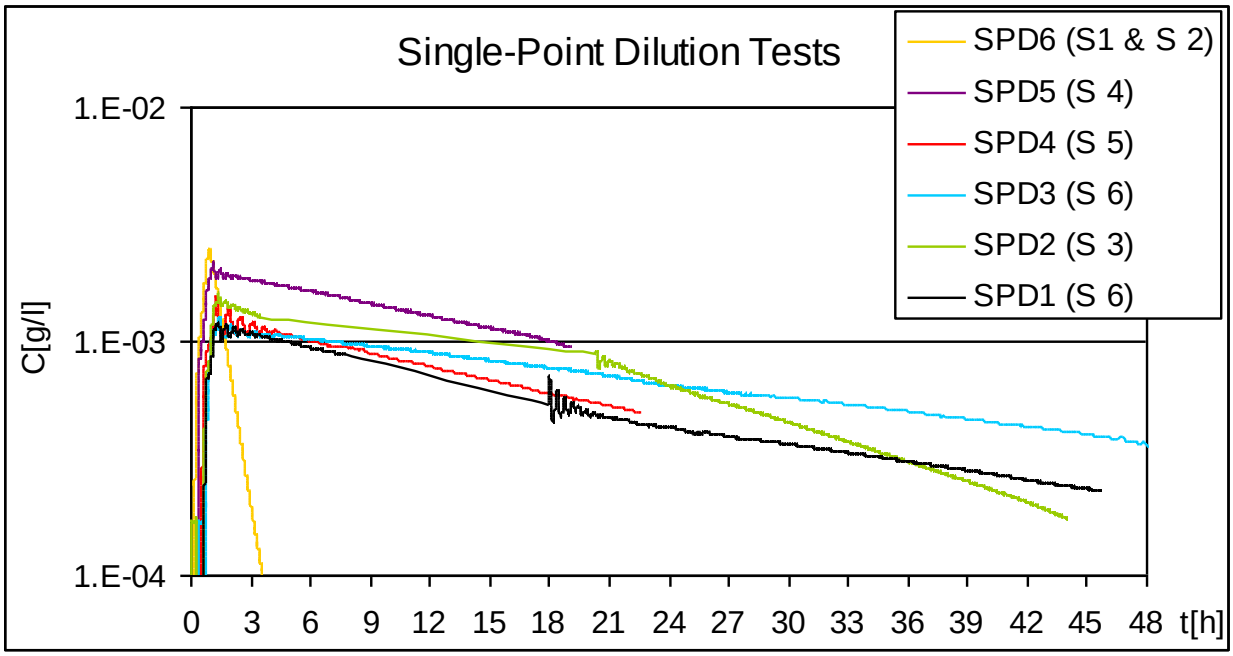

Figure 6.3: Semi-log plot of the measured RWT concentration over time of the single-point dilution tests SPD 1 to SPD 6.

6.9.4 Interpretation of the Point Dilution Tests

The assumptions 1 to 4 described above required for the theory of point dilution tests were fulfilled. However, it became obvious that assumption 2) was not met during the initial part of the tracer tests. The measured tracer concentration of all tests oscillated for few hours after the test had started (Figure 6.3). The same oscillation of the tracer concentration was observed when the pump had to be restarted due to an electricity breakdown during test SPD 1 after 18 hours and SPD 2 after approximately 21 hours. The oscillating shape of the tracer concentration over time was caused by the mixing procedure of the injection interval. The water volume of the test interval was pumped through a commercial garden hose up to the surface where the tracer was injected, and pumped down through the garden hose back into the packered section. The oscillating intervals of the measured tracer concentration over time, however, did not match with the time intervals which were necessary to pump the volume of the injection interval plus the volume of the garden hose up to the surface to the injection point and back into the test interval again. Nevertheless, the oscillation of the tracer concentration during the first 3 hours of the tests was assumed to be caused by the mixing of the tracer in the injection interval. After about 3 hours, the oscillation of the tracer concentration decreased, and the concentration of RWT tracer in the injection interval seemed to be constant. This so-measured mixing effect of tracer in an injection interval was not described previously.

The apparent velocity v^*, the linear groundwater velocity v, and the hydraulic gradient i are listed in Table 6.6. Values of the effective porosity n_e were not measured for core samples of the test site. Values gained for the porosity from examined cores from BH4 (Mitchener, 2003) were considered as first estimate to calculate the average linear velocity v of the sandstone

aquifer or adjacent. The hydraulic conductivity K was taken from the pumping test results calculated for S1 to S7. The well-shape factor α of test SPD 6 was calculated according to equation 6.5 (Table 6.5). Well-shape factors α of the tests SPD 1-5, as listed in Table 6.6, were calculated according to equation 6.6 under the assumption that $r_1 = r_2$ and $K_1 = K_3$, as borehole BH 1 was drilled in the sandstone without the installation of a wellscreen or gravel pack.

Table 6.5: Well-shape factor α of SPD 6, calculated according to Equation 6.3.

	r1 [m]	r2 [m]	r3 [m]	K1 [m/d]	K2 [m/d]	K3 [m/d]	α
SPD 6	0.0635	0.0675	0.1016	302*	539**	8.53	**3.44**

*K1 well screen permeability applied by Dorst et al. (1968) 0.35 cm/s
**K2 given by Driscoll (1995) 539 m/d

Table 6.6: Calculated values of the hydraulic gradient *i* after Freeze and Cherry (1979). Porosity values after Mitchener (2003) were listed under *n** and *K* values as calculated for the pumping tests. *K* value for S4 was taken from Test 10. Test SPD 6 was processed in BH2 all other tests in BH1.

Aquifer Layer	Test	*v** [m/d]	*K* [m/d]	*n**	*α*	*v* [m/d]	*v*/*K*=*i*
S1 + S2	SPD6	2.778	11.41	0.246	3.44	3.282	0.288
S3	SPD2	0.253	6.21	0.260	2	0.488	0.079
S4	SPD5	0.147	2.55	0.252	2	0.293	0.115
S5	SPD4	0.166	1.9	0.239	2	0.349	0.183
S6	SPD3	0.088	4.72	0.280	2	0.156	0.033
S6	SPD1	0.101	4.72	0.280	2	0.180	0.038

The calculated apparent and linear groundwater velocities *v** and *v*, as well as the hydraulic gradient *i* listed in Table 6.6, decrease with increasing depth of the tested aquifer layer. Hydraulic gradients in the range of $i = 0.01$ to $i = 0.1$ within the Triassic Sandstone of the UK were considered to be typical by Tellam and Barker (2006). Thus typical values were calculated for S3 and S6. The hydraulic gradients of S1+S2, S4 andS5 were higher than those proposed by Tellam and Barker (2006). A calculated value 0.278 for the natural hydraulic gradient in layer S1 and S2 should have a different reason, as the value is much higher than

those proposed by Tellam and Barker (2006). One possible reason for such a high value seems to be vertical up-flow in BH2 from S2 towards S1. Up flow was measured in BH1 but not in these layers as those were cased. Up-flow was also measured in the wells of the Great Hall borehole array (Figure 3.2).

6.9.5 Conclusion of the Point Dilution Tests

In conclusion, six point dilution tests were carried out successfully on the test site. Aquifer layers S3 to S6 were tested as single layer in BH1, applying the double packer system of Greswell (1999). S1 and S2 were tested in BH2. Aquifer layer S7, unfortunately, was not tested due to lack of time. The calculated values for the average linear velocity v of the sandstone aquifers were achieved by using the porosity values measured by Mitchener (2003), as no other data for the effective porosity were available for the test site. The calculated average linear velocity v and hydraulic gradient i, as listed in Table 6.6 were considered to be higher if lower values for the effective porosity were available than those measured for the porosity by Mitchener (2003). The calculated hydraulic gradients in Table 6.6, however, were considered to be acceptable to define boundary conditions of the aquifer layers for a computer model of the test site.

The mixing process of the injected RWT in the injection or test interval was observed for the first time. An oscillating tracer concentration of tracer during the first hours could be measured for the point dilution tests.

6.10 Horizontal Convergent Flow Tracer Tests

6.10.1 Test Setup of the Horizontal Convergent Flow Tracer Tests

Five horizontal convergent flow tracer tests were conducted in S2 (injection in S1 and S2), S5 and S7. The tests were set up as forced gradient or combined pumping and tracer tests. The pumped well created a convergent radial flow field into which a tracer was injected. Fluorescein and RWT were chosen as tracers. BH1 was the pumping well for all tests. For each test, the double packer system of Greswell (1999) was applied to packer off S2, S5 and S7 in BH1. BH2, BH3 and BH5 were used as injection wells. Tracer was injected after about half an hour of pumping, assuming that the heads in the wells had reached steady state. During the tests, the heads were monitored with transducers. The concentration in the pumping well, BH1, was measured with the GGUN-FL 20 (Schnegg and Doerflieger, 1992) in intervals of 10 seconds. The concentration of tracer in the injection well was measured with water samples taken at different intervals. Later, the samples of the injection well were analysed in the laboratory using the Perkin-Elmer fluorometer. Figure 6.4 gives a schematic overview of the setup of the horizontal convergent flow tracer tests TT1 to TT5. TT3 was a repetition of TT2 and TT5 was a reptition of TT4.

The horizontal tracer tests were started by a rapid or slug injection of tracer into a recirculation loop which entered the aquifer layer of the injection wells. For the slug injection, the tracer was diluted in less than half a litre of previously pumped ground water. Injecting the diluted tracer and flushing the injection equipment required about 3 litres of solute in total, which were injected into the recirculating loop. The same in-hole recirculation method employed for the point dilution tests was adopted for the injection well for the horizontal gradient tracer testing. Table 6.7 lists the horizontal convergent flow tracer test pumping rates,

pumping times, total discharges, and injected mass of tracers, as well as recovered and not recovered mass of tracers However, TT2 is not discussed any further as records of the fluormeter were disturbed by different problems of the test setup (e.g. air in the hose connected to the GGUN-FL 20 (Schnegg and Doerflieger, 1992, generator failure, pump failure).

Table 6.7: Details of the horizontal tracer tests. Discharge well was BH1 at all times.

Tracer Test	Layer	Injection well	Abstraction Rate [m³/d]	Pumping Time [d]	Total Discharge [m³]	Injected Tracer [g]		Recovered Tracer [g]		Not Recovered Tracer [g]	
						Fluorescein	RWT	Fluorescein	RWT	Fluorescein	RWT
TT 1	S 7	BH 5	224.64	0.77	172.41	2	2	1.84	2	0.16	0
TT 2	S 5	BH 3	66.44	3.19	211.64	0.5	1	-	-	-	-
TT 3	S 5	BH 3	61.71	2.37	146.22	3	1	1.73	0.48	1.27	0.52
TT 4	S 1 & S 2	BH 2	65.92	1.66	109.43	1	1	0.72	0.75	0.28	0.25
TT 5	S 1 & S 2	BH 2	65.66	4.34	284.91	4	-	3.73		0.27	-

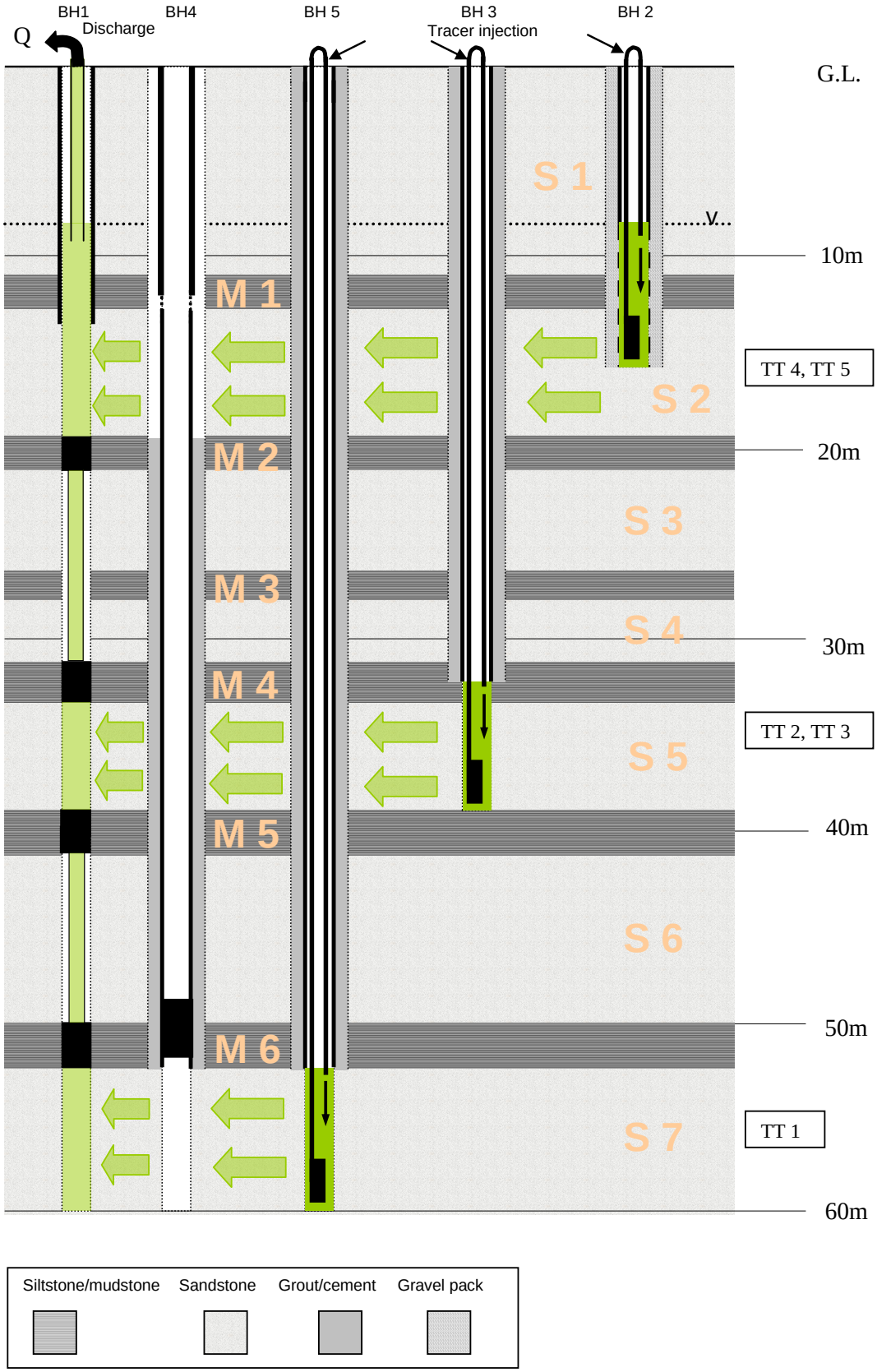

Figure 6.4: Schematic cross-section of the test setup of the horizontal convergent flow tracer tests.

6.10.2 Tracer Test 1 (TT 1)

In Figure 6.5, the tracer concentrations (*C* in g/l) over time were plotted for the injection well, BH5, and for the pumping well, BH1. The concentration curve of the injection well showed a rapid increase of tracer concentration and four peaks for fluorescein and RWT. About 66 minutes after the injection had started, a concentration of less than $1x10^{-6}$g/l tracer (fluorescein and RWT) was detected in the injection well and nearly all tracers had left the injection well BH5.

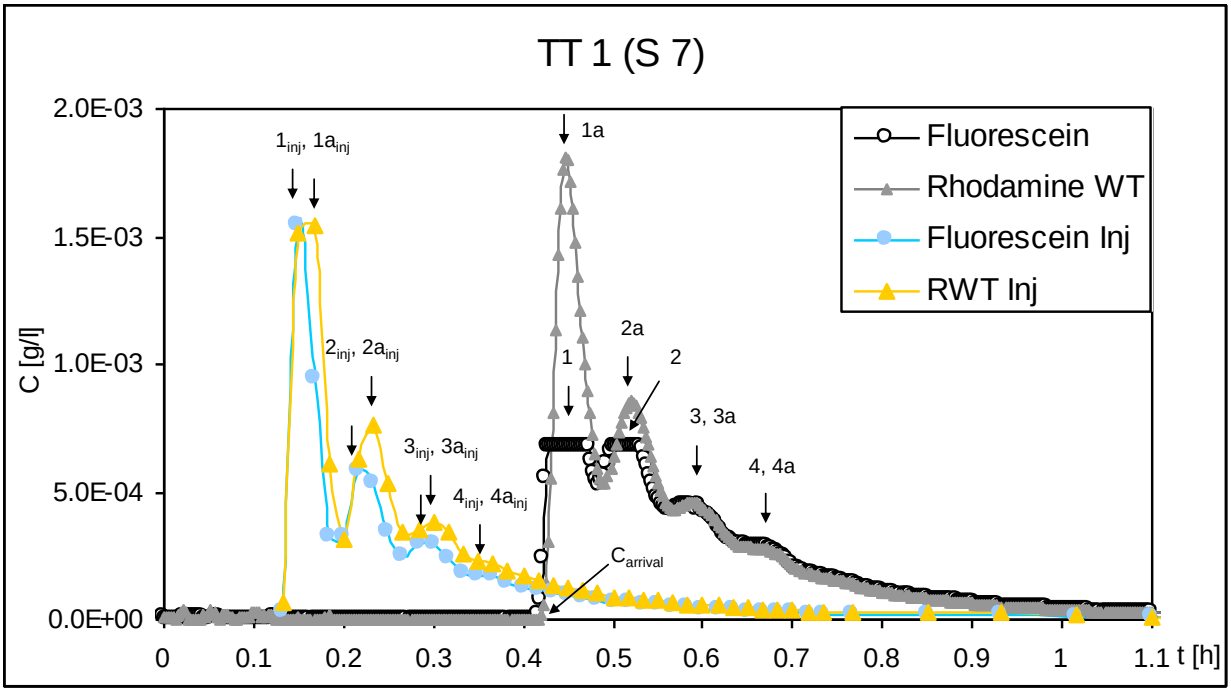

Figure 6.5: Concentration versus time of the tracer concentrations in the injection well BH5 (Fluorescein Inj and RWT Inj) and in the pumping well BH1 of TT 1. The first appearance of the tracers on the breakthrough-curves in BH1 is marked with $C_{arrival}$. Four peaks for each tracer in the injection well (Fluorescein 1_{inj} to 4_{inj}, RWT $1a_{inj}$ to $4a_{inj}$) and pumping well (Fluorescein 1 to 4, RWT 1a to 4a) were distinguished. Lower tracer concentrations plotted for the injection well shall be considered as relative values, as the reason for lower tracer concentrations compared to higher concentrations in the pumped well are unresolved (see also 6.10.2.1 TT 1 - Discussion and Interpretation).

The shape of the breakthrough-curve was very similar to the shape of the tracer concentration versus time, as printed for the injection well BH1. The detection limit of the GGUN-FL 20

fluorometer for fluorescein was exceeded for Peak 1 and Peak 2. Table 6.8 lists tracer test details and calculated values for $v_{arrival}$ and v_{peak} for each peak of each tracer. 2g of RWT were recovered 3 hours after TT 1 had started. At the same time, 1.68g of fluorescein was recovered. Concentrations above the detection limit of Peak 1 and Peak 2 were not recorded and were considered to include the missing 0.32g fluorescein, being listed as not recovered 3 hours after the test had started.

Table 6.8: TT 1 – Tracer concentrations C and time t of peak concentrations measured in the injection well, BH5, and tracer concentrations C and time t of arrival and peak concentrations in the pumping well BH1 (S7). For Peak 1 and Peak 2 of fluorescein in the discharge well, the time interval is listed when the detection limit has been reached. Distance BH1 to BH5 is 6.85m.

TT 1 Injection Well BH5					
Tracer	Injection	C [g/l]	t [h]	t [d]	
Fluorescein	Peak 1_{inj}	1.54×10^{-3}	0.15	0.006	
	Peak 2_{inj}	5.83×10^{-4}	0.216	0.009	
	Peak 3_{inj}	2.94×10^{-4}	0.283	0.012	
	Peak 4_{inj}	1.7×10^{-4}	0.35	0.015	
RWT	Peak $1a_{inj}$	1.54×10^{-3}	0.166	0.007	
	Peak $2a_{inj}$	7.59×10^{-4}	0.233	0.010	
	Peak $3a_{inj}$	3.82×10^{-4}	0.3	0.013	
	Peak $4a_{inj}$	2.25×10^{-4}	0.35	0.015	
TT 1 Discharge Well BH1 (S7)					
Tracer	Breakthrough	C [g/l]	t [h]	t [d]	*v* [m/d]
Fluorescein	$C_{arrival}$	1.91×10^{-6}	0.41	0.017	403
	Peak 1	*6.74×10^{-3}*	*0.44*	*0.018-0.019*	-
	Peak 2	*6.74×10^{-3}*	*0.514*	*0.021-0.022*	-
	Peak 3	4.55×10^{-4}	0.59	0.025	274
	Peak 4	2.61×10^{-4}	0.68	0.028	244
RWT	$C_{arrival}$	1.12×10^{-6}	0.41	0.017	420
	Peak 1a	1.80×10^{-3}	0.45	0.019	361
	Peak 2a	8.53×10^{-4}	0.52	0.022	311
	Peak 3a	4.55×10^{-4}	0.59	0.025	274
	Peak 4a	2.61×10^{-4}	0.68	0.028	244

6.10.2.1 TT 1 Discussion and Interpretation

The tracer was injected more than 30 minutes after pumping had started, assuming that nearly steady state and radial flow conditions adjusted in S7 on the test site. The injection interval was pumped in a recirculating loop for more than 30 minutes before tracer injection, too. Tracer was injected in one slug into the injection interval of the injection borehole. Despite the attempts to mix the tracer concentrations homogenously over the injection interval, the tracer in the injection well was not homogenously mixed and four injection peaks were observed in BH5 instead of one expected peak of a slug injection. The reason for such an oscillation is that the tracer was not instantaneously mixed. The time between the measured four peak concentrations in the injection well, BH5, was 0.066h to 0.067h, with one exemption of 0.05h between Peak $3a_{inj}$ and Peak $4a_{inj}$ (Table 6.9). This time interval was shorter than pumping the volume of the test interval from the bottom of the test interval up to the surface and back to the top of the injection interval (about 0.0967 hours). The tracer was injected into the test interval with one part of the tracer probably entering S7 and the rest being pumped through the hoses and the injection interval in BH5. This happened four times until about all tracer was transported out of BH5 in the direction of BH1. The same oscillation of tracer concentrations, as measured in the point-dilution tests was observed for the slug injection.

For TT1 (see Figure 6.5), the shape of the tracer concentration curves imply that less tracer was injected than breaking through: However, it was expected that the measured tracer concentrations of the injection well would be higher than those measured in the pumped well, by about one order of magnitude. After rechecking the data files no obvious mistakes were found for the calibration of the flurometer and measurements taken in the abstraction well. The same applies for the injection well. The manual sampling procedure for later analysis

seemed not to be the reason for any wrong measurements. Tracer concentrations of the samples taken at the injection well could have been decayed due to influence of daylight or storage failure, although all samples were stored in bottles in dark boxes and later in cupboards in the laboratory. A sufficient explanation for such lower tracer concentrations in the injection well was not found and the problem remains unresolved. Therefore the measured data of the injection well should be considered as relative rather than absolute values and the shape of the tracer concentration curve can be considered for discussion. The data of the pumped well recorded for fluorescein and rhodamine concentrations are considered to be reasonable and therefore can be taken as absolute values.

Even though, the time intervals $t_{peak\ to\ peak}$ between the peak concentrations of the tracers in the injection well (Peak 1_{inj} to Peak 4_{inj}, and Peak $1a_{inj}$ to Peak $4a_{inj}$) and the correlating peaks of the breakthrough curve in the pumped well (Peak 1 to Peak 4, and Peak 1a to Peak 4a) were used to calculate travel velocity $v_{peak\ to\ peak}$ for each slug injection of tracer, as listed in Table 6.9. Similar time intervals and travel velocities were calculated for the tracer to travel through the fracture from BH5 to BH1 for Peak 1 to Peak 4.

Table 6.9: TT 1 – Tracer concentrations C of peak concentrations measured in the injection well BH5 and in the pumping well BH1. Calculated $t_{peak\ to\ peak}$ and $v_{peak\ to\ peak}$ are given between the recorded peak concentrations in the injection and discharge well.

Tracer	Injection	Breakthrough	$C_{injection\ BH\ 5}$ [g/l]	$C_{discharge\ BH\ 1}$ [g/l]	$t_{peak\ to\ peak}$ [d]	$v_{peak\ to\ peak}$ [m/d]
Fluorescein	Peak 1_{inj}	Peak 1	1.54×10^{-3}	*6.74×10^{-3}*	*0.0120*	*571*
	Peak 2_{inj}	Peak 2	5.83×10^{-4}	*6.74×10^{-3}*	*0.0124*	*552*
	Peak 3_{inj}	Peak 3	2.94×10^{-4}	4.55×10^{-4}	0.0128	*535*
	Peak 4_{inj}	Peak 4	1.7×10^{-4}	2.61×10^{-4}	0.0138	*496*
RWT	Peak $1a_{inj}$	Peak 1a	1.54×10^{-3}	1.80×10^{-3}	0.0118	*581*
	Peak $2a_{inj}$	Peak 2a	7.59×10^{-4}	8.53×10^{-4}	0.012	*571*
	Peak $3a_{inj}$	Peak 3a	3.82×10^{-4}	4.55×10^{-4}	0.012	*571*
	Peak $4a_{inj}$	Peak 4a	2.25×10^{-4}	2.61×10^{-4}	0.0138	*496*

According to Lenda and Zuber (1970), the effective porosity, n_e, was calculated with Equation 6.9 for a combined pumping-tracer (radial) flow experiment (1D-solution), assuming a horizontal bedded layer or fracture:

$$n_e = \frac{Qt_0}{\pi x^2 H} \qquad \text{(Equation 6.9)}$$

with x being the distance between injection and pumping well and H being the mean aquifer thickness of S2. Values of n_e were between 0.225% to 0.263% for S7 (Table 6.10).

Table 6.10: TT 1 – Calculation of the effective porosity n_e with the mean transient time, t_0 = $t_{peak\ to\ peak}$ (after Lenda and Zuber, 1970).

Tracer Test	Tracer	Breakthrough	t_0 mean transient time [d]	n_e
TT 1	RWT	Peak 1	0.012	0.00229
		Peak 2	0.012	0.00236
		Peak 3	0.013	0.00244
		Peak 4	0.014	0.00263
TT 1	Fluorescein	Peak 1	0.0118	0.00225
		Peak 2	0.012	0.00229
		Peak 3	0.012	0.00229
		Peak 4	0.0138	0.00263

Superimposing test data on the Sauty-type curves allowed to determine the peclet number, P, and to calculate the longitudinal dispersivity, α_L (Sauty, 1984) by superimposing breakthrough on Sauty-type curves. For analysis, radial flow was assumed as well as an instant tracer injection. The longitudinal dispersivity, α_L for peak 1 of RWT is <0.00725m.

6.10.3 Tracer Test 3 (TT 3)

The tracer concentrations (C in g/l) over time are plotted in Figure 6.6 for the injection well (BH3) and in Figure 6.7 for the pumping well (BH1). Table 6.12 lists the tracer concentration (C [g/l]) at the beginning of the test, and the peak concentrations measured in the injection and pumping well.

For the first 45 minutes, a sample of the injection well was taken every 5 minutes. The sample intervals were gradually increased and the last sample was taken 23 hours after injection had started. In total, 37 samples were taken. The fuorescein samples were not diluted enough to measure the actual concentrations of the samples which was above 10^{-3}g/l, as shown in Figure 6.6. The samples were already lost after the measurements and repetition was not possible. However, it was assumed that the shape of the fluorescein injection curve had a shape similar to that of RWT.

The breakthrough curves of fluorescein and RWT of TT 3 are shown in Figure 6.24. Both breakthrough curves had a similar shape. Three peaks were defined on each breakthrough curve. A forth peak was defined for the fluorescein breakthrough curve, resembling a plateau rather than a peak. The tracer test details and calculated values for $v_{arrival}$ and v_{peak} are listed in Table 6.11. Remaining tracers in the system of TT 2 were detected between the start of TT 3 and $C_{arrival}$.

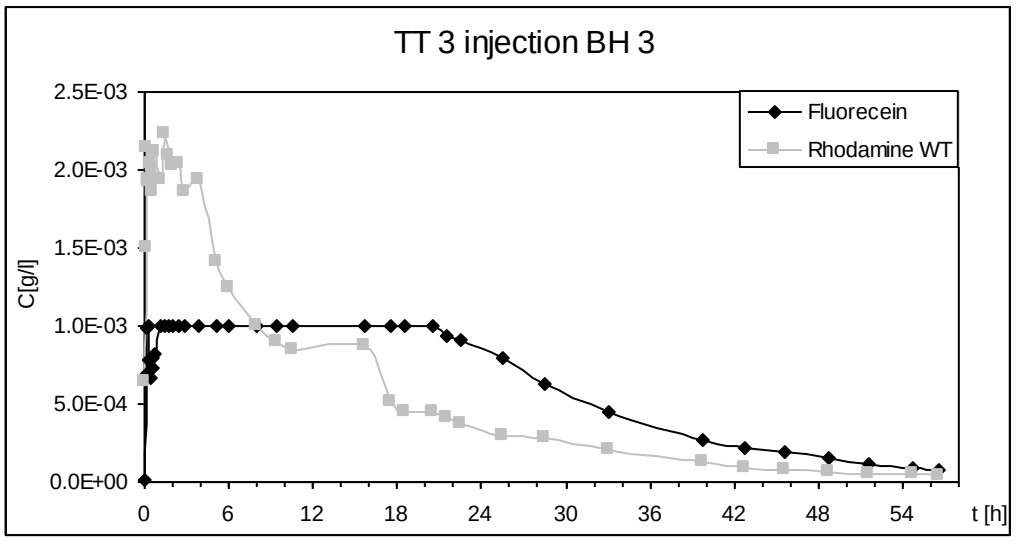

Figure 6.6: TT 3 – Tracer concentrations of fluorescein and RWT in the injection BH3.

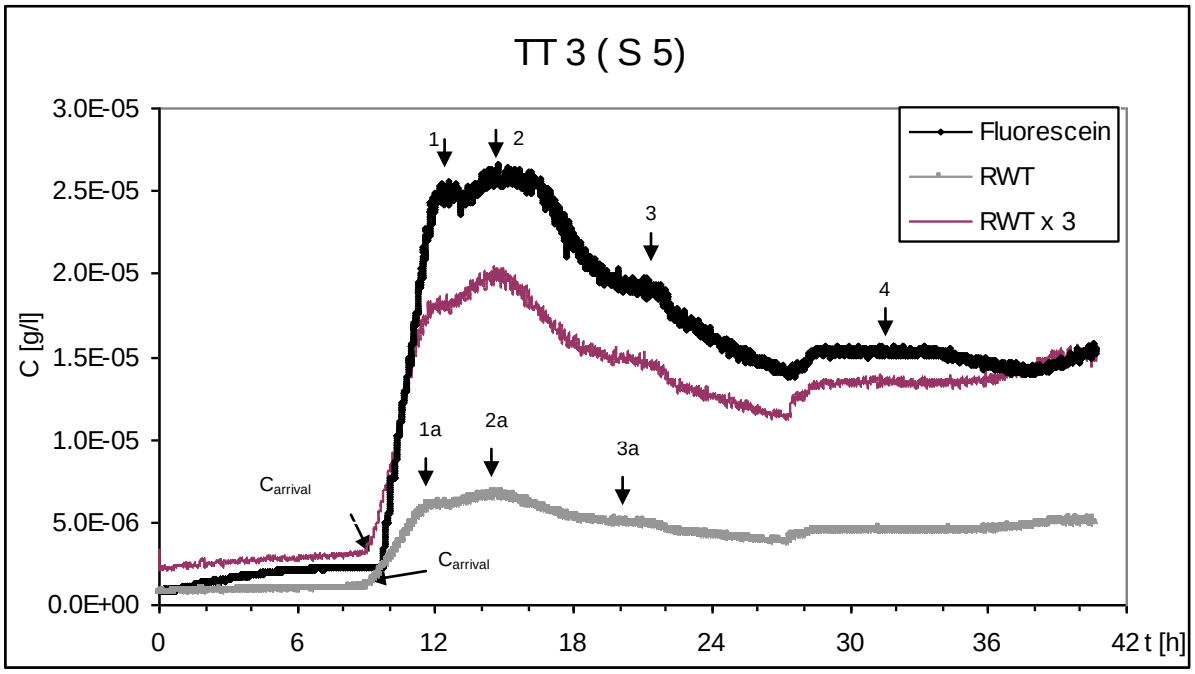

Figure 6.7: TT 3 – Tracer concentrations of fluorescein and RWT measured in S5 in BH1. The first appearance of the tracers on the breakthrough curve is marked with $C_{arrival}$. Four peaks of fluorescein (1-4) and 3 of RWT (1a-3a) were distinguished. The recorded data are plotted as running average of 4 minutes. The purple curve, RWT x 3, is the tracer concentration of RWT multiplied by 3 to compare the breakthrough of fluorescein and RWT for the same calculated mass of tracer injected.

The breakthrough curve of RWT recorded lower concentrations than the fluorescein breakthrough curve as 1g RWT was injected instead of 3g Fluorescein. To explore whether the breakthrough concentrations of RWT matched those of Fluorescein, the recorded concentrations of the RWT breakthrough curve were multiplied by 3 (RWTx3) and plotted in purple in Figure 6.7. If both tracers were injected with the same concentration and both were to travel through the same pathways, the breakthrough curves should be of the same shape. However, the purple RWTx3 tracer concentration curve in Figure 6.24 had the same shape as the breakthrough curve of Fluorescein, but at much lower concentrations. Only after about 37 hours towards the end of TT 3, the fluorescein and RWTx3 concentrations became nearly identical.

6.10.3.1 TT 3 Discussion and Interpretation

Compared to TT 1, the tracer concentration in TT 3 took much longer to reach the pumping well and the tracer concentration between peak concentrations varied smoothly over several hours instead of oscillating tracer concentration changes within minutes. 57.66% of fluorescein and 48% RWT were recovered in BH1 during TT 3.

According to Lenda and Zuber (1970), the effective porosity, n_e, was calculated with equation 6.9 for a combined pumping-tracer (radial) flow experiment (1D-solution), assuming a horizontal bedded layer or fracture, as for TT 1 (Table 6.12). Values of n_e of S5 were between 11.5% to 29.4% for S7.

Table 6.11: TT 3 – Tracer concentrations C and time t of peak concentrations measured in the injection well BH3 and tracer concentrations C and time t of arrival and peak concentrations in the pumping well BH1 (S5). Peak 4a is no identified peak value but the measured RWT concentration is listed to compare with Peak 4 of the fluorescein breakthrough curve. Distance between BH1 and BH3 is 4m.

TT 3 Discharge Well BH3 (S5)					
Tracer	Breakthrough	C [g/l]	t [h]	t [d]	*v* [m/d]
Fluorescein	start	8.77×10^{-7}	0.00	0.000	-
	$C_{arrival}$	2.65×10^{-6}	9.39	0.391	10.23
	Peak 1	2.56×10^{-5}	12.61	0.526	7.61
	Peak 2	2.61×10^{-5}	15.30	0.638	6.27
	Peak 3	1.92×10^{-5}	21.78	0.907	4,41
	Peak 4	1.57×10^{-5}	31.59	1.316	3.04
	End of Test	1.55×10^{-5}	40.65	1.694	-
RWT	start	7.02×10^{-7}	0.00	0.000	-
	$C_{arrival}$	1.20×10^{-6}	9.03	0.376	10.90
	Peak 1a	6.18×10^{-6}	12.39	0.516	7.94
	Peak 2a	6.74×10^{-6}	14.87	0.620	6.62
	Peak 3a	5.04×10^{-6}	21.08	0.878	4.67
	Peak 4a	*4.58×10^{-6}*	*31.59*	*1.316*	*3.12*
	End of Test	5.00×10^{-6}	40.65	1.694	-

Table 6.12: TT 1 – Calculation of the effective porosity, n_e, after Lenda and Zuber (1970). For Peak 4a the RWT concentration was listed to compare with Peak 4 of the fluorescein breakthrough curve.

Tracer Test	Tracer	Breakthrough	t_0 mean transient time	n_e
TT 3	Fluorescein	Peak 1	0.526	0.117
(S5)		Peak 2	0.638	0.142
		Peak 3	0.907	0.203
		Peak 4	1.316	0.294
	RWT	Peak 1a	0.516	0.115
		Peak 2a	0.620	0.138
		Peak 3a	0.878	0.196
		Peak 4a	1.316	0.294

Even after TT 3 was terminated a concentration of 2.15x10-4g fluorescein and 9.5x10-5g RWT still could be measured in the injection well BH3. Figure 6.8 shows the RWT concentration over time when BH3 was pumped to withdraw tracer from S5 after TT 3 was terminated. The pumping rate was the same as applied during the tracer test. However, the tracer concentration in BH3 could not be reduced significantly.

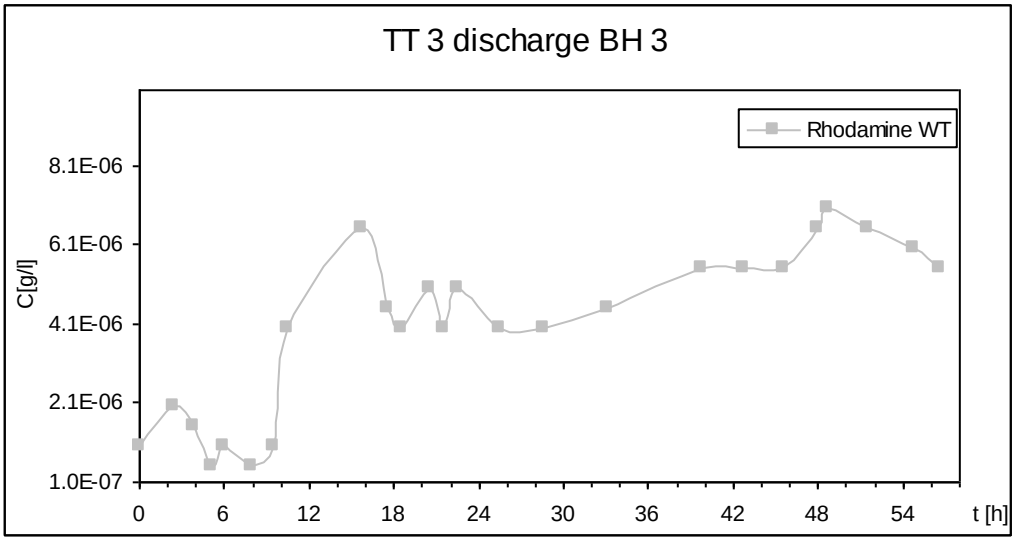

Figure 6.8: TT 3, BH3 discharge – Tracer concentrations in BH3 measured during pumping of BH3. Start of discharge about 24 hours after TT 3 has ended.

6.10.4 Tracer Tests 4 (TT 4)

The tracer concentration during TT 4 in the injection well BH2 rapidly increased to its maximum within about 0.5 hours after the slug injection and continuously decreased until the end of the tracer test (Figure 6.9).

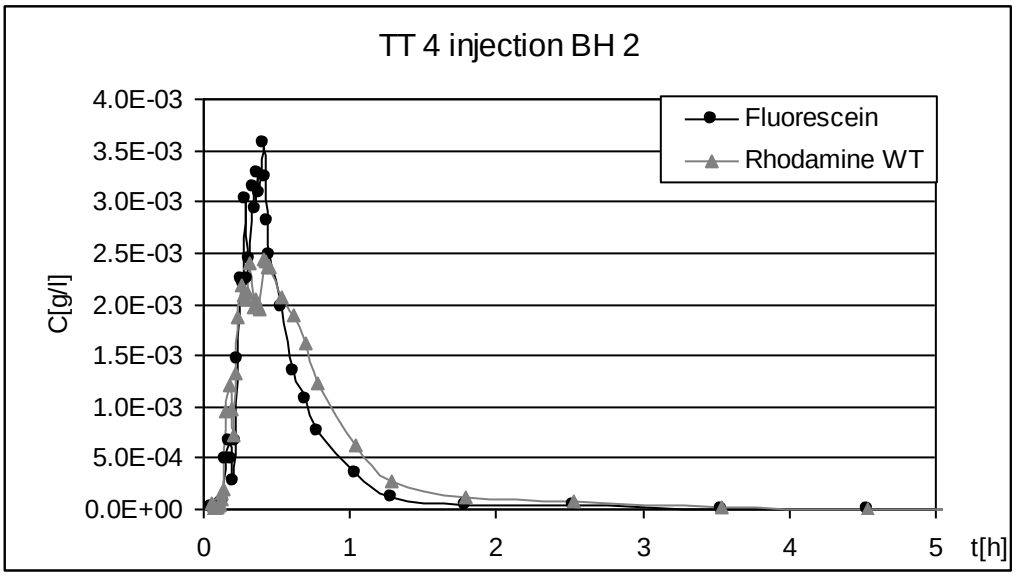

Figure 6.9: Tracer concentrations of fluorescein and RWT of TT 4 measured in the injection well BH2.

The breakthrough curve of the tracers in BH1 is shown in Figure 6.10. Two peaks on the breakthrough curves of fluorescein and RWT were marked. Tracer test details and calculated values for $v_{arrival}$ and v_{peak} for each peak are listed in Table 6.13. Both tracer breakthrough curves had similar shapes, but RWT was recorded about 18 minutes earlier than fluorescein at BH1. Furthermore, the RWT breakthrough curve showed irregular amplitudes with high RWT concentrations during the first 6 hours and after 25 hours, until the end of the test. These sudden increased values of RWT concentration corresponded with the measured turbidity values in BH1, which were recorded with the GGUN-FL 20 fluorometer (Schnegg and Doerflieger, 1992) along with the tracers during TT 4. In total, 61.05 % of fluorescein and 55.62 % of RWT were recovered in BH1 after 27.50 hours.

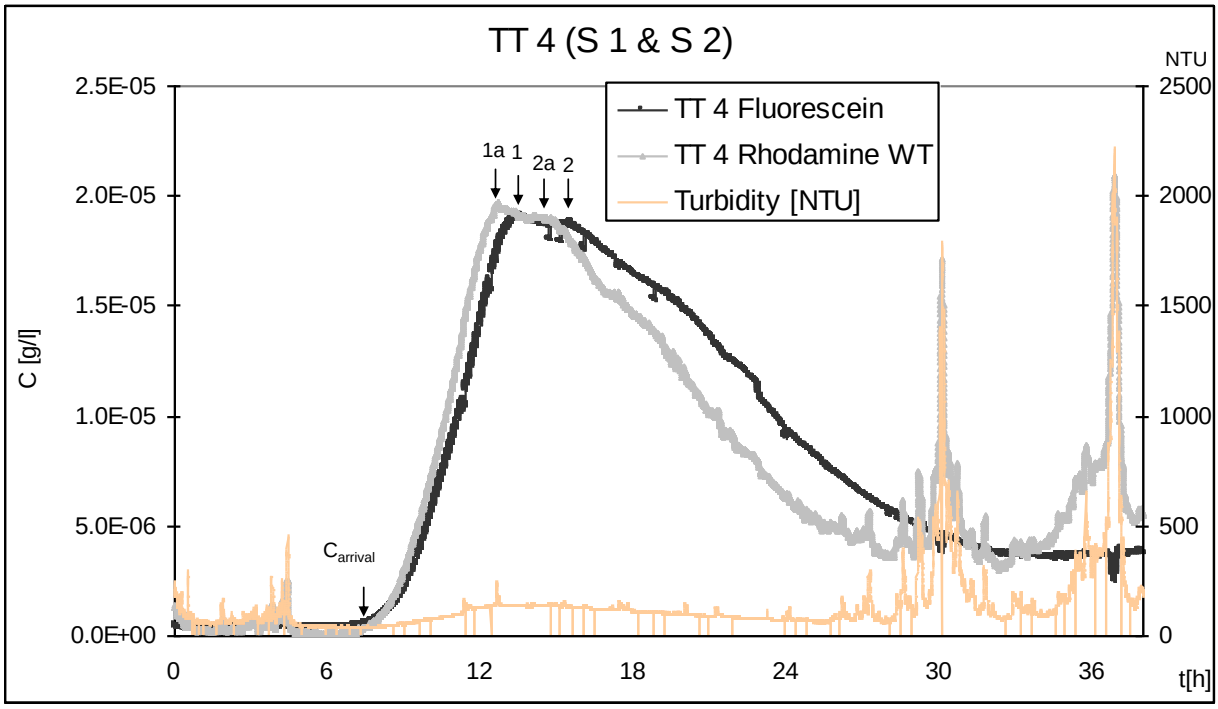

Figure 6.10: TT 4 –Breakthrough curve of fluorescein and RWT measured in S2 of BH1. The first appearance of the tracers on the breakthrough curves is marked with $C_{arrival}$. Two peaks for fluorescein (1 and 2) and for RWT (1a and 2a) were distinguished. The recorded data are plotted as running average of 4 minutes. The light orange curve is the measured turbidity in Nephelometric Turbidity Units (NTU).

Table 6.13: TT 4 – Tracer concentrations C and time t of arrival and peak concentrations in the pumping well BH1 (S2).

TT 4 Discharge Well BH1 (S1& S2)					
Tracer	Breakthrough	C [g/l]	t [h]	t [d]	*v* [m/d]
Fluorescein	start	4.47×10^{-7}	0.00	0.000	-
	$C_{arrival}$	1.87×10^{-7}	6.67	0.278	15.11
	Peak 1	1.91×10^{-5}	13.17	0.549	7,29
	Peak 2	1.87×10^{-5}	15.44	0.643	6,22
	End of Test	3.9×10^{-6}	40.65	1.694	-
RWT	start	1.28×10^{-6}	0.00	0.000	-
	$C_{arrival}$	1.55×10^{-7}	6.79	0.283	14,13
	Peak 1a	1.95×10^{-5}	12.48	0.520	7.69
	Peak 2a	1.91×10^{-5}	14.41	0.600	6.66
	End of Test	3.80×10^{-6}	27.85	1.160	-

6.10.4.1 TT 4 Discussion and Interpretation

RWT showed a lower maximum peak than fluorescein in the injection well and seemed to have remained slightly longer in the injection well with higher concentrations measured than fluorescein during the first 2.5 hours. The setup of TT 4, as shown in Figure 6.18, illustrates the injection of tracer into S1, S2 and M2 in BH2, because of the construction of the slotted casing and gravel pack around BH2. Discharge happened only in S2, as BH1 only approached this aquifer layer. This could be a reason for the different remaining times of the injected tracer in BH2. However, the difference in concentrations in the injection well seemed to be more likely a problem of accuracy of measurement of the RWT concentration than a sorbtion of RWT to the borehole wall of the injection well or the pipe work to inject tracer into the test interval.

The recorded RWT breakthrough during the first 6 hours and after 25 hours (Figure 6.27), until the end of the test, had the same shape as the measured NTU. It is probable that the scattering of light caused by the sediment falsely influenced the RWT sensor of the GGUN-FL 20 fluorometer (Schnegg and Doerflieger, 1992), as the detector and emitter filters were fairly crude with overlapping transmission wavelengths. In contrast, the fluorescein filters seemed to separate the excitation and emission wavelength more effectively. The measured turbidity particles could be caused by silt or clay particles, typically occurring in S5, according to the core analysis of Mitchener (2003). As the NTU concentration was abstracted from the recorded data after the test was finished, no representative samples turbidity particles were taken for confirmation.

According to Lenda and Zuber (1970), the effective porosity, n_e, was calculated as described for TT 2 (Table 6.14). The effective porosity, n_e, of Peak 1 and Peak 2 of both tracers were

very close together. It is likely that Peak 1 represented one pathway and Peak 2 could be neglected.

Table 6.14: TT 4 – Calculation of the effective porosity, n_e, (after Lenda and Zuber, 1970).

Tracer Test	Tracer	Breakthrough	t_0	n_e
TT 4	Fluorescein	Peak 1	0.549	0.112
(S 1 & S 2)		Peak 2	0.643	0.130
	RWT	Peak 1a	0.520	0.121
		Peak 2a	0.600	0.139

BH2 was pumped after TT 4 was finished to discharge the remaining tracer in S2. The discharge period started about 24 hours after TT 4 was finished and lasted for 46.53 hours. At the end of the discharge period, tracer concentrations of 3 x 10^{-6} g/l fluorescein and 6 x 10^{-6}g/l RWT were measured.

6.10.5 Tracer Tests 5 (TT 5)

TT 5 was a repetition of TT 4 which was terminated after 1.66 days. The goal of TT 5 was the measurement of the final tail of the breakthrough curve. This was also the reason to run the test for 4.34 days. To receive better signal than in TT 4, 4g fluorescein were injected. RWT was not injected because of concerns that the breakthrough concentration values might be disturbed by turbidity.

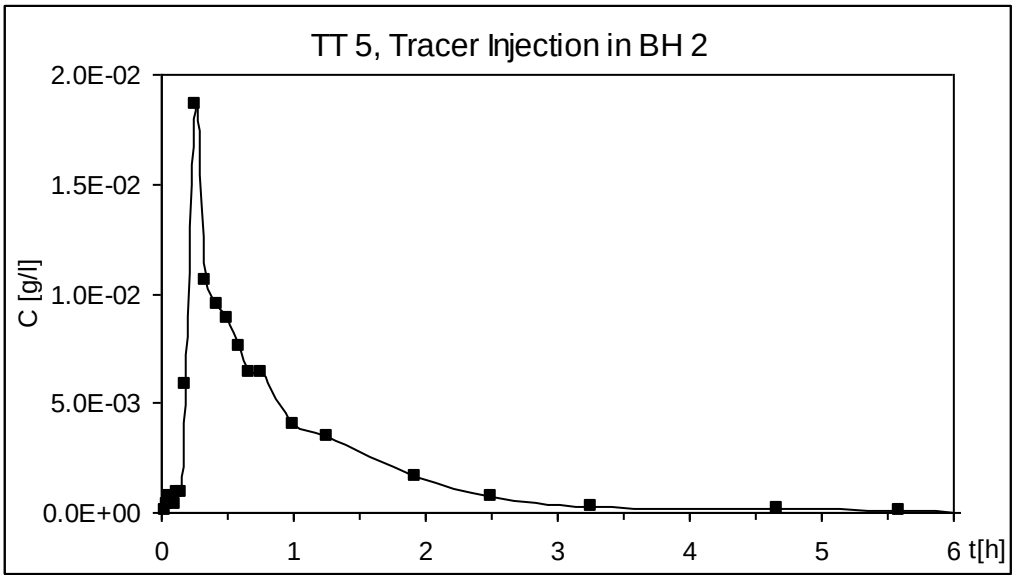

Figure 6.11: Tracer concentration curve of fluorescein of TT 5, measured in the injection well BH2.

The breakthrough of fluorescein of TT 5 in BH1 is shown in Figure 6.12. The shape of the breakthrough curve was similar to those of TT 4. The first peak was identified at about the same time and a second peak was measured after 40.36 hours. Two large gaps in the tracer breakthrough record were observed between 14.34 hours and 22.99 hours and between 37.12 hours and 37.46 hours. These gaps were caused by air and particle clogging of the fluorometer and the connecting hose to the rising main, and by total power failures of the generator providing the test site with electricity. The power failure problem with the generator continued during the whole test campaign and was corrected manually. At the end of TT 5, after 104.14 hours, 3.73g (93.44%) of fluorescein were recovered. Table 6.15 lists tracer test details and calculated values for $v_{arrival}$ and v_{peak} for the peaks.

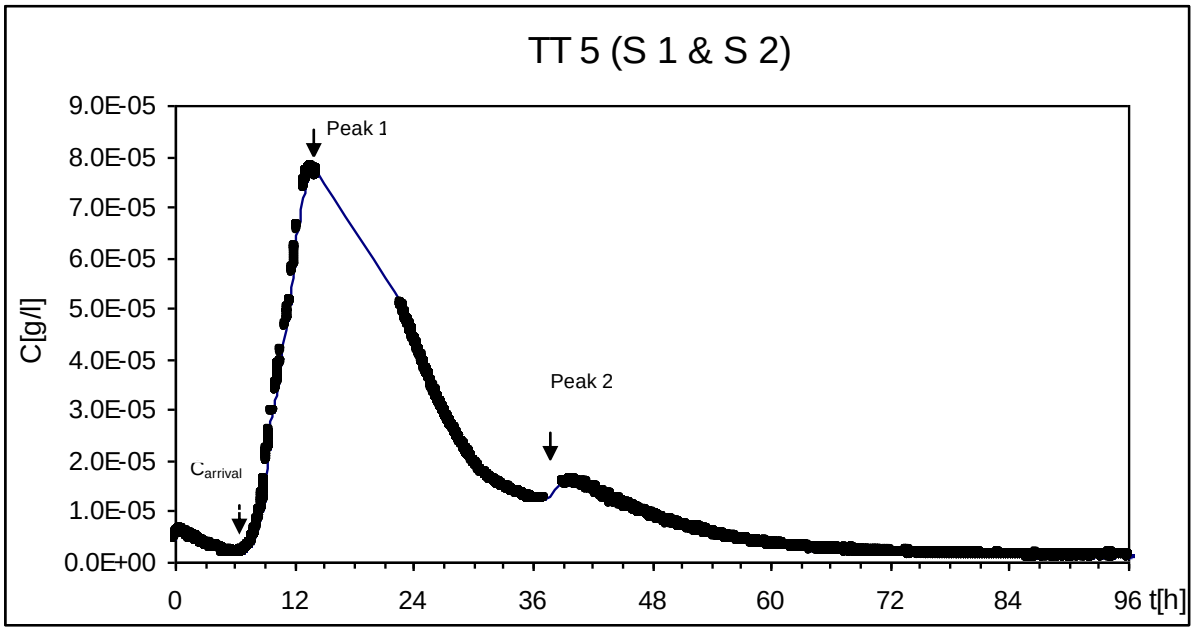

Figure 6.12: TT 5 –Breakthrough of fluorescein measured in S2 of BH1. The first appearance of the tracer is marked with $C_{arrival}$. Two peaks for fluorescein (1 and 2) were distinguished. The recorded data are plotted as running average of 4 minutes.

Table 6.15: TT 5 – Tracer concentrations C and time t of arrival and peak concentrations in the pumping well BH1 (S2)..

TT 5 Discharge Well BH1 (S2)						
Tracer	Breakthrough	distance BH2 to BH1 [m]	C [g/l]	t [h]	t [d]	*v* [m/d]
Fluorescein	start	4.1	4.57×10^{-6}	0.00	0.000	-
	$C_{arrival}$	4.1	2.05×10^{-6}	6.51	0.271	15.12
	Peak 1	4.1	7.78×10^{-5}	13.79	0.575	7.14
	Peak 2	4.1	1.62×10^{-5}	40.36	1.682	2.44
	End of Test	4.1	1.25×10^{-6}	104.14	4.339	-

6.10.5.1 TT 5 Discussion and Interpretation

Injection of tracer was carried out into S1, S2 and M2. S1 and S2 were only partially penetrated by BH2. Discharge occurred only in S2, as BH1 only approached this aquifer layer. The water in the injection interval was constantly mixed during the test, but analogue to TT 4, it is most likely that the tracer travelled down in BH2 into S2 and there towards the pumped well BH1.

Figure 6.13 shows the breakthrough curves of the tracers in TT 4 and TT 5. To compare the graphs, the fluorescein concentration of TT 5 was divided by 4. The breakthrough curves of fluorescein of TT 5 came close to match with the breakthrough curve of TT 4, from $C_{arrival}$ until peak 1 was reached. The recorded tracer concentration after peak 1 in TT 5 deviated from the breakthrough curve of fluorescein in TT 4, caused by the failures of the generator, but had a similar shape.

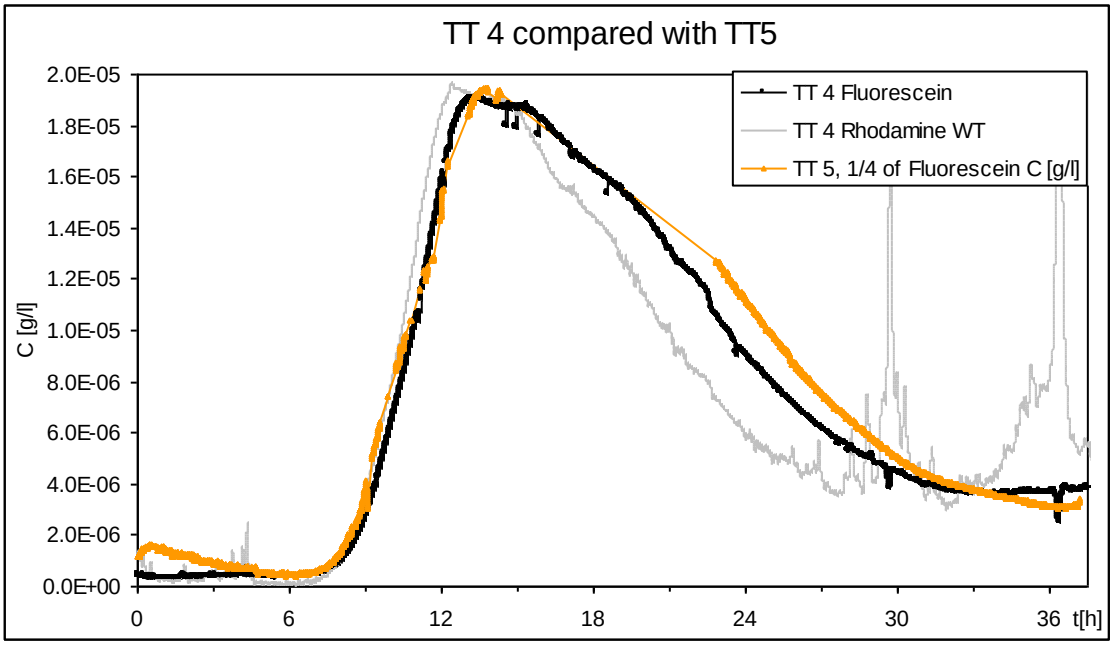

Figure 6.13: TT 5 compared with TT 4 – Tracer concentration of fluorescein and RWT of TT 4, and ¼ of the measured tracer concentration of TT 5 recorded in BH1. The recorded data are plotted as running average of 4 minutes.

Table 6.16: TT 5 – Calculation of the mean transient time, t_0, and effective porosity, n_e, (after Lenda and Zuber, 1970).

Tracer Test	Tracer	Breakthrough	t_0 mean transient time [d]	n_e
TT 5	Fluorescein	Peak 1	0.575	0.128
(S 1 & S 2)		Peak 2	1.682	0.346

According to Lenda and Zuber (1970), the effective porosity, n_e, was calculated as described for TT 2 (Table 6.16).

6.10.6 Conclusion of the Horizontal Tracer Tests

Four forced gradient tracer tests were successfully carried out in three aquifer layers of the test site. Rapid flow pathways and slower pathways through which the bulk of the tracer moved were identified in the Triassic Sandstone between the wells of the test site. Velocities and first calculated porosity values, assuming radial flow in horizontal layers, were newly gained for particular layers in Triassic Sandstone, (UK). A fast pathway was identified in TT 1 which seemed to be the fracture or group of fractures as identified with the CCTV, connecting the injection and discharge hole of the forced gradient tracer test. The measurements matched porosity values of Streetly et al. (2002) calculated with a 1-D tracer test model in Triassic sandstone north of Liverpool, where effective porosity values of n_e = 0.002 for early peaks on the breakthrough curves of fractured sandstone aquifers and matrix flow dominated sandstone aquifers.

For the first time, the very close relationship of tracer injection and breakthrough in TT 1 was measured in such an obvious relation that the tracer concentration curve in the injection well came close to match the breakthrough. TT 1 underlined that the injection well should be observed with the same intensity and time intervals as the breakthrough in the discharge well. If the injection well had not been monitored, four different fast pathways of fractured sandstone would have been identified, instead of one.

Tracer tests could be repeated successfully in the same sandstone layer measuring the same shape of breakthrough curve for TT 4 and TT 5. Fluorescein, as a conservative tracer, could be confirmed by comparing the breakthrough curves of both tests.

6.11 Vertical Tracer Tests (VTT)

6.11.1 Setup of the Vertical Convergent Flow Tracer Tests

The aim of the vertical tracer tests was to explore vertical pathways between aquifer layers, which were separated by mudstone layers. Tracer was injected in BH1 into a sandstone layer, confined by mudstone layers. Water was pumped from the sandstone layers above and below the injection layer. Three vertical tracer tests VTT 1 to VTT 3 were conducted on the test site during summer and autumn 2000. Tracer was injected after about two hours pumping, assuming that the heads in the well had reached steady state. The heads were monitored with transducers (Geokon Model 4500 Vibrating Wire Piezometers, see Chapter 5.3.2). The recorded signal, however, was heavily disturbed by electrical current interferences with other electrical equipment run on the test site. The concentration of tracer was logged with the GGUN-FL 20 fluorometer (Schnegg and Doerflieger, 1992) in one pumping well. In the other pumping well, a self constructed fluorometer ("Schneggli" by Richard Greswell in 2000) was applied to measure the fluorescein concentration. The concentration of tracer in the injection well was measured with a Perkin-Elmer fluorometer (at water samples taken) or with the self constructed fluorometer mentioned above (Greswell, 2000). The setup of the vertical tracer tests, VTT 1 to VTT 3, is schematically shown in Figure 6.14. The recirculation loop, mixing the tracer over the whole depth of the injection layer in the injection well, was constructed with a hose of one centimetre diameter. The recirculated water was injected at the top of the test interval in BH1. The Grundfos MP1 pump was connected to the hose or the recirculating loop and placed at the bottom end of the test interval. Water was pumped up to the well top and down into the well, releasing the water through the hose at the top elevation of the injection interval with a recirculation loop of 18.75 m^3/d.

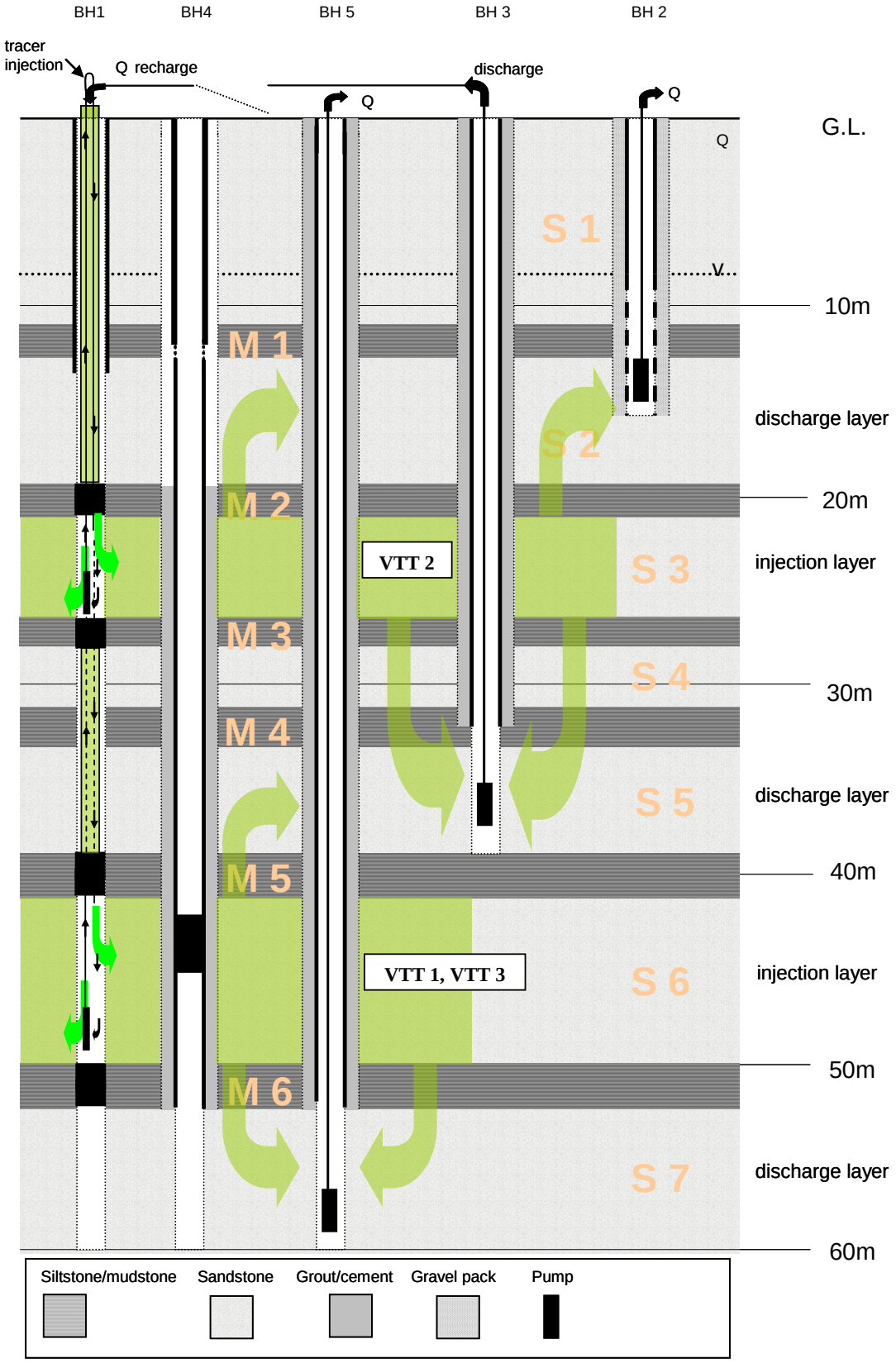

Figure 6.14: Schematic setup of the vertical tracer tests VTT 1, VTT 2 and VTT 3. The injection interval in BH1 was constantly mixed during the tests. The tracer was injected in the injection layers in BH5 and breakthrough was observed in the discharge layers in BH2, BH3, and BH5.

A deviation to a fluorometer as well as a deviation to take samples or inject tracer was installed on the surface of the test interval. Table 6.17 gives an overview of the pumping rate, pumping time and injected mass of tracer. The tracer concentration in the injection well and discharge wells was measured with online fluorometers and by taking water samples which were later analysed in the laboratory.

Table 6.17: Details of the vertical tracer tests: Injected tracer amount, injection layer, injection length, pumping rates, and length of the vertical tracer test are listed.

Tracer Test	Injection			Pumping			Recovered Tracer	
	Layer	Tracer	Period [h]	Well/Layer	Rate [m³/d]	Period [h]		
VTT 1	S6	57 g Fluorescein	79.83	BH3 / S5	61.34	184.40	2.32g	4.07%
				BH5 / S7	190.99	16.93	1.075g	1.89%
VTT 2	S3	57 g Fluorescein	81.3	BH2 / S1&S2	55.30	120.76	9.49g	16.65%
				BH3 / S5	61.34	309.00	n.a.	
VTT 3	S6	57 g Fluorescein	64.5	BH3 / S5	61.71	117.75	n.a.	
				BH5 / S7	115.77	93.50	4.34g	7.61%

6.11.2 Forced Tracer Injection during the Vertical Tracer Tests

Processing the vertical tracer tests, it was expected that the aquifer layers were leaky aquifers and that connections in the mudstones between the aquifers existed functioning as pathways for tracers. Tracer was injected into the injection layer over the whole depth of the injection interval in BH1. The tracer was forced into the injection layer by recharge. In an ideal homogenous injection layer, the tracer plume should have a disk shape over the whole depth of the injection layer with the same radius in all directions around the injection well BH1. However, flow was measured in the injection layer, and water was abstracted in the aquifer above and below the recharge layer. It was expected that such an injected tracer plume would

not be as sensitive to the natural flow fields induced by the natural gradient as a slug injected tracer and would therefore remain within the area of the pumped wells and the created head differences by pumping the sandstone layers above and below the injection layer. The goal in each vertical tracer test was to inject a plume of tracer over the whole thickness of the aquifer around the injection well BH1. During all vertical tracer tests, BH3 was pumped and the water was used as recharge for the injection interval in BH1. 57g of fluorescein tracer, diluted in 216 litres of prior pumped groundwater, were injected at a constant concentration level over several hours into the recirculation loop in the injection well with a peristaltic pump. The tracer mass to be injected was dimensioned in such a way that under perfect conditions a minimum and evenly distributed tracer concentration of 1×10^{-5} g/l in the injection layer was maintained, high enough to be detectable by the applied flurometer in the abstraction wells. The injection of tracer was started after about one hour pumping when nearly steady state had been reached in the pumped and recharged aquifer layers. The tracer concentration in the injection well was monitored by taking water samples for later analysis in the laboratory.

A first estimation of the dimension and radii of the injected tracer plumes created in the injection layer were calculated by applying the porosity values defined by Mitchener (2003) listed in Table 6.18, assuming no flow in the layers and no abstraction of water in the borehole array. The used porosity values of Mitchener (2003) for the calculation were presumably higher than the effective porosity (n_e) into which the tracer was forced by the injection. Applying values for n_e half the size of those from Mitchener (2003), but as calculated for S5 and S2 for horizontal tracer tests, would double the size of the injection plume and vice versa. Using values n_e as of TT 1 for a fracture or high permeable zone in the Triassic Sandstone would result in a radius of tracer injection between 600m and 800m. However, using values for n_e in the range of 14% to 28% to calculate the radius of the

injected tracer plumes confirmed that the tracer was forced into the injected layer, above or below the pumped boreholes in neighbouring aquifer layers.

Table 6.18: Radius of injected tracer plume in the injection layers S3 and S6 ascalculated for VTT 1, VTT 2, and VTT 3 (applying values *n* of Mitchener (2003)).

Tracer Test	Injection Rate [m³/d]	Injection Time [d]	Injection Layer Thickness [m]	Porosity *n*	Rock Volume Recharged [m³]	Injected Area in Sandstone [m²]	Tracer Plume Radius [m]
VTT 1	61.34	3.32	9	0.28	727.32	80.81	4.79
VTT 2	61.34	3.39	6.5	0.26	799.78	123.04	6.14
VTT 3	61.34	2.69	9	0.28	589.30	65.48	4.31

6.11.3 Vertical Tracer Test VTT 1

During the first vertical tracer test, VTT 1, tracer was injected in the aquifer layer S6 in borehole BH1. Mudstone layers M5 and M6 were packered in BH1 with the double packer system (Greswell, 1999). Water was abstracted at the same time in S7 (BH5) and in S5 (BH3) (Table 6.18). All pumped water of S5 was used as recharge for S6 and was injected together with the tracer through BH1. The schematic test setup of the VTT 1 is shown in Figure 6.14.

6.11.3.1 VTT 1 – S6 towards S7

Tracer was injected over about 80 hours. The tracer concentration was observed with the Perkin-Elmer flurometer, using water samples, taken during the first 16 hours (Figure 6.15). The initial oscillation of the injected tracer concentration in S6 of BH1 was caused by different pumping rates of a peristaltic pump used to inject the tracer. During the test differences in the pumping rate of the peristaltic pump were observed caused by electrical current differences in the electrical supply system including the generator and the connected pumps. The pumping rate of the peristaltic pump was adjusted manually.

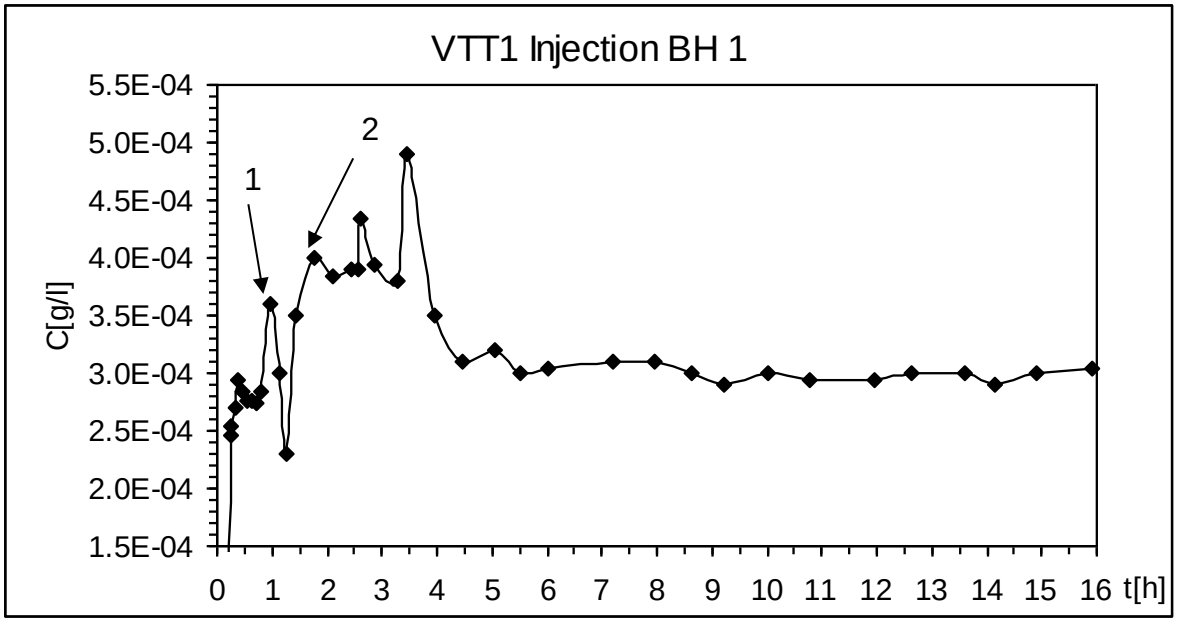

Figure 6.15: VTT 1 – fluorescein concentration versus time in the injection well BH1 (S6) during the first 16 hours, when BH5 was pumped. Two peaks were marked with 1 and 2 to be compared with the breakthrough in BH5.

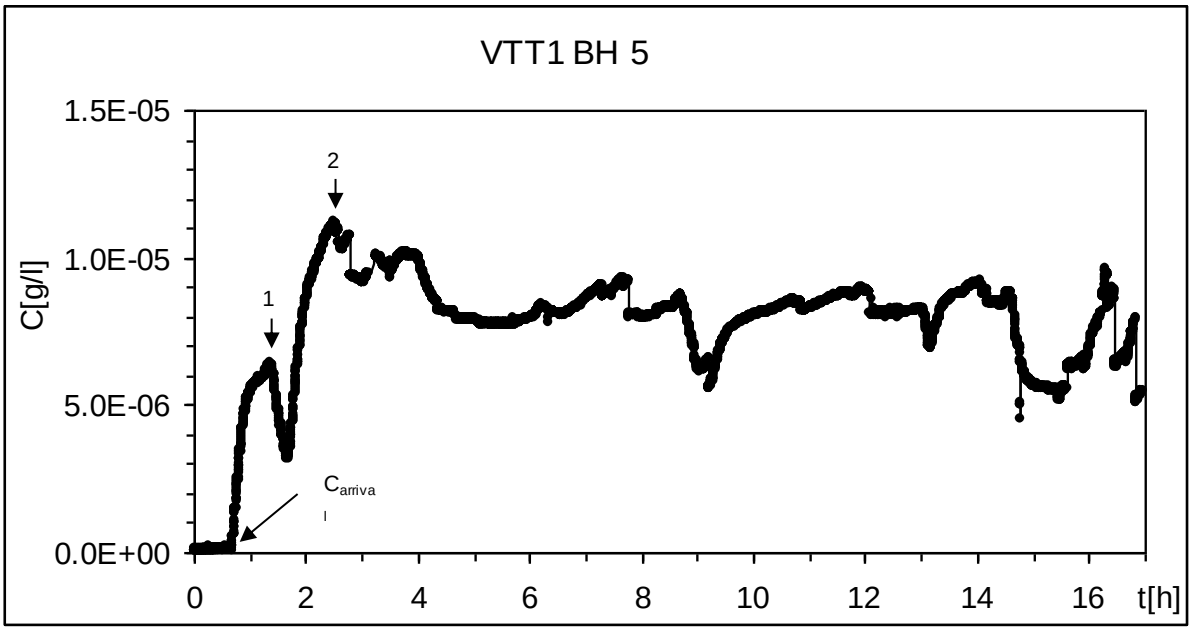

Figure 6.16: VTT 1 - Breakthrough of fluorescein tracer in the pumped well BH5 in S7. The first appearance of the tracers on the breakthrough curves in BH5 is marked with $C_{arrival}$. Two peaks marked with 1 and 2 could be compared with peaks recorded for the tracer concentration in the injection well.

The fluorescein tracer breakthrough curve in S7 (BH5) is shown in Figure 6.16. Pumping of BH5 was stopped after about 17 hours, as breakthrough in BH5 was recorded. At the termination of VTT 1 in BH5, 1,075g (1.9%) of tracer were recovered.

6.11.3.2 VTT 1 – S6 towards S7 Discussion

The test recorded a rapid breakthrough in BH5. Details are listed in Table 6.19. The drop of fluorescein concentration on the breakthrough curve after the first peak correlated with the drop of tracer concentration on the injection curve after about 1.25 hours (Figure 6.15). On the tracer concentration curve of the injection well, the tracer concentration increased again correlating with the increasing tracer concentration of the breakthrough curve towards peak 2. Following peak 2 on the breakthrough curve, no higher concentration than peak 2 was detected. If another pathway existed, it was to be expected that the tracer concentration had increased above the concentration of peak 2 (Figure 6.16). Because of the rapid breakthrough, it was assumed that the tracer travelled through a vertical fracture or a group of vertical fractures in the mudstone from the injection layer, S6, towards the pumping layer (S7).

As first estimation, average linear velocities for the peaks and peak to peak velocities (as for TT 1) were calculated under the assumption that the tracer travelled directly between BH1 and BH5 and through M5 in vertical direction (Table 6.19).

Table 6.19: VTT 1 – BH5 (S7): Measured tracer concentrations C, peak concentrations and time. Distance BH1 to BH5 is 6.85 m and the thickness of M6 is 2m.

VTT 1 Discharge Well BH5 (S7)						
Breakthrough	C [g/l]	t [h]	t [d]	v [m/d]	$t_{peak\ to\ peak}$ [d]	$v_{peak\ to\ peak}$ [m/d]
start	6.8×10^{-8}	0.00	0.000	-	-	-
$C_{arrival}$	2.16×10^{-7}	0.67	0.028	330.26	-	-
Peak 1	6.36×10^{-6}	1.38	0.057	161.13	0,0179	494
Peak 2	1.12×10^{-5}	2.50	0.104	88.80	0,0299	296
End of Test	5.5×10^{-6}	16.94	0.706	-	-	-

6.11.3.3 VTT 1 – S6 towards S5

BH5 was stopped after about 17 hours because no further changes in breakthrough towards BH5 were expected and also to increase the vertical head difference between the S6 and S5 pumped in BH3, where no tracer arrival was recorded at that time. The GGUN-FL 20 fluorometer (Schnegg and Doerflieger, 1992) was connected to measure the tracer concentration of BH3 after BH5 was switched off. At the same time BH 1 was connected to a self constructed fluorometer ("Schneggli" by Richard Greswell in 2000) to monitor the tracer concentration in the injection well (Figure 6.17). The measured tracer concentration of BH3 could not be interpreted as the recorded data were disturbed due to equipment failure. Steps in the concentration curve of Figure 6.17 were caused by different data download intervals of the self constructed fluorometer. After each interval the recorded data started at different concentrations. To avoid this a calibration of the "Schneggli" should have been processed prior to every start of a measurement interval. However, the recorded tracer measurements could be used as general observation data of the tracer concentration in the injection well. The tracer injection and recharge of water into S6 was stopped after 79.83 hours (Figure 6.17). After 83.68 hours, the maximum concentration was measured in the injection well. The

breakthrough curve for BH3 is shown in Figure 6.18. 2.32g fluorescein (4.1%) of the injected tracer could be recovered in BH3 after 175 hours.

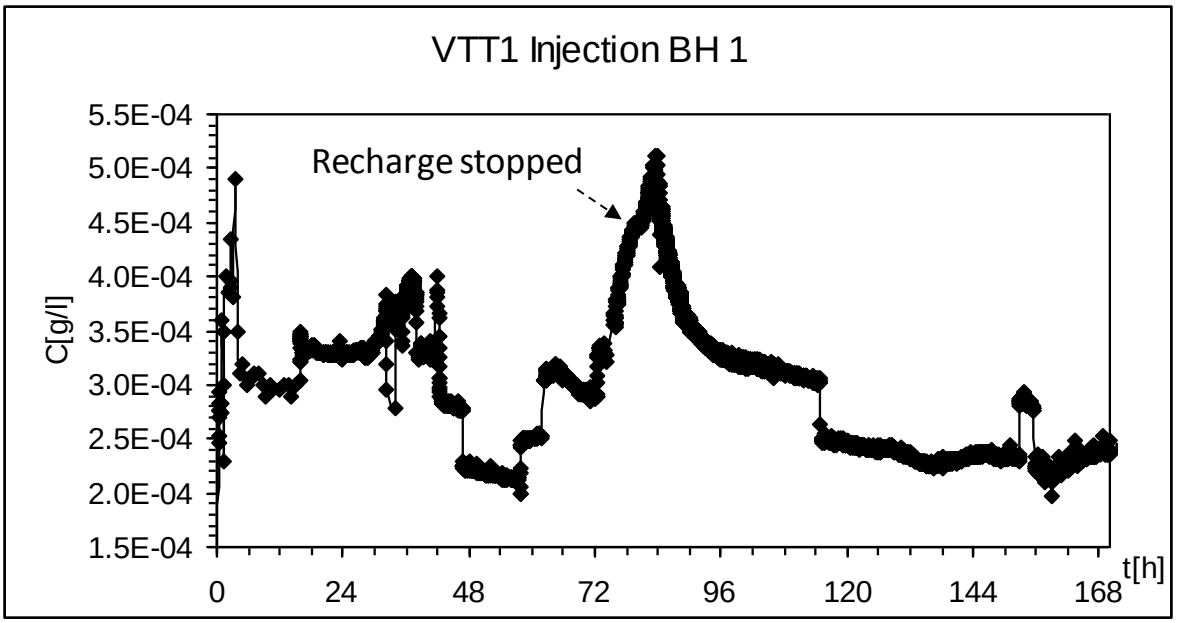

Figure 6.17: VTT 1 – fluorescein concentration in the injection well BH1 (S6) during the whole test.

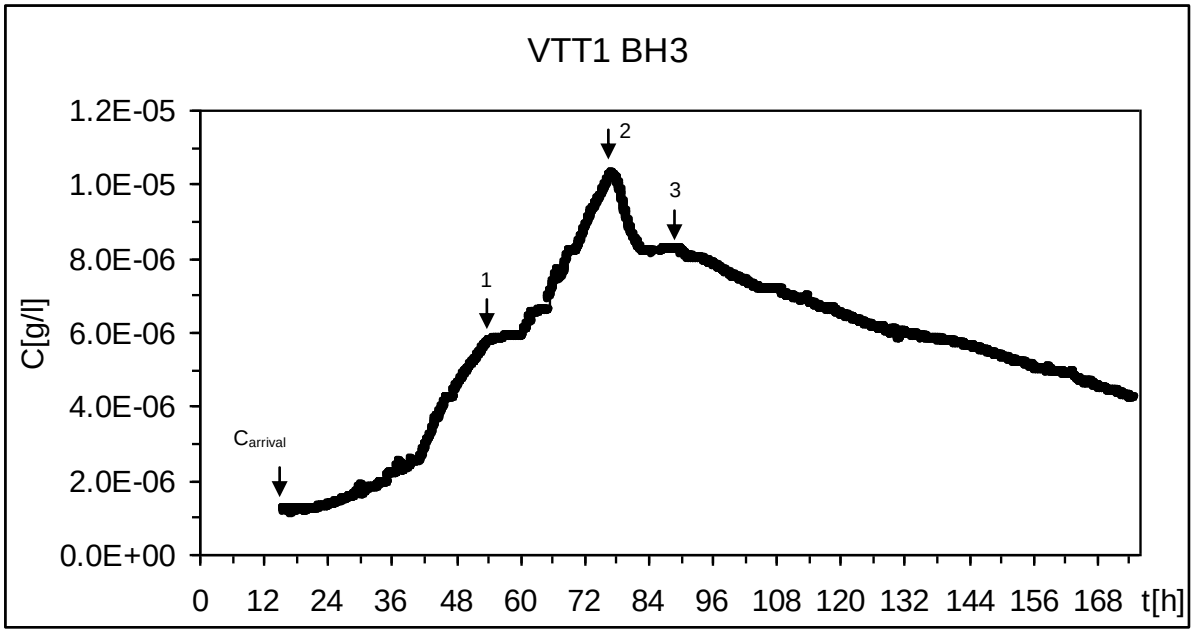

Figure 6.18: VTT 1 – Breakthrough of fluorescein in the pumped well BH3 in S5. The first appearance of the tracers on the breakthrough curves in BH3 is marked with $C_{arrival}$. Three peaks (1, 2 and 3) were distinguished.

6.11.3.4 VTT 1 – S6 towards S5 Discussion

Compared to VTT 1 in BH5, tracer breakthrough in BH3 was recorded much later with a three times smaller pumping rate (Table 6.20). Peak 2 was recorded before the recharge was stopped, and the tracer concentration started to decrease before the recharge was finished. Peak 3, however, was recorded a few hours after the maximum concentration in the injection well was measured. Under the assumption that the tracer travelled directly between BH1 in S6 and BH3 in S5, the average linear velocities for the peaks were calculated.

Table 6.20: VTT 1 – BH3 (S5): Measured tracer concentrations C, peak concentrations and time, and the calculated velocities for tracer arrival ($C_{arrival}$) of the peaks are listed. Distance BH1 to BH3: 4.90 m. Thickness of M5: 2m.

VTT 1 Discharge Well BH3 (S5)				
Breakthrough	C [g/l]	t [h]	t [d]	*v* [m/d]
start GGUN-FL 20*	1.23×10^{-6}	16.12	0.672	-
$C_{arrival}$	1.25×10^{-6}	22.59	0.941	6.38
Peak 1	5.84×10^{-6}	57.32	2.388	2.51
Peak 2	1.03×10^{-5}	77.28	3.220	1.86
Peak 3	8.22×10^{-6}	86.92	3.622	1.66
End of Test	4.20×10^{-6}	175.08	7.295	-

6.11.4 Vertical Tracer Test VTT 2

VTT 2 was processed over 309 hours. BH2 was pumped for 127.87 hours. BH2 was switched off, after breakthrough of tracer could be recorded and to also increase the head difference between the injection layer and BH3. BH3was continuously pumped until the end of the tracer test VTT 2. The schematic test setup of VTT 2 is shown in Figure 6.14.

During the first 127.78 hours, the tracer concentration in the injection well was measured by taking water samples for later analysis in the laboratory. Figure 6.19 shows the tracer concentration in the injection well. The fluorescein concentration decreased after 6, 24 and 74 hours caused by power failure and the interruption of tracer injection. The sharp increase after

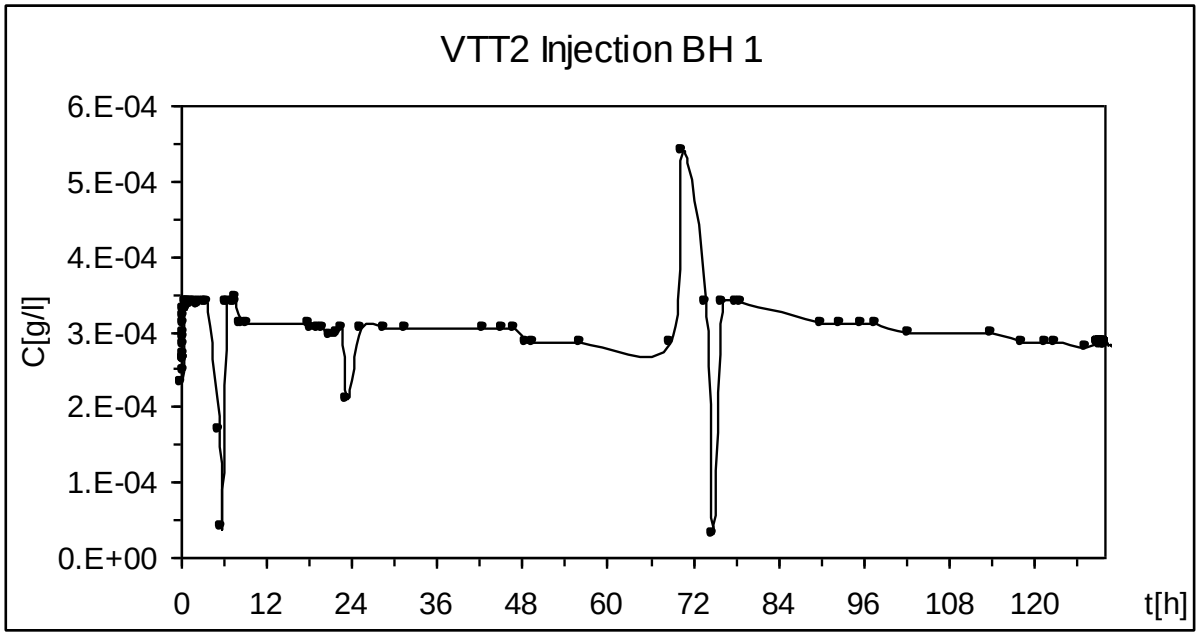

Figure 6.19: VTT 2 - Development of the fluorescein concentration in the injection well BH1 in S3 over 128 hours.

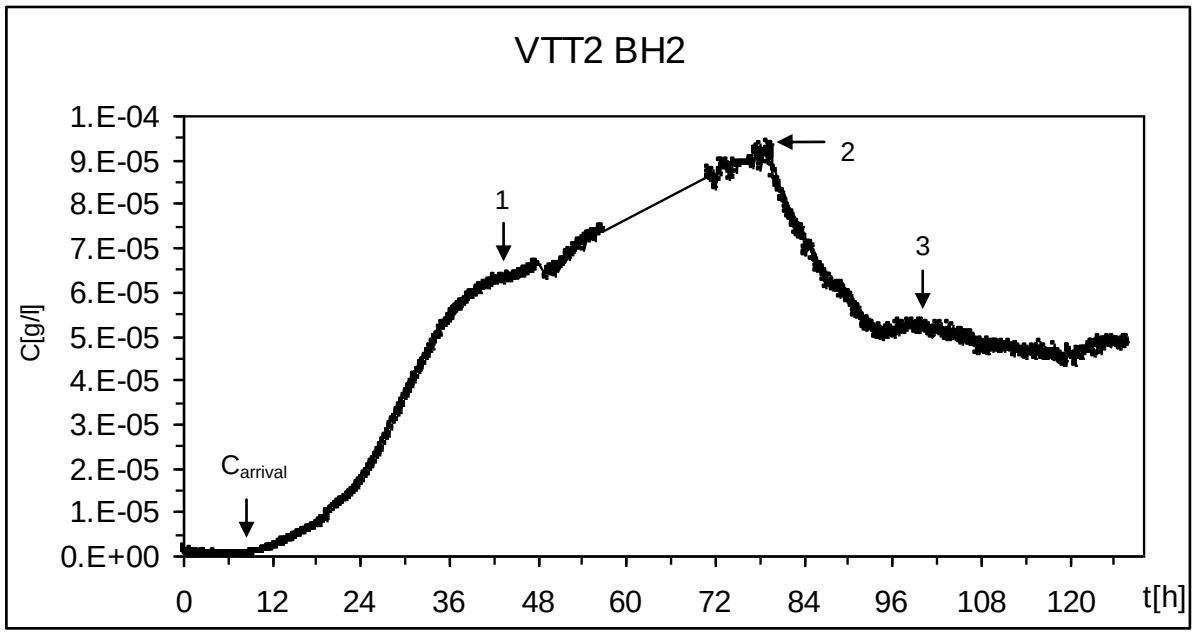

Figure 6.20: VTT 2 – Breakthough of fluorescein in the pumped well BH2 in S2. The first appearance of the tracers on the breakthrough-curves in BH2 is marked with $C_{arrival}$. Three peaks were distinguished.

70 hours caused by increased injection of tracer with the peristaltic pump, due to problems with the stability of the power supply. However, both problems were recognized and could be solved so that the tracer concentration was recorded at about 3 x 10^{-5}g/l during the first 130 hours of the test. The tracer injection and recharge of water into S3 was stopped after 81.30 hours (Figure 6.17).

6.11.4.1VTT 2 – S3 towards S2

The breakthrough curve for BH2 is given in Figure 6.20. The concentration of fluorescein increased slowly over 38 hours towards peak 1, or rather a shoulder, of the curve towards the highest concentration measured at peak 2. Between approximately 56 hours and 70 hours, the tracer concentration could not be measured as the fluorometer was blocked by air in the detection cell. It was assumed, however that the tracer concentration continuously rose during that time towards peak 2. A slight rise in tracer concentration was marked with peak 3. After 120.76 hours, 12.30g (21.70%) of the injected fluorescein were recovered in BH2.

Table 6.21: VTT 2 – BH2 (S1 & S2): Measured tracer concentrations C, peak concentrations and time, and the calculated velocities, *v*, for tracer arrival ($C_{arrival}$) of peak 1, peak 2, and peak 3 are listed. Distance BH1 to BH2: 4.2 m. Thickness of M6: 2m.

VTT 2 Discharge Well BH2 (S1 & S2)				
Breakthrough	C [g/l]	t [h]	t [d]	*v* [m/d]
start	2.22 x 10^{-6}	0.00	0.000	-
$C_{arrival}$	7.28 x 10^{-7}	9.08	0.378	16.40
Peak 1	6.6 x 10^{-5}	47.29	1.970	3.15
Peak 2	9.39 x 10^{-5}	79.67	3.320	1.87
Peak 3	5.57 x 10^{-5}	99.63	4.151	1.49
End of Test	4.95 x 10^{-6}	120.76	5.032	-

6.11.4.2 VTT 2 – S3 towards S2 Discussion

The highest tracer concentration listed for peak 2 was measured shortly before recharge was stopped. The closest distance between BH1 and BH2, equal to the horizontal distance between the injection and pumping well plus the thickness of M2 was used to calculate the average linear velocities for three peaks observed in BH2, as listed in Table 6.21.

6.11.4.3 VTT 2 – S3 towards S5

The breakthrough of tracer in BH3 delivered only poor data, due to sediments in the detection chamber of the self constructed fluorometer ("Schneggli" by Richard Greswell in 2000) during the first 130 hours. Despite cleaning and maintenance of the used equipment, the tracer concentration measured consisted of three blocks with decreasing steps in tracer concentration from one block to the other. The data are not discussed any further.

6.11.5 Vertical Tracer Test VTT3

The setup of the vertical tracer test VTT 3 was analysed to VTT 1 as schematically shown in Figure 6.14. The tracer test was processed for about 120 hours. During the tracer injection of the first 62 hours, the concentration of fluorescein in borehole BH1 varied between 2.25×10^{-4} g/l and 3.25×10^{-4} g/l (Figure 6.21). After injection of tracer and recharge in BH1 was stopped (after 64.5 hours) the tracer concentration dropped to about 7.5×10^{-5} g/l.

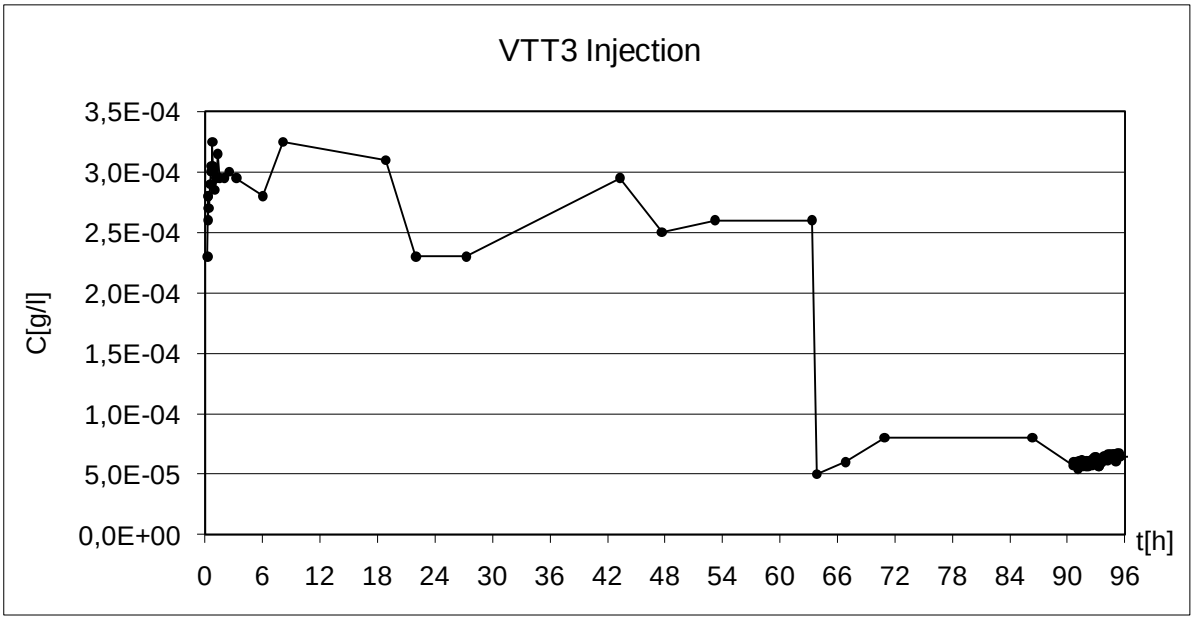

Figure 6.21: VTT 3 - Development of the tracer concentration versus time in the injection well BH1 in S5.

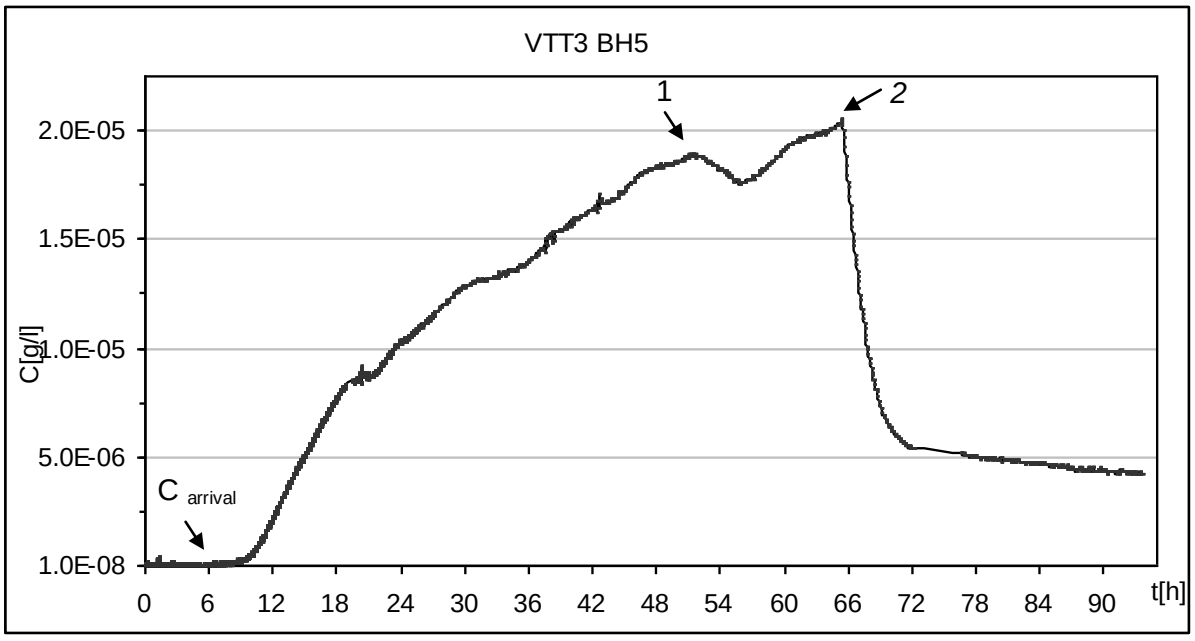

Figure 6.22: VTT 3 – Concentration versus time of fluorescein tracer in the pumped well BH5 in S7. The first appearance of the tracers on the breakthrough-curves in BH2 is marked with $C_{arrival}$. Two peaks were distinguished.

6.11.5.1 VTT 3 – S6 towards S7

The tracer concentration in BH5 was measured with the GGUN-FL 20 fluorometer (Schnegg and Doerflieger, 1992). The pumping rate was 115.77m³/d, about 40% lower than in VTT 1. A lower pumping rate was applied to avoid such a rapid breakthrough as in VTT 1. The breakthrough was continuously recorded. The only interruption was after 72 hours to read out data and to change the power supply of the logger box. The tracer concentration rose nearly continuously to peak 1 dropped slightly and rose again to peak 2 after 65.44 hours.

6.11.5.2 VTT 3 – S6 towards S7 Discussion

The breakthrough recorded in BH5 (S7) was quite different from the breakthrough curve recorded for the same test setup in BH5 (S7) of VTT 1. The breakthrough started not before 6 ½ hours and not after a few minutes. The different shape of the breakthrough curve was caused by the 40% reduced pumping rate. Furthermore, the new test setup and placement of the packers in BH1 might have blocked the connection to the pathway detected in VTT 1 and in VTT 3. A different connection between S6 and S7 was observed. Under the assumption that the tracer travelled directly between BH1 and BH5 as assumed for VTT 1, but for different connection, the average linear velocity could be calculated in Table 6.22.

Table 6.22: VTT 3 – BH5 (S7): Measured tracer concentrations C, peak concentrations and time, and the calculated velocities, *v*, for tracer arrival ($C_{arrival}$) and Peak 1 to Peak 2 are listed. Distance BH1 to BH5: 6.85 m. Thickness of M6: 2m.

VTT 3 Discharge Well BH5				
Breakthrough	C [g/l]	t [h]	t [d]	*v* [m/d]
start	4.26×10^{-8}	0.00	0.000	-
$C_{arrival}$	8.27×10^{-8}	6.09	0.254	34.84
Peak 1	1.90×10^{-5}	51.37	2.14	4.14
Peak 2	2.05×10^{-5}	65.44	2.73	3,24
End of Test	4.22×10^{-6}	93.57	3.90	-

6.11.5.3 VTT 3 – S6 towards S5

The breakthrough in BH3 was measured with the self constructed fluorometer (Greswell, 2000). The same problems as described for the breakthrough in BH3 of VTT2 occurred. The vertical tracer test between S6 in BH1 and S5 in BH3 was considered as failed, as one third of the data was recorded below the detection limit and the recorded data above the detection limit were not reliable.

6.11.6 Conclusion of the Vertical Tracer Tests

Three different vertical tracer tests were carried out in the Triassic Sandstone. Breakthrough could be monitored in all abstraction wells. Vertical hydraulic connections for solute transport of a conservative tracer between two sandstone layers, separated by a mudstone layer, were found from:

- S3 to S2, through M3.
- S6 to S5, through M5.
- S6 to S7, through M6.

Between 1.89% and 16.65% of the injected 57g fluorescein tracer were recovered during the test in the pumped wells. As a first assumption, velocities between the injection well and the pumped wells were calculated. A strong relationship between the tracer concentration in the injection well and the breakthrough curve was observed. Changes of tracer concentration in the injection well could be measured in tracer concentration changes of the breakthrough. The termination of the recharge could be observed with a corresponding rapid decrease of tracer concentration in the observation wells, however, measured with different delays on the breakthrough curve. Tracer tests could be repeated, although different pumping rates were applied. The breakthrough curve of the repeated tests (VTT 1 – S5 towards S7 and VTT 3 –

S6 towards S7) had different shapes and different quantities of tracer recovered. It is assumed that different pathways were detected by the repetition.

6.12 Tracer Tests Conclusion

A number of tracer tests could be carried out successfully on the test site in the Triassic Sandstone of the UK.:

- Point Dilution Tracer Tests delivered first linear groundwater flow velocities for six aquifer layers. A first assumption of the hydraulic gradient of these six layers could be calculated.
- Horizontal convergent flow tracer tests were carried out successfully in three different sandstone layers approached by the borehole array. Rapid breakthrough and slower breakthrough curves were recorded. First values for the effective porosity could be gained. The strong correlation between the concentration measured in the injection well and the breakthrough curve was approved to be very important, as for one horizontal tracer test, for example, four different ways might defined instead of one path of solute transport.
- Vertical convergent flow tracer tests were carried out for the first time, injecting tracer in one sandstone layer and pumping in sandstone layers above and below the injection layer. The tests were successful and tracer could be recovered and quantified in almost all pumped wells and was quantified (recovered tracer 1.89% to16.65% of the injected tracer).

For further interpretation, modelling of the horizontal and vertical tracer tests was required to quantify values of effective porosities and dispersivities for the sandstone and mudstone layers.

CHAPTER 7: Computer Modeling

7.1 Aim

The computer modeling of the test site is necessary to characterize its hydraulic conditions, solute movement and transport conditions, in addition to the analytical interpretations described in the chapters above. The computer codes MODFLOW (Harbaugh, A.W. and McDonald, M.G., 1996a and b, Harbaugh et al. 2000) and MT3D (Zheng, C., 1990, 1996) were chosen to set up a computer model of the test site and to run simulations of the pumping tests and tracer tests carried out.

The following chapter describes the:

- The setup of the conceptual model.

- The hydraulic modelling of the:
    - upflow conditions, taking the calculated natural gradient into account
    - pumping tests of the sandstone layers.

- The solute movement and transport modeling of the:
    - horizontal forced gradient tracer tests and
    - vertical forced gradient tracer tests.

Measurements taken during various test were entered into a computer model or were taken into consideration to calibrate the model.

7.2 Groundwater Modeling Software and Code Used

The groundwater modeling software Processing Modflow for WINdows (PMWIN; Chiang and Kinzelbach, 2001; PMWINpro7, Chiang, 2005) was used to model the flow and solute transport measured in various tests on the borehole array of the test site. PMWINpro7 is a pre- and postprocessor initially developed for the groundwater flow code MODFLOW (Harbaugh, A.W. and McDonald, M.G., 1996a and b, Harbaugh et al. 2000). MODFLOW is a block-centered finite difference method (FDM) and was originally designed to simulate saturated three-dimensional groundwater flow through porous media. To solve further specific problems related to groundwater flow and solute transport, PMWIN handles a variety of MODFLOW related codes (Chiang, 2005). One of those is the modular three-dimensional transport model, MT3D (Zheng, C., 1990, 1996). MT3D was chosen to model the solute transport of the tracer tests. MT3D is a transport model which uses a mixed Eulerian-Lagrangian approach to solute the three-dimensional advective-dispersive-reactive transport equation. MT3D is based on the assumption that changes in the concentration field will not affect the flow field significantly. This allows the setup and the calibration of a flow model independently. After a flow simulation is complete, MT3D simulates solute transport by using the calculated hydraulic heads and various flow terms saved by MODFLOW. MT3D was used to simulate changes in concentration of tracer concentrations in groundwater considering advection, dispersion but no chemical reactions.

7.3 Conceptual Computer Model of the Test Site

Anderson and Woessner (1991) gave an overview of groundwater flow and transport modeling. Further discussions and descriptions can be also found in Zheng and Bennett (1995) or Spitz and Moreno (1996).

Setting up the conceptual model, the block-centred finite difference grid in MODFLOW replaced the test site by a discretised domain consisting of an array of nodes and associated finite difference blocks (or cells). The sandstone and mudstone layers and their location were spatially discretised in terms of layers, rows, and columns (PMWIN: pro index notation [Layer, Row, Column]) for each cell. To represent the flow around wells it was decided to create a square mesh of rows and columns, with a wider mesh (cell diameter) at the boundaries and a gradually finer mesh towards the centre. The grid cell setup in the centre was built by a square mesh with cells of the same size of 0.15m width. The central part should be considered by a small sized cell setup to especially represent the boreholes with diameters of about 0.1m to 0.2m and to model the vertical flow of the borehole array. One cell represents a well. This was assumed to be acceptable for later hydraulic and transport modeling (Figure 7.1). According to the conceptual model, S1 to S7 and M1 to M6 were set up in 40 layers to mirror the thickness of these layers. The surface elevation in the model was considered to be flat. Table 7.1 lists the details of the grid setup of the conceptual model (Appendix VII.1 shows the size of each layer, row and column).

Table 7.1: Details of the grid geometry of the conceptual model setup in MODFLOW

Horizontal grid geometry	
Number of cells	90 rows and 90 columns
Grid size	197.24m x 197.24m
Maximum cell size	20.91m
Minimum cell size	0.15m
Number of cells in the center covering the test site	50 rows and 50 columns
Grid size covering the test site	7.5m x 7.5m
Cell size covering the test site	0.15m (uniform cell size)
Vertical grid geometry	
Vertical grid geometry	
Number of Layers	40
Top Elevation	60m
Bottom Elevation	0m

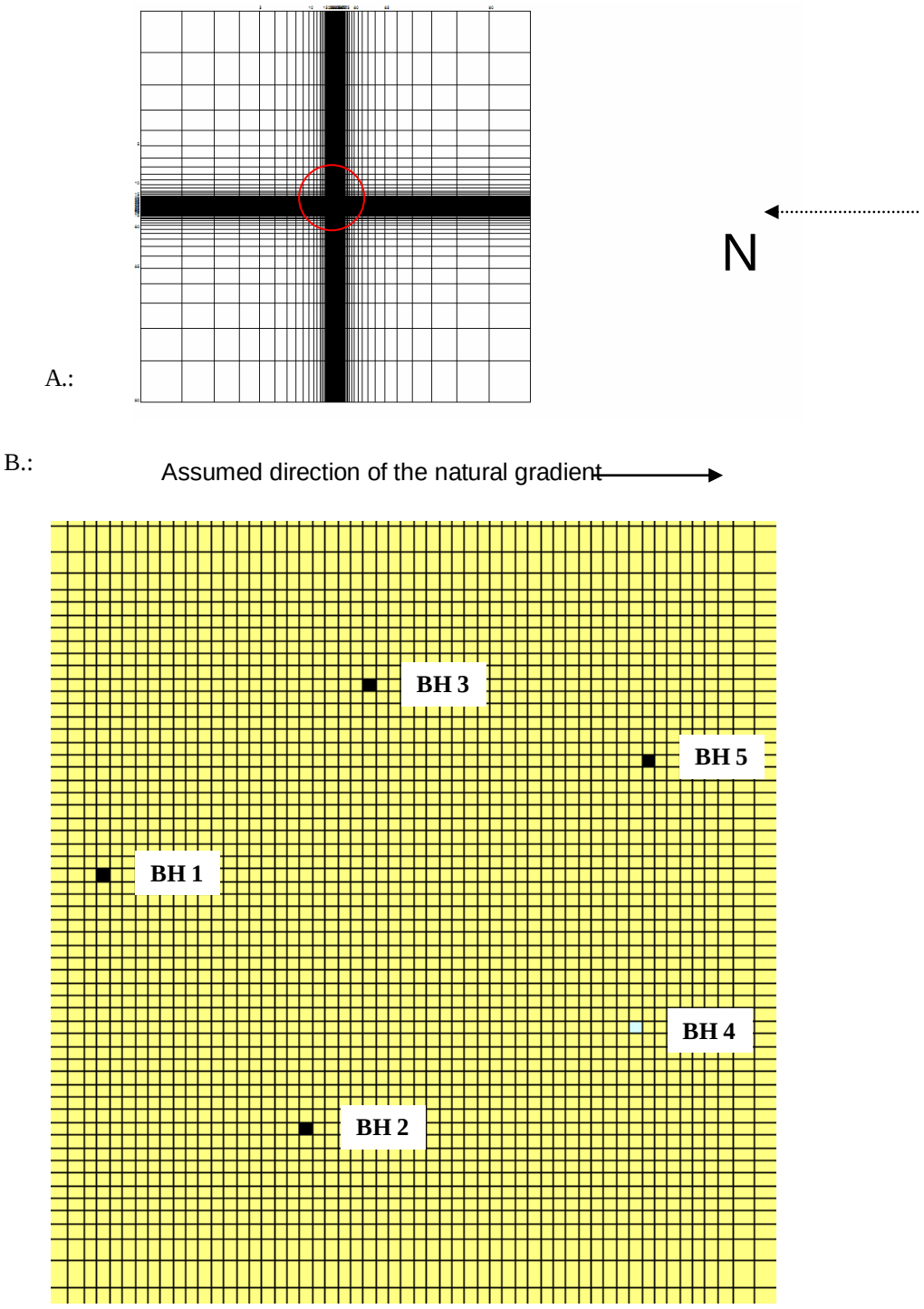

Figure 7.1: Grid setup of the University test site. A shows the boundaries of the grid. The circle marks the area of B with the central test site and the location of the boreholes BH1 to BH5.

7.4 Hydraulic Properties

The hydraulic properties achieved from the pumping test and from core data were used as initial input for the conceptual model of the layers S1 to S7 and M1 to M6. Table 7.2 lists the hydraulic parameters used for the initial groundwater flow model. Wells were defined by cells.

Table 7.2: Hydraulic input parameter to the initial groundwater model. Values for the porosity, *n*, were taken from Mitchener (2003) and Curião et al. (2001). *Kh* – horizontal hydraulic conductivity, *Kv* – vertical hydraulic conductivity, *Sc* – specific storage, *Sy* specific yield.

		Layer	*Kh* [m/d]	*Kv* [m/d]	*Sc*	*Sy*	*n*
S1		1-5	11.41	1.141	2.43×10^{-4}	0.2	0.246
M1		6+7	10^{-3}	10^{-3}	10^{-3}	0.01	0.01
S2		8-11	11.41	1.141	2.43×10^{-4}	0.2	0.246
M2		12+13	10^{-3}	10^{-3}	10^{-3}	0.01	0.01
S3		14-16	6.21	0.621	10^{-4}	0.2	0.246
M3		17+18	10^{-3}	10^{-3}	10^{-3}	0.01	0.01
S4		19-21	2.55	0.255	1.32×10^{-3}	0.2	0.246
M4		22-24	10^{-3}	10^{-3}	10^{-3}	0.01	0.01
S5		25-27	1.9	0.19	3.23×10^{-4}	0.2	0.246
M5		28+29	10^{-3}	10^{-3}	10^{-3}	0.01	0.01
S6		30-34	4.72	0.472	10^{-4}	0.2	0.246
M6		35+36	10^{-3}	10^{-3}	10^{-3}	0.01	0.01
S7		37-40	12.13	1.213	9.58×10^{-5}	0.2	0.246
BH1	cased well	1-7	10^{-6}	10^{6}	10^{-6}	1	1
	open well	8-40	100	10^{6}	10^{-6}	1	1
BH2	cased well	1-3	10^{-6}	10^{6}	10^{-6}	1	1
	slotted casing	4-9	100	10^{6}	10^{-6}	1	1
BH3	cased well	1-22	10^{-6}	10^{6}	10^{-6}	1	1
	open well	23-26	100	10^{6}	10^{-6}	1	1
BH4	ruptured casing	1-7	10	10^{6}	10^{-6}	1	1
	cased part	8-36	10^{-6}	10^{6}	10^{-6}	1	1
	grouted /flushedl	37-40	100	10^{6}	10^{-6}	1	1
BH5	cased well	1-36	10^{-6}	10^{6}	10^{-6}	1	1
	open well	37-40	100	10^{6}	10	1	1
Packer BH4		33	10^{-6}	10^{-6}	10^{-6}	10^{-6}	10^{-6}
Packer			10^{-6}	10^{-6}	10^{-6}	10^{-6}	10^{-6}

7.5 Boundary Conditions

It was assumed that the natural groundwater flow occurred from North to South (see Bouch et al., 2006), or from the left side of the model towards the right side (Figure 7.1). The boundary conditions were defined for the up-flow and down-flow boundaries at the left and the right side of the model, using the natural hydraulic gradient defined with the point dilution test. The ground water level at the boundaries of the different aquifer layers was calculated with the natural hydraulic gradient in wells, defined with the point dilution tests as shown in Appendix VII.2.

7.6 Applying Up-flow in BH1 in the Initial Model

The initial model was used to calibrate the boundary conditions against the measured hydraulic head changes in borehole BH1 due to up-flow. The head changes were calculated by sealing of M1 to M6 in the computer model under steady-state flow conditions. The values were compared with the measured head changes of the test site. Adjustment of the up-flow in BH1 was achieved by moving the heads at the boundaries up or down. After empirical adjustment of the boundary conditions, the calculated model head differences in BH1, as shown in Figure 7.2, appeared to be reasonable and could be used as definition of the mean heads in the boundaries of the model, taking the natural hydraulic gradient and upflow within the borehole array into account (Appendix VII.2). Figure 7.3 shows the up flow conditions with an open BH1 and Figure 7.4 shows an onview of Layer 11 with an open BH1. Figure 7.5 shows the cross-section with interrupted up-flow conditions with an installed packer in M2 of BH1. In Figure 7.6 the same set up with a packer in M2 is shown, but for a cross-section in flow direction.

Figure 7.2: Modelled head increase and head decrease above and below the packered mudstone layer compared to the measured data.

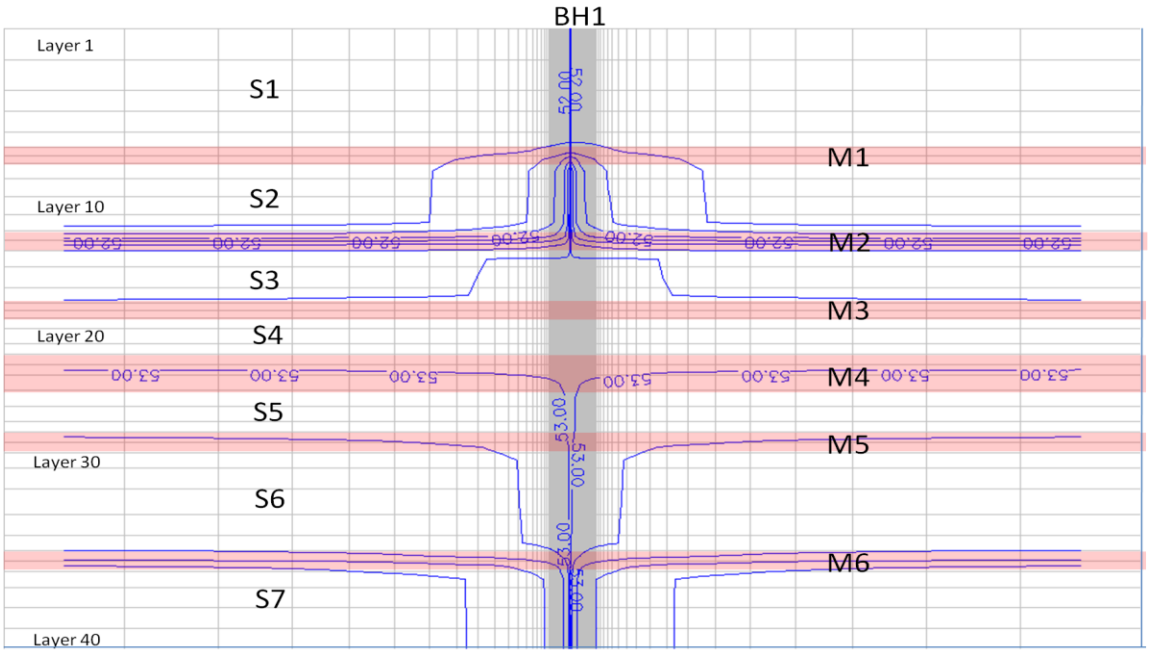

Figure 7.3: Flow conditions of the test site with an open-borehole BH1. Cross-Section at column 22.

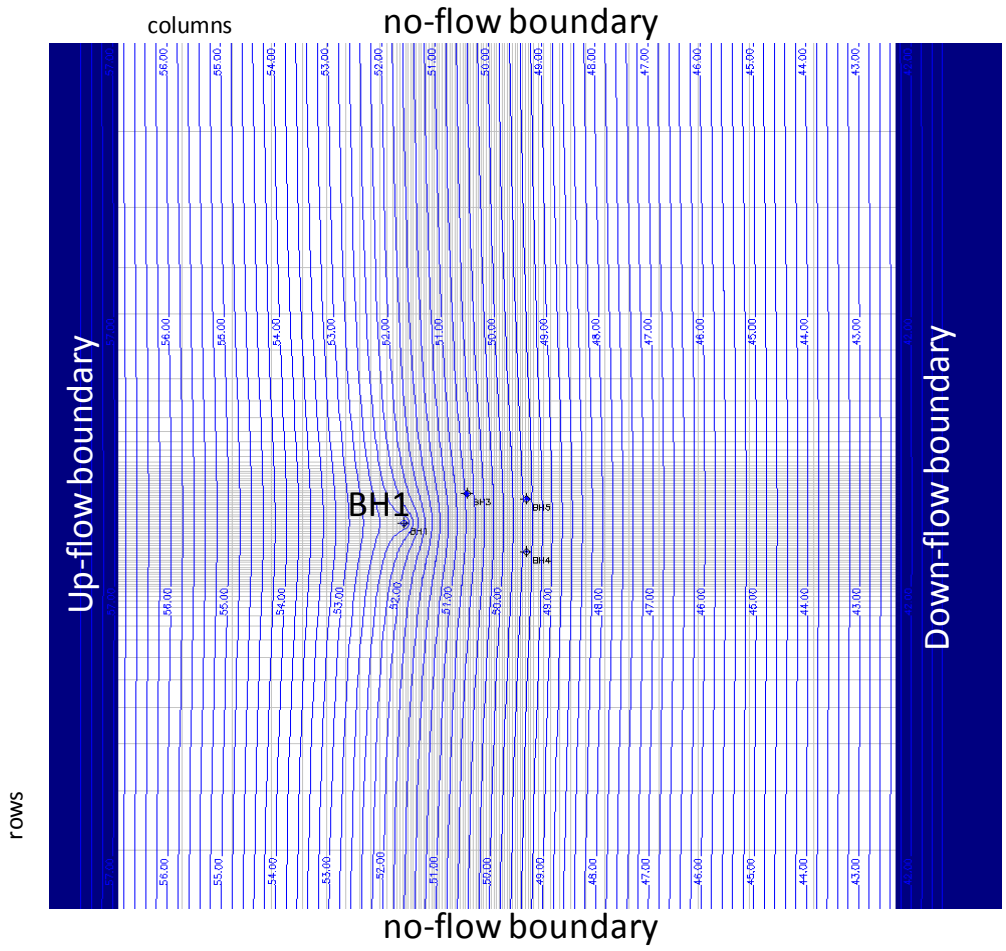

Figure 7.4: Overview on Layer 11 with an open-borehole BH1.

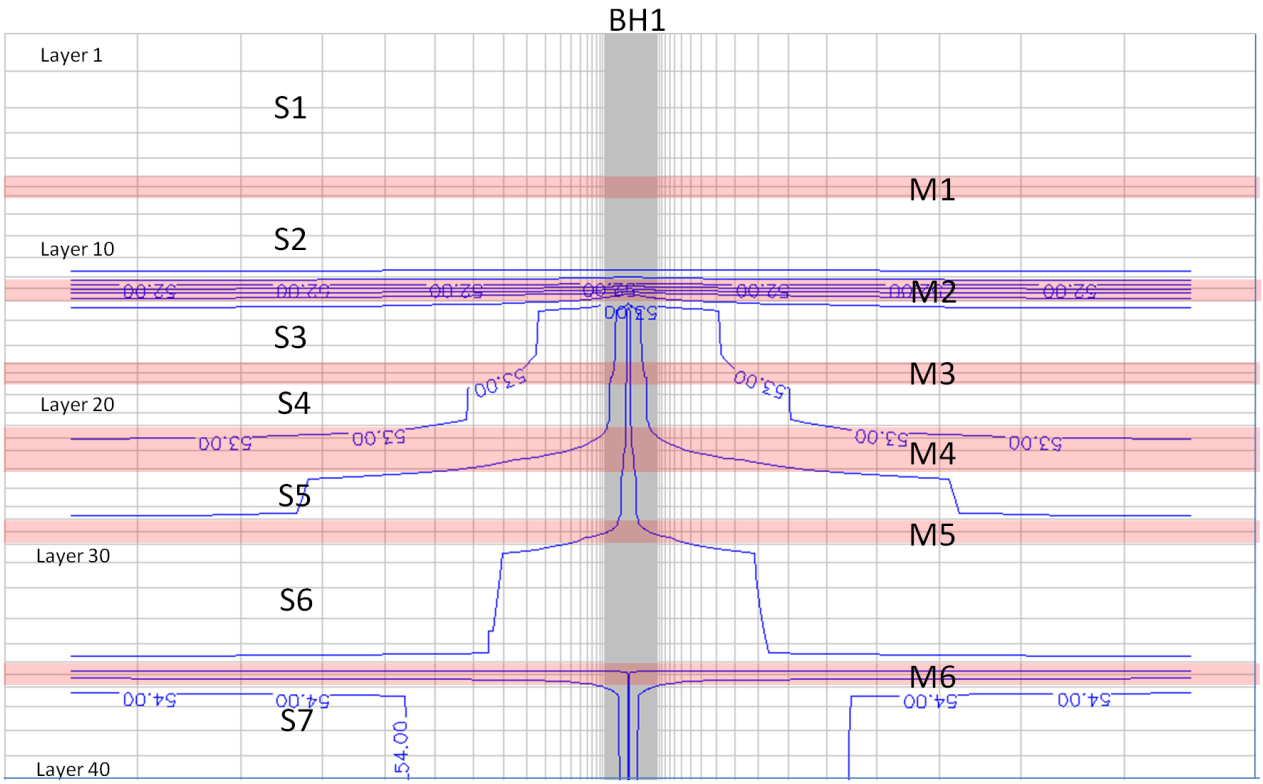

Figure 7.5: Flow conditions of the test site with a packered M2 in BH1. Cross-Section at column 22 (BH1).

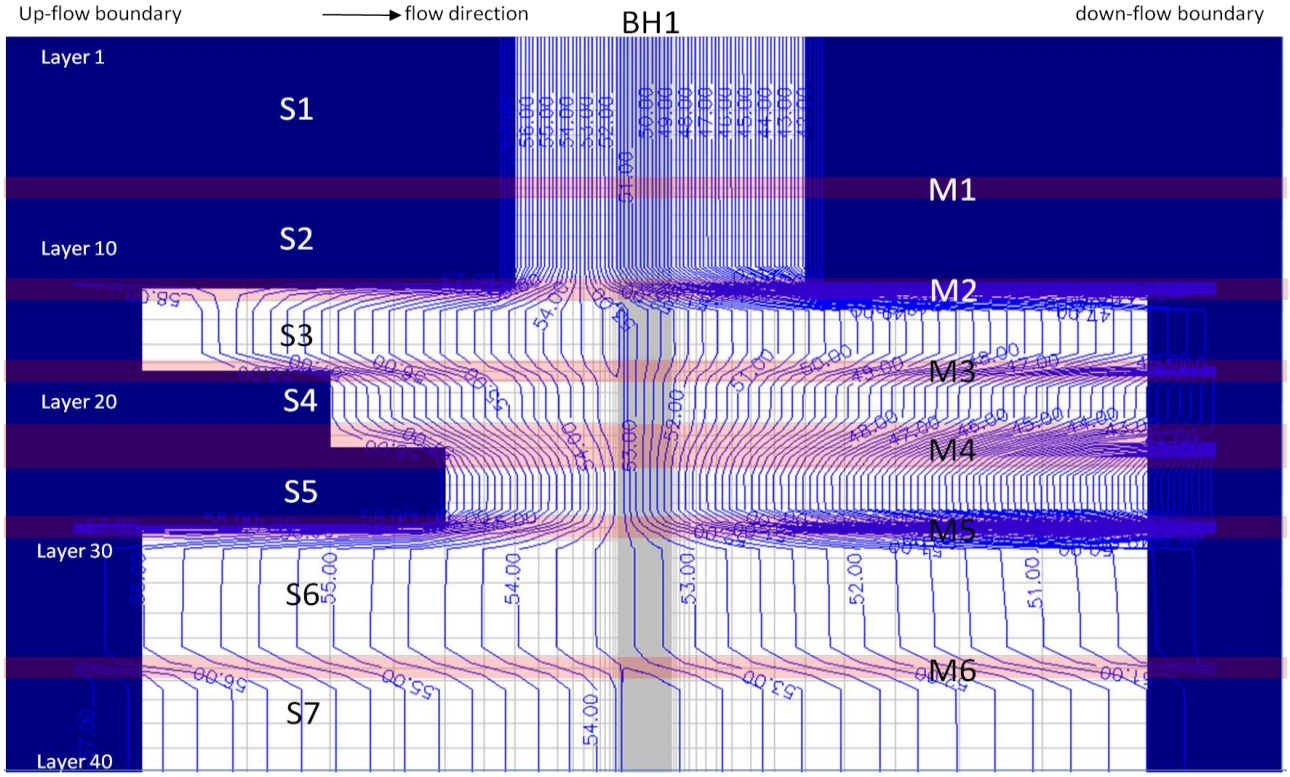

Figure 7.6: Flow conditions of the test site with a packered M2 in BH1. Cross-Section at row 43 (BH1).Blue areas are up-flow and down-flow boundaries of the different layers.

7.7 Model Calibration with Pumping Test Data

The pumping tests Test 1 to Test 9 and Test 11 to Test 14 were used to calibrate the flow model in the particular sandstone layers. The calibrated hydraulic data are listed in Table 7.3. Figure 7.7 a/b shows onviews of the test site and Figure 7.8 shows a two-dimensional cross-section during Test 7 in BH1. In Appendix VII.3, the drawdown graphs of the pumping tests fitted against the drawdown graphs of the model results are printed.

Table 7.3: Calibrated hydraulic input parameter for the groundwater model.

Aquifer layer	Test	Borehole	K[m/d]	S
S1 and S2	1	BH2	4.5	$4x10^{-4}$
	13	BH2	3.75	$6x10^{-4}$
S2	4	BH1	3.32	$5x10^{-4}$
	5	BH1	3.25	$6x10^{-5}$
S3	6	BH1	4.35	$9.5x10^{-5}$
S5	2	BH3	1.475	$2.5x10^{-5}$
	7	BH3	1.525	$2.5x10^{-4}$
	11	BH3	1.7	$2.5x10^{-4}$
	12	ob. well BH3	3.4	$2.25x10^{-4}$
S6	8	BH1	1.98	$3x10^{-5}$
S7	9	BH1	5.74	$1.75x10^{-4}$
	14	BH5	12	$3x10^{-3}$

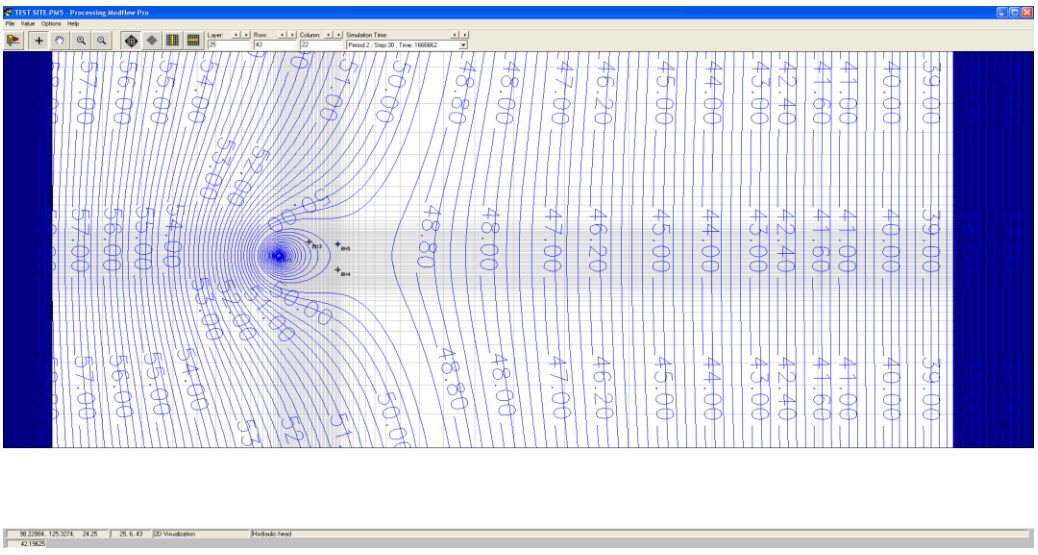

Figure 7.7 a: Overview of Test 7 pumping BH1 in S5.

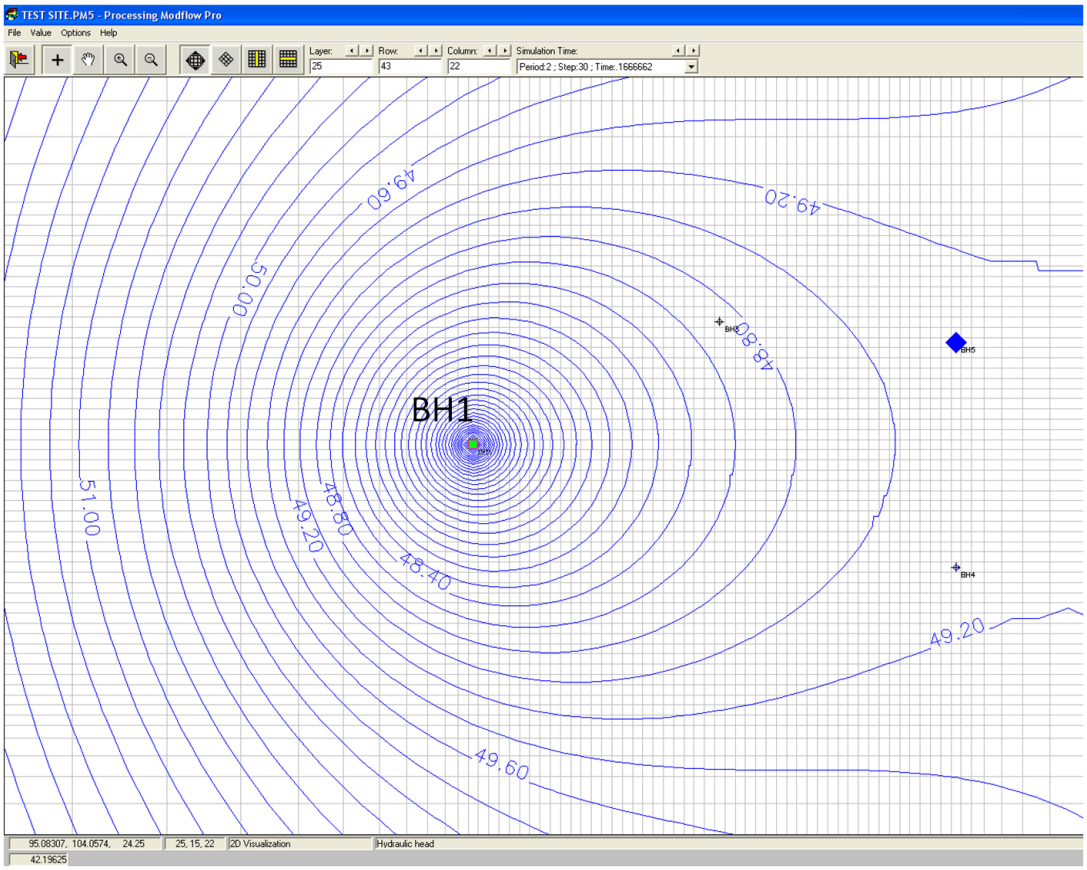

Figure 7.7 b: Detailed overview of Test 7 pumping BH1 in S5.

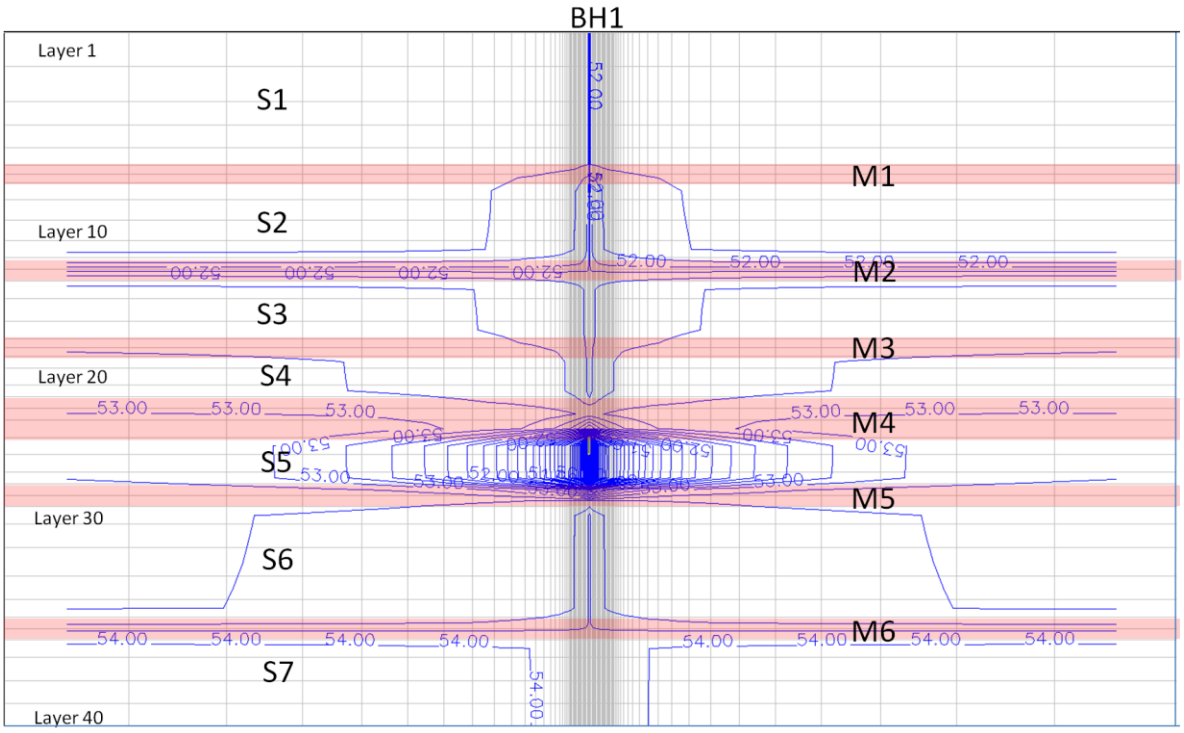

Figure 7.8: Cross-section column 22 of Test 7 pumping BH1 in S5.

7.8 Model Calibration of the Horizontal Forced Gradient Tracer Tests

TT1, TT2 and TT3 were used to calibrate the model and to calculate values of effective porosity and dispersivity. for S7, S5 and S2. In the advection package applied whenusing MT3D in PMWIN, the solution scheme for the advection term MOC method of characteristics was used. MOC is virtually free of numerical dispersion, however it can be slow and requires a large amount of computer memory when a large number of particles is required. Further, the computed concentrations can show artificial oscillations. The 1st order Eulerian approach was used to solve the transport.

As artificial oscillations were calculate during the computer modeling applying the prior described flow model, a simple three-dimensional model with the same grid setup, but only two layers was applied. One layer represented the aquifer layer and a layer on top functions as confining layer. For all test, a correlation 1:10 of longitudinal to transversal and vertical dispersion was applied.

7.8.1 Model Calibration of TT 1

Figure 7.9: shows the computer calibration of TT 1 in S7. As the transport is very fast it was difficult to match enough time steps to match the first peak of measured the breakthrough curve. A mass of 2g of tracer was injected. Calculated values of the effective porosity and dispersivity were listed in Table 7.4. The first peak of TT 1 was calibrated, because the other peaks reflect the mixing process of the tracer in the injection well (see Chapter 6). The results are similar to those calculated as first assumption (Lenda and Zuber, 1970; Sauty, 1984).

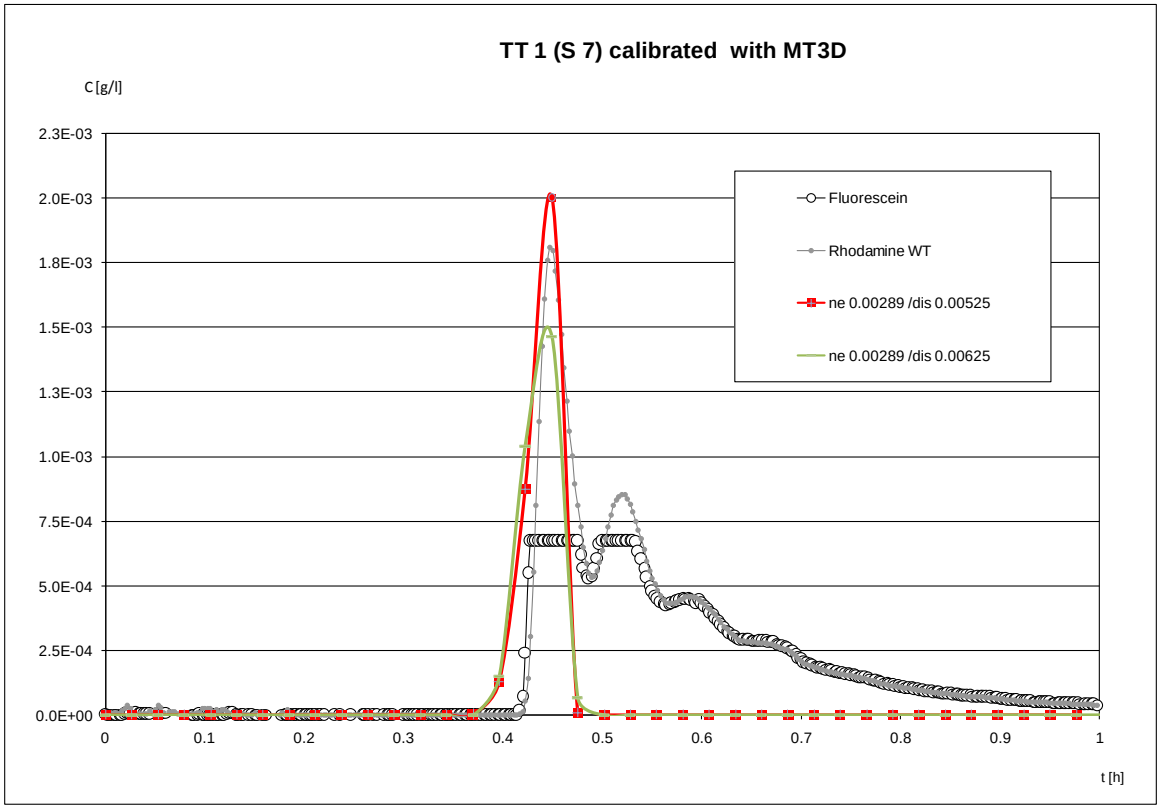

Figure 7.9: Calibration of TT 1 with MT3D.

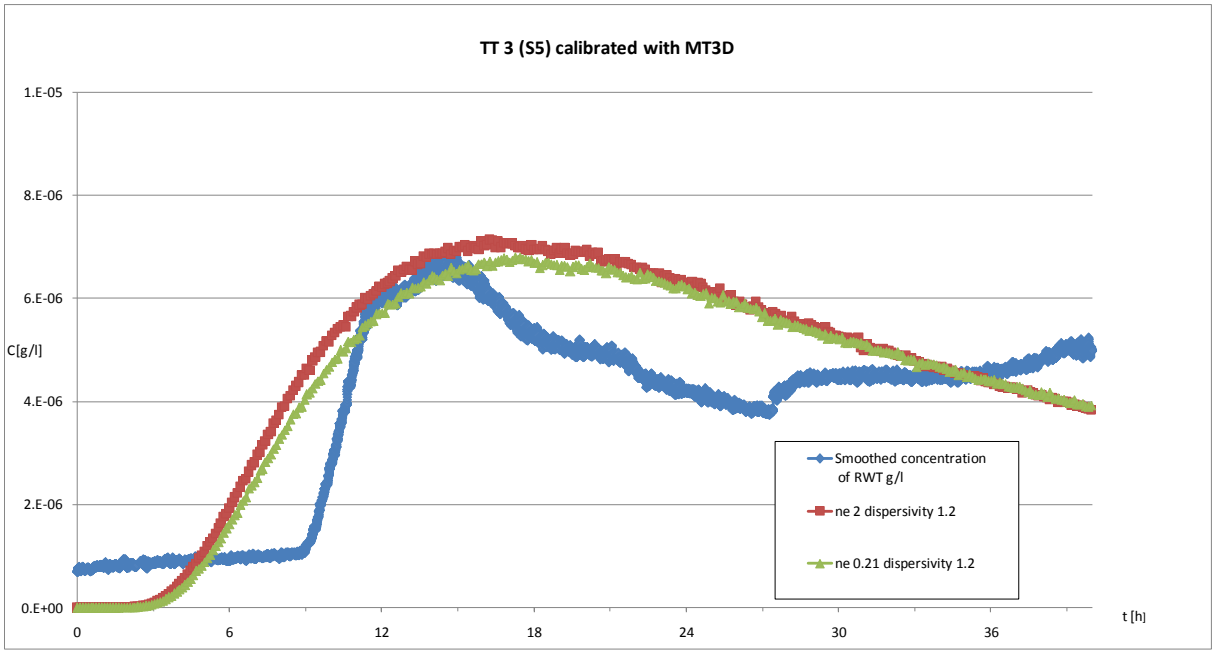

Figure 7.10: Calibration of TT 3 with MT3D. 48% of the injected tracer were applied as initial concentration for the computer model.

7.8.2 Model Calibration of TT 3

Figure 7.10: shows the computer calibration of TT 3 in S5. Entering the initial tracer concentration injected of 1g RWT, breakthrough curves of much higher concentration were computed than measured. As only 48% of tracer were recovered in TT3, 48% of tracer were injected as inital injection. The results seem to be reasonable, as the computed peak matches the peak of the breakthrough curve (Figure 7.11). Calculated values of the effective porosity and dispersivity were listed in Table 7.4.

7.8.3 Model Calibration of TT 5

Figure 7.11: shows the computer calibration of TT 3 in S1 and S2. As described above, a simple 2 layer model was applied, thus, calibrating TT5 only S2 was taken into consideration as aquifer layer. 4 g were injected as initial tracer concentration. The results were considered to be reasonable. Calculated values of the effective porosity and dispersivity were listed in Table 7.4.

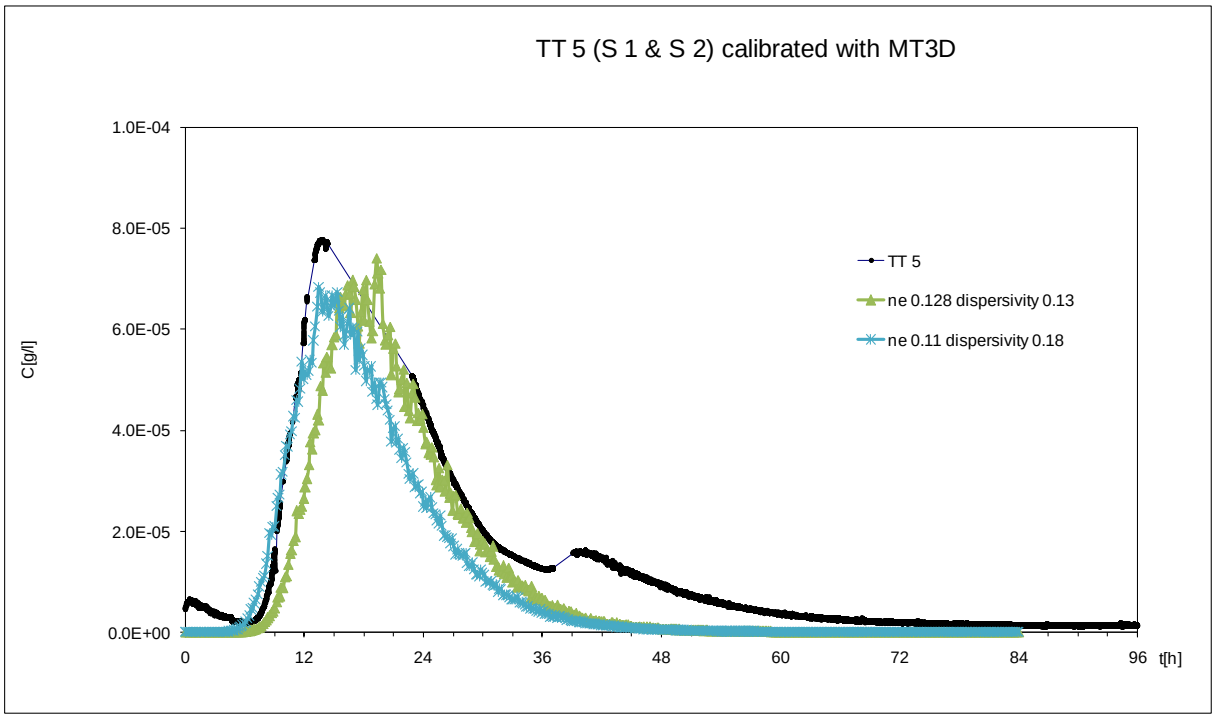

Figure 7.11: Calibration of TT 5 with MT3D.

Table 7.4: Details of the calibrated horizontal forced gradient tracer tests with MT3D

	TT1	TT3	TT5
Initially Injected Tracer Concnetartion	2 g	0.48g	4g
n_e used in MT3D	0.00289	0.2 - 0.21	0.128
α_L (longitudinal dispersivity) used in MT3D	0.00525 - 0.00625 m	1.2 m	0.13 - 0.18 m

7.9. Model Calibration of the Vertical Forced Gradient Tracer Test

As described for the horizontal forced gradient tracer test, artificial oscillation applying MT3D occurred. Despite attempts in reducing the number of layers, the test could not be modelled.

7.10 Conclusion Computer Modeling

A computer model was successfully set up with MODFLOW (Harbaugh, A.W. and McDonald, M.G., 1996a and b, Harbaugh et al. 2000) using the groundwater modelling software PMWINpro7 (Chiang, 2005). A detailed flow model was set up, taking the upflow into account and using the natural hydraulic gradient to define the boundaries. The flow model could be calibrated against the pumping tests carried out in S1 to S3 and S5 to S7. Test 10, could not be calibrated and would have required adjustment of the hydraulic parameters in all seven aquifer layers. However, the calibrated individual layers were considered to be sufficient to calibrate the horizontal forced gradient tracer tests.

MT3D (Zheng, C., 1990, 1996) was used as transport model to calibrate the horizontal forced gradient tracer tests. As artificial oscillations occurred using the model with 40 layers, a simplified model with the same mesh, but only two layers was applied to model the solute transport. TT 1 and TT 5 could be matched reasonable. TT 3 was difficult to match as only

48% of tracer broke through. The quantified values of n_e and α_L are considered to be reasonable.

CHAPTER 8: Discussion and Conclusion

8.1 Discussion

The study was setup to examine the solute transport in horizontal and vertical direction within a sandstone aquifer at the borehole scale within a radius of less than 10m around a pumping well. Due to the rising groundwater issue in conurbations, especially Birmingham, the vertical flow around pumping wells is important. The values to be studied were hydraulic parameters describing the flow filed and transport parameters describing the solute transport.

Geophysical logging of the five boreholes of the test site confirmed a good correlation between the different wells and methods applied to conclude that the borehole array was drilled into a horizontally layered part of the Wildmoor Sandstone. A core taken (Mitchener, 2003) and drilling log of BH1 confirmed the geophysical measurements.

The natural hydraulic gradients calculated according to the measured concentration decreases in S1 to S6 on the test site, recorded with point dilution tracer test, gave higher values than those generally proposed by Tellam and Barker (2006) for the Triassic Sandstone. One reason for higher hydraulic gradients could be the surface elevation of the area around the test site and the close location to the Birmingham fault.

The measured upflow corresponds to those reported by Taylor et al. (2003), Joyce et al. (2006), and Tellam and Barker (2006). It could be measured and was considered in the flow model of the test site.

The fourteen pumping test were used to calibrate the flow model for the individual sandstone layers. The especially build double-packer system (Greswell, 1999) was successfully applied. The results gained were analytically analysed and entered the calibration of the flow model.

The big packer, consisting of a plastic tube filled with water when it was used successfully, when introduced into BH1, sealing this borehole off. Pumping tests, analysed with curve-fitting methods, delivered week results, however, the flow model delivered reasonable to good results, supporting the application of such a big packer.

Three horizontal tracer tests were successfully carried out, recording breakthrough of RWT and fluorescein. Both tracers showed no retardation and behaved conservative. During TT 3, the RWT concentration record was disturbed by particles or turbidity, causing the flurometer to record higher RWT concentrations. The tracer was injected instantaneously and pumped from a second well. In TT 1 (S7) the mixing procedure in the injection well instigated an injection of four pulses of tracer. A connecting fracture between BH1 and BH5, initiated by the drilling process, which caused a "blow out" (verbal confirmation of Richard Greswell) was detected, resulting in a fast breakthrough. The opposite represents TT3 (S5) with remaining tracer in the injection well of about 50% and a slower break through. TT5 (S1&S2) seems to be on peak breakthrough with an intermediate decrease of tracer in the injection well and a smooth breakthrough in the pumped well. All quantified values received from calibration of the horizontal tracer test with the computer modeling are similar to those of Streetly et al. (2002), Coleby (1996) an Joyce et al. (2006).

8.2 Conclusion

Hydraulic and solute transport properties could be quantified for the unconfined Birmingham aquifer in the Triassic Sandstone. The values measured and interpreted with analytical calculations and computer modelling were in the range of property values expected by Tellam and Barker (2006) or Allen et al. (1998):

- Hydraulic conductivity values and storage coefficients were defined.

- Point dilution test were newly carried out in the Triassic Sandstone aquifer
- Average linear flow velocities of sandstone layers were calculated.
- Effective porosity values and dispersivity values could be quantified
- Fast to slow solute transport pathways could be defined by the horizontal forced gradient tracer test
- Newly carried out vertical forced gradient tracer test could confirm the existence of vertical connection in mudstone layers, connecting sandstone layers of different levels.
- The importance of measuring the tracer injection as accurate as the breakthrough was shown and possible misinterpretations were discussed.

As proposed by Tellam and Barker (2006), fracture flow in the vicinity of pumped wells was proven to be important for contaminate transport in horizontal direction within sandstone layers, as shown in TT1. Simulated with tracer, it took only a few minutes for the tracer to travel over distances of a few metres. All vertical forced gradient tracer tests confirmed the existence of vertical connections through the mudstone layers. In some vertical tracer test, tracer required only a few hours to pass vertical distances of a few metre of mudstone. The findings can be used for future calculations of catchment areas around pumped well for example. The calculated values of effective porosities and dispersivity values can be used for the prediction of travel times of contamination at a certain point towards a pumped well in Triassic Sandstone and vice versa.

8.3 Future Work

Future work would be:

- Quantification of the correlation of injection and breakthrough of tracer, according to the test setups of this work.
- A quantification of the vertical tracer migration using other particle tracing methods, giving a quantification of the effective porosity and dispersivity of the mudstone layers

Literature

Aeby, P., Schultze, U., Braichotte, D., Bundt, M., Moser-Broroumand, F., Wydler, H., and Flühler, H., 2001, Fluorescence imaging of tracer distributions in soil profiles, Environ. Sci. Technol., 35, 753-760

Allen, D.J., Bloomfield, J.P., Gibbs, B.R. and Wagstaff, S.J., 1998, Fracturing and the Hydrogeology of the Permo-Triassic Sandstones in England Wales.

Allen, D.J., Brewerton, L.J., Coleby, L.M., Gibbs, B.R., Lewis, M.A., MacDonald, A.M., Wagstaff, S.J. and Williams, A.T., 1997, The physical properties of major aquifers in England and Wales, BGS Technical Report WD/97/34 equivalent to Environment Agency R&D Publication 8

Anderson, M.P. and Woessner, W.W., 1992, Applied Ggroundwater modeling, Academic Press, San Diego, 381p.

Atkinson, T.C. and Smart, P.L., 1980, Artificial tracers in hydrogeology, in a survey of British hydrology, The Royal Society

Audley-Charles, M.G., 1970, Triassic palaeogeography of the British Isles. Quarterly Journal of the Geological Society of .ondon 126, 49-89.

Barclay, T., 1898, The future water supply of Birmingham, Cornish Brothers, Birmingham, (3.rd edition)

Barker, A.P., Newton, R.J., Bottrell, S.M., and Tellam, J.H., 1998, Processes affecting groundwater chemistry in a zone of saline intrusion into an urban sandstone aquifer, Applied Geochemistry, 6, 735-750

Bashar K., 1997, Developing a conceptual model of intergranular conservative solute transport processes for water flow through laboratory-scale samples of the UK Triassic Sandstone, Unpub. PhD thesis, Earth Sciences, University of Birmingham, 306p

Bateman, A.S., Hiscock, K.M., and Anderson, T.C., 2001, Qualitative risk assessment using tracer tests and groundwater modeling in an unconfined sand and gravel aquifer, In: Seiler, K.-P. And Wohnlich, S., 2001, New approaches characterizing groundwater flow, Swets and Zeitlinger, Lisse, 251-255

Bath, A., Milodowski, A.E., Ruotsalainen, P., Tullborg, E.-L., Cortes ruiz, A., and Aranyossy, J.F., 2000, EUR 19613 – Evidence from mineralogy and geochemistry for the evolution of groundwater systems during the Quaternary for use in radioactive waste repository safety assessment (EQUIP project), project report, Nuclear Science and Technology Series, 2000-XIV, Luxembourg Office for Official Publications of the European Communities

Batu, V., 2006, Applied flow and solute transport medeling in aquifers, Tylor and Francis, 667p.

Bear, J. And Buchlin, J.-M., 1991, Modelling and applications of transport phenomena in porous media, Kluwer Academic Publishers, 380p.

Bear, J., 1961a, Some experiments on dispersion, Journal of Geophysical Research, 66, 1185-1197

Bear, J., 1961b, Some experiments on dispersion, Journal of Geophysical Research, 66, 2455-2467

Bear, J., 1972, Dynamics of fluids in porous media, New York, American Elsevier Publishing Company, 764p.

Behrens, H., 2001, German Federal Environmental Agency Working Group: Toxicological and ecotoxicological assessment of water tracers, Journal Hydrogeology, 9, 321-325

Betts, C., 1996, A tracer test in the Triassic Sandstone at Haskayne, Lancashire, unpublished MSc project report, Earth Sciences, University of Birmingham

Bouch, J.E, Milodowski, A.E. and Ambrose, K., 2004, Dolomitisation, fracturing and pore-systems in Dinantian carbonates from Leicestershire, South Derbyshire and West Cumbria, UK, In: Braithwaite, C.J.R., Rizzi, G. and Darke, G (eds),, 2004, The geometry and petrogenesis of dolomite hydrocarbon reservoirs, Geological Society, London, Special Publications, 235, 325-369

Bouch, J.E, Hough, E.D., Kemp, S.J., McKervey, J.A., Williams, G.M. and Greswell, R.B., 2006, Sedimentary and diagenetic environments of the Wildmoor Sandstone Formation (United Kingdom): implications for groundwater and contaminant transport and sand production, In: Tellam, J.H. and Barker, R.D. (eds), Fluid Flow and Solute Movement in Sandstones: The Offshore UK Permo-Triassic Red Bed Sequence, Geological Society, London, Special Publications, 263, 129-153

Brassington, F.C. and Walthall, S., 1985, Field techniques using borehole packers in hydrogeological investigations. Q. J. Eng. Geol., 18, pp. 181-193

Brassington, F.C., 1992, Measurements of head variations within observation boreholes and their implications for groundwater monitoring, J. Inst. Wat. Env. Mgmt., 6, 81-100

Brouyère, S, 2003, Modeling tracer injection and well-aquifer interactions: A new mathematical and numerical approach, Water Resources and Research, 39, no.3, 1070

Brouyère, S, Carabin, G., and Dassargues A., 2005, Influence of tracer injection on field tracer experiments, Ground Water, Vol. 43, 389-400

Burley, S.D., 1984, Patterns of diagenesis in the Sherwood Sandstone Group (Triassic), United Kingdom. Clay Minerals, 19, 403-440

Campell, J.E., 1982, Permeability characteristics of the Permo-Triassic sandstones of the Lower Mersey Basin, MSc thesis, University of Birmingham

Chadwick, R.A. and Smith, N.J.P., 1988, Evidence of negative structural inversion beneath central Ebgland from new seismic data, Journal of the Geological Society, 145, 519-522

Chiang, W.-H. and Kinzelbach W., 2001, 3D-Groundwater modeling with PMWIN, First Edition. Springer Berlin Heidelberg New York, 346 pp

Chiang, W.-H., 2005, 3D-Groundwater modeling with PMWIN, Second Edition, A simulation system for modeling groundwater flow and transport processes, Springer Berlin, Heidelberg, New York, 397 pp

Coleby L.M., 1996, Heath house tracer test data report, British Geological Survey Technical Report, WD/96/74

Cooper, H.H., and Jacob, C.E., 1946, A generalized graphical method for evaluating formation constants and summarizing well field history, Am. Geophys. Union Trans., vol. 27, pp.526-534.

Curião, V., Tellam, J. and Greswell, R., 2001, The effect of mudstones on flow in the Triassic Sandstone (UK) – Laboratory measurements of mudstone permeability, School of Earth Sciences, University of Birmingham, unpublished

Curtis, G.P., Reinhard, M., and Roberts , P.V., 1986, A natural gradient experiment on solute transport in a sand aquifer, 4. Sorption of organic solutes and its influence on mobility, Water Resources Research, 22, 2058-2072

Davis, S.N., Campell, D.J., Bentley, H.W. and Flynn, T.J., 1985, Ground Water Tracers, National Groundwater Association, EPA, 199p

De Marsily, G., 1986, Quantitative Hydrogeology, Academic Press, London, 440 pp

Derouane, J., and Dassargues, AQ., 1998, Delineation of groundwater protection zones based on tracer tests and transport modeling in alluvial sediments, Environ. Geol., 36(1-2), 27-36

Drew, B.P., 1968, A review of the available methods for tracing underground waters, Pro. Br. Speleol. Assoc., 6, 1-19

Driscoll, F., G., 1995, Groundwater and Wells, 2nd Edition, published by U.S: Filter/Johnson Screens, St Paul, MN 55112

Drost, W., Klotz, D., Koch, A., Moser, H., Neumaier, F. and Rauert W., 1968, Point dilution methods of investigating groundwater flow by means of radioisotopes, Water Resources Research, Vol.4, No.1, p.125-146

Eastwood, T., Whitehead, T.H., and Robertson, T., 1925. The Geology of the country around Birmingham, Sheet 168 England, Geological Survey of Great Britain

Edwards, H.E., Becker, A.D. and Howell, J.A., 1993, Compartmentalization of an Aeolian sandstone by structural heterogeneities: Permo-Triassic Sandstone, Moray Firth, Scotland, In: North, C.P. and Prosser, D.J. (eds), Characterization of fluvial and aeolian reservoirs, Geological Society, London, Special Publications, 73, 339-365

Fetter, C.W., 1994, Applied Hydrogeology, 3.rd edition, Prentice Hall Inc., 691p

Fetter, C.W., 1999, Contaminat Hydrogeology, 2.rd edition, Prentice Hall Inc., 500p

Fisher, Q.L. and Knipe, R.J., 1998, Fault sealing processes in siliclastic sediments, In: Jones,

G. Et al. (eds.), Faulting and Fault Sealing in Hydrocarbon Reservoirs, Geological Society, London, Special Publications, 147, 117-134

Flury, M., and Wai, N., N., 2003, Dyes as tracer for vadose zone hydrology, Reviews of Geophysics, 1, American Geophysical Union

Fowels, J. and Burley, S., 1994. Textural and permeability characteristics of faulted, high porosity sandstones, Marine and Petroleum Geology, 11, 608-623

Freeze, R.A. and Cherry, J.A., 1979, Groundwater, Prentice-Hall; Englewood Cliffs, NJ, 604 p.

Freyberg, D.L., 1986, A natural gradient experiment on solute transport in a sand aquifer, 2. Spaitial moments and the advection and dispersion of nonreactive tracers, Water Resources Research, 22, 2073-2093

Galloway, W.E. and Sharp, Jr., J.M., 1998, Characterizing aquifer heterogeneity within terrigenious clastic depositional systems, in Hydrogeologic models of sedimentary aquifers, ed. by Fraser, G.S. and Davis, J.M., SEPM, pp. 85-90

Garabedian, S.P., LeBlanc, D.R., Gelhar, L.W., and Celia, M.A., 1991, Large-scale natural gradient tracer test in sand and gravel, Cape Cod, Massachusetts - 2. Analysis of spatial moments for a nonreactive tracer, Water Resources Research, 27, 911-924

Gasper, E., 1987, Modern trends in tracer hydrology (Vol. II), CRC Press, Boca Raton, FL

Gasper, E. and Oncescu, M., 1972, Developments in Hydrology: Radio-Active Tracers in Hydrology, Elsevier, Amsterdam, 342p.

Geokon, Inc., 1989, Instruction Manual Vibrating Wire Piezometers Model 4500

Green, H., 1994. A tracer test in the Triassic Sandstone at the Haskayne cutting, west Lancashire, unpublished MSc project report, Earth Sciences, University of Birmingham

Greswell, R. 1995, A laboratory investigation of flow and transport processes in the Lincolnshire limestones, unpublished PhD Thesis University of Birmingham

Greswell, R.B., 1999, Design of Packer System, In: Using urban aquifers: Sustainability at a different time and space scales, unpublished Third Progress Report, School of Earth Sciences, University of Birmingham

Greswell, R., Thomas, A., Shepherd, K.A., Sauer, R. I., Mitchenrer, R.G.R., Harris, J.M., Mackay, R., Tellam, J.H. and Rivett, M.O., 2000, Using urban aquifers: Assessing water quality issues, in: Sililo, O. et al., 2000, Past achievements and future challenges, Proceedings of the XXX IAH Congress on Groundwater.

Gutmanis, J.C., Lanyon, G.W., Wynn, T.J. and Watson, C.R., 1998, Fluid flow in faults: A study of fault hydrogeology in Triassic sandstone and Ordovician volcaniclastic rocks at Sellafield, north-west England, Proceedings of the Yorkshire Geological Society, 52, 159-175

Halevy, E, Moser, H., Zellhofer, O., and Zuber, A., 1967, Borehole dilution techniques: a critical review. Proceedings of the 1966 Symposium of the International Atomic Energy Agnecy, pp.531-564

Hamilton, C.A.L., 1995, Tracer test in the Triassic Sandstone at the Haskayne, Lancashire, unpublished MSc project report, Earth Sciences, University of Birmingham

Hantush, M.S. and C.E. Jacob, 1955, Non-steady radial flow in an infinite leaky aquifer, Am. Geophys. Union Trans., v. 36, no. 1, pp. 95-100.

Hantush, M.S., 1960, Modification of the theory of leaky aquifers, Jj. Geophys. Res., vol. 65, pp.3713-3725.

Harbaugh, A.W. and McDonald, M.G., 1996a, User's documentation for MODFLOW-96, an update to the U.S. Geological Survey modular finite-difference ground-water flow model, USGS Open-File Report 96-485

Harbaugh, A.W. and McDonald, M.G., 1996b, Programmer's documentation for MODFLOW-96, an update to the U.S. Geological Survey modular finite-difference ground-water flow model, USGS Open-File Report 96-486

Harbaugh, A.W., Banta E.R., Hill, M.C, and McDonald, M.G., 2000, MODFLOW-2000, The U.S. Geological Survey modular ground-water model User guide to modularization concepts and the ground-water flow process, U. S. Geological Survey, Open-file report 00-92.

Hess, K.M., Wolf, S.H., and Celia, M.A., 1992, Large-scale natural gradient tracer test in sand and gravel, Cape Cod, Massachusetts – 3. Hydraulic conductivity, variability and calculated macrodispersivities, Water Resources Research, 28, 2011-2027

Hiscock, K.M., 1982, Hydraulic properties of the chalk at Ludgershall sewage treatment works, BSc. Thesis, University of East Anglia, Norwich

Hiscock, K.M., 2005, Hydrogeology: principles and practice, Blackwell, 389pp.

Hofstraat, M.S., Vriezekolk, G., Schreurs, W., Broer, J.A.A., and Wijnstok, N., 1991, Determination of rhodamine WT in surface water by solid-phase extraction and HPLC with fluorescence detection, Water Resources Research, 25(7), 883-890

Horton, A., 1974, Engineering geology of the Pleistocene deposits of Birmingham. IGS Report 75/4

Ireland, R., 1981, Investigation of the hydrogeology of the Bromsgrove sandstone by downhole packer techniques. Research and Development Project Report, Severn-Trent Water Authority

Iwatsuki, T., Satake, H., Metcalfe, R., Yoshida, H., and Hama, K., 2002, Isotopic and morphological features of fracture calcite from granitic of the Tono area, Japan: a promising paleohydrogeological tool, Applied Geochemistry, 17, 1241-1257

Jackson, D. and Lloyd, J.W., 1983, Groundwater chemistry of the Birmingham Triassic sandstone aquifer and its relation to structure, Quarterly Journal of Engineering Geology, 16,

135-142

Jeffcoat, A.M., 2002, Exploring the hydraulic properties of discontinuity geometry in the UK Triassic Sandstones, PhD Thesis, University of Birmingham

Joyce, E., Rueedi, J., Cronin, A., Pedley, S, Tellam, J. and Greswell, R., 2006, Fate and transport of phage and viruses in UK Permo-Triassic Sandstone aquifers, Final report, Submitted November 2006, Environment Agency of England and Wales, Robens Centre for Public and Environmental Health, University of Surrey & Environmental Sciences & University of Birmingham, Joint Research Project (NC/02/47)

Käss, W, 1998, Tracing technique in geohydrology, A. A. Balkema, Brookfields, Vt.

Käss, W, 2004, Lehrbuch der Hydrogeologie 9. Geohydrologische Markierungstechnik. Gebrüder Bornträger, Stuttgart, 557 pp.

Kearl, P.M., Dexter, J.J. and Price, J.E., 1988, Procedures, analysis, and comparison of groundwater velocity measurement methods for unconfined aquifers, UNC/GJ-TMC-3, UNC Geotech, Grand Junction, CO.

Kelly, M., 1964. The Middle Pleistocene of north Birmingham. Philosophical Transaction of the Royal Society, 247, p.533

Keys, S.W., 1989, Borehole geophysics applied to ground-water investigations, National Water Well Association, 313 p.

Keys, S.W., 1994, Borehole geophysics applied to ground-water investigations, Chapter E2 in: Techniques of water-resources investigations of the United States Geological Survey, Book 2, Collection of environmental data, (Http://pubs.usgs.gov/Twri/twri2-e2/pdf/TWRL2-E2.pdf)

Killeen, P.G., 1982, Gamma-ray logging and interpretation, in Fitch, A.A., ed., Developments in geophysical exploration methods: London, England Elsevier Applied Science Publishers, bk 3, chap.7, p.95-150

Knipe, C.V., Lloyd, J.W., Lerner, D.N. and Greswell, R.B., 1993, Rising groundwater levels in Birmingham and the engineering implications, CIRIA Special Publication 92, Construction Industry Research and Information Association, London. 114pp

Knopp, A., 1875, Über die hydrographischen Beziehungen zwischen der Donau und der Aachquelle im badischen Oberlande, Neues Jahrb. Mineral. Geol. Paleontol., 942-958

Knopp, A., 1878, Über die hydrographischen Beziehungen zwischen der Donau und der Aachquelle im badischen Oberlande - Schluss, Neues Jahrb. Mineral. Geol. Paleontol., 350-363

Kruseman, G.P. and N.A. de Ridder, 1994, Analysis and evaluation of pumping test data, Second Edition, ILRI publication 47, International Institute for Land Reclamation and Improvement, The Netherlands, 377 p.

Lamontagne, S., Dighton, j., and Ullman, w., 2002, Estimation of groundwater velocity in riparian zones using point dilution tests, Technical Report 14/02, CSIRO Land and Water

Land, D., 1966, Hydrogeology of the Triassic Sandstone in the Birmingham Lichfield District, Water supply paper of the Geological Survey, Hydrological Report, no. 2

LeBlanc, D.R., Garabedian, S.P., Hess, K.M., Gelhar, L.W., Quadri, R.D., Stollenwerk, K.G., and Wood, W.W., 1991, Large-scale natural gradient tracer test in sand and gravel, Cape Cod, Massachusetts – 1. Experimental-design and observed tracer movement, Water Resources Research, 27, 895-910

Lenda, A., and Zuber, A., 1970, Tracer dispersion in groundwater experiments, Proc. Isotope Hydrol.: 619-641, IAEA, Vienna

Lerner, D., 2000, Depth and extent of penetration of urban recharge and contamination into UK aquifers, 3rd Progress Report, URGENT project

Lloyd, J.W., Ramanathan, C. and Pacey, N., 1979, The use of point dilution methods in determining the permeabilities of land-fill materials, Water Services, p.843-846

Lovelock, P.E.R., 1977, Aquifer properties of Permo-Triassic sandstones in the United Kingdom, Bulletin of the Geological Survey of Great Britain, 56

Mader, D., 1992, Evolution of paleoecology and paleoenvironment of Permian and Triassic fluvial basins in Europe, 1, Gustav Fischer Verlag

Mackay, D.M., Freyberg, D.L., and Roberts, P.V, 1986, A natural gradient experiment on solute transport in a sand aquifer, 1. Approach and overview of plume movement, Water Resources Research, 22, 2017-2029

Maloszewski, P., Wohnlich, S. and Mieseler, T., 2007, Tracer techniques in hydrogeology (in German), FH-DGG and Ruhr University Bochum

Manzocchi, T., Ringrose, P.S. and Underhill, J.R., 1998, Flow through fault systems in high-porosity sandstones. In Conward, M.P., Daltaban, T.S. and Johnson, H. (eds.) Structural geology in reservoir characterization, Geological Society, London, Special Publications, 127, 65-82

Metcalf, R.R., Savage, D. and Higgo, J.W., 1994. Fluid-rock interactions during continental red bed diagenesis: Implications for theoretical models of mineralization in sedimentary basins. In Parnell, J. (ed) Geofluids: Origin, migration and evolution of fluids in sedimentary basins, Geological Society, London, Special Publications, 78, 301-324

Metcalfe, R., 1998, The petrology and paragenesis of fracture mineralization in the Sellafield area, west Cumbria, Processing of the Yorkshire Geological Society, 52, 215-242

Miall, A.D., 1988, Reservoir heterogeneities in fluvial sandstones: Lessons from outcrop studies, The American Association of Petroleum Geologists Bulletin, 72, pp. 682-697

Milodowski, A.E. and Strong, G.E., 1999, Diagenesis of the Permo-Triassic rocks, In: Plant, J.A., Jones, D.G. and Haslam, H.W. (eds), The Cheshire Basin, British Geological Survey, Keyworth, 125-175

Mitchener, R.G.R., 2003, Hydraulic and chemical property correlations of the Triassic Sandstone of Birmingham, PhD thesis, University of Birmingham

Moench, A.F., 1989. Convergent radial dispersion: A Laplace transform solution for aquifer tracer testing, Water Resources Research, 25, 439-447

Monkhouse, R.A. and Richards, H.J.,1982, Groundwater resources of the United Kingdom. Commission of the European Communities, Th. Schäfer Druckerei GmbH, Hannover

Moser, H., and Neumaier, F., 1957, Die Anwendung radioaktiver Isotopen in der Hydrologie, Atomkernenergie I and II, 26-34, 225-231

Moser, H. and Sagl, H., 1967, Die Direktmessung hydrologischer Farbtracer im Gelände, Steirische Beitr. Hydrogeolo., 1966/1967, 179-183

Mountney, N.P.T. and Thompson, D.B., 2002, Stratigraphic evolution and preservation of Aeolian dune and damp/wet interdune strata: An example from the Triassic Helsby Sandstone Formation, Cheshire Basin, U.K., Sedimentology, 49, 805-833

Mull, D.S., Liebermann, T.D., Smoot, J.L., and Woosley, L.H., 1988, Application of dye-tracing techniques for determining solute transport characteristics of ground water in karst terranes, Rep. EPA904/688-001, US. Environ. Prot. Agency

Neumaier, F., 1960, Experiences concerning the use of radioactive isotopes in hydrology, Publ. No. 52, IASH Comm. Subterr. Waters, 542-547

Newell, A.J., 2006, Calcrete as a source of heterogeneity in Triassic fluvial sandstone aquifers (Otter Sandstone Formation, SW England), In: Tellam, J.H. and Barker, R.D. (eds), Fluid flow and solute movement in sandstones: The onshore UK Permo-Triassic Red Bed Sequence, Geological Society, London, Special Publications, 263, 119-127

Noy, D.J., 1993, FORTRAN 77 program to calculate breakthrough concentrations for radially converging tracer tests according to the method of Moench (1989), British Geological Survey, unpublished Report

Ogilvi, N.A., 1958, An electrolytical method of determining the filtration velocity of undergroundwaters (in Russian), Bull. Sci.-Tech. Inf.No.4(16), Gosgeoltekhizdat, Moscow

Olsen, L.D., and Tenbus, F.J., 2004, Design and analysis of a natural-gradient groundwater tracer test in a freshwater tidal wetland, West Branch Canal Creek, Aberdeen Proving Ground, Maryland, U.S. GEOLOGICAL SURVEY, Scientific Investigation Report 2004-5190

Pang, L., Close, M., and Nonan, M., 1998, Rhodamine WT and Bacillus subtilis transport through an alluvial gravel aquifer, Groundwater, 36(1), 112-122

Papadopulos, I.S. and Cooper H.H. Jr., 1967, Drawdown in a well of large diameter, Water Resources Res., Vol. 3, 241-244

Pedersen, K., Ekendahl, S., Tullborg, E.-L., Furnes, H., Thorseth, I., and Tumyr, o., 1997, Evidence of ancient life at 207m depth in a granitic aquifer, Geology, 25, 827-830

Pettijohn, F.J., 1975. Sedimentary rocks, 3rd edition, Harper and Row, New York

Pickering, R., 1957. Pleistocene geology of south Birmingham, Quaterly Journal of the Geological Society, 113, 223-239

Pitrak et al. (2007), A simple borehole dilution technique in measuring horizontal groundwater flow, Ground Water 4, no.1, 89-92

Powell, J.H., Glover, B.W. and Waters, C.N., 2000, Geology of the Birmingham area, Memoir for 1:50 000 Geological Sheet 168 (England and Wales), BGS

Ptak, T., and Schmid, G., 1996, Dual-tracer transport experiments in a physically and chemically heterogeneous porous aquifer: Effective transport parameters and spatial variability, J. Hydrol., 183(1-2), 117-138

Reeves, M.J., Skinner, A.C., and Wilkinson, W.B., 1975, The relevance of aquifer flow mechanisms to exploration and development of groundwater resources, Journal of Hydrology, 25, 1-21

Rivett, M.O., Shepherd, K.A., Keeys, L.L., Brennan, A.E., 2005, Chlorinated solvents in the Birmingham Aquifer, UK: 1986-2001, Quarterly Journal of Engineering Geology and Hydrogeology, 28, 337-350

Roberts, P.V, Goltz, M.N., and Mackay, D.M., 1986, A natural gradient experiment on solute transport in a sand aquifer, 3. Retardation estimates and mass balances for organic solutes, Water Resources Research, 22, 2047-2058

Roberts, P.V, Hopkins, G.D., Mackay, D.M., and Semprini, L, 1990, A field evaluation of in-situ biodegradation of chlorinated ethenes, Part 1 Methodology and field site characterization, Ground Water, 28, no.4, 591-604

Robertson Research Engineering Ltd, 1982, Robertson Pota-Log, Manual

Rumbaugh, J., and Rumbaugh, D., 1997, AquiferWIN32

Rushton, K.R. and Salmon, S., 1993, Significance of flow through low-conductivity zones in Bromsgrove Sandstone aquifer, Journal of Hydrology, 152, 131-152

Sabatini, D.A., and Austin, T.A. 1991, Characteristics of rhodamine WT and fluorescein as Adsorbing. Ground-water Tracers, Ground Water, 29, p. 341

Salmon, S., 1990, The significance of vertical components of flow in groundwater, with special reference to the Bromsgrove aquifer. PhD, University of Birmingham, School of Civil Engineering

Sauty, J.P., 1984, An analysis of hydrodispersive transfer in aquifers, Water Resources Research, 16, 1, 145-158

Scheidegger, A.E., 1961, General theory of dispersion in porous media, J. Geophys. Res., 66, 3273-3278

Schlumberger, C. And Doll, D., 1927, Electrical logs and correlations in drill holes, Mining and Metallurgy, 10, no.275, 515-518

Schnegg and Doerflieger, 1992, An inexpensive flow-through field fluorimeter, in Geomagnetism Group University of Neuchâtel

Scott, J.H., Dodd, P.H., Droullard, R.F., and Mudra, P.J., 1961, Quantitative interpretation of gamma-ray logs, Geophysics, 26, no.2, p.182-191

Segar, D.A., 1993, The effect of open boreholes on groundwater flows and chemistry, PhD thesis, University of Birmingham

Semprini, L., Roberts, P.V., Hopkins, G.D., and McCarty, 1990, A field evaluation of in-situ biodegradation of chlorinated ethenes, Part 2, Results of biostimulation and biotransformation experiments, Ground Water, 28, no.5, 715-727

Shepherd, K.A., 2003, Contamination and groundwater quality in the Birmingham Aquifer, PhD thesis, University of Birmingham

Shepherd, K.A., Ellis, P.A. and Rivett, M.O., 2006, Integrated understanding of urban land, groundwater, baseflow and surface-water quality The City of Birmingham, U.K., Science of the total Environment

Shiau, B.J., 1993, Influence on rhodamine WT on sorption and transport in subsurface media, Ground Water, 31, no.6, 913-920

Smart, P.L. and Laidlaw, I.M.S, 1977, An evaluation of some fluorescent dyes for water tracing, Water Resources Research, 13, 15-33

Smart, P.L., 1984, A review on the toxicity of twelve fluorescent dyes used for water tracing, NSS Bull, 46, 21-33

Spitz, K. and Moreno, J., 1996, A practical guide to groundwater and solute transport modeling, 461 pp. John Wiley & Sons, New York. ISBN: 0-471-13687-5

Steel, R.J. and Thompson, D.B., 1983. Structures and textures in Triassic braided stream conglomerates ("Bunter Pebble Beds") in the Sherwood Sandstone Group, north Staffordshire, England, Sedimentology, 30, 341-367

Steventon-Barnes, H., 2001. Solid organic carbon in UK aquifers: Its role in sorption of organic contaminants, PhD thesis, University of London

Streetly, H.R., Hamilton, A.C.L, Betts, C., Tellam, J.H., and Herbert, A.W., 2002, Reconnaissance tracer tests in the Triassic Sandstone Aquifer north of Liverpool, UK, Quarterly Journal of Engineering Geology and Hydrogeology, 35, 167-178

Strong. G.E., 1993. Diagenesis of Triassic Sherwood Sandstone Group rocks, Preston, Lancashire, UK: A possible evaporitic cement precursor to secondary porosity?, in North, C.P. and Prosser, D.J., 1993, Characterization of Fluvial and Aeolian Reservoirs, Geological Society Special Publication, 73, pp. 279-289

Sudicky, E.A., 1986, A natural gradient experiment on solute transport in a sand aquifer: Spaitial variability of hydraulic conductivity and its role in the dispersion process, Water Resources Research, 22

Sutton, D.J., and Kabala, Z.J., 2001, Limitations and potential of commercially available rhodamine WT as a groundwater tracer, Water Resources Research, 37, 6, 1641-1656

Taylor, R.G., Cronin, A.A., Trowsdale, S.A., Baines, O.P., Barrett, M.H. and Lerner, D.N., 2003. Vertical groundwater flow in Permo-Triassic sediments underlying two cities in the Trent River Basin (U.K.), Journal of Hydrology, 284, 92-113

Tellam, J.H. and Lloyd, J.W., 1981, A review of the hydrogeology of British onshore non-carbonate mudrocks, Quarterly Journal of Engineering Geology and Hydrogeology, 14, 347-355

Tellam, J.H., 1995, Urban groundwater pollution in the Birmingham Triassic Sandstone Aquifer, 4.th annual conference on groundwater pollution, London

Tellam, J.H., 2004, 19th century studies of the hydrogeology of the Permo-Triassic Sandstones of the northern Cheshire Basin, England. In: Mather, J. (ed) 200 Years of British Hydrogeology, Geological Society, London, Special Publications, 225, 89-105

Tellam, J.H. and Barker, R.D., 2006, Fluid Flow and Solute Movement in Sandstones: The onshore UK Permo-Triassic Red Bed Sequence, Geological Society, London, Special Publications, 263

Theis, C.V., 1935, The relation between the lowering of the piezometric surface and the rate and duration of discharge of a well using groundwater storage, Trans. Amer. Geophys. Union, Vol. 16, pp. 519-524.

Thomas, A, 2001, A geographic information system methodology for modeling urban groundwater recharge and pollution , PhD thesis, University of Birmingham

Thompson D.B., 1970, Sedimentation of the Triassic Cheshire Basin and its margins, Geological Journal, 7, 183-216

Trillat, M.A., 1899, Sur l'emploi des matières colorantes pour la recherche de l'origine des sources et des eaux d'inflitration, C.R. Hebd. Seances Acad. Sci., 128, 698-702

Towsdale, S.A. and Lerner, D.N., 2003. Implications of flow patterns in the sandstone aquifer beneath the mature conurbation of Nottingham (UK) for source protection, Quarterly Journal of Engineering Geology and Hydrogeology, 36, 197-206

Umweltbundesamt, Institut für Wasser-, Boden- und Lufthygiene, 1997, Human- und ökotoxikologische Bewertung von Markierungsmitteln in Gewässern, Grundwasser, 2/97, 61-64

Vanderborght, J., Gähwiller, P., Flühler, H., 2002, Identification of transport processes in soil cores using fluorescent tracers, Soil Sci. Soc. Am. J., 64, 1305-1317

Viriot, M.L. and André, J.C., 1989, A search for new tracer for hydrology, Analusis, 17, 97-111

Walker, T.R., Waugh, B., and Grone, A.J., 1978, Diagenesis in first-cycle desert alluvium of Cenozoic age, southwestern United States and northwestern Mexico, Geological Society of America Bulletin, 89, 19-32

Walton, W.C., 1962, Selected Analytical Methods for Well and Aquifer Evaluation, Illinoise State Water Survey Bull., No. 49, 81 pp.

Ward, R.S., Williams, A.T., Barker, J.A., Brewerton, L.J., and Gale, I.N., 1998, Groundwater tracer tests: a review and guidelines for their use in British aquifers, British Geological Survey Report WD/98/19

Warrington, G., Audley-Charles, M.G., Elliot, R.E., Evens, R.E., Ivimey-Cook, H.C., Kent, P.E., Robinson, P.L., Shotton, F.W. & Taylor, F.M., 1980, A correlation of the Triassic rocks in the British Isles, Special Report 13: London, Geological Society, 78 p.

Weber, K.J., and van Geuns, L.C., 1990, Framework for constructing clastic reservoir simulation models, Journal of Petroleum Technology, 42, PP12-48, 1296-1297

Williams, G.M., Stuart, A., and Holmes, D.C., 1985, Investigation of the geology of the low-level radioactive waste burial site at Drigg Cumbria, British Geological Survey Report, 17, no.3

Wills, L.J., 1970, The Triassic succession in the central Midlands in its regional setting, Journal of the Geological Society, London, 126, 225-283

Wills, L.J., 1976. The Trias of Worcestershire and Warwickshire. HMSO, London

Wilson, J.T., Leach, L.E., Henson, M., and Jones, J.N., 1986, In situ biorestoration as a ground water remediation technique, Ground Water Monit. Rev., 6, 56-64

Yang, Y., Lerner, D.N., Barrett, M.H. and Tellam, J.H., 1999, Quantification of groundwater recharge in the city of Nottingham, U.K., Environmental Geology, 38(3), 183-198

Zheng, C., 1990, MT3D, a modular three-dimensional transport model, S.S. Papadopulos and Associates, Inc., Rockville, Maryland

Zheng, C. and Bennett, G.D., 1995, Applied contaminant transport modeling: Theory and practice, 440 pp. Van Nostrand Reinhold, New York

Zheng, C., .1996, MT3D99 A modular 3D multispecies transport simulator, S.S. Papadopulos and Associates, Inc. Bethesda, Maryland

Appendices

Appendix III.3.1: Drilling Log of BH1 (Note: The elevations (AOD) given are not correct! See Figure 3.7).

Appendix III.3.2: Double-tube core barrel drilling BH4. A: Core bit removed, B: Taking off the Core Catcher. C & D: Pulling out of the inner tube with the core of the double-tube core barrel

Appendix III.3.3: Core Bits applied to drill Borehole BH 4

Appendix IV 4.1: BH 4 Core Log (Mitchener, 2003)

Appendix IV 4.2: Temperature Logs

Appendix IV 4.3: Conductivity Logs

Appendix IV 4.4: Caliper Logs

Appendix VII.1 a: Computer Model Mesh Size, Rows and Columns

Appendix VII.1 b: Computer Model Layer Setup

Appendix VII.1 c: Computer Model Borehole Coordinates

Appendix VII.2: Computer Model Heads at the Boundaries

Appendix VII.3: Drawdown graphs of the pumping tests fitted against the drawdown graphs of the model results

Appendix III.3.1: Drilling Log of BH1 (Note : The elevations (AOD) given are not correct! See Firgure 3.7).

Appendix III.3.2: Double-tube core barrel drilling BH4. A.: Core bit removed, B.: Taking off the Core Catcher. C.& D: Pulling out of the inner tube with the core of the double-tube core barrel

Appendix III.3.3: Core Bits applied to drill Borehole BH 4

Appendix IV 4.1: Drilling Log of BH4 (Mitchener, 2003).

Coring Log

BOREHOLE No
URGENT1

Project: URGENT Project

Client: University of Birmingham

Project No:	Date Started: Date Started:	Ground Level (m)	Co-Ordinates () E N	Sheet 1 of 8

SAMPLES & TESTS			Water	STRATA				Instrument/ Backfill
Depth	Type No	Test Result		Reduced Level	Legend	Depth (Thick-ness)	DESCRIPTION	
						0.13	TOPSOIL	
						0.50	Red-brown course sand, clay and silt with some organic matter CLAY AND SAND	
						(1.00)	NO RECOVERY	
						1.50		
						(0.40)	moderate reddish brown (10-R-4/6) course grained, well sorted, very poorly cemented, no structures visible. Less than 5% white mica present. COURSE SAND	
						1.90		
						(1.10)	NO RECOVERY	
						3.00		
						3.25	pale reddish brown (10-R-5/4) course grained. some speckling with darked red coloration. No cementation, 5% white mica present COURSE SAND	
						(1.75)	NO RECOVERY	
						5.00		
						5.18	pale reddish brown (10-R-5/4) course grained. some speckling with darked red coloration. No cementation, 5% white mica present COURSE SAND	
						(2.72)	NO RECOVERY	
						7.90		
						8.00		

Boring Progress and Water Observations						Chiselling			Water Added		GENERAL REMARKS
Date	Time	Depth	Casing	Casing Dia	Water Dpt	From	To	Hours	From	To	

All dimensions in metres Scale 1:50	Contractor :	Logged By Richard Mitchener	Approved By

Form SLR BOREHOLE LOG File PHD.GPJ 17-02-03

SLR Consulting Ltd, Wheeley Ridge, Wheeley Road, ALVECHURCH, B48 7DD, Telephone: 0121 447 8040, Fax: 0121 447 8076

Coring Log

BOREHOLE No
URGENT1

Project: URGENT Project

Client: University of Birmingham

Project No:	Date Started: Date Started:	Ground Level (m)	Co-Ordinates () E N	Sheet 2 of 8

SAMPLES & TESTS			Water	STRATA				Instrument/ Backfill
Depth	Type No	Test Result		Reduced Level	Legend	Depth (Thick-ness)	DESCRIPTION	
							Dark reddish brown (10-R-3/4) medium grained well sorted, well cemented. 5% white mica. MEDIUM SANDSTONE NO RECOVERY	
						(4.00) 12.00		
						(0.50) 12.50	dark reddish brown (10-R-3/4) CLAY with bands of greenish grey (5-G-6/1) SILTY SANDSTONE	
						12.70	grey MUDSTONE	
						(0.45) 13.15	red with silty bands MUDSTONE	
						13.16	grey CLAYEY SANDSTONE	
						13.50	moderate reddish brown (10-R-4/6) with minor clays FINE SANDSTONE	
						13.85	moderate reddish brown (10-R-4/6) very friable MEDIUM SANDSTONE	
						14.00	moderate reddish brown (10-R-4/6) wel cemented with white mica COURSE SANDSTONE	

Boring Progress and Water Observations						Chiselling			Water Added		GENERAL REMARKS
Date	Time	Depth	Casing	Casing Dia	Water Dpt	From	To	Hours	From	To	

All dimensions in metres Scale 1:50	Contractor :	Logged By Richard Mitchener	Approved By

Form SLR BOREHOLE LOG File PHD.GPJ 17-02-03

SLR Consulting Ltd, Wheeley Ridge, Wheeley Road, ALVECHURCH, B48 7DD, Telephone: 0121 447 8040, Fax: 0121 447 8076

Coring Log

BOREHOLE No
URGENT1

Project: URGENT Project

Client: University of Birmingham

Project No:	Date Started: Date Started:	Ground Level (m)	Co-Ordinates () E N	Sheet 3 of 8

SAMPLES & TESTS			Water	STRATA				Instrument/ Backfill
Depth	Type No	Test Result		Reduced Level	Legend	Depth (Thick-ness)	DESCRIPTION	
						16.09	very dusky red (10-R-2/2) (Manganese rich) with minor silt and white mica FINE SANDSTONE	
						16.22	dark reddish brown (10-R-3/4) MEDIUM SANDSTONE	
						16.45	Mottled, moderate red (5-R-5/4) and dark reddish brown (10-R-3/4) with minor silt and small hard, well rounded red pebbles MEDIUM SANDSTONE	
						16.62	heavily fractured, mottled, dark reddish brown (10-R-3/4) MEDIUM SANSTONE with minor small pebbles MEDIUM SANDSTONE	
						16.70	moderate pink (5-R-7/4) well sorted medium-course grained COURSE SANDSTONE	
						17.00	moderate red (5-R-7/4) well cemented fine-medium grained. Hard pale band at 16.71 at 45 degrees MEDIUM SANDSTONE	
						17.05	dark reddish brown (10-R-3/4) with mica MEDIUM SANDSTONE	
						17.10	moderate red (5-R-4/6) poorly cemented FINE SANDSTONE	
						17.20 (0.50)	moderate red (5-R-4/6) MUDSTONE	
						17.70	moderate red (5-R-5/4), well sorted clean FINE SANDSTONE	
						17.80	dark reddish brown (10-R-3/4) well sorted, clean MEDIUM SANDSTONE	
						18.10	dark reddish brown (10-R-3/4) laminated SILTY MUDSTONE	
						18.25	dark reddish brown (10-R-3/4) laminated SILTSTONE	
						18.47	moderate reddish brown (10-R-4/6) MEDUIM SANDSTONE	
						19.25	moderate red (5-R-4/6) well cemented MEDIUM SANDSTONE	
						19.35	dusky red (5-R-3/4) MUDSTONE	
						19.40	dusky red (5-R-3/4) uncemented SAND	
						19.50	grey, sand fine-grained ARENACEOUS MUDSTONE	
						(0.90)	dark reddish brown (10-R-3/4), hard. Grey weathering along fractures SILTSTONE	
						20.40	moderate red (5-R-4/6) well sorted, clean well cementedMEDIUM SANDSTONE	
						(1.60)		
						22.00	pale reddish brown (10-R-5/4) Paler harder bands seen at 22.01-22.05 m and 23.4 - 23.5 m COURSE SANDSTONE	
						(2.00)		
						24.00		

Boring Progress and Water Observations						Chiselling			Water Added		GENERAL REMARKS
Date	Time	Depth	Casing	Casing Dia	Water Dpt	From	To	Hours	From	To	

All dimensions in metres Scale 1:50	Contractor :	Logged By Richard Mitchener	Approved By

Form SLR BOREHOLE LOG File PHD.GPJ 17-02-03

SLR Consulting Ltd, Wheeley Ridge, Wheeley Road, ALVECHURCH, B48 7DD, Telephone: 0121 447 8040, Fax: 0121 447 8076

Coring Log

BOREHOLE No
URGENT1

Project: URGENT Project

Client: University of Birmingham

Project No:	Date Started: Date Started:	Ground Level (m)	Co-Ordinates () E N	Sheet 4 of 8

SAMPLES & TESTS			Water	STRATA				Instrument/ Backfill
Depth	Type No	Test Result		Reduced Level	Legend	Depth (Thick-ness)	DESCRIPTION	
						(0.90) 24.90	Greyish Red (5-R-4/2) Hard bands at 24.4 -24.5 m and 24.6 - 24.7 m COURSE SANDSTONE	
						(0.60) 25.50	moderate red (5-R-4/6) COURSE SANDSTONE. Clay content increasing downwards	
						25.51 (0.55) 26.05	MUDSTONE Moderate red (5-R-4/6) course grained ARGILLACEOUS SANDSTONE	
						26.20	Moderate red (5-R-4/6) MEDIUM SANDSTONE	
						26.25	uncemented fine-grained GRAVEL	
						26.40	Moderate red (5-R-4/6) MEDIUM SANDSTONE	
						26.41 (0.04) 26.46	MUDSTONE Moderate red (5-R-4/6) MEDIUM SANDSTONE	
						26.47	MUDSTONE	
						27.10	Moderate red (5-R-4/6) MEDIUM SANDSTONE	
						27.25	Dark reddish brown (10-R-3/4) broken, hard MUDSTONE	
						(0.55) 27.80	moderate red (5-R-4/6) well sorted COURSE SANDSTONE	
						28.00	Moderate red (5-R-4/6)ARENACEOUS MUDSTONE	
						28.25	dark reddish brown (10-R-3/4) with small micas and dark minerals MEDIUM SANDSTONE	
						(2.45) 30.70	Moderate red (5-R-5/4) fine-medium grained at top coursening downwards to course-medium grained. Fine lighter bands below 28.66 m, darker (very dark red (5-R-2/6)) 1 mm bands below 29.30 m MEDIUM SANDSTONE	
						30.80	moderate red (5-R-5/4) soft CLAY	
						30.90	moderate red (5-R-5/4) SANDY SILTSTONE	
						31.00	moderate red (5-R-5/4) COURSE SANDSTONE	
						31.20	moderate red (5-R-5/4) fine -medium grained CLAYEY SANDSTONE	
						31.40	Moderate red (5-R-5/4) very course grained (some 3 mm quartz clasts) SILTY SANDSTONE	
						31.75	Moderate reddishy brown (10-R-4/6) heavily broken CLAYEY	

Boring Progress and Water Observations						Chiselling			Water Added		GENERAL REMARKS
Date	Time	Depth	Casing	Casing Dia	Water Dpt	From	To	Hours	From	To	

All dimensions in metres Scale 1:50	Contractor :	Logged By Richard Mitchener	Approved By

Form SLR BOREHOLE LOG File PHD.GPJ 17-02-03

SLR Consulting Ltd, Wheeley Ridge, Wheeley Road, ALVECHURCH, B48 7DD, Telephone: 0121 447 8040, Fax: 0121 447 8076

Coring Log

BOREHOLE No
URGENT1

Project: URGENT Project

Client: University of Birmingham

Project No:	Date Started: Date Started:	Ground Level (m)	Co-Ordinates () E N	Sheet 5 of 8

SAMPLES & TESTS			Water	STRATA				Instrument/ Backfill
Depth	Type No	Test Result		Reduced Level	Legend	Depth (Thick-ness)	DESCRIPTION	
						32.10	SILTSTONE	
						32.30	Moderate reddish brown (10-R-4/6) SANDY SILTSTONE	
						32.39	Moderate Reddish Brown (10-R-4/6) heavily broken SILTSTONE	
						32.72	moderate red (5-R-4/6) FINE SANDSTONE	
						33.06	moderate red (5-R-4/6) finely laminated, fine grained SILTY SANDSTONE	
						33.10	Moderate reddish brown (10-R-4/6) well sorted, clean medium-course grained COURSE SANDSTONE	
						33.15	Moderate reddish brown (10-R-4/6) SILTY MUDSTONE	
						33.35	moderate red (5-R-4/6) very fine grained FINE SANDSTONE	
						(0.40)	Dusky red (5-R-3/4) finely interbedded SANDSTONE AND SILTSTONE	
						33.75	Moderate red (5-R-4/6, heavily broken below 33.70 m MEDIUM SANDSTONE	
						34.10	dark reddish brown (10-R-3/4) FINE SANDSTONE	
						(0.82)	Dark reddish brown (10-R-3/4) fine grained. bands of very dark red (5-R-2/6). CLAYEY SANDSTONE	
						34.92		
						35.05	Dark reddish brown (10-R-3/4) with fine bands of greyish green (5-G-5/2) SILTY CLAYSTONE	
						(1.20)	Dark reddish brown (10-R-3/4) with ~5% clay lenses below 36.04 m COURSE SANDSTONE	
						36.25		
						(0.75)	Dark reddish brown (10-R-3/4) well rounded micaceous fine-medium grained, coursening downwards to course-medium grained. MEDIUM SANDSTONE	
						37.00		
						(1.10)	dark reddish brown (10-R-3/4) some grains very heavily stained with Mn. Darker, clay-rich bands at ~5cm intervals MEDIUM SANDSTONE	
						38.10		
						(0.60)	dark reddish brown (10-R-3/4) poorly cemented fine-medium grained reduced to greenish grey (5-G-6/1) below 38.63 m MEDIUM SANDSTONE	
						38.70		
						38.72	dark reddish brown (10-R-3/4) course grained CLAYEY SANDSTONE	
						39.05	pale red (5-R-6/2) COURSE SANDSTONE	
						(0.45)	Dark reddish brown (10-R-3/4) MUDSTONE. Pale red (5-R-6/2) bands at 39.12 - 29.15 m and 39,22 - 39.35 m. Highly broken below 39.30 m MUDSTONE	
						39.50		
						(0.50)	moderate reddish brown (10-R-4/6) well sorted, clean MEDIUM SANDSTONE	
						40.00		

Boring Progress and Water Observations					
Date	Time	Depth	Casing	Casing Dia	Water Dpt

Chiselling			Water Added	
From	To	Hours	From	To

GENERAL REMARKS

All dimensions in metres Scale 1:50	Contractor :	Logged By Richard Mitchener	Approved By

Form SLR BOREHOLE LOG File PHD.GPJ 17-02-03

SLR Consulting Ltd, Wheeley Ridge, Wheeley Road, ALVECHURCH, B48 7DD, Telephone: 0121 447 8040, Fax: 0121 447 8076

Coring Log

BOREHOLE No
URGENT1

Project: URGENT Project

Client: University of Birmingham

Project No:	Date Started: Date Started:	Ground Level (m)	Co-Ordinates () E N	Sheet 6 of 8

SAMPLES & TESTS			Water	STRATA				Instrument/ Backfill
Depth	Type No	Test Result		Reduced Level	Legend	Depth (Thick-ness)	DESCRIPTION	
						(0.40) 40.40	Dusky red (5-R-3/4) clean uncemented COURSE SAND	
						40.60	dark reddish brown (10-R-3/4) CLAY PELLETS in uncemented CLAYEY SAND	
						40.80	dark reddish brown (10-R-3/4) clean MEDIUM SANDSTONE	
						(0.38) 41.18	dark reddish brown (10-R-3/4) with minor small clay lenses COURSE SANDSTONE	
						41.23	Dusky red (5-R-3/4) MUDSTONE	
						(0.47) 41.70	Dark reddish brown (10-R-3/4) medium grained CLAYEY SANDSTONE	
						(0.73) 42.43	Moderate red (5-R-5/4) with fine clay bands (Moderate reddish brown (10-R-4/6)) above 42.00 m. Course bands present below this.FINE SANDSTONE	
						42.60	Dark reddish brown (10-R-3/4) fine-grained, very clayey CLAYEY SANDSTONE	
						(0.40) 43.00	dark reddish brown (10-R-3/4) clean COURSE SANDSTONE	
						(4.05) 47.05	Moderate red (5-R-4/6) well cemented course-medium grained. Heavily broken bands at 44.39 - 44.42 m, 46.21 - 46.42 and 46.67 - 46.82 m. MEDIUM SANDSTONE	
						(0.65) 47.70	Moderate red (5-R-4/6) well cemented course-medium grained with fine Mn rich banding. MEDIUM SANDSTONE	
						(0.40)	Moderate red (5-R-4/6) well cemented micaceous course MEDIUM	

Boring Progress and Water Observations						Chiselling			Water Added		GENERAL REMARKS
Date	Time	Depth	Casing	Casing Dia	Water Dpt	From	To	Hours	From	To	

All dimensions in metres Scale 1:50	Contractor :	Logged By Richard Mitchener	Approved By

Form SLR BOREHOLE LOG File PHD.GPJ 17-02-03

SLR Consulting Ltd, Wheeley Ridge, Wheeley Road, ALVECHURCH, B48 7DD, Telephone: 0121 447 8040, Fax: 0121 447 8076

Coring Log

BOREHOLE No
URGENT1

Project: URGENT Project

Client: University of Birmingham

Project No:	Date Started: Date Started:	Ground Level (m)	Co-Ordinates () E N	Sheet 7 of 8

SAMPLES & TESTS			Water	STRATA				Instrument/ Backfill
Depth	Type No	Test Result		Reduced Level	Legend	Depth (Thick-ness)	DESCRIPTION	
						48.10	SANDSTONE	
						48.13	Grey MUDSTONE	
						(0.87)	Moderate red (5-R-4/6) well cemented micaceous course-medium grained MEDIUM SANDSTONE	
						49.00		
						49.31	Dark reddish brown (10-R-3/4) partially cemented micaceous (white and dark) fine - medium grained.CLAYEY SANDSTONE	
						49.34	Dark reddish brown (10-R-3/4) partially cemented micaceous (white and dark) fine - medium grained with clay pellets CLAYEY SANDSTONE	
						49.69	Dark reddish brown (10-R-3/4) partially cemented micaceous (white and dark) fine - medium grained. Broken band at 49.65 - 49.69 m CLAYEY SANDSTONE	
						(0.61)		
						50.30	Pale reddish brown (10-R-5/4) clean well cemented meduim grained coursening downwards to very course grained at base COURSE SANDSTONE	
						(0.90)	moderate reddish brown (10-R-5/4) very broken and micaceous to 50.60 m SILTY MUDSTONE	
						51.20		
						51.43	greenish grey (5-GY-6/1) FINE SANDSTONE	
						(0.57)	Very dark red (5-R-2/6) COURSE SANDSTONE	
						52.00		
						52.29	dark reddish brown (10-R-3/4) well sorted very-fine grained FINE SANDSTONE	
						52.39	Greenish grey (5-G-6/1) FINE SANDSTONE	
						52.54	dark reddish brown (10-R-3/4) well sorted, very fine grained FINE SANDSTONE	
						(2.36)	dark reddish brown (10-R-3/4) well sorted, very course grained. silty lenses between 54.40 and 54.70 m COURSE SANDSTONE	
						54.90		
						(1.00)	Very dark red (5-R-2/6) poorly cemented. medium grained sand particles. Becoming more silty and finer grained downwards to 55.50. Becoming more sorted below this, and colour grading to moderate reddish brown (10-R-4/6). Micas appearing. -56.00 SILTY SANDSTONE	
						56.00		

Boring Progress and Water Observations					
Date	Time	Depth	Casing	Casing Dia	Water Dpt

Chiselling			Water Added	
From	To	Hours	From	To

GENERAL REMARKS

All dimensions in metres Scale 1:50	Contractor :	Logged By Richard Mitchener	Approved By

Form SLR BOREHOLE LOG File PHD.GPJ 17-02-03

SLR Consulting Ltd, Wheeley Ridge, Wheeley Road, ALVECHURCH, B48 7DD, Telephone: 0121 447 8040, Fax: 0121 447 8076

Coring Log

BOREHOLE No
URGENT1

Project: URGENT Project

Client: University of Birmingham

Project No:	Date Started: Date Started:	Ground Level (m)	Co-Ordinates () E N	Sheet 8 of 8

SAMPLES & TESTS			Water	STRATA				Instrument/ Backfill
Depth	Type No	Test Result		Reduced Level	Legend	Depth (Thick-ness)	DESCRIPTION	
						57.12	Moderate reddish brown (10-R-4/6) medium grained. Sub vertical very hard band presen SILTY SANDSTONE	
						(0.56) 57.68	moderate reddish brown (10-R-4/6) very course. Cross bedded. Good channel base at bottom COURSE SANDSTONE	
						58.00	moderate reddish brown (10-R-4/6) fine grained. Fining downwards to very silty sandstone SILTY SANDSTONE	
						(0.60) 58.60	moderate reddish brown (10-R-4/6)cross bedded, some dark mineralsFINE SANDSTONE	
						(0.40) 59.00	moderate reddish brown (10-R-4/6) fine grained. Course (up to 2 mm) grains present singly and in bands SILTY SANDSTONE	
						(0.55) 59.55	moderate reddish brown (10-R-3/4) with bands of course and finer material. Matrix coursens downwards -59.55 MEDIUM SANDSTONE	
						(0.45) 60.00	dark reddish brown (10-R-3/4) some fine and course sand present SILTSTONE	

Boring Progress and Water Observations					
Date	Time	Depth	Casing	Casing Dia	Water Dpt

Chiselling			Water Added	
From	To	Hours	From	To

GENERAL REMARKS

All dimensions in metres Scale 1:50	Contractor :	Logged By Richard Mitchener	Approved By

Form SLR BOREHOLE LOG File PHD.GPJ 17-02-03

SLR Consulting Ltd, Wheeley Ridge, Wheeley Road, ALVECHURCH, B48 7DD, Telephone: 0121 447 8040, Fax: 0121 447 8076

Appendix IV 4.2: Temperature Logs

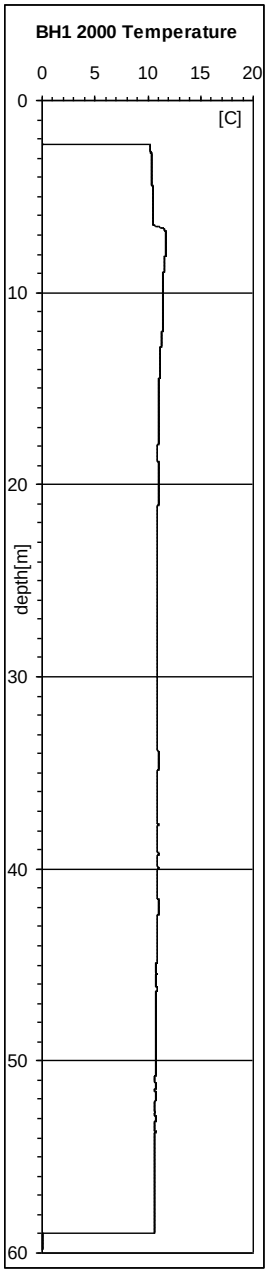

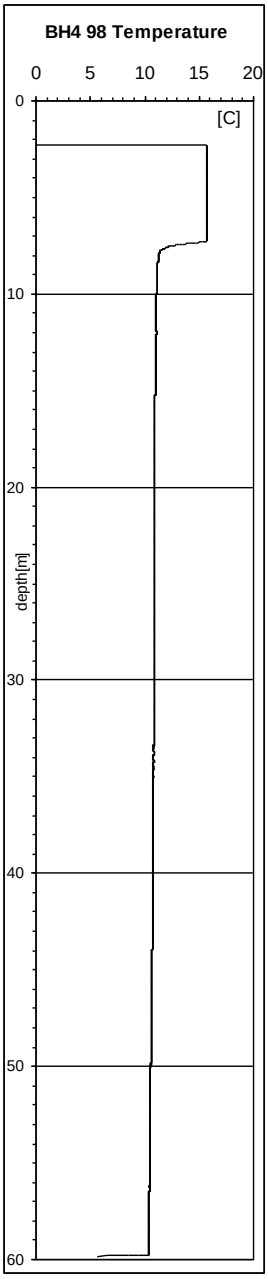

Appendix IV 4.3: Conductivity Logs.

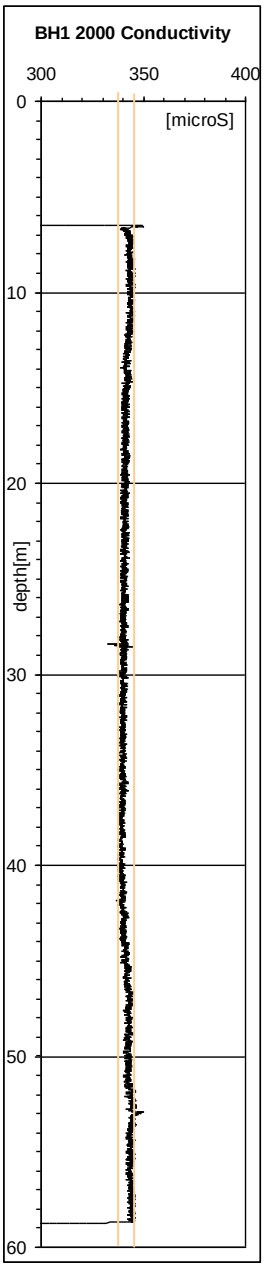

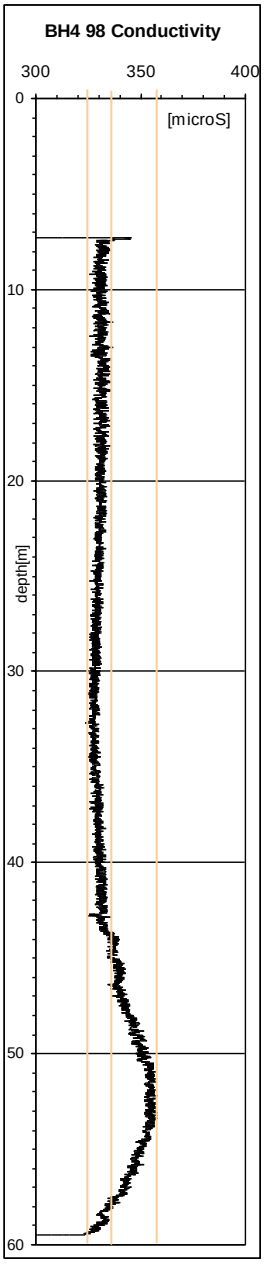

Appendix IV 4.4: Caliper Logs

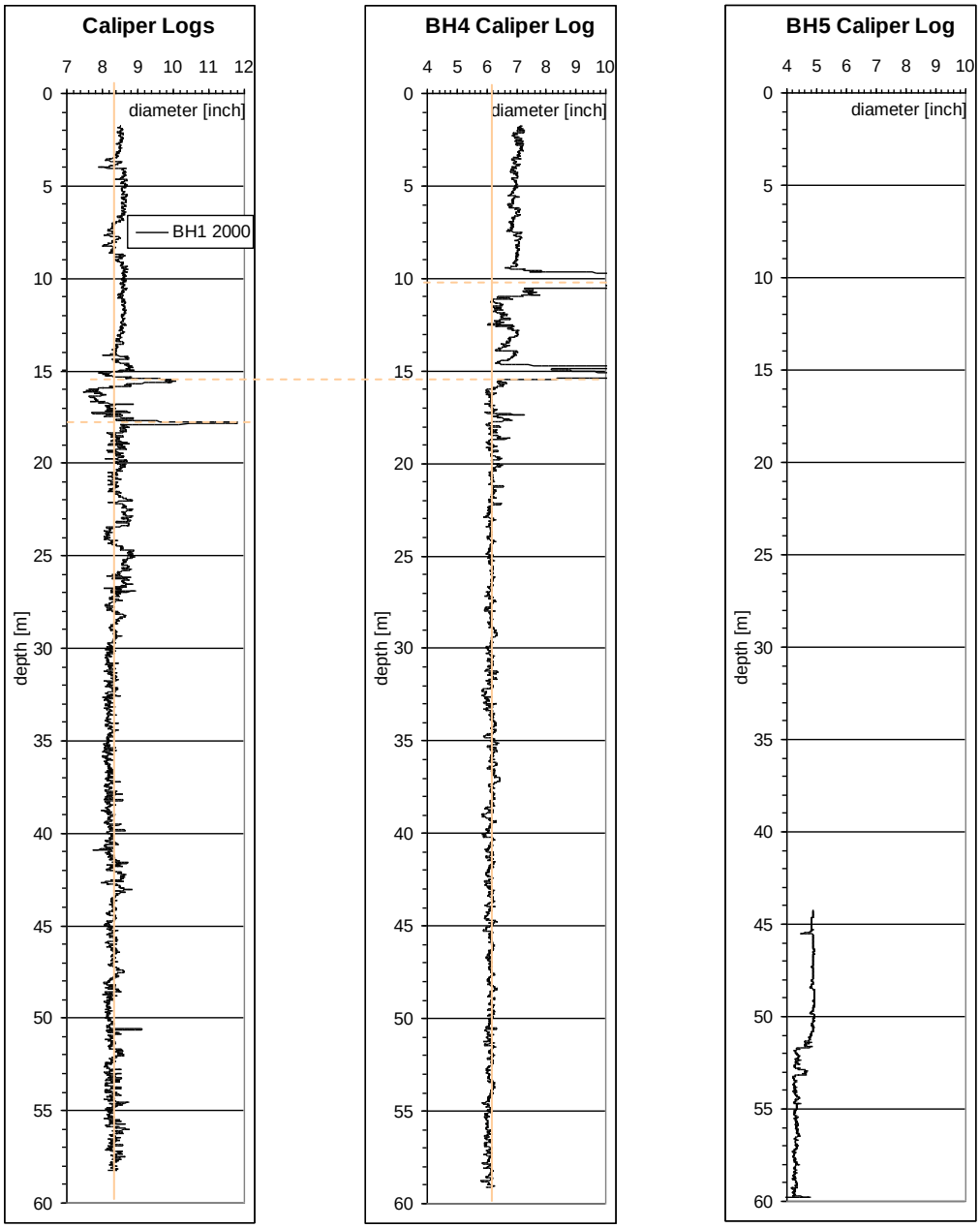

Appendix VII.1 a

Row and Column No.	Mesh Size (m)	Row and Column No.	Mesh Size (m)
1	20.91	46	0.15
2	16.33	47	0.15
3	12.76	48	0.15
4	9.97	49	0.15
5	7.79	50	0.15
6	6.08	51	0.15
7	4.75	52	0.15
8	3.71	53	0.15
9	2.9	54	0.15
10	2.27	55	0.15
11	1.77	56	0.15
12	1.38	57	0.15
13	1.08	58	0.15
14	0.84	59	0.15
15	0.66	60	0.15
16	0.52	61	0.15
17	0.4	62	0.15
18	0.31	63	0.15
19	0.25	64	0.15
20	0.19	65	0.15
21	0.15	66	0.15
22	0.15	67	0.15
23	0.15	68	0.15
24	0.15	69	0.15
25	0.15	70	0.15
26	0.15	71	0.19
27	0.15	72	0.25
28	0.15	73	0.31
29	0.15	74	0.4
30	0.15	75	0.52
31	0.15	76	0.66
32	0.15	77	0.84
33	0.15	78	1.08
34	0.15	79	1.38
35	0.15	80	1.77
36	0.15	81	2.27
37	0.15	82	2.9
38	0.15	83	3.71
39	0.15	84	4.75
40	0.15	85	6.08
41	0.15	86	7.79
42	0.15	87	9.97
43	0.15	88	12.76
44	0.15	89	16.33
45	0.15	90	20.91

Appendix VII.1 b

Layer No.	Layer in [m]	Depth bgl [m]	Top Elevation	Bottom Elevation
1	3	3	60	57
2	3	6	57	54
3	2	8	54	52
4	2	10	52	50
5	1.5	11.5	50	48.5
6	0.75	12.25	48.5	47.75
7	0.75	13	47.75	47
8	1.5	14.5	47	45.5
9	1.75	16.25	45.5	43.75
10	1.75	18	43.75	42
11	1.5	19.5	42	40.5
12	1	20.5	40.5	39.5
13	1	21.5	39.5	38.5
14	1.5	23	38.5	37
15	2	25	37	35
16	1.5	26.5	35	33.5
17	0.75	27.25	33.5	32.75
18	0.75	28	32.75	32
19	1	29	32	31
20	1.5	30.5	31	29.5
21	1	31.5	29.5	28.5
22	1	32.5	28.5	27.5
23	1	33.5	27.5	26.5
24	1.5	35	26.5	25
25	1.5	36.5	25	23.5
26	1.5	38	23.5	22
27	1	39	22	21
28	1	40	21	20
29	1	41	20	19
30	1.5	42.5	19	17.5
31	2	44.5	17.5	15.5
32	2.5	47	15.5	13
33	2	49	13	11
34	1.5	50.5	11	9.5
35	1	51.5	9.5	8.5
36	1	52.5	8.5	7.5
37	1.5	54	7.5	6
38	2	56	6	4
39	2	58	4	2
40	2	60	2	0

Appendix VII.1c

	Layer	Row	Column
BH1	1 - 40	43	22
BH2	1 - 9	63	44
BH3	1 - 27	31	46
BH4	1 - 40	55	69
BH5	1 - 40	33	69

Natural Gradient transferd to model input data							Initial Head Conditions at the Boundary Natural Gradient and Up-Flow in BH1	
Aquifer Layer S1& S2	BH2 average head (rest water levels)		7.75	[m] bgl				
	84.64	distance to boundary [m]	91.54	distance to boundary [m]	**Head MODFLOW Boundary**		**Head MODFLOW Boundary Natural Gradient and Up-Flow in BH1**	
	head up-flow end of the model area		head down-flow end of the model area		Column 1	Column 90	Column 1	Column 90
i	head increase [m]	total head increase [m]	head decrease [m]	total head decrease [m]	up-flow boundary	down-flow boundary	up-flow boundary	down-flow boundary
0.288	24.35	16.60	26.33	34.08	76.60	25.92	94.08	34.08
Adjusted	18.88	distance to boundary [m]	38.13	distance to boundary [m]	**Column 7**	**Column 85**	**Column 7**	**Column 85**
i	head increase [m]	total head increase [m]	head decrease [m]	total head decrease [m]	**up-flow boundary**	**down-flow boundary**	**up-flow boundary**	**down-flow boundary**
0.288	5.43	-2.32	10.97	18.72	**57.68**	**41.28**	**78.72**	**18.72**
Aquifer Layer S3	BH1 average head (rest water levels)		7.15	[m] bgl				
	84.64	distance [m]	88.54	distance [m]	**Head MODFLOW Boundary**		**Head MODFLOW Boundary**	
	head up-flow end of the model area		head down-flow end of the model area		**Column 1**	**Column 90**	**Column 1**	**Column 90**
i	head increase [m]	Total head [m bgl]	head decrease [m]	Total head [m bgl]	**up-flow boundary**	**down-flow boundary**	**up-flow boundary**	**down-flow boundary**
0.079	6.65	-0.50	6.96	14.11	**59.50**	**45.89**	**74.11**	**14.11**
Aquifer Layer S4	BH1average head (rest water levels)		7.15	[m] bgl				
	84.64	distance to boundary [m]	91.54	distance to boundary [m]	**Head MODFLOW Boundary**		**Head MODFLOW Boundary**	
	head up-flow end of the model area		head down-flow end of the model area		Column 1	**Column 90**	Column 1	**Column 90**
i	head increase [m]	total head increase [m]	head decrease [m]	total head decrease [m]	up-flow boundary	**down-flow boundary**	up-flow boundary	**down-flow boundary**
0.115	9.71	2.56	10.50	17.65	62.56	**42.35**	77.65	**17.65**
	51.475	distance to boundary [m]			**Column 3**		**Column 3**	
i	head increase [m]	total head increase [m]			**up-flow boundary**		**up-flow boundary**	
0.115	5.90	-1.25			**58.75**		**60.00**	
Aquifer Layer S5	BH1average head (rest water levels)		7.15	[m] bgl				
	84.64	distance to boundary [m]	91.54	distance to boundary [m]	**Head MODFLOW Boundary**		**Head MODFLOW Boundary**	
	head up-flow end of the model area		head down-flow end of the model area		Column 1	**Column 90**	Column 1	**Column 90**
i	head increase [m]	total head increase [m]	head decrease [m]	total head decrease [m]	up-flow boundary	**down-flow boundary**	up-flow boundary	**down-flow boundary**
0.183	15.53	8.38	16.80	23.95	68.38	**36.05**	83.95	**23.95**
	31.23	distance to boundary [m]			**Column 5**		**Column 5**	
i	head increase [m]	total head increase [m]			**up-flow boundary**		**up-flow boundary**	
0.183	5.73	-1.42			**58.58**		**60.00**	
Aquifer Layer S6	BH1average head (rest water levels)		7.15	[m] bgl				
	84.64	distance to boundary [m]	91.54	distance to boundary [m]	**Head MODFLOW Boundary**		**Head MODFLOW Boundary**	
	head up-flow end of the model area		head down-flow end of the model area		**Column 1**	**Column 90**	**Column 1**	**Column 90**
i	head increase [m]	total head increase [m]	head decrease [m]	total head decrease [m]	**up-flow boundary**	**down-flow boundary**	**up-flow boundary**	**down-flow boundary**
0.036	3.01	-4.14	3.26	10.41	**55.86**	**49.59**	**70.41**	**10.41**

Appendix VII.2: It is assumed that the flow on the Test site is from the right side of the model to the left side of the model (nearly North_South direction). The head increase at the up-flow and down-flow boundaries is calculated with the gradients i gained with the dilution tracer tests. The total head increase at the up-flow and down-flow boundaries is the head increase minus the average head of BH1 (S3 to S6) or BH2 (S1&S2) and vice versa for the total head decrease. The head of the Modflow boundary at the up-flow end is 60 m (the top elevation of the model) plus the total head increase. The head of the Modflow boundary at the down-flow end is 60 m (the top elevation of the model) minus the total head decrease.

Appendix VII.3, the drawdown graphs of the pumping tests fitted against the drawdown graphs of the model results.

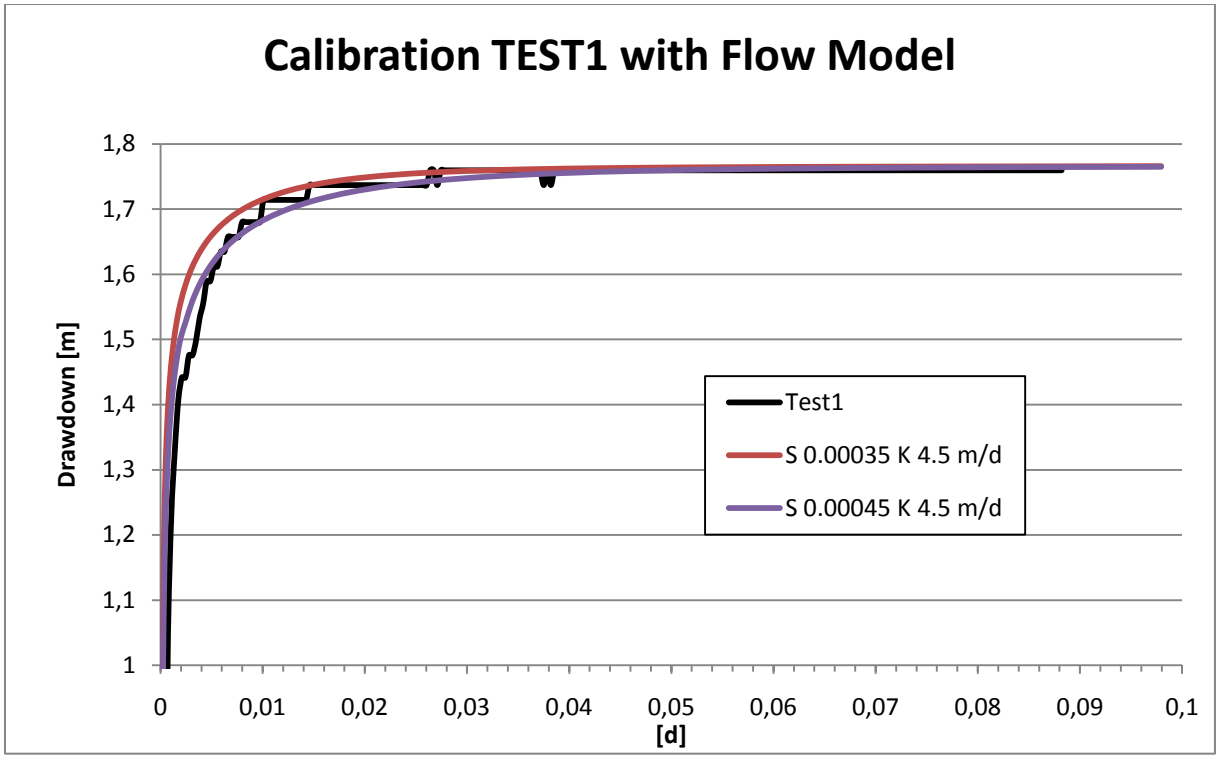

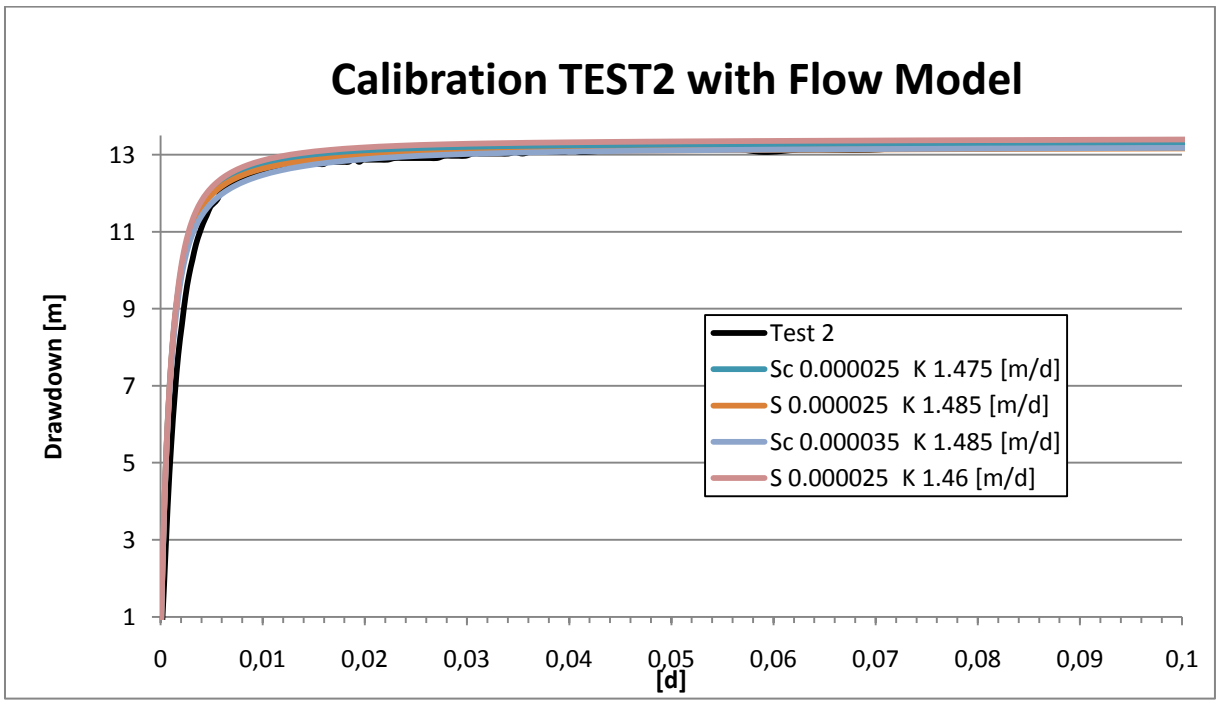

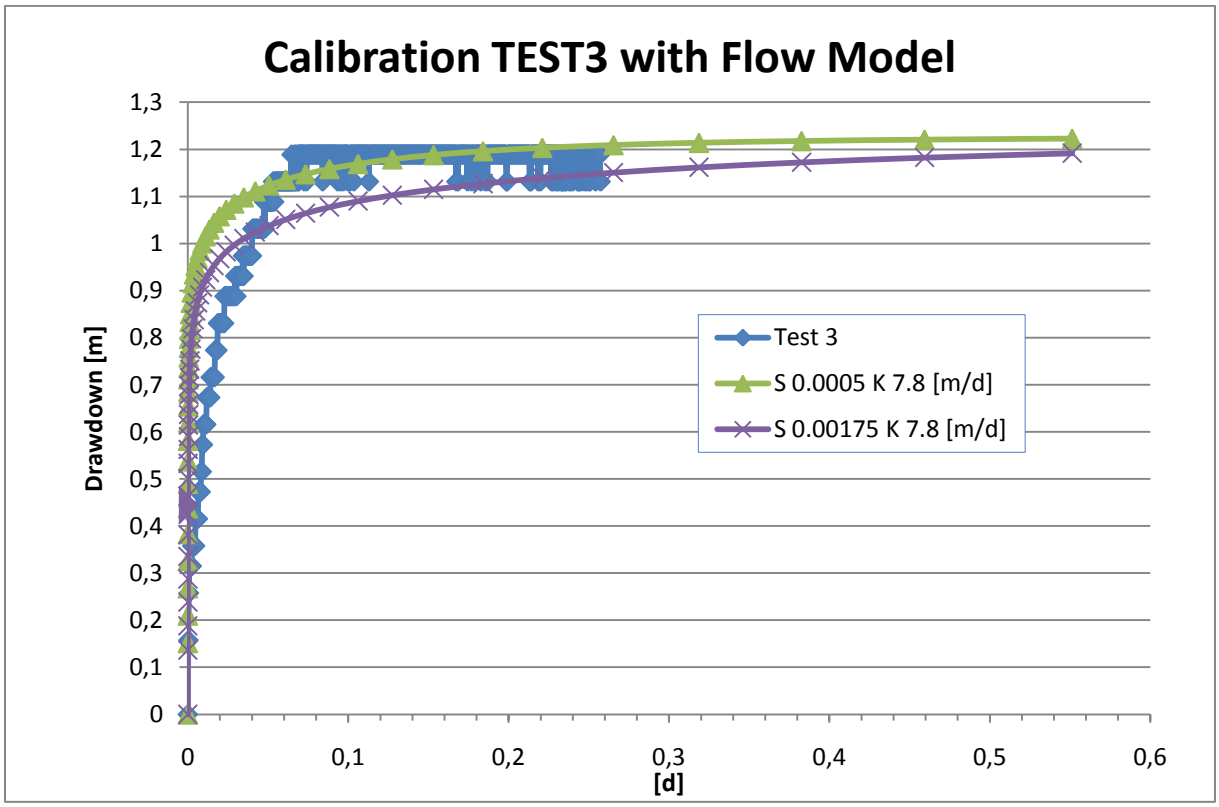
Calibration TEST3 with Flow Model
Drawdown [m]
1,3
1,2
1,1
1
0,9
0,8
0,7
0,6
0,5
0,4
0,3
0,2
0,1
0
0
0,1
0,2
0,3
0,4
0,5
0,6
[d]
Test 3
S 0.0005 K 7.8 [m/d]
S 0.00175 K 7.8 [m/d]

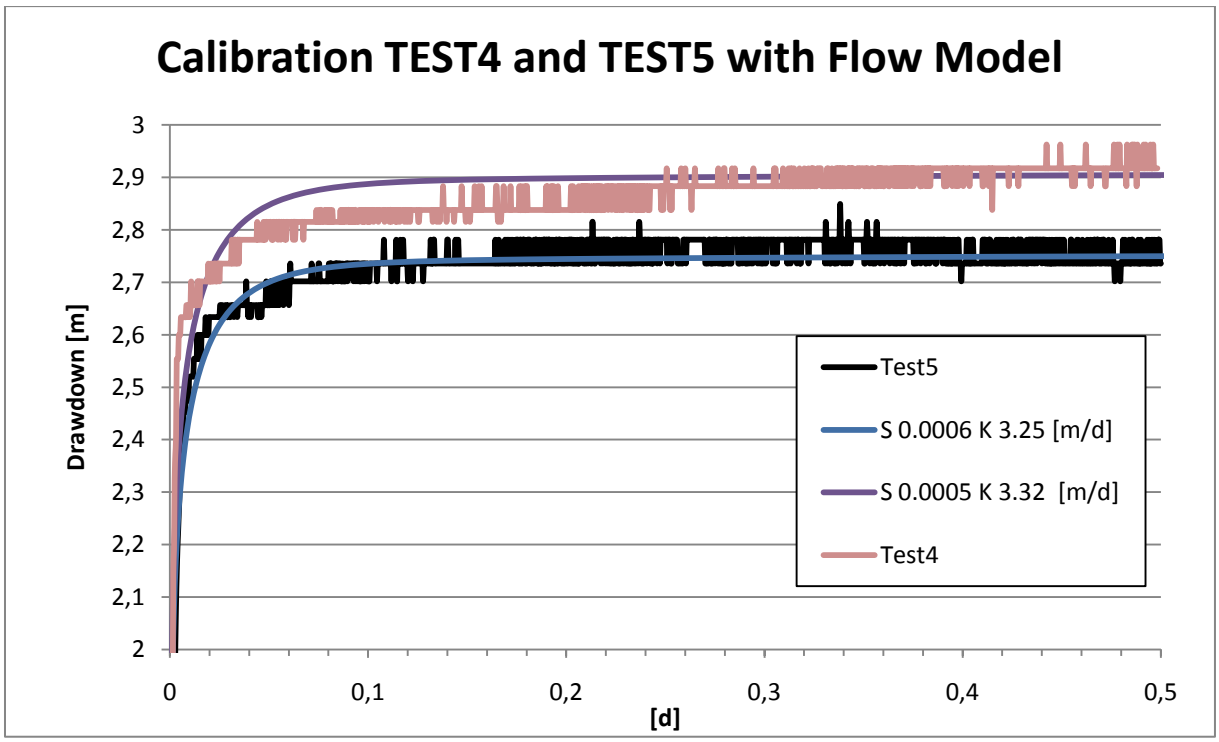
Calibration TEST4 and TEST5 with Flow Model
Drawdown [m]
3
2,9
2,8
2,7
2,6
2,5
2,4
2,3
2,2
2,1
2
0
0,1
0,2
0,3
0,4
0,5
[d]
Test5
S 0.0006 K 3.25 [m/d]
S 0.0005 K 3.32 [m/d]
Test4

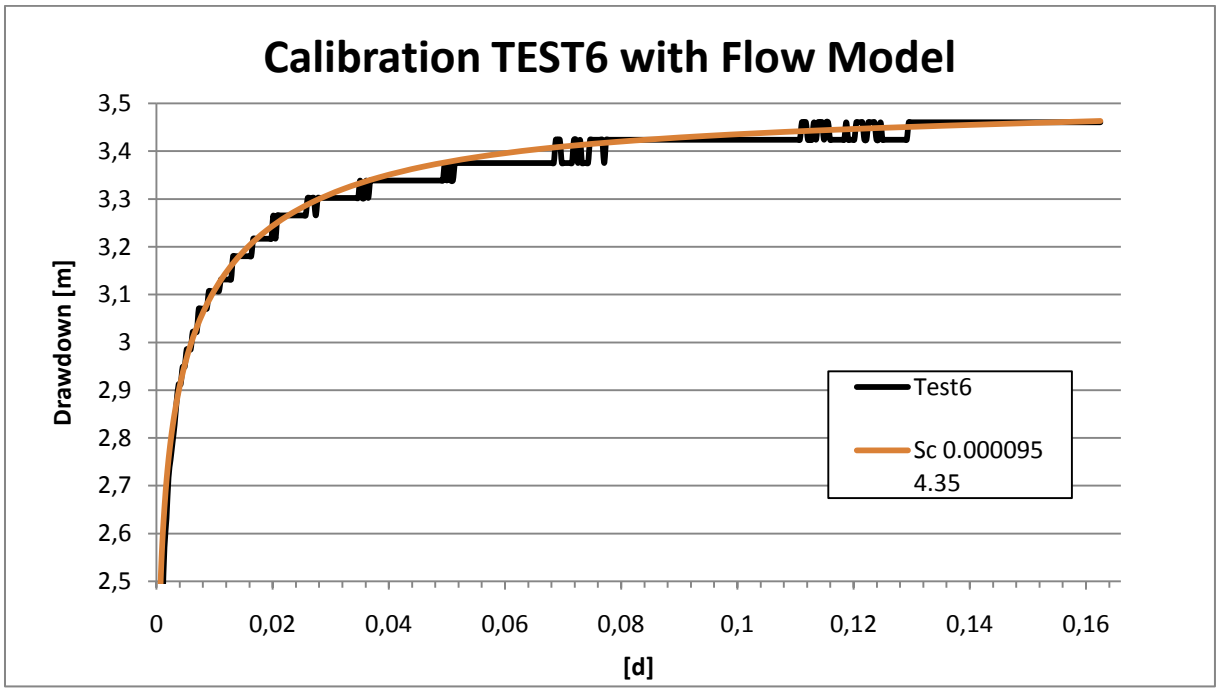
Calibration TEST6 with Flow Model
Drawdown [m]
3,5
3,4
3,3
3,2
3,1
3
2,9
2,8
2,7
2,6
2,5
0
0,02
0,04
0,06
0,08
0,1
0,12
0,14
0,16
[d]
Test6
Sc 0.000095
4.35

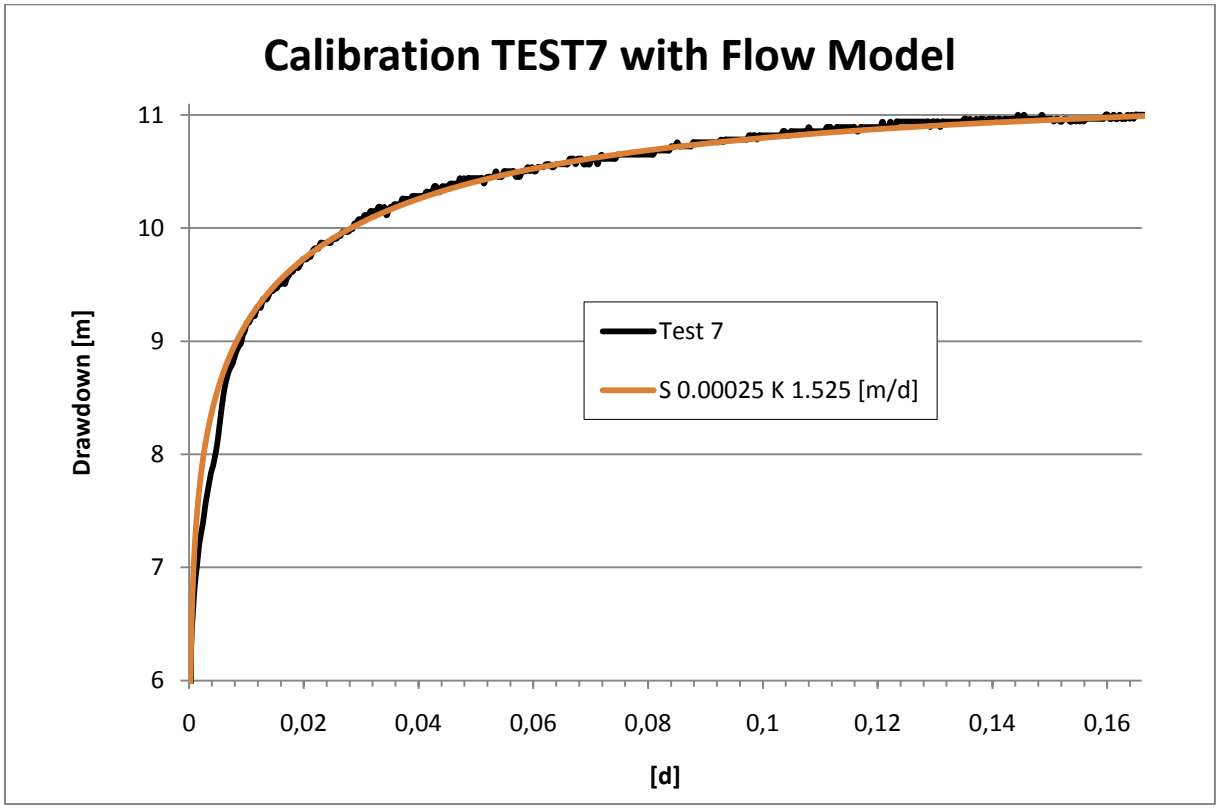
Calibration TEST7 with Flow Model
Drawdown [m]
11
10
9
8
7
6
0
0,02
0,04
0,06
0,08
0,1
0,12
0,14
0,16
[d]
Test 7
S 0.00025 K 1.525 [m/d]

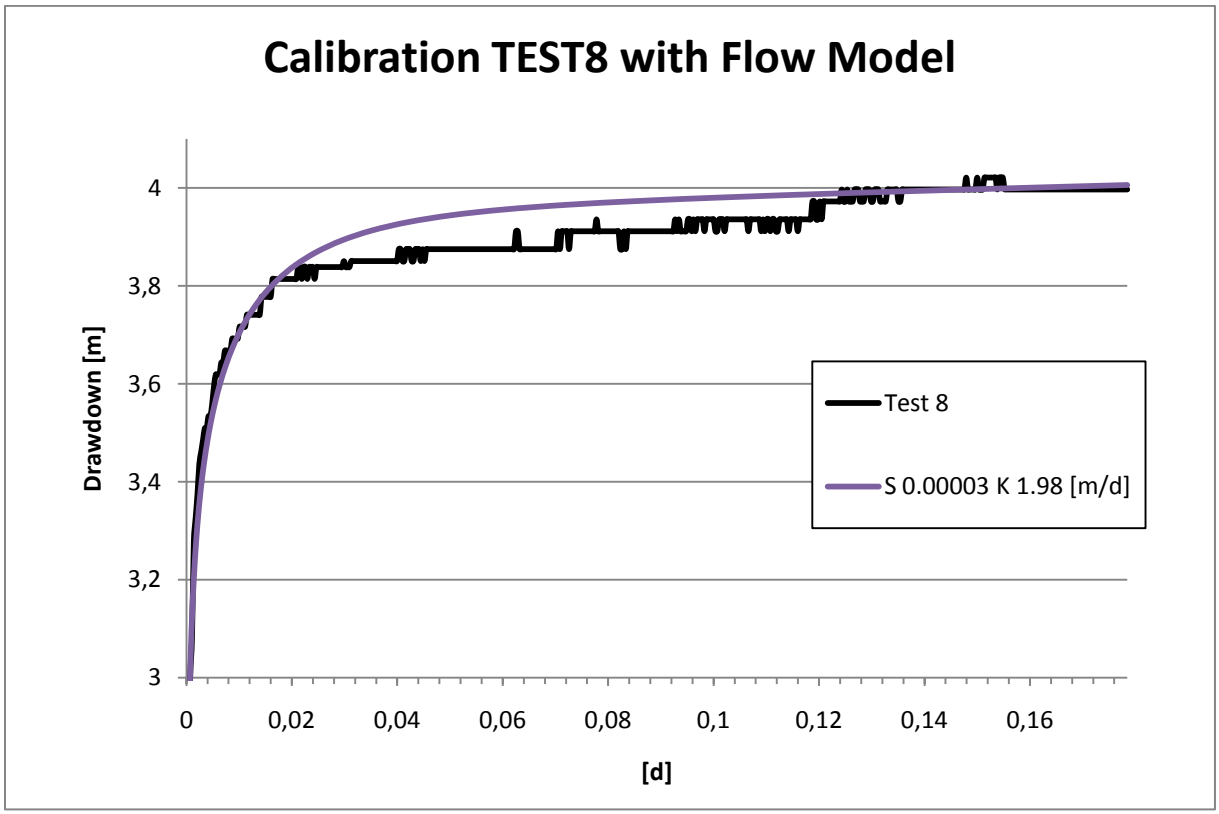
Calibration TEST8 with Flow Model
Drawdown [m]
4
3,8
3,6
3,4
3,2
3
0
0,02
0,04
0,06
0,08
0,1
0,12
0,14
0,16
[d]
Test 8
S 0.00003 K 1.98 [m/d]

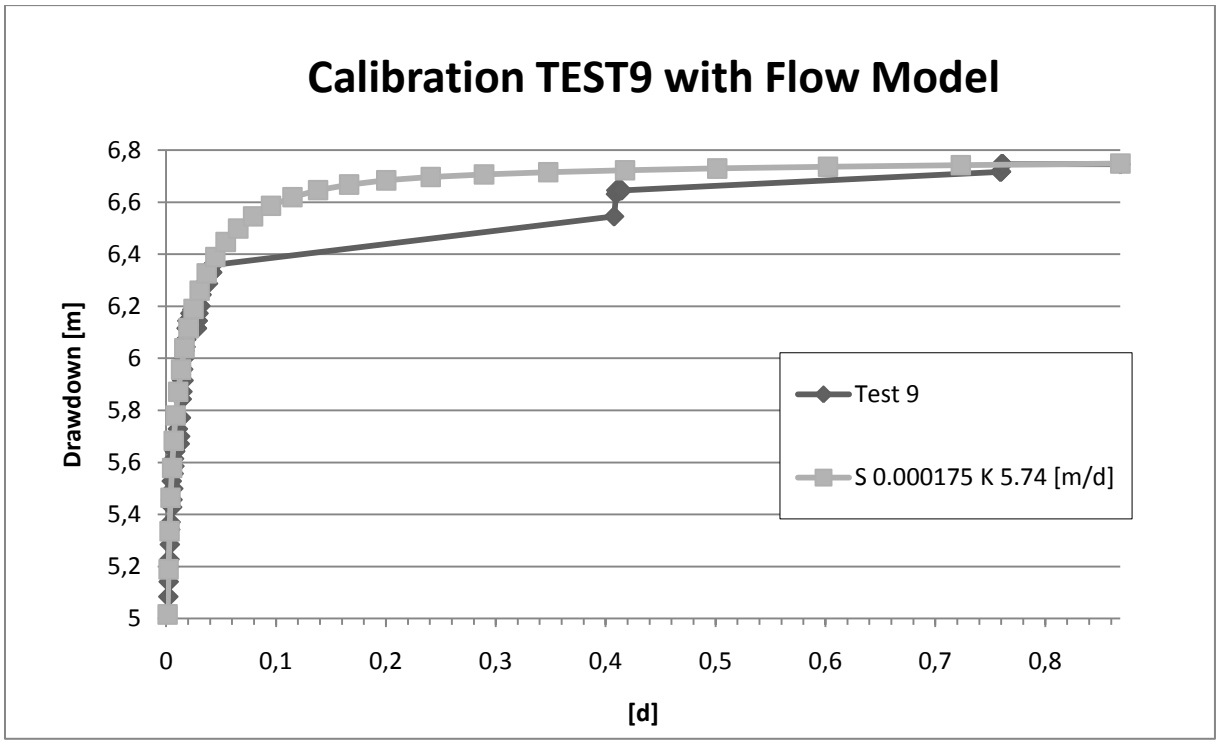
Calibration TEST9 with Flow Model
Drawdown [m]
6,8
6,6
6,4
6,2
6
5,8
5,6
5,4
5,2
5
0
0,1
0,2
0,3
0,4
0,5
0,6
0,7
0,8
[d]
Test 9
S 0.000175 K 5.74 [m/d]

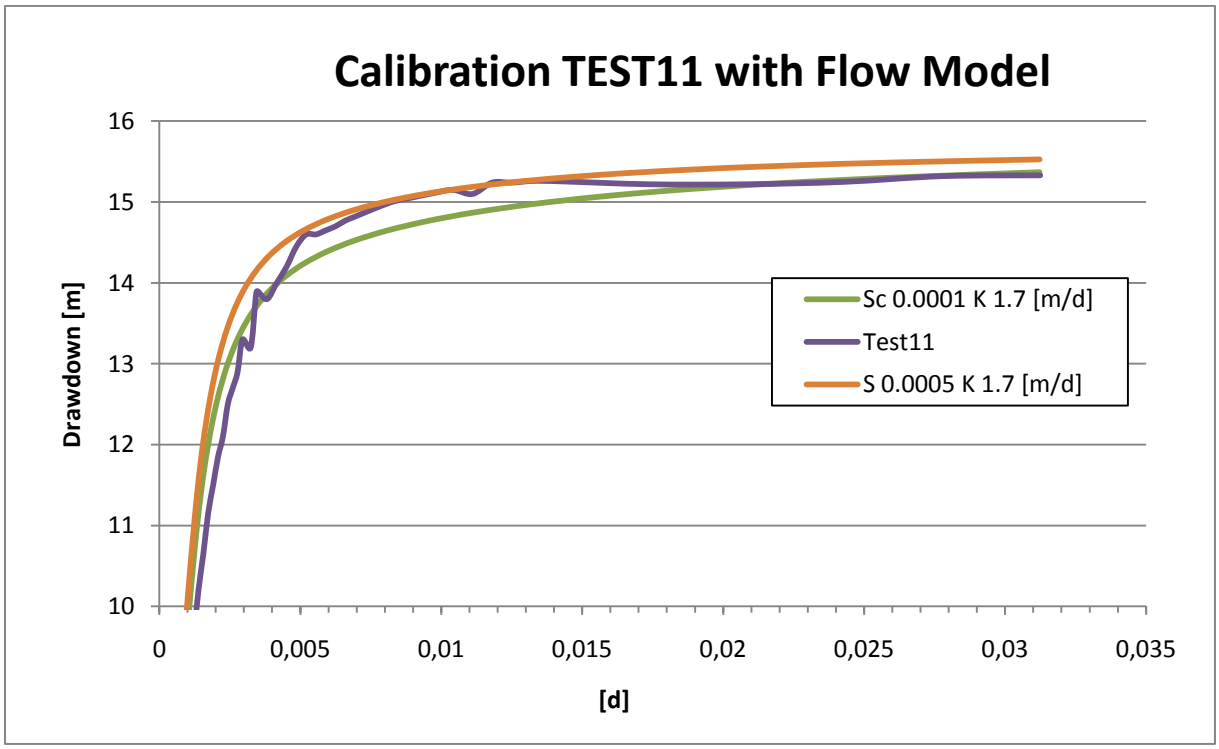
Calibration TEST11 with Flow Model
Drawdown [m]
16
15
14
13
12
11
10
0
0,005
0,01
0,015
0,02
0,025
0,03
0,035
[d]
Sc 0.0001 K 1.7 [m/d]
Test11
S 0.0005 K 1.7 [m/d]

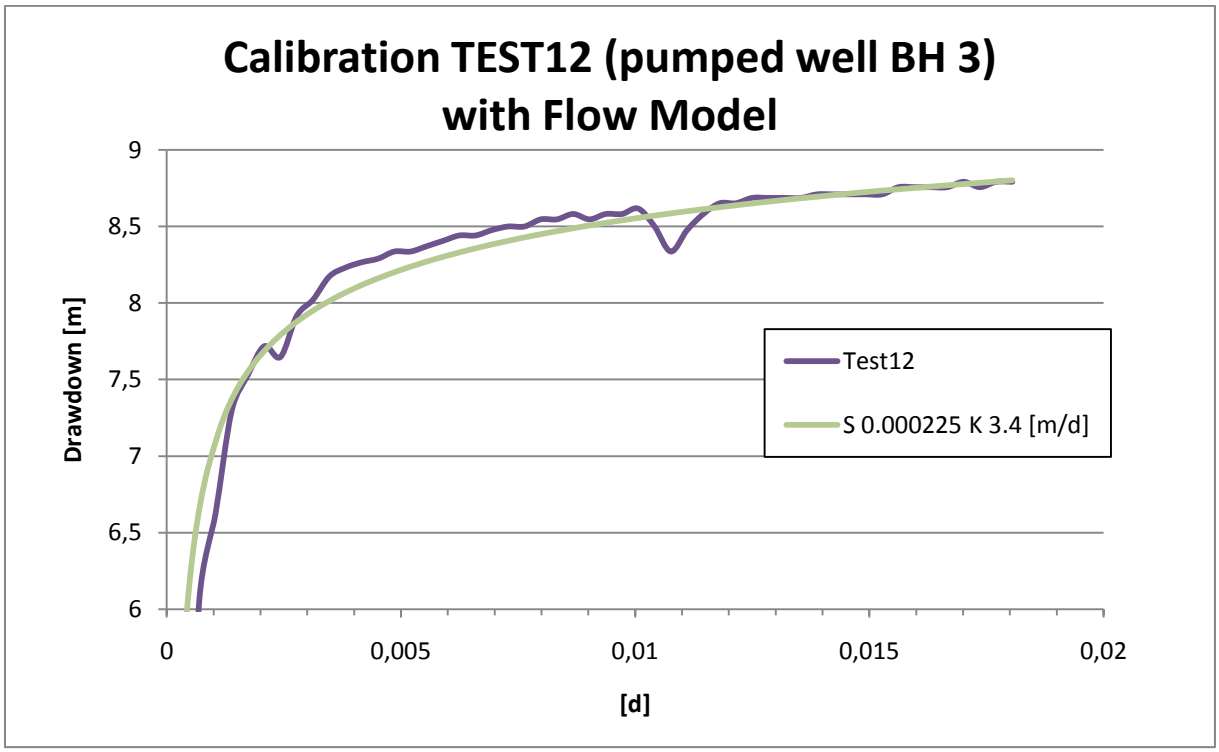
Calibration TEST12 (pumped well BH 3)
with Flow Model
Drawdown [m]
9
8,5
8
7,5
7
6,5
6
0
0,005
0,01
0,015
0,02
[d]
Test12
S 0.000225 K 3.4 [m/d]

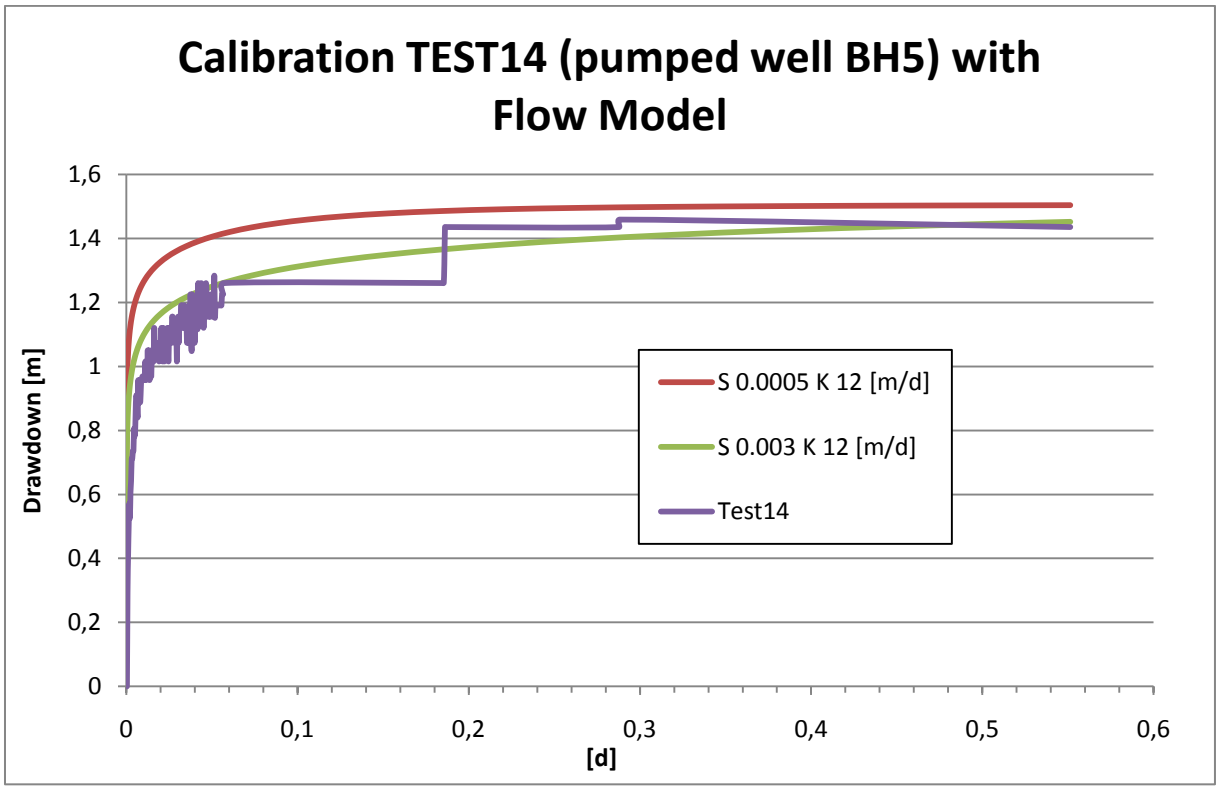
Calibration TEST14 (pumped well BH5) with Flow Model
Drawdown [m]
1,6
1,4
1,2
1
0,8
0,6
0,4
0,2
0
0
0,1
0,2
0,3
0,4
0,5
0,6
[d]
S 0.0005 K 12 [m/d]
S 0.003 K 12 [m/d]
Test14